

DEVELOPMENT OF NOVEL COMBINATIONAL IMPLANTS FOR THE LOCALISED TREATMENT OF BRAIN TUMOURS.

By

Sarah Lastakchi

A thesis submitted to
The University of Birmingham
for the degree of
DOCTOR OF PHILOSOPHY

School of Pharmacy

College of Medical and Dental Sciences

The University of Birmingham

November 2019

UNIVERSITY OF
BIRMINGHAM

University of Birmingham Research Archive

e-theses repository

This unpublished thesis/dissertation is copyright of the author and/or third parties. The intellectual property rights of the author or third parties in respect of this work are as defined by The Copyright Designs and Patents Act 1988 or as modified by any successor legislation.

Any use made of information contained in this thesis/dissertation must be in accordance with that legislation and must be properly acknowledged. Further distribution or reproduction in any format is prohibited without the permission of the copyright holder.

ABSTRACT

This thesis will show the discovery of two highly potent multidrug treatments against Glioma brain tumour and their subsequent development into an implantable drug delivery device.

Glioblastoma is a highly malignant cancer with fewer than 10% of patients surviving longer than 5 years. Initially through using patient derived primary tissue we have demonstrated that at low dose (<100 μ M) repurposed drug treatments such as Pitavastatin, Irinotecan and Celecoxib are more effective than the current standard of care, Temozolomide. Of the 14 Glioma patients, only one (7 %) responded to Temozolomide, while 8 (57 %), 11 (79 %) and 12 (86 %) responded to Irinotecan, Pitavastatin and Celecoxib, respectively. We then examined drugs that had evidence of enhanced antitumor activity when combined, and two multi drug treatments were discovered. The first drug combination consisted of Irinotecan, Pitavastatin, Disulfiram and Copper Gluconate and the second combination was Irinotecan, Captopril and Disulfiram. Both were significantly more effective at killing Glioma cells and reducing reoccurrence than the individual drugs. To develop those two highly potent drug combinations into a pharmaceutical product, an analytical HPLC technique that is capable of separating, detecting and quantifying each drug within the implantable device was developed and subsequently validated for specificity, linearity, accuracy, precision, and robustness.

Finally, each drug combination was designed into a formulation. Rheology was performed to identify the most suitable matrix components, while swellability and DSC studies were used to measure implants physical and chemical stability. From all of the gathered data we have successfully formulated each of those multi-drug treatments into a novel multilayer drug delivery device, consisting of each drug incorporated homogeneously within either a 50:50 poly(lactic-co-glycolic acid) polymer or polymer plus Kolliphor® P 188 plasticiser additive, for the localised treatment of Glioblastoma.

In conclusion the significant cancer cell killing capability of Irinotecan-Pitavastatin-Disulfiram-Copper Gluconate and Irinotecan-Captopril-Disulfiram drug combinations as well as their successful formulation into a poly(lactic-co-glycolic acid) based drug delivery

device demonstrates their future clinical translation potential and the need to continue further with product development and testing.

ACKNOWLEDGMENTS

I would like to thank my supervisor Dr Christopher Mcconville, for his help, support and guidance throughout this project, I could not have asked for a better mentor throughout my time at university. I would like to thank Dr Hannah Batchelor for her incredible encouragement and support which really impacted on my success. I would also like to acknowledge Extruded Pharmaceuticals Ltd for funding which enabled this work to be completed.

My gratitude also goes to my family and friends. Firstly, my mother who initially encouraged me to peruse this PhD and without her I wouldn't have accomplished it. My friends, Justyna Hofmanová, Pavel Hofmanová, Nagina Rashid, Dennis van Soest, Shaun Ryan Huo, Muhammed Rassul, Pam Nicklin and Dan Nicklin for their love and support. Finally, I extend my gratitude to all my colleagues within the School of Pharmacy for their daily kindness and positivity.

PUBLICATIONS

1. Major I, Lastakchi S, Dalton M, McConville C: Chapter 7. **Implantable drug delivery systems**. In: Engineering Drug Delivery Systems. Edited by Ali Seyfoddin SD: Woodhead Publishing; 2020.
2. Garrett A-M, Lastakchi S, McConville C: **The Personalisation of Glioblastoma Treatment using Whole Exome Sequencing: A Pilot Study**. Journal of Molecular Genetics and Genomics 2020.

In progress

1. Gawley M, Almond L, Daniel S, Lastakchi S, Kaur S, Detta A, Cruickshank G, Miller R, Hingtgen S, Sheets K, McConville C: **Development and in vivo evaluation of Irinotecan-loaded Drug Eluting Seeds (iDES) for the Localised treatment of recurrent Glioblastoma Multiforme**. Journal of Controlled Release. (Submitted for initial review 2020)
2. Lastakchi S, Olaloko MK, McConville C: **Repurposed drug treatments are highly toxic against both tumour core and tumour infiltrating glioma tissue**. Journal of Neuro-Oncology. (Submitted for initial review 2020)
3. Lastakchi S, Olaloko MK, McConville C: **A combination of cytotoxic and non-cytotoxic drugs are highly toxic against both tumour core and tumour infiltrating glioma tissue**. Journal of Neuro-Oncology. (Forthcoming Summer 2020)

CONTENTS

1. CHAPTER ONE: BACKGROUND.....	1-1
1.1 Glioblastoma: description and incidence	1-1
1.2 Current therapy for Glioblastoma.....	1-3
1.2.1 Current systemically administered chemotherapeutic treatments.....	1-3
1.2.2 Current locally administered chemotherapy treatment.....	1-7
1.3 Rationale for localised therapy	1-8
1.3.1 Blood Brain Barrier (BBB).....	1-9
1.3.2 Location of tumour growth	1-13
1.3.3 Heterogeneity	1-14
1.3.4 Re-occurrence.....	1-16
1.4 Drugs that may be suitable for repurposing to treat Glioblastoma	1-17
1.4.1 Irinotecan	1-21
1.4.2 Pitavastatin	1-22
1.4.3 Disulfiram/Copper Gluconate	1-23
1.4.4 Captopril	1-25
1.4.5 Celecoxib	1-26
1.4.6 Ticlopidine	1-28
1.4.7 Itraconazole	1-29
1.5 Conclusion.....	1-30
2. CHAPTER TWO: TISSUE CULTURE SINGLE DRUG TREATMENT..	2-31
2.1 Abstract	2-31
2.2 Introduction.....	2-31
2.3 Materials and methods	2-33
2.3.1 Materials	2-33
2.3.2 Biopsy collection and dispersion.....	2-34
2.3.3 Histological evaluation and biopsy protein expression	2-35
2.3.4 Whole exome sequencing	2-35
2.3.5 Cell culture.....	2-35
2.3.6 Drug solution.....	2-37
2.3.7 MTT cell metabolism and IncuCyte cell proliferation imaging assays	2-37
2.3.8 Statistical Analysis	2-39
2.4 Results.....	2-40
2.4.1 Clinical demographics.....	2-40
2.4.2 Defining cell culture and test conditions.....	2-42
2.4.3 Cell metabolism assay (MTT).....	2-47
2.4.4 IncuCyte cell proliferation imaging assay	2-70
2.5 Discussion.....	2-94
2.5.1 Patient demographic vs cytotoxicity drug response	2-94
2.5.2 Patient abrupt protein expression vs tumour growth and drug response.....	2-94
2.5.3 MTT Data analysis and visualisation	2-95
2.5.6 IncuCyte data analysis and visualisation.....	2-99
2.6 Conclusion	2-101
Acknowledgment	2-102
3. CHAPTER THREE: TISSUE CULTURE COMBINATION DRUG TREATMENT	3-103

3.1 Abstract	3-103
3.2 Introduction.....	3-103
3.3 Materials and methods	3-107
3.1 Drug solution	3-107
3.2 MTT cell metabolism and Incucyte cell proliferation assay	3-108
3.3 Statistical analysis	3-109
3.4 Results.....	3-110
3.4.1 clinical demographics.....	3-110
3.4.2 Cell metabolism assay (MTT).....	3-111
3.4.3 IncuCyte cell proliferation assay	3-123
3.4.4 Re-occurrence of residual BAT tumour	3-141
3.5 Discussion	3-142
3.5.1 Patient demographic vs cytotoxicity drug response	3-142
3.5.2 Tumour protein expression vs tumour growth and drug response.....	3-143
3.5.3 MTT data analysis and visualisation.....	3-144
3.5.4 IncuCyte data analysis and visualisation	3-147
3.5.5 Resistance against multidrug treatment.....	3-148
3.6 Conclusion	3-149
Acknowledgment	3-150
4. CHAPTER FOUR: HPLC METHOD DEVELOPMENT AND VALIDATION	4-151
4.1 Abstract	4-151
4.2 Introduction.....	4-151
4.3 Materials and methods	4-153
4.3.1 Materials and reagents.....	4-153
4.3.2 Placebo extraction procedure.....	4-154
4.3.3 Instrument and chromatographic condition	4-154
4.3.4 Methods development	4-155
4.3.5 Preparation of solutions	4-155
4.3.6 Methods validation	4-156
4.4 Results and discussion.....	4-157
4.4.1 Scope and applicability	4-157
4.4.2 Method development and optimization	4-158
4.4.3 Specificity	4-162
4.4.4 Linearity	4-162
4.4.5 Range	4-164
4.4.6 Accuracy	4-165
4.4.7 Precision- Repeatability.....	4-167
4.4.8 Precision- Intermediate precision	4-169
4.4.9 Limit of detection and quantitation	4-172
4.4.10 System suitability	4-173
4.5 Conclusion	4-174
5. CHAPTER FIVE: FORMULATION AND DEVELOPMENT OF A MULT- DRUG IMPLANTABLE DRUG DELIVERY DEVICE	5-176
5.1 Abstract	5-176
5.2 Introduction.....	5-177
5.2.1 Selection of excipients	5-178

5.2.2 Thermal stability and interaction.....	5-180
5.2.3 Drug release characteristics.....	5-181
5.3 Materials and methods.....	5-183
5.3.1 Materials and Reagents.....	5-183
5.3.2 Rheology	5-183
5.3.3 Thermal stability	5-183
5.3.4 HPLC.....	5-184
5.3.5 Swelling study.....	5-184
5.3.6 Micro extrusion	5-185
5.3.7 Implant drug content	5-186
5.3.8 Dissolution test, <i>in-vitro</i> drug release	5-186
5.4 Results and discussion	5-186
5.4.1 Rheological assessment of polymer and plasticisers.....	5-186
5.4.2 Influence of plasticiser type and loading on the swelling of the implants.....	5-191
5.4.3 Thermal stability during manufacture.....	5-193
5.4.4 Micro-extrusion and characterisation of implants	5-197
5.6 Conclusion	5-201
6. CHAPTER SIX: CONCLUSION	6-203
REFERENCES.....	6-206
Appendix A	6-231
Appendix B	6-232

LIST OF FIGURES

Figure 1.1: Central Brain Tumor Registry of the United States (CBTRUS) diagnosis database from 2007-2011. (a) Incidence rate by age group (b) One, Two, Three, Five and Ten-Year relative survival rates by age group [8].....	1-2
Figure 1.2: Schematic representation of the BBB.	1-9
Figure 1.3: Schematic representation of drug transport mechanisms across the BBB. 1) Passive diffusion across endothelial cell, 2) Passive diffusion via tight junctions, 3) Endocytosis 4) Carrier-mediated transport 5) Carrier-mediated efflux	1-10
Figure 1.4: Cancer cell population consisting of non-differentiated tumorigenic stem cells and fast growing differentiated cancer cells.....	1-17
Figure 1.5: Metabolism of IRN into its active SN-38 metabolite	1-21
Figure 1.6: bis(N,N-diethyl dithiocarbamate)copper(II) complex	1-24
Figure 2.1: 96 well plate cytotoxicity assay layout.	2-38
Figure 2.2: Summary of patient cohort and grade of GBM tumours.....	2-40
Figure 2.3: Cellular growth measurement of three glioma primary cells under either F-12 serum or F-12 serum-free culture medium.....	2-43
Figure 2.4: Summary of cell survival assay for MTT method validation. Glioma cells were seeded in a 96-well plate at 2000, 4,000, 10,000 and 20,000 cells/well density. Cellular confluence and medium colour change are observed over a 16-day incubation period.....	2-45
Figure 2.5: Patient 1 TC sample MTT cell viability graphs prior to and following method development. In pre-method development all wells within a 96 well-plate were used for the assay. In post-method development only non-perimeter wells were used, perimeter wells were filled with 250 μ L SDW. \pm SEM is indicated as error bars.....	2-46
Figure 2.6: LogIC ₅₀ cytotoxicity curves and data table of TMZ chemotherapy tested against primary cells. Eight number assigned grade IV TC samples were evaluated using MTT assay. \pm SEM is indicated as error bars.....	2-48
Figure 2.7: LogIC ₅₀ cytotoxicity curves and data table of IRN drug tested against primary cells. Eight number assigned grade IV TC samples were evaluated using MTT assay. \pm SEM is indicated as error bars.	2-49
Figure 2.8: LogIC ₅₀ cytotoxicity curves and data table of PTV drug tested against primary cells. Seven number assigned grade IV TC samples were evaluated using MTT assay. \pm SEM is indicated as error bars.....	2-50
Figure 2.9: LogIC ₅₀ cytotoxicity curves and data table of DSF drug tested against primary cells. Seven number assigned grade IV TC samples were evaluated using MTT assay. \pm SEM is indicated as error bars.....	2-51
Figure 2.10: LogIC ₅₀ cytotoxicity curves and data table of CoGlu drug tested against primary cells. Seven number assigned grade IV TC samples were evaluated using MTT assay. \pm SEM is indicated as error bars.....	2-52
Figure 2.11: LogIC ₅₀ cytotoxicity curves and data table of CAP drug tested against primary cells. Seven number assigned grade IV TC samples were evaluated using MTT assay. \pm SEM is indicated as error bars.....	2-53
Figure 2.12: LogIC ₅₀ cytotoxicity curves and data table of CXB drug tested against primary cells. Seven number assigned grade IV TC samples were evaluated using MTT assay. \pm SEM is indicated as error bars.....	2-54

Figure 2.13: LogIC ₅₀ cytotoxicity curves and data table of TCL drug tested against primary cells. Seven number assigned grade IV TC samples were evaluated using MTT assay. ± SEM is indicated as error bars.....	2-55
Figure 2.14: LogIC ₅₀ cytotoxicity curves and data table of ITZ drug tested against primary cells. Seven number assigned grade IV TC samples were evaluated using MTT assay. ± SEM is indicated as error bars.....	2-56
Figure 2.15: LogIC ₅₀ cytotoxicity curves and data table of TMZ chemotherapy tested against primary cells. Two number assigned grade III TC samples were evaluated using MTT assay. ± SEM is indicated as error bars.	2-57
Figure 2.16: LogIC ₅₀ cytotoxicity curves and data table of IRN drug tested against primary cells. Two number assigned grade III TC samples were evaluated using MTT assay. ± SEM is indicated as error bars.	2-58
Figure 2.17: LogIC ₅₀ cytotoxicity curves and data table of PTV drug tested against primary cells. Two number assigned grade III TC samples were evaluated using MTT assay. ± SEM is indicated as error bars.	2-59
Figure 2.18: LogIC ₅₀ cytotoxicity curves and data table of DSF drug tested against primary cells. Two number assigned grade III TC samples were evaluated using MTT assay. ± SEM is indicated as error bars.	2-60
Figure 2.19: LogIC ₅₀ cytotoxicity curves and data table of CoGlu drug tested against primary cells. Two number assigned grade III TC samples were evaluated using MTT assay; Patient 6 and 12. ± SD is indicated as error bars.....	2-60
Figure 2.20: LogIC ₅₀ cytotoxicity curves and data table of CAP drug tested against primary cells. Two number assigned grade III TC samples were evaluated using MTT assay. ± SEM is indicated as error bars.	2-61
Figure 2.21: LogIC ₅₀ cytotoxicity curves and data table of CXB drug tested against primary cells. Two number assigned grade III TC samples were evaluated using MTT assay. ± SEM is indicated as error bars.	2-61
Figure 2.22: LogIC ₅₀ cytotoxicity curves and data table of TCL drug tested against primary cells. Two number assigned grade III TC samples were evaluated using MTT assay. ± SEM is indicated as error bars.	2-62
Figure 2.23: LogIC ₅₀ cytotoxicity curves and data table of ITZ drug tested against primary cells. Two number assigned grade III TC samples were evaluated using MTT assay. ± SEM is indicated as error bars.	2-62
Figure 2.24: LogIC ₅₀ cytotoxicity curves and data table of TMZ chemotherapy tested against primary cells. Four number assigned grade IV BAT samples were evaluated using MTT assay. ± SEM is indicated as error bars.....	2-63
Figure 2.25: LogIC ₅₀ cytotoxicity curves and data table of IRN drug tested against primary cells. Four number assigned grade IV BAT samples were evaluated using MTT assay. ± SEM is indicated as error bars.....	2-64
Figure 2.26: LogIC ₅₀ cytotoxicity curves and data table of PTV drug tested against primary cells. Four number assigned grade IV BAT samples were evaluated using MTT assay. ± SEM is indicated as error bars.....	2-65
Figure 2.27: LogIC ₅₀ cytotoxicity curves and data table of DSF drug tested against primary cells. Four number assigned grade IV BAT samples were evaluated using MTT assay. ± SEM is indicated as error bars.....	2-66
Figure 2.28: LogIC ₅₀ cytotoxicity curves and data table of CoGlu drug tested against primary cells. Four number assigned grade IV BAT samples were evaluated using MTT assay. ± SEM is indicated as error bars.....	2-67

Figure 2.29: LogIC ₅₀ cytotoxicity curves and data table of CAP drug tested against primary cells. Four number assigned grade IV BAT samples were evaluated using MTT assay. ± SEM is indicated as error bars.	2-68
Figure 2.30: LogIC ₅₀ cytotoxicity curves and data table of CXB drug tested against primary cells. Four number assigned grade IV BAT samples were evaluated using MTT assay. ± SEM is indicated as error bars.	2-68
Figure 2.31: LogIC ₅₀ cytotoxicity curves and data table of TCL drug tested against primary cells. Four number assigned grade IV BAT samples were evaluated using MTT assay. ± SEM is indicated as error bars.	2-69
Figure 2.32: LogIC ₅₀ cytotoxicity curves and data table of ITZ drug tested against primary cells. Four number assigned grade IV BAT samples were evaluated using MTT assay. ± SEM is indicated as error bars.	2-70
Figure 2.33: LogIC ₅₀ cytotoxicity curves and data table of mono-therapeutic drug treatments tested against patient 4 TC cells using IncuCyte assay. ± SEM is indicated as error bars.	2-72
Figure 2.34: IncuCyte cell confluence and representative images data of patient 4 derived TC cells treated with TMZ. Drug concentration from left to right: control, 0.1 µM low, 1 µM medium and 100 µM high.	2-73
Figure 2.35: IncuCyte cell confluence and representative images data of patient 4 derived TC cells treated with IRN. Drug concentration from left to right: control, 0.1 µM low, 1 µM medium and 100 µM high.	2-74
Figure 2.36: IncuCyte cell confluence and representative images data of patient 4 derived TC cells treated with PTV. Drug concentration from left to right: control, 0.1 µM low, 1 µM medium and 100 µM high.	2-76
Figure 2.37: IncuCyte cell confluence and representative images data of patient 4 derived TC cells treated with DSF. Drug concentration from left to right: control, 0.1 µM low, 1 µM medium and 100 µM high.	2-77
Figure 2.38: IncuCyte cell confluence and representative images data of patient 4 derived TC cells treated with CoGlu. Drug concentration from left to right: control, 0.1 µM low, 1 µM medium and 100 µM high.	2-78
Figure 2.39: IncuCyte cell confluence and representative images data of patient 4 derived TC cells treated with CAP. Drug concentration from left to right: control, 0.1 µM low, 1 µM medium and 100 µM high.	2-79
Figure 2.40: IncuCyte cell confluence and representative images data of patient 4 derived TC cells treated with CXB. Drug concentration from left to right: control, 0.1 µM low, 1 µM medium and 100 µM high.	2-80
Figure 2.41: IncuCyte cell confluence and representative images data of patient 4 derived TC cells treated with TCL. Drug concentration from left to right: control, 0.1 µM low, 1 µM medium and 100 µM high.	2-81
Figure 2.42: IncuCyte cell confluence and representative images data of patient 4 derived TC cells treated with ITZ. Drug concentration from left to right: control, 0.1 µM low, 1 µM medium and 100 µM high.	2-82
Figure 2.43: LogIC ₅₀ cytotoxicity curves and data table of mono-therapeutic drug treatments tested against patient 4 BAT cells using IncuCyte assay. ± SEM is indicated as error bars.	2-84
Figure 2.44: IncuCyte cell confluence and representative images data of patient 4 derived BAT cells treated with TMZ. Drug concentration from left to right: control, 0.1 µM low, 1 µM medium and 100 µM high.	2-85
Figure 2.45: IncuCyte cell confluence and representative images data of patient 4 derived BAT cells treated with IRN. Drug concentration from left to right: control, 0.1 µM low, 1 µM medium and 100 µM high.	2-86

Figure 2.46: IncuCyte cell confluence and representative images data of patient 4 derived BAT cells treated with PTV. Drug concentration from left to right: control, 0.1 μ M low, 1 μ M medium and 100 μ M high.	2-87
Figure 2.47: IncuCyte cell confluence and representative images data of patient 4 derived BAT cells treated with DSF. Drug concentration from left to right: control, 0.1 μ M low, 1 μ M medium and 100 μ M high.	2-88
Figure 2.48: IncuCyte cell confluence and representative images data of patient 4 derived BAT cells treated with CoGlu. Drug concentration from left to right: control, 0.1 μ M low, 1 μ M medium and 100 μ M high.	2-89
Figure 2.49: IncuCyte cell confluence and representative images data of patient 4 derived BAT cells treated with CAP. Drug concentration from left to right: control, 0.1 μ M low, 1 μ M medium and 100 μ M high.	2-90
Figure 2.50: IncuCyte cell confluence and representative images data of patient 4 derived BAT cells treated with CXB. Drug concentration from left to right: control, 0.1 μ M low, 1 μ M medium and 100 μ M high.	2-91
Figure 2.51: IncuCyte cell confluence and representative images data of patient 4 derived BAT cells treated with TCL. Drug concentration from left to right: control, 0.1 μ M low, 1 μ M medium and 100 μ M high.	2-92
Figure 2.52: IncuCyte cell confluence and representative images data of patient 4 derived BAT cells treated with ITZ. Drug concentration from left to right: control, 0.1 μ M low, 1 μ M medium and 100 μ M high.	2-93
Figure 2.53: MTT LogIC ₅₀ cytotoxicity data of, grade IV patients 2-4, 7-11 and grade III patients 6 and 12, TC sample population. For ineffective drug treatments predicted Graphpad Prism LogIC ₅₀ values were used.	2-95
Figure 2.54 Average LogIC ₅₀ data for 10 TC and 4 BAT samples tested against mono-therapeutic drug treatments. To plot data for ineffective drug treatments predicted Graphpad Prism LogIC ₅₀ values were used. \pm SD is indicated as error bars. Significance between groups is denoted by * $P < 0.05$, ** $P < 0.01$, *** $P < 0.001$, if no line is drawn $P > 0.05$	2-99
Figure 2.55: MTT vs IncuCyte LogIC ₅₀ cell viability data for patient 4 tumour fragments a) Tumour Core b) Brain around tumour.....	2-100
Figure 3.1: Protocol for making 3 and 4 drug combination assay solutions.	3-107
Figure 3.2: LogIC ₅₀ cytotoxicity curves and data table of IRN-PTV-DSF-CoGlu drug combination tested against primary cells. Seven number assigned grade IV TC samples were evaluated using MTT assay. \pm SEM is indicated as error bars.....	3-112
Figure 3.3: LogIC ₅₀ cytotoxicity curves and data table of IRN-CAP-CXB-ITZ drug combination tested against primary cells. Seven number assigned grade IV TC samples were evaluated using MTT assay. \pm SEM is indicated as error bars.	3-113
Figure 3.4: LogIC ₅₀ cytotoxicity curves and data table of IRN-CAP-DSF drug combination tested against primary cells. Seven number assigned grade IV TC samples were evaluated using MTT assay. \pm SEM is indicated as error bars.	3-114
Figure 3.5: LogIC ₅₀ cytotoxicity curves and data table of IRN-PTV-CAP-TCL drug combination tested against primary cells. Seven number assigned grade IV TC samples were evaluated using MTT assay. \pm SEM is indicated as error bars.....	3-115
Figure 3.6: LogIC ₅₀ cytotoxicity curves and data table of IRN-PTV-DSF-CoGlu drug combination tested against primary cells. Two number assigned grade III TC samples were evaluated using MTT assay. \pm SEM is indicated as error bars.....	3-116
Figure 3.7: LogIC ₅₀ cytotoxicity curves and data table of IRN-CAP-CXB-ITZ drug combination tested against primary cells. Two number assigned grade III TC samples were evaluated using MTT assay. \pm SEM is indicated as error bars.....	3-117

Figure 3.8: LogIC ₅₀ cytotoxicity curves and data table of IRN-CAP-DSF drug combination tested against primary cells. Two number assigned grade III TC samples were evaluated using MTT assay. ± SEM is indicated as error bars.	3-118
Figure 3.9: LogIC ₅₀ cytotoxicity curves and data table of IRN-PTV-CAP-TCL drug combination tested against primary cells. Two number assigned grade III TC samples were evaluated using MTT assay. ± SEM is indicated as error bars.	3-119
Figure 3.10: LogIC ₅₀ cytotoxicity curves and data table of IRN-PTV-DSF-CoGlu drug combination tested against primary cells. Four number assigned grade IV BAT samples were evaluated using MTT assay. ± SEM is indicated as error bars.	3-120
Figure 3.11: LogIC ₅₀ cytotoxicity curves and data table of IRN-CAP-CXB-ITZ drug combination tested against primary cells. Four number assigned grade IV BAT samples were evaluated using MTT assay. ± SEM is indicated as error.	3-121
Figure 3.12: LogIC ₅₀ cytotoxicity curves and data table of IRN-CAP-DSF drug combination tested against primary cells. Four number assigned grade IV BAT samples were evaluated using MTT assay. ± SEM is indicated as error.	3-122
Figure 3.13: LogIC ₅₀ cytotoxicity curves and data table of IRN-PTV-CAP-TCL drug combination tested against primary cells. Four number assigned grade IV BAT samples were evaluated using MTT assay. ± SEM is indicated as error.	3-123
Figure 3.14: IncuCyte 3-day cytotoxicity assay, LogIC ₅₀ curves and data table of combination drug treatments tested against patient 4 TC cells. ± SEM is indicated as error.	3-125
Figure 3.15: IncuCyte cell confluence and representative images data of patient 4 derived TC cells treated with IRN-PTV-DSF-CoGlu drug combination. Drug concentration from left to right: control, 0.1 µM low, 1 µM medium and 100 µM high.	3-127
Figure 3.16: IncuCyte cell confluence and representative images data of patient 4 derived TC cells treated with IRN-CAP-CXB-ITZ drug combination. Drug concentration from left to right: control, 0.1 µM low, 1 µM medium and 100 µM high.	3-128
Figure 3.17: IncuCyte cell confluence and representative images data of patient 4 derived TC cells treated with IRN-DSF-CAP drug combination. Drug concentration from left to right: control, 0.1 µM low, 1 µM medium and 100 µM high.	3-129
Figure 3.18: IncuCyte cell confluence and representative images data of patient 4 derived TC cells treated with IRN-PTV-CAP-TCL drug combination. Drug concentration from left to right: control, 0.1 µM low, 1 µM medium and 100 µM high.	3-130
Figure 3.19: IncuCyte 3-day cytotoxicity assay, LogIC ₅₀ curves and data table of combination drug treatments tested against patient 4 BAT cells. ± SEM is indicated as error.	3-131
Figure 3.20: IncuCyte cell confluence and representative images data of patient 4 derived BAT cells treated with TMZ monotherapy. Drug concentration from left to right: control, 0.1 µM low, 1 µM medium and 100 µM high.	3-133
Figure 3.21: IncuCyte cell confluence and representative images data of patient 4 derived BAT cells treated with IRN-PTV-DSF-CoGlu drug combination. Drug concentration from left to right: control, 0.1 µM low, 1 µM medium and 100 µM high.	3-135
Figure 3.22: IncuCyte cell confluence and representative images data of patient 4 derived BAT cells treated with IRN-CAP-CXB-ITZ drug combination. Drug concentration from left to right: control, 0.1 µM low, 1 µM medium and 100 µM high.	3-137
Figure 3.23: IncuCyte cell confluence and representative images data of patient 4 derived BAT cells treated with IRN-CAP-DSF drug combination. Drug concentration from left to right: control, 0.1 µM low, 1 µM medium and 100 µM high.	3-138
Figure 3.24: IncuCyte cell confluence and representative images data of patient 4 derived BAT cells treated with IRN-PTV-CAP-TCL drug combination. Drug concentration from left to right: control, 0.1 µM low, 1 µM medium and 100 µM high.	3-140

Figure 3.25: Tumour relapse assessment of current standard treatment, TMZ and four combination drug treatment; i) IRN-PTV-DSF-CoGlu ii) IRN-CAP-CXB-ITZ iii) IRN-CAP-DSF iv) IRN-PTV-CAP-TCL tested against residual tumour BAT cells via two distinct cytotoxicity assay: a) MTT, average LogIC ₅₀ data of patient 2, 4, 5, 8 and 9 ± SEM is indicated as error bars b) IncuCyte, LogIC ₅₀ data of patient 4 only.	3-142
Figure 3.26: MTT LogIC ₅₀ cytotoxicity data of, grade IV patients 3, 4, 7-11 and grade III patients 6 and 12, TC sample population. For ineffective drug treatments predicted Graphpad Prism LogIC ₅₀ values were used.	3-144
Figure 3.27: Average LogIC ₅₀ data for 9 TC and 4 BAT samples tested against combination drug treatments. To plot data for ineffective drug treatments predicted Graphpad Prism LogIC ₅₀ values were used. ± SD is indicated as error bars	3-147
Figure 4.1: Disulfiram and copper gluconate reaction scheme to form a bis(N,N-diethyl dithiocarbamate)copper(II) complex.....	4-153
Figure 4.2: Structures of the four captopril stereoisomers (2R,2R, 2S,2R, 2S,2S, and 2R,2S).....	4-160
Figure 4.3: Chromatograms depicting the specificity of each drug combinations. The top chromatogram is of IRN-PTV-DSF-DDC_Cu combination measured at 245 and 270 nM wavelengths. Whereas the bottom chromatogram shows IRN-CAP-DSF combination measured at 245 nM wavelength.	4-162
Figure 5.1: Dimensions (diameter x height) of Gliadel® wafer implant compared to our 4-layer multi-drug delivery device.....	5-180
Figure 5.2: Drug release profile of reservoir and surface eroding biodegradable implants. With permission from [162]......	5-182
Figure 5.3: Temperature sweep data between 80 to 180 °C for PLGA 5002, 5004 and 5010. Optimum viscosity range for extrusion (10 ³ -10 ⁴ Pa.s) is represent by red lines.....	5-187
Figure 5.4: Temperature sweep data for the drug-polymer mixture at 30:70 % ratio. Drugs investigated were IRN, PTV, DSF, CAP and CoGlu, and polymers were PLGA 5002a and 5004. For the 5002 polymer the temperature sweep was performed at 80-170 °C, slightly higher temperature range, 90-180 °C, was selected for the 5004 polymer due its higher viscosity. Optimum viscosity range for extrusion (10 ³ -10 ⁴ Pa.s) is represent by red lines.	5-189
Figure 5.5: Temperature sweep data for the polymer-plasticiser mixture at different ratios. Plasticisers investigated were RH40, P188 and P237, and polymers were PLGA 5004 and 5010. For the 5004:plasticiser (90:10) and 5010:plasticiser (70:30) ratio the temperature sweep was performed at 90-180 °C, slightly higher initial temperature was selected for 5010:plasticiser (90:10) due to its higher viscosity. Optimum viscosity range for extrusion (10 ³ -10 ⁴ Pa.s) is represent by red lines....	5-190
Figure 5.6: Swelling profile of IRN-PTV-DSF-CoGlu and IRN-CAP-DSF drug combination implants made from 5004 polymer and either RH40, P188 or P237 plasticiser.	5-192
Figure 5.7: Thermal stability % recovery data for IRN, PTV, DSF and CAP. n=4, ± %RSD is indicated as error bars.	5-193
Figure 5.8: DSC diagram of (A) All excipients tested individually: PLGA 5002A, PLGA 5004 and P188 Plasticisers (B) Drug product tested three times; as pure compound (100% drug), drug in combination with p188 and PLGA 5004 (Drug:P188:PLGA 5004, 30:20:50%) and drug in combination with PLGA 5002 (Drug:5002A 30:70%).....	5-196
Figure 5.9: Simultaneous drug dissolution profiles of IRN, PTV, CAP and DSF within three (IRN-CAP-DSF) or four (IRN-PTV-DSF-CoGlu) layer combination drug implant. The dissolution profiles of two distinct formulations: 5004 and 5002 were tested under both sink and biorelevant conditions. ..	5-201

LIST OF TABLES

Table 1.1: Genomic GBM alterations and target molecular pathways [132, 138].	1-15
Table 1.2: List of promising drug treatments. Recorded with their Chemical structure, Physicochemical properties, Mechanism of action and clinical trial findings.	1-19
Table 1.3: Clinical trials involving disulfiram in GBM. Identifiers in reference to www.clinicaltrials.gov online database, table last updated 27 th -11-2018.	1-25
Table 1.4: ITZ mechanism of action against cancers.	1-29
Table 2.1: Summary of sample collection.	2-34
Table 2.2: TMZ, IRN, PTV, DSF, CoGlu, CAP, TCL, CXB & ITZ stock solutions	2-37
Table 2.3: The result of IDH1, ATRX, p53 and MGMT immunoexpression in tissue biopsy. N/A indicates that the data could not be determined	2-41
Table 2.4: Summary of whole exome sequencing of all non-somatic variants for patient's tissue biopsy and corresponding tissue cultured cells grown in serum-based medium.	2-44
Table 2.5: Colour coded MTT assay logIC ₅₀ data chart of patients 1-12 derived TC and BAT cells treated with TMZ, IRN, PTV, DSF, CoGlu, CAP, CXB, TCL and ITZ.	2-97
Table 2.6: IC ₅₀ and LogIC ₅₀ cytotoxicity data of ITZ, PTV, IRN, DSF, CAP, CoGlu+DSF and CXB, tested against glioma cell lines. [142, 173-175, 253, 262, 327, 328]	2-98
Table 3.1: Combination drug treatment LogIC ₅₀ values comparison between MTT and IncuCyte assays for the TC samples.	3-126
Table 3.2: Combination drug treatment LogIC ₅₀ values comparison between MTT and IncuCyte assays for the BAT samples.	3-132
Table 3.3: Colour coded MTT assay logIC ₅₀ data chart. Listing patients 3-4, 6-12 derived TC and BAT cells treated with IRN-PTV-DSF-CoGlu, IRN-CAP-CXB-ITZ, IRN-CAP-DSF, IRN-PTV-CAP-TCL.	3-146
Table 4.1: Results of regression analysis for the linearity data of IRN, PTV, DSF and DDC_Cu	4-163
Table 4.2: Results of regression analysis for the linearity data of IRN, CAP and DSF.	4-164
Table 4.3: Intra-day accuracy measurements of HPLC assay for IRN-PTV-DSF-DDC_Cu combination.	4-165
Table 4.4: Intra-day accuracy measurements of HPLC assay for IRN-CAP-DSF combination.	4-166
Table 4.5: Intra-day precision of HPLC assay for IRN-PTV-DSF-DDC_Cu combination.	4-167
Table 4.6: Intra-day precision of HPLC assay for IRN-CAP-DSF combination.	4-168
Table 4.7: Intermediate precision of HPLC assay for IRN-PTV-DSF-DDC_Cu combination. Instrument 1 was Dionex Ultimate 3000 LC system and instrument 2 was Agilent LC system.	4-170
Table 4.8: Intermediate precision of HPLC assay for IRN-CAP-DSF combination. Instrument 1 was Agilent LC system and instrument 2 was Dionex Ultimate 3000 LC system.	4-171
Table 4.9: LOD and LOQ data of HPLC assay for IRN-PTV-DSF-DDC_Cu combination.	4-172
Table 4.10: LOD and LOQ data of HPLC assay for IRN-CAP-DSF combination.	4-172
Table 4.11: system suitability data of HPLC assay for IRN-PTV-DSF-DDC_Cu combination.	4-173
Table 4.12: system suitability data of HPLC assay for IRN-CAP-DSF combination.	4-174
Table 5.1: Studies performed for drug delivery device development with target product profile.	5-178

Table 5.2: Components ratio and processing temperature for each drug formulation. Each drug was either formulated using PLGA 5004 or 5002.	5-185
Table 5.3: Mass distribution data for the individual drug 2x2mm implants.....	5-197
Table 5.4: Drug content, RSD and % RSD values for each drug within IRN-PTV-DSF-CoGlu, IRN-CAP-DSF and DSF only drug delivery devices.....	5-198

LIST OF ABBREVIATIONS

% RSD	Percentage Relative Standard Deviation
5-ALA	5-Aminolevulinic Acid
ACE	Angiotensin-Converting Enzyme
ADP	Adenosine Diphosphate
ALDH	Aldehyde Dehydrogenase
ALP	Raised Alkaline phosphatase
ALT	Raised Alanine Transaminase
ATRX	Alpha Thalassemia/Mental Retardation Syndrome X-linked
BAT	Brain Around Tumour
BBB	Blood Brain Barrier
bFGF	Fibroblast Growth Factor basic
CAP	Captopril
CED	Convection enhanced delivery
CNS	Central Nervous System
CoGlu	Copper Gluconate
COX-2	Cyclooxygenase-2
CSF	Cerebrospinal Fluid
CT	Computed Tomography
Cu	Copper
CXB	Celecoxib

DCM	Dichloromethane
DDC	Diethyldithiocarbamic Acid
DDC_Cu	bis(N,N-diethyl dithiocarbamate)copper(II) complex
DDS	Drug delivery system(s)
DDD	Drug delivery device
DMC	2,5-dimethyl-celecoxib
DMEM-F12	Dulbecco's Modified Eagle Medium
DMSO	Dimethyl Sulfoxide
DNA	Deoxyribonucleic Acid
DNA's	Deoxyribonuclease I
DSC	Differential Scanning Calorimetry
DSF	Disulfiram
EGF	Epidermal Growth Factor
EGFR	Epidermal Growth Factor Receptor
EIAEDs	Enzyme-Inducing Antiepileptic Drugs
FBS	Fetal Bovine Serum
FDA	Food and Drug Administration
FIGR	5-Aminolevulinic Acid -Induced Fluorescence to Guide Surgery
GBM	Glioblastoma
HBSS	Hank's Balanced Salt Solution
HGG	High Grade Glioma

HP	Human Plasma
IDH	Isocitrate Dehydrogenase
IRN	Irinotecan Hydrochloride
ITZ	Itraconazole
MGMT	O(6)-methylguanine-DNA methyltransferase
MRI	Magnetic Resonance Imaging
MTT	Thiazolyl Blue Tetrazolium Bromide
NaHCO ₃	Sodium Bicarbonate
NF1	Neurofibromin 1
NFkB	Nuclear Factor Kappa-Light-Chain-Enhancer of Activated B Cells
NSAI	Non-Steroidal Anti-Inflammator
OS	Overall Survival
OSR	Overall Survival Rate
PBS	Phosphate Buffer Saline
PDGFRA	Platelet-Derived Growth Factor Receptors
PLGA	Poly Lactic-co-Glycolic Acid
PLK1	Serine/Threonine-Protein Kinase
PTEN	Phosphatase and Tensin Homolog
PTV	Pitavastatin
RNA	Ribonucleic Acid
SD	Standard Deviation

SEM	Standard Error of Mean
SN-38	7-ethyl-10-hydroxycamptothecin
TC	Tumour Core
TCGA	The Cancer Genome Atlas Research Network
TCL	Ticlopidine
TMZ	Temozolomide
VEGF	Vascular Endothelial Growth Factor

1. CHAPTER ONE: BACKGROUND

1.1 Glioblastoma: description and incidence

Glioblastoma (GBM), also classified as grade IV astrocytoma, is the most common brain tumour in adults [1]. GBM has shown to arise from astrocytes, supportive brain tissue or progress from lower grade gliomas. It usually develops within the cerebral hemisphere of the brain with the frontal lobe being the most common site (about 25% of cases), however it can develop anywhere within the brain or spinal cord [1]. Despite advances in medical treatment survival rates remain low with most deaths occurring in the first 15 months after diagnosis [1, 2]. GBM is considered highly malignant as the cells divide quickly and are surrounded by a large network of blood vessels that provide a continuous supply of nutrients for fast growth [3].

Several classifications of GBM exists, depending on tumour origin and various genetic expressions. The 2016 World Health Organization (WHO) have classified GBM into: (i) primary or *de novo* GBM, which corresponds to approximately 90% of cases and occurs in predominantly older patients. (ii) Secondary GBM, corresponding to approximately 10% of cases, which occurs because of disease progression from lower grade astrocytoma and is predominant in younger patients [4-6].

The annual incident rate in England is 4-5 per 100,000 per year [1]. Known factors influencing diagnosis and survival length include age, ethnicity and gender. GBM can occur in both children and adults; however, incident number increases with age, while long-term survival decreases (Figure 1.1) [1, 7, 8].

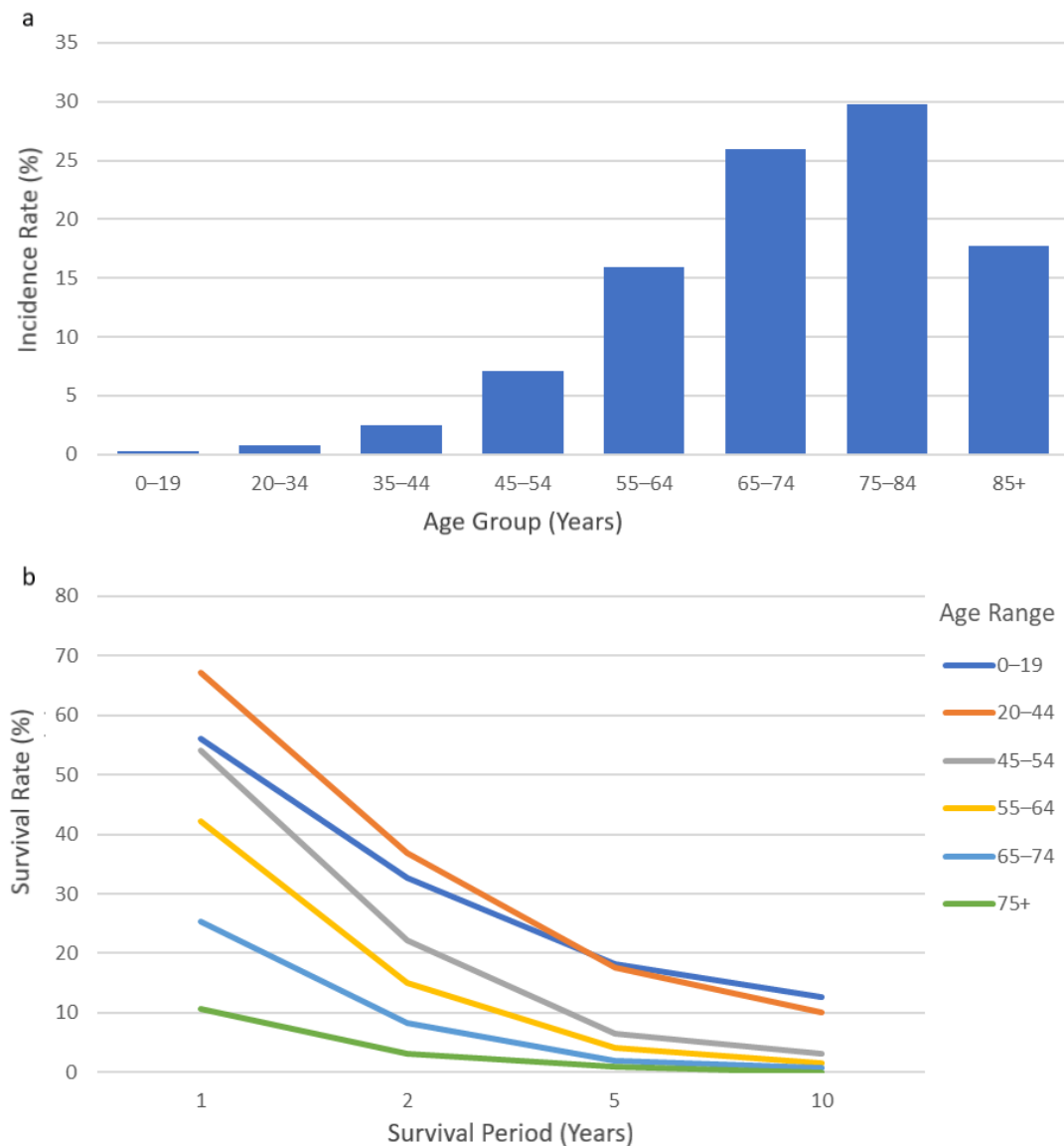


Figure 1.1: Central Brain Tumor Registry of the United States (CBTRUS) diagnosis database from 2007-2011. **(a)** Incidence rate by age group **(b)** One, Two, Three, Five and Ten-Year relative survival rates by age group [8].

White non-Hispanic people have a two-fold higher incidence rate than Hispanic and Black people [8]. GBM is also 1.6 times more common in men than women [1, 8]. One study carried out by Tao Sun demonstrated that the retinoblastoma protein, a protein known to reduce cancer risk, is significantly less active in men's brain and could explain why men are more at risk [9].

Other minor evidence of factors linked to risk of developing GBM include, exposure to ionising radiation, and several heritable genetic factors [10-13]. However, these do not account for a significant increase in diagnosis [12].

Symptoms can vary largely dependent on the location of growth. Some of the more common symptoms such as headache, nausea, vomiting, and drowsiness are caused by the increase in intracranial pressure of the brain [13].

For diagnosis, computed tomography (CT) and magnetic resonance imaging (MRI) scans are combined with tissue biopsy [14]. Imaging techniques are utilised to detect and locate the tumour. Imaging characteristics of high infiltration, necrosis and irregular rim of enhancement are typical but not specific for GBM [15]. Hence tissue biopsy is required to confirm the grade of the tumour, any specific genetic mutations and sub classification (i.e. primary or secondary) [6, 16].

1.2 Current therapy for Glioblastoma

The current standard of treatment is the STUPP protocol, which involves maximal safe resection surgery of the tumour followed by radiation therapy and chemotherapy with the oral alkylating agent Temozolomide (TMZ) [17]. Approximately 34% of UK patients undergo the STUPP protocol [1] enhancing patient survival by ~ 11 months compared to no treatment [17, 18]. The STUPP's NICE 2001 UK NHS cost estimate was £11,900 per patient, this is likely to have increased since 2001 but no recent cost estimation were found [19]. Due to the high cost, a careful evaluation of treatment outcome for each patient is made and thus for some patients this treatment may be deemed cost ineffective [20].

Other FDA approved drugs such as Carmustine, Bevacizumab and Lomustine could also be prescribed for the treatment of GBM, however these can only stabilise and/or extend survival for a short period of time, usually no more than 2-6 months [21-27]. For an individual patient selection of drug treatment can be dependent on a number of factors including genetic mutation of tumour, resectability of tumour and feasibility of treatment for the individual, where cost, drug safety and effectiveness are weighed [20].

1.2.1 Current systemically administered chemotherapeutic treatments

Current chemotherapeutic treatments for GBM mainly rely on the oral and intravenous delivery route. Although these certainly offer flexibility in administration, drug delivery to

the brain is often hindered by the Blood Brain Barrier (BBB) (Chapter one, 1.3 Rationale for localised therapy, 1.3.1 Blood Brain Barrier (BBB)) These therapeutic agents have shown some clinical viability but increased systemic toxicities are observed because of the high drug distribution rate within the systemic circulation [28].

Temozolomide

TMZ (Trade name: Temodar®) is utilized within the STUPP protocol and is administered at a dose of 150–200 mg/m² either orally as tablets or injection via intravenous infusion [29-31]. In combination with radiotherapy it has shown to prolong the overall survival rate (OSR) for patients, from 12.1 months for radiotherapy alone to 14.6 months when combined with TMZ treatment [17]. It's mechanism of action is dependent on its ability to alkylate Deoxyribonucleic acid (DNA) by supplying a methyl group to purine bases damaging it and triggering cell death. An estimated 40% of patients are resistant to TMZ because of MGMT gene activation through a mutation enabling it to repair the DNA damage induced by TMZ [25]. The two-year survival rate for TMZ treated patients with either the expressed or silenced MGMT DNA repair gene is 14 % and 46 %, respectively [25]. Patients undergoing TMZ treatment are carefully evaluated prior to and during treatment. With patients more likely to experience myelosuppression, including prolonged pancytopenia and eventually death [32, 33]. Neutrophil, platelet and complete blood counts are regularly checked via weekly assessments [22].

Because of its small size, neutral charge and lipophilic nature, it possesses good bioavailability. A clinical study reported by Portnow, using a microdialysis catheter placed in peritumoral brain tissue, recorded that following oral administration of single dose TMZ, an average of 17.8% reached the brain interstitium compared to drug concentration in plasma. Maximum TMZ plasma concentration was reached within 1.8 ± 1.2 hours, and 2.0 ± 0.8 hours in the brain interstitium [34].

TMZ toxicity is mainly systemic, with some of the most common side effects being thrombocytopenia, lymphocytopenia, neutropenia, leukopenia, anaemia, nausea, vomiting,

anorexia, constipation, infection, raised alanine transaminase (ALT), raised alkaline phosphatase (ALP) and mucositis [32, 33].

Bevacizumab

Vascular Endothelial Growth Factor (VEGF) secretion is used by GBM to promote the formation of blood vessels and aid growth [3, 35-38]. Bevacizumab (Trade name: Avastin®) is a humanized monoclonal antibody that is administered by intravenous infusion to inhibit VEGF [39, 40]. Bevacizumab is utilised as a single agent therapy in patients with progressive disease. It is often provided for patients as a mean for best supportive care treatment following previous treatment failure [41-43]. There is no evidence for bevacizumab demonstrating improvement in disease-related symptoms or survival length for patients [23, 44, 45]. Its effectiveness is established on patients' objective response rate based on WHO radiographic criteria and steady or decreasing corticosteroids use [23, 44, 46].

It was granted accelerated FDA approval in 2009, following two clinical trials, evaluating bevacizumab in patients with documented disease progression who had undergone prior TMZ and radiation treatments [44, 47]. The first trial was a multicentre randomised assessment of 85 patients receiving bevacizumab 10 mg/kg dose every 2 weeks alone or in combination with Irinotecan, until disease progression or unacceptable toxicity [23, 44]. The objective response rate was found in 25.9% of patients. The second trial was a single arm, single institution trial of 56 patients, receiving 10 mg/kg dose every 2 weeks. The objective response rate was found in 19.6% of patients [44]. With no other alternative of therapy for patients with progressive disease, bevacizumab was deemed to be effective and approval was granted based on the risk to benefit ratio for patients [44]. However, the studies showed that more than 10% of bevacizumab treated patients, which was twice as many when compared to the control arm, were more likely to experience epistaxis, rhinitis, proteinuria, taste alteration, headache, hypertension, dry skin, rectal hemorrhage, lacrimation disorder and exfoliative dermatitis [44]. Hence, during bevacizumab treatment, careful monitoring of the patient's response to therapy is vital.

Lomustine

Lomustine (Trade name: Gleostine®) was FDA approved in 1977 [48-50]. It is a chloroethylating nitrosoureas drug that alkylates DNA and Ribonucleic acid (RNA) and can also inhibit several enzymatic processes within the cancer cells. It has proven to prolong OSR by 8 months and just like TMZ, its mechanism of action is dependent on MGMT gene methylation and thus its ability to alkylate DNA [51-53].

Lomustine is administered as a single oral dose. Due to extremely high toxicity, including fatal outcome, only one dose is prescribed for patients to administer every 6 weeks [26]. Since the introduction of the STUPP's protocol's lomustine is rarely prescribed for GBM as it has the potential to cause irreversible systemic side effects including kidney damage, renal failure, thrombocytopenia and leukopenia [21, 26]. Patients undergoing lomustine treatment are required to undertake frequent assessment for blood count, liver function, renal function and electrolyte level [26].

Lomustine is predicted to have good bioavailability due to its small size, neutral charge and lipophilic nature [54, 55]. However, no data was found to quantify drug passage into the Central Nervous System (CNS).

Carmustine

Carmustine for intravenous infusion was approved in 1977. Equivalent to lomustine, it is a chloroethylating nitrosoureas drug that alkylates DNA and RNA and can also inhibit several enzymatic processes within the cancer cells. Similar to TMZ and lomustine, carmustine's activity is correlated with MGMT gene methylation [56-61]. Carmustine is known to cause extravasation, so to minimise this it is administered via a slow intravenous infusion every 6 weeks either as a single dose or divided into two doses over 2 consecutive days [27].

With physicochemical properties of low molecular weight, lipophilicity and neutral charge, carmustine is known to readily pass the BBB. However, due to its excessive metabolism in the liver it possess a relatively short half-life of 15-70 minutes, hence a high systemic dose is required for a therapeutic concentration to reach the brain [55, 62].

Carmustine treated patients are more likely to experience myelosuppression, pulmonary toxicity, administration reactions, carcinogenicity and ocular toxicity [24, 27, 55]. Patients undergoing systemically administered carmustine treatment are required to undertake frequent assessment of their blood count and renal function with the dosage adjusted based on these results [27]. This treatment is not associated with a significant prolongation in the OSR of patients so this treatment became rarely prescribed following the FDA approval of TMZ and Gliadel® therapies [63].

1.2.2 Current locally administered chemotherapy treatment

Carmustine wafer (Gliadel®)

Gliadel® is an implantable chemotherapeutic wafer, it was initially developed to enhance the therapeutic efficacy of carmustine by delivering the drug locally. Large drug distribution and fast elimination rate by the liver were avoided, subsequently prolonging carmustine stability and minimising the dosage requirement [64, 65]. Gliadel® consist of carmustine incorporated homogenously within 1,3-bis(p-carboxyphenoxy) propane:sebacic acid (20:80 ratio) polymer [63]. During brain resection surgery up to 8 wafers are placed on the tumour bed. Each providing 7.7 mg of controlled and sustained carmustine release [65]. Carmustine implants have been utilized significantly and are often considered as the second line treatment therapy for GBM. This therapy has revealed significant reduction in haematological toxicity with maximum effectiveness at the site of action. In two clinical trials involving 32 and 240 patients, Gliadel® improved the OSR of newly diagnosed GBM patients by 2.9 and 2.3 months respectively when compared to placebo implanted wafers [66-69].

In-vivo, the wafers are known to release carmustine over a period of 5 days, the remaining polymer then degrades over a period of 6-8 weeks [65]. The sebacic acid monomers are excreted from the body as expired CO₂, whereas the 1,3-bis-(p-carboxyphenoxy)propane monomers and carmustine drug degradation products are excreted through the urine [65].

One drawback for Gliadel® treatment is that it is not suitable for all patients. Wafers can only be implanted if the size, shape and location of the resection cavity allows it. As each wafer is 1.45 cm in diameter and 1 mm thick, a large resection cavity is needed to host 8 wafers [70].

Also depending on the location of GBM growth, tumour resection might not be viable, hence wafer implantation cannot occur. Another drawback is that for recurrent tumour Gliadel® is ineffective. A Cochrane report evaluated the clinical effectiveness of Gliadel® implants and concluded that for newly diagnosed patients, Gliadel® was clinically effective in improving survival without an increase in toxic side effects, however for recurrent patients, Gliadel® showed no clinical improvement [71].

When compared to systemically administered carmustine, the locally delivered drug does suffer from increased local toxicity such as seizures, intracranial hypertension, meningitis, cerebral oedema and impaired neurosurgical wound healing [66, 67]. Despite the toxicity issues associated with Gliadel®, the implants offer the best option for overcoming the BBB. Gliadel® has demonstrated therapeutic drug concentrations at the site of the tumour [67]. With many drugs possessing excellent anticancer properties but are limited by their ability to cross the BBB this local delivery approach could potentially enable some of these substances to be utilised in GBM treatment (Chapter one, 1.3 Rationale for localised therapy, Table 1.2). Overall Gliadel® serves as a rationale that intracavity drug delivery is both feasible and successful in improving drug efficacy when compared to the systemically delivered drug, it represents one of the few current therapies clinically approved for the treatment of GBM when many other treatments have failed in the clinic.

1.3 Rationale for localised therapy

This form of treatment is particularly viable for GBM as tumour reoccurrence following debulking surgery is usually localised, within 2 to 3 cm of the primary lesion border. Therefore, a local delivery approach could be used to concentrate chemotherapeutic drugs in this precise location [72]. Reduced toxicity is also possible due to the lower dosage requirement and avoidance of systemic circulation [63]. Of course, local toxicity may become more prevalent. However, this can be minimised with intelligent dosage form design and non-toxic drug selection.

Localised treatment could also be developed to target the four main disease specific obstacles that are currently responsible for treatment failures including the BBB, tumour location, tumour heterogeneity and disease re-occurrence.

1.3.1 Blood Brain Barrier (BBB)

Between the systemic circulation and CNS, there exist three unique physiological barriers: the arachnoid–subarachnoid cerebrospinal fluid (CSF), the choroid plexus–ventricular CSF and Blood Brain Barrier (BBB) [73]. Of these, the BBB is the most important in controlling passage of solutes between blood and CNS.

The BBB consist of a monolayer of endothelial cells in brain capillaries. In between endothelial cells, a seal consisting of claudins and other proteins is formed, known as tight junctions. The endothelial cells are also surrounded by a basal membrane, which comprise of collagen, fibronectin, laminin, tenascin and proteoglycans [74] (Figure 1.2). The complete surface area of the BBB is approximately 20 m² and total capillaries length is 600,000 m [74, 75].

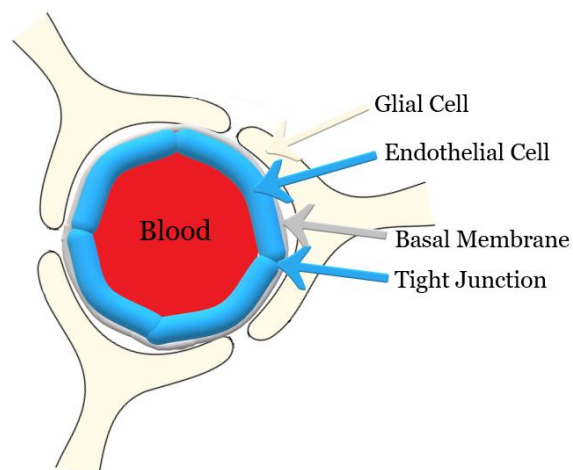


Figure 1.2: Schematic representation of the BBB.

Drug molecules may transport across the BBB via a number of mechanisms 1) passive diffusion across endothelial cell, 2) passive diffusion via tight junctions, 3) endocytosis 4) carrier-mediated transport 5) carrier-mediated efflux (Figure 1.3).

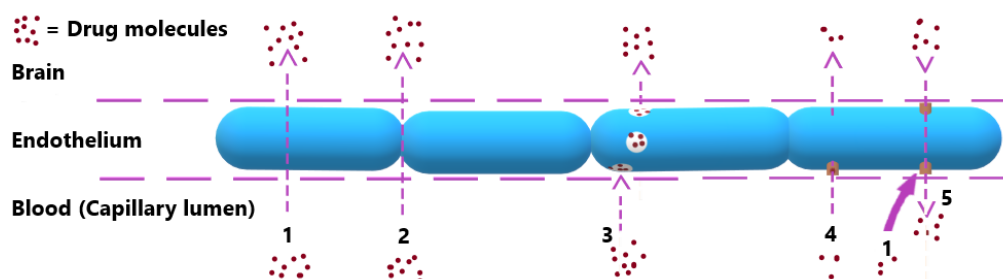


Figure 1.3: Schematic representation of drug transport mechanisms across the BBB. 1) Passive diffusion across endothelial cell, 2) Passive diffusion via tight junctions, 3) Endocytosis 4) Carrier-mediated transport 5) Carrier-mediated efflux

Large molecules, >500 Daltons are transported across the BBB via carrier-mediated vehicles. Whereas small molecules rely on passive transport, with the transport rate dependent on molecular weight, electrical charge and lipophilicity [76].

The BBB is a great obstacle for many pharmaceutical agents to cross with most drug trials focusing on delivering the drug orally or intravenously, most are bound to fail not due to their inability to target and kill cancer cells but their ability to reach the site of the tumour at therapeutic concentrations [67]. Even with drug molecules that have optimum physiochemical properties to cross the BBB (i.e small size, neutral charge and lipophilicity) bioavailability can still be unpredictable. Brain tumours, such as GBM alter the BBB permeability through elevated cellular secretion of humoral factors such as bradykinin, histamine, serotonin and platelet-activating factor leading to increased cerebral pressure, upregulation of carrier mediated efflux and vascular permeability [73, 77]. Additionally, rapid cellular growth induced changes are associated with enhanced production of vascular endothelial growth, often referred to as the blood–tumour barrier [78]. These changes may enhance BBB permeability but can also reduce the residence time of drugs in the brain, where chemotherapy agents that successfully cross the BBB are quickly efflux transported back into the capillary lumen [73]. The increase vasculature system in GBM patients have previously been argued as a theory that drug permeability to the brain is much higher in

patients with brain tumour, however the overwhelming clinical evidence demonstrates that drugs with poor BBB permeability still cannot penetrate the barrier [79].

Since many anticancer agents do not have the appropriate physicochemical properties to cross the BBB, a variety of drug delivery options have been explored such as the use of small lipophilic drugs that could easily pass the BBB, the incorporation of drugs into nanocarriers and the use of implantable drug delivery devices or injectable systems such as convection enhanced delivery (CED) [80-83]. There has also been research done on modifying the BBB permeability through the use of focused ultrasound [84].

Many successful preclinical studies for the use of nanocarriers in GBM treatments have been developed with the aim of enhancing the bioavailability of systemically administered chemotherapeutic agents [85-92]. By specifically designing the nanocarriers to be small sized, lipophilic and neutrally charged, optimum BBB permeability can be obtained. Additionally, the encapsulated drug could in principle hold an extended systemic circulation period by being protected from degradation in physiological environment [93-95]. Saucier-sawyer et al developed a camptothecin loaded polymeric nanoparticle system, consisting of a copolymer of polylactic acid and hyperbranched polyglycerol, surface modified with adenosine. The drug brain uptake increased by 0.8% of injected dose (200 mg/kg) compared with free drug in mice [96]. Another study by Wilson et al investigated the possibility of targeting Alzheimer using tacrine loaded poly(n-butylcyanoacrylate) nanoparticles, in rats the formulation significantly increased the uptake of tacrine into the brain with the drug concentration reaching 251.49 ± 17.25 ng/mL compared to 61.79 ± 4.98 ng/mL with free drug alone [97].

Injectable systems such as CED involves the implantation of catheters into the brain. The drug can be infused through a pressure gradient for sustained targeted delivery of the chemotherapeutic agent [82]. This method of delivery is currently utilised for the treatments of Diffuse Intrinsic Pontine Glioma [98]. Its main advantage is the delivery of chemotherapeutic agents deep into parts of the brain that they cannot reach through

diffusion alone. A GBM clinical trial assessing citredekine besudotox, a chimeric pseudomonas exotoxin with recombinant human interleukin-13, infusion using CED have revealed no improvement in outcome when compared to current Gliadel® therapy [99]. However, although for this particular therapy, clinical success was not attained, it does provide a prospect for GBM patients with unresectable tumour [100]. An injectable system may offer a solution for localised delivery deep into parts of the brain not reachable by current therapy. Brachytherapy, another example of injectable therapy, may provide inspiration for reaching unresectable tumours; Brachytherapy is used for the treatment of cancer via insertion of radioactive seeds directly into the cancerous tissue [101]. It has been utilised for the treatment of brain, prostate, cervical, breast and liver cancer [101-106]. Typically after accurate positioning of the tumour, small seeds (3mm x 7 mm) are inserted into the tumour via a specialised delivery device (e.g. needle or catheter) [106]. In a GBM clinical trial patients were treated with 28 to 171 of radioactive seeds that were directly inserted into the tumour margin. The insertion procedure was shown to be safe, however adverse side effects were reported due to the radiation [106]. Thus, although this radiation therapy was proven to be unsuccessful the injection of therapy into the tumour boarder could be utilized for the administration of implantable drug delivery systems.

One of the most successful drug delivery strategies to circumvent the BBB has been the use of drug loaded polymer implants [64, 67]. Drug-loaded polymer implants have been utilized for the delivery of chemotherapeutics [107-110], proteins [111, 112], antibiotics [113, 114], anti-inflammatory drugs [115] etc. With clinical success reached when the Food and Drug Administration (FDA) approved the use of biodegradable drug-loaded wafer, Gliadel®. Drug loaded polymer implants have the advantage of obtaining site-specific, controlled release of therapeutic agents and enhanced efficacy owing to lower dose requirements. For GBM specifically, it has the additional advantage of providing a non-delayed immediate therapy following surgery, which is particularly important because with systemic drug delivery a lead time between surgery and drug treatment is required to aid healing. However, during this time residual tumour is left untreated and can grow rapidly.

1.3.2 Location of tumour growth

Even without the issues of the BBB, the location of the tumour presents some difficulty for treatment with systemically administered chemotherapy. Drug distribution across the body and in peripheral tissues, particularly for highly lipid soluble drugs, result in reduced bioavailability in the brain.

Glioma mainly arise within the anterior subcortical structures of the brain, with 40% of cases occurring in the frontal lobe, 29 % in temporal lobe, 14% in parietal lobe, 3% in occipital lobe, and 14% in the deeper structures [116]. The main prognosis factor for GBM is the extent of tumour resection. The mean OSR for patients who undergo resection surgery is 3.5 months greater than biopsy alone [117, 118]. The location of the tumour and level of infiltration into normal brain tissue plays a vital role in the extent of tumour resectability.

Advancements in surgery have helped to achieve maximal resection of the tumour. One of the greatest advances is the use of 5-aminolevulinic acid (5-ALA)-induced fluorescence to guide surgery (FIGR) [119-126]. Helping the operating surgeon to distinguish between tumour and normal brain tissue enabling to resect more of the tumour without increasing neurological damage [127]. However even with this significant advancement, the infiltrative nature of GBM makes gross total resection surgery (Total removal of tumour) impossible without damaging the neurological tissue and affecting the cognitive ability of patients. Therefore, a therapeutic strategy that targets the residual tumour left behind following surgery is crucial for successful treatment.

In selected patients, surgical procedure is limited to stereotactic biopsy [100]. This is often due to the tumour being located deep within the brain and the increased probability for permanent neurological complications. For this minority subset of patients, prognosis is really short even with radiation and chemotherapy [100]. OncoSeed, a form of Brachytherapy, is a radioactive implantable material that is inserted into the tumour location and could provide treatment that is minimally invasive [128-131]. A study undertaken by Lopes et. al on the use of 4.5×0.8 mm OncoSeed metal rods in ten low grade stem glioma patients have

concluded that it is a safe and effective method to treat brain tumour [128]. Hence patients with an unresectable tumour could benefit from localised treatment.

1.3.3 Heterogeneity

GBM is highly molecularly and genetically diverse, which has an impact on treatment.

Following tissue biopsy, a genetic profile of common GBM mutations are performed, including isocitrate dehydrogenase (IDH), alpha thalassemia/mental retardation syndrome X-linked (ATRX), P53 and O(6)-methylguanine-DNA methyltransferase (MGMT). This mutation profile can then serve as an indicator for prognosis and suitable treatment.

IDH1, P53, and ATRX are all associated with growth control genes [132]. Whereas MGMT is utilised to select appropriate treatment. MGMT gene encodes for a DNA repair enzyme [133]. A methylation process is known to stop DNA transcription and therefore, expression of the MGMT enzyme. MGMT expression can protect non-cancerous cells from carcinogens. Unfortunately, it also inactivates the effect of alkylating agents such as TMZ making the tumour resistant to this form of chemotherapeutic treatment.

Approximately 10, 15 and 48 % of GBMs are IDH1, ATRX and P53 mutant respectively.

Patients with mutant IDH and ATRX proteins have improved prognosis [51, 132, 134]. ATRX mutation is usually accompanied with IDH and P53 mutation [132, 135]. A combination of ATRX mutant, IDH mutant and P53 wildtype genes lead to significant improvement in both OSR and progression free survival (PFS) [132].

The Cancer Genome Atlas Research Network (TCGA) has reviewed the genetic variability between different GBM patient samples and classified GBM tumours into four categories based on their genetic type; Classical, Proneural, Mesenchymal and Neural [136].

Classical are classified by increased levels of Epidermal Growth Factor Receptor (EGFR) and P53 wildtype. EGFR is a protein attached to the surface of some cells that initiates cell signalling and increases tumour cellular growth. In Proneural tumours, TP53, IDH1 and Platelet-derived growth factor receptors (PDGFRA) are frequently mutated. All of which can contribute to fast growing uncontrollable cellular division when altered. The Mesenchymal

subgroup is characterized by high rates of mutation in the neurofibromin 1 (NF1), Phosphatase and tensin homolog (PTEN) and TP53 tumour suppressor genes [136].

Finally, the Neural subgroup does not have a significantly higher or lower rate of genetic mutations compared to the other groups. The Neural subgroup is characterized by several gene expressions that are also typically found within normal non-cancerous brain and nerve cells or neurons [136].

Unfortunately, heterogeneity is further complicated by intra-tumoural heterogeneity (within the same patient), as well as tumour evolution over time. A better understanding of GBM genetic mutations has led to the development of many specific molecular pathways targeting therapies. Some of those pathways are involved in the regulation of growth, cell cycle, DNA repair and apoptosis (Table 1.1) [137, 138]. Although this drug development approach does support a well-grounded notion, no successful single agent therapy has been found.

Table 1.1: Genomic GBM alterations and target molecular pathways [132, 138].

Gene	Alteration or target
Growth factor receptors	
EGFR	Deletion (EGFRvIII), mutation, translocation and/or amplification
KIT	Amplification, mutation
PDGFRA	Amplification
FGFR1, FGFR3	Translocation (e.g. FGFR3-TACC3)
MET	Amplification, translocation
MAPK and PI3K/mTOR signaling pathways	
PTEN	Deletion, mutation
PIK3CA	Amplification, mutation
NF1	Deletion, mutation
BRAF	Mutation (BRAF V600E)
Cell cycle pathways	
MDM2	Amplification
TP53	Wild-type (no mutations)
CDK4/6	Amplification
RB1	Wild-type (no mutations)
Others	
IDH1	Mutation
MYC, MYCN	Amplification
MGMT	Methylation
ATRX	Mutation

Following our recent understanding of GBM heterogeneity a shift in research focus has been centred on finding a treatment that could target multiple growth promoting pathways found within a single tumour [139-145]. Recent studies have suggested that intratumour heterogeneity is much more diverse than originally thought. GBM has been described as a collection of variable genetic colonies coexisting together with the most resistant colony existing as the dominant form within a specific time and space [146-149]. A personalised single drug therapy approach for a genetically diverse tumour sample will only lead to disease progression by creating resistance to therapy over time; once the most dominant genetic form of the disease is eradicated, a less dominant form will have the chance to grow and dominate [150]. Multiple drug treatment can target different colonies to enhance the efficacy of treatment and ultimately prognosis of patients. Few multidrug therapies have reached clinical studies with a much greater number currently developing within preclinical settings [51, 140, 141, 143-145, 151-154].

Few studies are aiming to develop this idea into personalised medicine, where each patients' tumour is assessed genetically and a suitable drug combination is selected for their tumour. Usefulness of this approach is yet to be explored [144].

1.3.4 Re-occurrence

GBM is characterised by a high proliferativion rate, angiogenesis, necrosis and the existence of brain tumour initiating cells, also known as cancer stem cells [118]. GBM reoccurrence is inevitable and usually occurs in the form of local continuous growth within 2 to 3 cm of the primary lesion border [72]. This new growth is often composed of a new genetic strain that is resistant to previous chemo and radiation therapy, making it difficult to treat [150, 155, 156]. GBM also extends into thread like structures that invades healthy tissue beyond the primary lesion contributing to its resistance [157].

Previous studies have revealed association of re-occurrence with the existence of cancer stem cells in GBM [149, 155, 157-161]. Cancer stem cells are associated with the ability to self-renew and differentiate into multiple cancer cell types. This leads to a population consisting of a rare fraction of tumorigenic cancer stem cells and dominant differentiated non-tumorigenic cells (Figure 1.4).

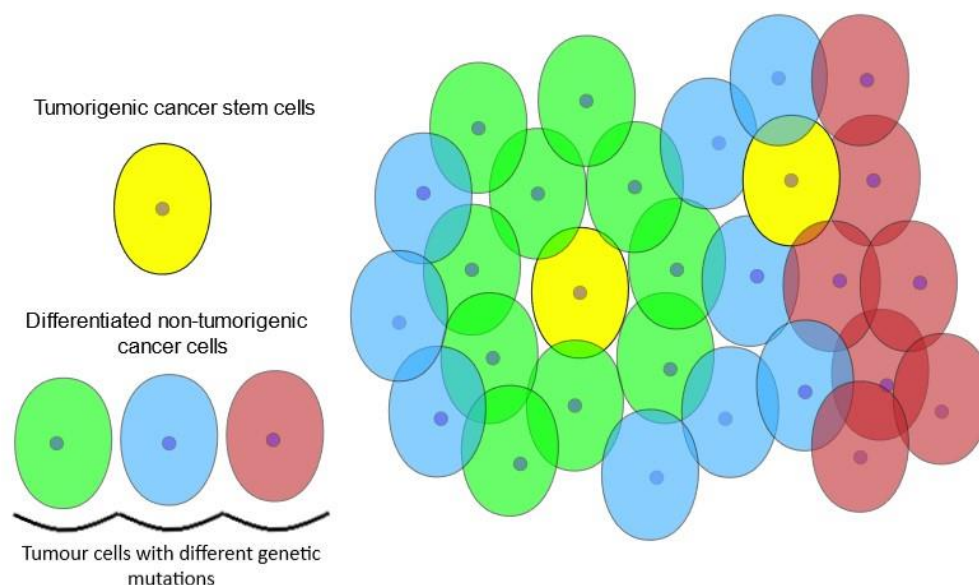


Figure 1.4: Cancer cell population consisting of non-differentiated tumorigenic stem cells and fast growing differentiated cancer cells.

Many studies have revealed GBM cancer stem cells to be highly resistant to standard treatments such as carmustine and TMZ [139, 140, 143, 144]. Cancer stem cells are thought to drive tumour growth and disease progression. Finding the perfect drug combination to target both the dominant subpopulation as well as the less dominant cancer stem cells could eradicate GBM.

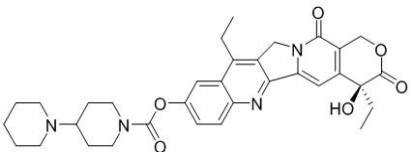
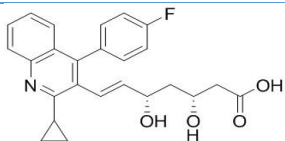
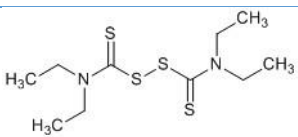
1.4 Drugs that may be suitable for repurposing to treat Glioblastoma

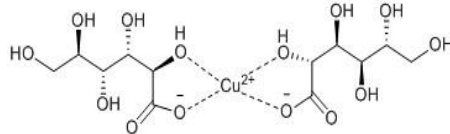
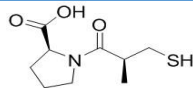
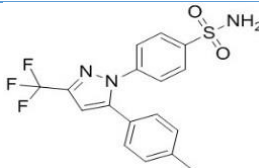
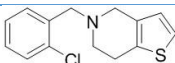
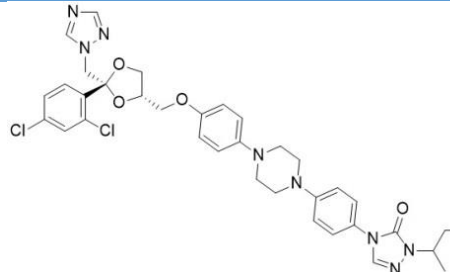
The high cost of new drug development as well as the fact that GBM is a rare disease limit the financial incentive for companies to develop new treatments, thus repurposing and reformulating of promising drug candidates has seen an increase in interest as a potential treatment for GBM.

This project will investigate the repurposing of eight approved drugs as a potential treatments for GBM. The selected list of drugs were determined following a literature review

using both scopus and google scholar journal search engines. The inclusion criteria comprised of drugs that were already FDA approved, have shown potential for GBM treatment through either *in-vivo* or *in-vitro* studies, are relatively hydrophobic ($\log P > -0.5$ for faster diffusion into the tumour), with low melting point ($<270\text{ }^{\circ}\text{C}$) and low molecular weight ($<800\text{ g/mol}$). The exclusion criteria were drugs that presented high toxicity in patient leading to death. The search terminology included the words drug AND FDA OR repurposed AND glioblastoma OR glioma. Only articles in English were included. Following the search irinotecan hydrochloride (IRN), pitavastatin (PTV), disulfiram (DSF), copper gluconate (CoGlu), captopril (CAP), celecoxib (CXB), itraconazole (ITZ) and ticlopidine (TCL) were selected because they are pharmacologically well characterized, had a low likelihood of either inducing local toxicity or adding to a patient's side effect burden, had evidence for interfering with a recognized, well-characterized growth promoting element of GBM, and when combined had a reasonable likelihood of concerted activity against key biological features of GBM growth (Table 1.2). Furthermore, their physicochemical properties (Log P, molecular weight and melt temperature) make them suitable for formulation into an implant using a variety of techniques, such as extrusion, compression moulding, 3D printing and electrospinning [162, 163] (Chapter five: formulation and development).

Table 1.2: List of promising drug treatments. Recorded with their Chemical structure, Physicochemical properties, Mechanism of action and clinical trial findings.

Drug	Chemical structure	Log P	Molecular weight g.mol ⁻¹	Melting point °C	Mechanism of action	Clinical trial findings
Irinotecan		4.3 [164]	586.689	254 [165]	Inhibitor of topoisomerase I, an enzyme required for DNA transcription [166].	FDA approved for colorectal cancer. Clinical trials for glioma patients via intravenous delivery revealed some activity against cancer, enhanced efficacy is revealed when IRN is used in combination with other treatments, such as TMZ, bevacizumab, carmustine and thalidomide [41, 167].
Pitavastatin		1.45 [168]	421.468	184.9 [169]	Induce cell death and suppress tumour cell P-glycoprotein 1, which aids transfer of foreign substances out of the cell. Suppressing this protein would enhance potency of IRN combined treatment [142].	Statin drug, currently FDA approved as a cholesterol lowering agent.
Disulfiram		2.81 [170]	296.524	71.5 [171]	Few different mechanism have been proposed: Inhibitor of topoisomerase I and II, proteasome inhibition, Aldehyde Dehydrogenase (ALDH) inhibition, expression of serine/threonine-protein kinase (PLK1), MGMT and nuclear factor kappa-light-chain-enhancer of activated B cells (NFkB) activation inhibition [172-177]. DSF anticancer targeting activity is associated with naturally increased copper concentration within cancer cells [178]	FDA approved for the treatment of alcoholism. Current clinical trials are taking place where DSF is used alongside CoGlu and TMZ for GBM treatment.

Copper Gluconate		453.84	155-157 [179]	Have shown pre-clinical evidence for GBM growth inhibition when combined with aprepitant, artesunate, auranofin and DSF [180].	Dietary supplement. Current clinical trials are taking place where CoGlu is used in combination with other treatments.	
Captopril		-0.27 [181]	217.283	106 [181]	Inhibits activity of soluble matrix metalloproteinase (MMP) -2 and MMP-9, a growth facilitating factor in GBM [173, 182-186]. ACE inhibitors, including CAP, are well known to inhibit angiotensin. GBM is shown to develop new blood vessels at an enhanced rate, aiding with its migration and growth. Inhibiting angiotensin will suppress new GBM blood vessels growth [173, 186].	Utilised in the treatment of hypertension.
Celecoxib		2.82 [187]	381.373	161-162 [188]	Inhibits GBM growth by inducing DNA damage, leading to p53-dependent cell cycle arrest and autophagy [189, 190].	An anti-inflammatory drug. GBM clinical trials for orally delivered CXB have revealed dose related inhibition and some studies show that CXB sensitivity is enhanced with γ-irradiation [191-193].
Ticlopidine		4.39 [194]	263.783	204-207 [195]	Inhibits P2Y12 ADP receptor. A purinergic receptor, P2Y12 is expressed at higher levels in cancer cells [141].	FDA approved as anticoagulant for the prevention of strokes.
Itraconazole		5.66 [196]	705.641	168 [197]	Induce autophagy facilitated by inhibition of AKT1 MTOR signalling pathway, important for regulating cell cycle [198].	An antifungal drug. Widely used for the treatment of fungal diseases.

1.4.1 Irinotecan

IRN is a camptothecin derivative, which is an alkaloid isolated from the stem wood of the Chinese tree *Camptotheca acuminata* [199, 200]. IRN is currently utilized for use in colorectal cancer and has shown high activity against solid tumours in the gastrointestinal tract [199]. Preclinical studies have revealed activity against GBM cells with multidrug resistance [144]. Its mechanism of action involves the inhibition of the topoisomerase I enzyme [200, 201], which catalyses the breakage and re-sealing of the phosphodiester backbone of DNA and RNA. During transcription, Topoisomerase I causes the DNA strand to unfold and form a covalent linkage with the DNA. In this confirmation, IRN or its metabolites binds to Topoisomerase I preventing the DNA from re-sealing, causing S-phase specific killing [200, 201]. Following DNA damage topoisomerase I and II is shown to be particularly elevated in Glioma cells [202].

During metabolism of IRN within GBM cancer cells, several metabolites are formed. One of which is 7-ethyl-10-hydroxycamptothecin (SN-38) (Figure 1.5). This metabolite is shown to be 1000 times more potent than IRN at inducing cytotoxicity through apoptosis [200, 203, 204].

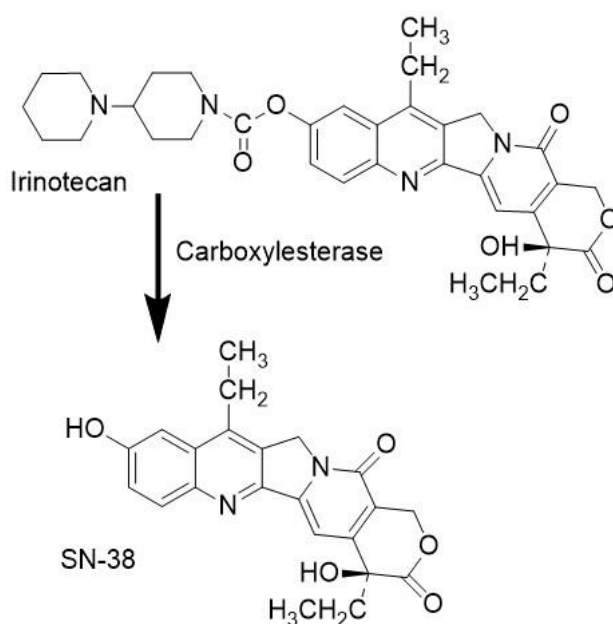


Figure 1.5: Metabolism of IRN into its active SN-38 metabolite

When given orally or via the intravenous route IRN suffers from rapid metabolism [205]. Furthermore, antiepileptic medications used during the treatment of GBM patients are known to accelerate the degradation of IRN and its active metabolites hindering its therapeutic effect [206].

The first IRN trial for Glioma was in 1999 [203], with 60 patients receiving 125 mg/m² IRN intravenously once a week for 4 weeks followed by a two week rest. The trial found that 15% of patients achieved a partial response, while 55% of patients attained stable disease lasting at least 2 weeks. A second phase II trial for patients undertaking a similar dosage and treatment cycle found a lower >10% response, a suggested reason was due to a larger number of patients undergoing anti-epileptic drug treatment [207].

More recent clinical studies have been performed to assess IRN in combination with other drugs, including TMZ, carmustine, thalidomide, cetuximab, carboplatin, and bevacizumab [205, 208-216]. All of which have confirmed IRN effectiveness in targeting GBM and that therapeutic efficacy is enhanced when used in combination with other chemotherapeutic agents, particularly TMZ and bevacizumab [41, 166, 209, 213, 214, 217, 218].

When administered intravenously IRN causes severe systemic toxicity, including neutropenia, severe diarrhoea and asthenia [205]. This has spurred the development of alternative IRN dosage forms. For example Ramsey et al developed an IRN loaded liposome formulation, known as Irinophore CTM. A preclinical study in mice revealed improved efficacy and an 8-fold increase in plasma half-life compared to standard intravenously administered IRN [219, 220].

1.4.2 Pitavastatin

PTV belongs to the statin class of drugs, which are used for lowering blood cholesterol levels. It received FDA approval in 2009. Soon after, *in-vitro* and *in-vivo* studies revealed that it exhibited antitumour properties in glioma, ovarian and colon cancers [142, 221-227]

A study undertaken by Jiang et al screened PTV monotherapy and in combination with IRN using patient-derived GBM cancer stem cell-like lines [142]. Results revealed that PTV

possess activity against GBM, via inducing cellular autophagy and cell cycle Go/G1 phase specific killing. It has also shown to be more potent than other statin drugs and forms synergic activity when combined with IRN [142]. One mechanism for GBM drug resistance is the overexpression of multi-drug resistance protein (MDR-1), also known as permeability glyco protein pump or P-glycoprotein 1 (PGP) [228, 229]. This protein forms an active transporter that uses ATP to transport cytotoxic substances, such as IRN, out of the cell [142, 230]. When PTV and IRN are combined an increased level of apoptosis is observed, which is due to PTV suppressing the glycosylation of MDR-1, thus inhibiting its effect and allowing an increased concentration of IRN to enter the GBM cells. *In-vivo* testing on mice confirmed this synergic effect [142]. It has been also suggested that the treatment of glioma cells with PTV is associated with the inhibition of nuclear factor-kappa B activation, a factor that suppresses autophagy, resulting in autophagic cellular death [223, 225].

Another study performed by Fan et al screened PTV and IRN individually and in combination, using a high throughput drug screening assay of GBM cell lines [231]. Results confirmed IRN plus PTV combinational drug treatment to be more effective than their respective monotherapies.

The ability of PTV to cross the BBB is predicted to be limited, with a calculated logarithm value of brain to plasma concentration ratio (-log BB) of -0.6499 [142]. Therefore, oral or intravenous delivery of PTV will result in sub-therapeutic concentrations in the brain and is thus not a viable route of administration for GBM treatment. The best option would be local administration.

1.4.3 Disulfiram/Copper Gluconate

DSF has been utilized for the treatment of alcoholism for the past few decades. It was originally prescribed orally in very high doses of 3000 mg per day and thus has a well-established safety profile [232]. Copper is naturally available in the body through diet, a healthy adult has 50-80 mg within their body. Dietary supplements such as CoGlu can be administered to enhance copper levels.

In-vitro testing of DSF has shown it to be potent against GBM cancer stem cells and it exhibits its activity when combined with copper. DSF/Copper activity is dependent on the formation of the bis(N,N-diethyl dithiocarbamato)copper(II) complex (Figure 1.6) [233]. *In-vitro* data demonstrate DSFs capability of inhibiting glioma stem cell proliferation, but a number of different mechanisms of action are proposed for its anticancer activity. Some have attributed it to proteasome inhibition, ALDH inhibition, expression of (PLK1), MGMT inhibition and NFkB activation inhibition [173-177]. Others have attributed it to the active reaction process of DSF plus Copper combination releasing reactive oxygen species such as H₂O₂ that potentiate apoptosis [233].

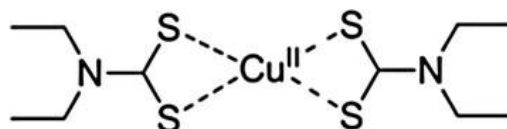


Figure 1.6: bis(N,N-diethyl dithiocarbamato)copper(II) complex

In-vivo studies with mice have demonstrated that low doses of DSF and Copper significantly improved TMZ activity [178]. Promising pre-clinical data for DSF and CoGlu combination treatment has spurred several clinical trials assessing treatment efficacy (Table 1.3).

The first DSF trial for GBM patients was in 2016, where 12 newly diagnosed GBM patients received dose-escalation of orally administered DSF in combination with TMZ. From this trial the maximum tolerated dose for orally administered DSF was established to be 500 mg daily. No significant change to survival length was observed [234]. Two years later a second Phase I clinical trial of newly diagnosed GBM patients investigated the same treatment, this time with or without copper [235]. 18 patients were enrolled, with 6 receiving orally administered DSF and CoGlu combinational treatment. Results found that a daily dose of 500 mg of DSF with 2 mg of CoGlu treatment to be tolerable, however no efficacy conclusions were drawn from the study due to limitations related to patient selection bias and small sample size.

Table 1.3: Clinical trials involving disulfiram in GBM. Identifiers in reference to www.clinicaltrials.gov online database, table last updated 27th-11-2018.

Clinical Trial Identifier	Study Phase	Drug(s)	Status	Start/Completion Dates
NCT03363659	Phase 2	TMZ, CoGlu, DSF	Not yet recruiting	Jan 2018- Jan 2027
NCT01907165	Early phase 1	TMZ, GoGlu, DSF	Completed	Oct 2013- Mar 2018
NCT01777919	Phase 2	TMZ, Copper, DSF	Not yet recruiting	Jan 2017- Jan 2020
NCT03034135	Phase 2	CoGlu, DSF	Completed	Mar 2017-Jun 2018 + 2 year follow up study
NCT02678975	Phase 2/3	Copper, DSF, Alkylating agent (TMZ, Lomustine or Procarbazine, Lomustine and Vincristine combination (PCV))	Recruiting	Jan 2017- Sep 2020
NCT02715609	Phase 1/2	TMZ, CoGlu, DSF	Recruiting	Jun 2016- Sep 2020
NCT02770378	Phase 1	9 repurposed drugs (Aprepitant, Auranofin, CAP, CXB, DSF, ITZ, Minocycline, Ritonavir and Sertraline) combined with metronomic TMZ	Active	Nov 2017- Mar 2018

Both DSF and Copper can pass the BBB, however with uncertain mechanism of action, it is difficult to predict efficacy through oral or intravenous delivery. After ingestion, DSF is rapidly convert into the bis(diethyldithiocarbamato) copper complex, which rapidly degrades again into diethyldithiocarbamic acid (DDC) which is unstable and is further degraded to form diethylamine and carbon disulphide [236, 237]. As the anticancer activity is achieved from either DSF or the bis(diethyldithiocarbamato) copper complex the efficacy of treatment will rely on those compounds reaching the cancer cells intact.

1.4.4 Captopril

CAP is an angiotensin-converting enzyme (ACE) inhibitor, an enzyme that converts angiotensin I to the potent vasoconstrictor angiotensin II and inactivates the bradykinins [238]. CAP is used for the treatment of hypertension and congestive heart failure. It has been widely prescribed since the 1980's [173]. As a monotherapy CAP does not induce cytotoxic effect on GBM cell lines but it has shown to inhibit cancer invasion, migration and adhesion, that are all essential processes used by GBM for growth and disease development [184, 239]. This mechanism of action is achieved through the downregulation of matrix

metalloproteinases-2 and -9 [184]. Another potential for CAP is its ability to scavenge free radicals, this could lead to the reduction of oxidative species that are raised through cytotoxic agents and radiation therapy lessening their toxicological effects [240]. Since the year 2000 research on CAP has mainly focused on its anticancer activity within combination drug treatments. General results of preclinical and clinical studies has revealed its antiangiogenesis therapeutic potential across a variety of cancer types, including renal, prostate, colorectal, breast, melanoma, lung etc [241-243].

Because of its small size, neutral charge and slight lipophilicity systemically administered CAP is predicted to be capable of partially passing the BBB (Table 2). However, CAP suffers from a relatively short half-life (<2 hours), hence significant degradation might occur prior to reaching the brain and thus high dosage would be required for systemic delivery and this might create further unpleasant toxicity to an already ill patient [244, 245].

Based on DSF and CAP mechanisms of action, their combination could exhibit enhanced antitumour activity by targeting multiple growth promoting pathways found within GBM such as proteasome, ALDH, MGMT, NFkB, ACE and bradykinins inhibitions [185]. CAP antioxidants ability may also reduce oxidative species that are raised during DSF metabolism, preventing elevated toxicity.

To date there has been limited research into CAP as a treatment for GBM. However, its anti-invasive properties could prove significant at slowing down GBM disease progression and increase survival.

1.4.5 Celecoxib

Celecoxib (CXB) is a cyclooxygenase-2 (COX-2) inhibitor used as an anti-inflammatory drug to treat pain and inflammation. Shortly after its clinical introduction in 1998, preclinical studies established its anticancer potential.

The anticancer effect of CXB is believed to be independent of its COX-2 inhibition ability, as its non-COX-2 analogue 2,5-dimethyl-celecoxib (DMC) can mimic CXB's anticancer potency [246-249]. One of CXB perceived anticancer mechanism of action is its triggering of

endoplasmic reticulum stress that causes leakage of calcium from the endoplasmic reticulum into the cytosol [250]. CXB has also been shown to induce p53-dependent G1 cell cycle arrest and autophagy as well as apoptosis via NF- κ B pathway in GBM cell lines [189, 190]. Other *in-vivo* research has shown that treatment with CXB led to lower levels of phospho-Akt, phospho-EGFR, Bcl-2 and Bcl-XL expressions [251]. Additional *In-vitro* and *vivo* testing shows that CXB can enhance tumour radiosensitivity through the inhibition of tumour angiogenesis and induced autophagy, particularly in hypoxic cells [191, 252, 253].

In combination with TMZ, systemically administered CXB demonstrated enhanced antitumour activity in rats GBM model [254]. Unfortunately, when the same study was replicated in humans CXB demonstrated no survival benefit compared to TMZ monotherapy in both newly diagnosed and recurrent glioma patients [193, 255, 256].

A phase II trial assessing combinational treatment of orally delivered CXB and intravenous delivered IRN revealed some activity among heavily pre-treated patients with a recurrent brain tumour [257]. 37 patients were enrolled, of which 92% were diagnosed with recurrent GBM and 8% recurrent anaplastic astrocytoma. A six week treatment cycle was established, with IRN administered weekly at 350 mg/m² dosage for patients receiving enzyme-inducing antiepileptic drugs (EIAEDs) and 125 mg/m² for patients not receiving EIAEDs, for both set of patients an additional 400 mg of CXB dosage was given twice daily. Following treatment, six patients achieved an objective radiographic response and an additional 13 patients achieved stable disease. Despite the heavy pre-treatment of the patients enrolled, the median OSR was 31.5 weeks and the median PFS was found to be slightly improved when compared with that achieved for IRN only treatment in previous clinical studies [258, 259].

When administered orally CXB has shown that it can pass the BBB barrier, but systemic administration can result in undesirable side effects, especially for patients with pre-existing renal dysfunction and heart failure. This risk increases with the doses required to achieve an anticancer effect [85, 260].

1.4.6 Ticlopidine

TCL is an adenosine diphosphate (ADP) receptor inhibitor antiplatelet drug, its main use is in preventing strokes and for patients with a new coronary stent to prevent occlusions. TCL's GBM anticancer properties is known to be from inhibiting adenosine diphosphate receptor P2Y₁₂. A purinergic receptor, which is expressed at higher levels in cancer cells [141].

A preclinical study in glioma bearing mice demonstrated that when TCL is used in combination with imipramine, a tricyclic antidepressant enhanced antitumour activity is formed [141].

So far limited research has been performed on TCL anticancer activity. This is perhaps due to it being an antiplatelet drug with some studies suggesting that with chronic use, there could be an increased risk of bleeding complications or cancer incidence. However, laboratory studies so far have demonstrated a combinational approach does provide superior results for anticancer treatment. Although some doubts exist, the successful experimental results justify the need to study antiplatelet drugs further [261].

1.4.7 Itraconazole

ITZ is an antifungal drug that has been used clinically since the 1980s and thus its clinical safety profile is well known [173, 262]. Pre-clinical and clinical studies have revealed that ITZ possess antitumour properties against a wide range of cancers including prostate, lung, basal cell carcinoma, leukaemia, ovarian, breast and pancreatic cancer. For GBM ITZ is shown to inhibit angiogenesis and induce autophagy through inhibition of the AKT-mTOR pathway (Table 1.4) [198].

Table 1.4: ITZ mechanism of action against cancers.

Mechanism	Target cancer
Anti-angiogenic	Non-small cell lung cancer [263]
	Prostate cancer [264]
	GBM [198]
Hedgehog pathway inhibition	Multiple myeloma [265]
	Medulloblastoma [266]
	Basal cell carcinoma [266, 267]
	Prostate cancer [264]
	Breast cancer [268]
	Malignant pleural mesothelioma [269]
Autophagy induction	GBM through inhibition of mTOR signalling [198]
	Endometrial cancer [270]
	Breast cancer [268]
Reversal of multi-drug resistance	Breast cancer [271]
	Leukemia [272, 273]

ITZ has been shown to possess enhanced anti-tumour activity when combined with a range of drugs including aprepitant, artesunate, auranofin, CAP, CXB, DSF, ITZ, ritonavir and sertraline, hence it could be worthwhile investigating ITZ in combination with a range of cytotoxic drugs that target different GBM survival mechanisms [173, 262].

Being a highly lipophilic drug, ITZ can pass the BBB and is generally well tolerated. Some rare side effects are headache, diarrhea, dyspepsia, abdominal pain, constipation, nausea, flatulence, rash, pruritus and urticaria [274].

1.5 Conclusion

So far, no effective drug treatment exists for GBM and thus survival rates remain low. The current first-line of treatment is the STUPP protocol, which consist of maximum resection surgery with radiation and chemotherapy with the oral alkylating agent TMZ, whereas the second line of treatment utilizes Gliadel® chemotherapy instead. Both of those treatment have been successful in extending the life expectancy of patients by 2-6 months. However, both TMZ and carmustine (in Gliadel®) potency is dependent on their ability to alkylate DNA through silencing of the MGMT DNA repair gene. Thus, for patients that are resistant to either form of treatments no other options are available for extended survival.

Considering that GBM is a rare disease significant investment in new research and drug development have been hindered. Additionally, the disease has proven to be particularly difficult to treat due to a number of disease specific obstacles including the BBB, tumour location, heterogeneity and re-occurrence. As a result of those complications, drug repurposing, combinational therapy and localised drug treatment are gaining focus. Because developing a new treatment from already FDA approved drugs is less costly and time consuming, utilizing combination drug treatment can target heterogeneity by bombarding multiple GBM cancer pathways and localised drug delivery approach can be used to surpass the BBB and improve drug efficacy as successfully demonstrated by current Gliadel® therapy for the local of delivery of carmustine.

A variety of FDA approved drugs have been shown to exhibit GBM anticancer properties, with IRN, PTV, DSF, CoGlu, CAP, CXB, TCP and ITZ being some of the most promising. Individually many of these drugs are weakly potent, however in combination there is a strong evidence of synergistic effect- for instance, PTV enhanced antitumour activity when combined with IRN (Chapter one, 1.4.2 Pitavastatin). This could lead to a potential treatment that can target multiple GBM cancer pathways. Furthermore, utilising a local administration method to deliver those drugs could enhance their efficacy by lowering drug toxicity through avoidance of systemic circulation, lower dosage requirement and a guarantee that the drugs reach the tumour at therapeutic concentrations.

2. CHAPTER TWO: TISSUE CULTURE SINGLE DRUG TREATMENT

2.1 Abstract

Background: Despite advances in surgical, radiation and chemotherapeutic-based treatment approaches, prognosis for glioma tumours remains low. This is mainly attributed to early disease recurrence, difficult to reach cancer location and tumour heterogeneity. Recently a number of FDA approved drugs for various other diseases have demonstrated cytotoxic activity against glioma, and these may offer a new means to fast track the development of an effective treatment. The aim of this study was to determine whether currently approved drugs used for the treatment of other diseases are effective against gliomas

Methods: To address this, *in-vitro* cytotoxicity testing of eight mono-therapeutic drug treatments: IRN, PTV, DSF, CoGlu, CAP, CXB, TCL and ITZ, were performed and compared against the current standard of care, TMZ. Twelve patient derived glioma cells were assessed, and each treatment was evaluated against two separate tumour fragments: the tumour core (TC) and brain around the tumour (BAT) cells. Furthermore, to ensure accuracy of our drug cytotoxicity data, the LogIC₅₀ results were compared across two separate cytotoxicity assays (MTT and IncuCyte)

Results: Our results demonstrate that at <100 µM dose, IRN, PTV and CXB were more efficacious than TMZ with data validated across different assays. Furthermore, those treatments were also effective across both the TC and BAT tumour fragments despite their varying phenotypic characteristics.

Conclusions: Repurposed drug treatments are potent against gliomas at lower doses than TMZ. This data was confirmed across separate tumour fragments and cytotoxicity assays ensuring the accuracy of our data.

2.2 Introduction

In cancer research cell culture methods have been fundamental in providing information on tumour biology and therapeutic cytotoxicity. It has allowed for the study of tumour cells in a controlled environment, which due to its ease of scale up and low cost makes it an attractive

option for high-throughput screening of therapeutic agents. However, the phenotypic and genetic characteristic found within cancer cell lines differ significantly to those found within primary cells derived from patients [275]. This is why so many successful pre-clinical studies using cell lines have failed in the clinic, and more importantly studying cell lines have led to some misleading results about important genetic pathways within cancers [276-279]. In contrast, primary cells isolated from human tissue samples can reproduce phenotypic and genetic populations that are much more representative of the original tumour tissue [275].

In GBM, one of the most important tumour characteristics that needs to be maintained during tissue culture is heterogeneity. This genetic diversity is generated through a minority of cancer cell population with stem cell characteristics that possess the ability to initiate tumour growth through self-renewal and differentiation [147, 148, 161, 280-283]. This characteristic of GBM is often what determines treatment failure and disease recurrence. Hence selecting an appropriate tissue culture technique is essential to translate research from the laboratory to the clinic.

Another important consideration for therapeutic screening that is not currently assessed within cell culture studies is the existence of intratumour heterogeneity. A study performed by S Tavaré et al confirmed that tumour fragments taken from the same patient can reveal significant variation in genetic make-up and could potentially be classified into a different GBM types [146]. This is of relevance in tissue culture because primary cell studies are usually undertaken using TC fragments attained from surgery. TC can often be phenotypically and genetically different from the residual cancer cells that are left behind. Within our study we have taken this into consideration and two separate tumour fragments were screened: TC and BAT.

There are a variety of techniques to screen the cytotoxicity of therapeutic agents, with the most established and well-known being the colorimetric MTT [3-(4,5-dimethyl-2-thiazolyl)-2,5-diphenyl-2H tetrazolium bromide] assay [284-286]. The MTT assay, which is an endpoint assay, taking a single measurement after a fixed incubation period has proven to be

a rapid, reliable and clinically relevant technique in screening therapeutic agents for their cytotoxicity against gliomas [285]. The IC₅₀ cytotoxicity data obtained from this assay is directly dependent on the cellular metabolic conversion of MTT to formazan and thus provides an indirect measure of cellular viability. Newly emerging cellular cytotoxicity techniques rely on the real-time measurement of cellular viability. One such technique is the IncuCyte live cell analysis method which relies on collecting snapshot images of cells as well as cell confluence data [287]. IncuCyte analysis is a real-time assay that allows for the tracking of cellular growth over time and is particularly useful for assessing the cytotoxicity of treatments, where subtle cytotoxic effects could be missed when using endpoint-based methods [287]. Within this study a comparison between the metabolic based MTT and the real-time based IncuCyte was performed, to ensure that our drug cytotoxicity data was true and reliable.

A range of FDA approved drugs (IRN, PTV, DSF, CoGlu, CAP, CXB, TCL and ITZ) have shown promise against glioma, either as monotherapies or in combination therapies. Within this chapter we will determine the cytotoxicity of the aforementioned drugs against primary glioma cells. The chapter presents a full discussion of sample clinical database, cytotoxicity test method refinement, MTT cytotoxicity data and IncuCyte cytotoxicity data.

2.3 Materials and methods

2.3.1 Materials

Irinotecan hydrochloride, pitavastatin calcium, were purchased from Jiangsu Hengrui Medicine Co. Ltd and LGM Pharma respectively.

Deoxyribonuclease I (DNA's), sodium pyruvate, sodium bicarbonate solution (NaHCO₃), fetal bovine serum (FBS), thiazolyl blue tetrazolium bromide (MTT) powder, dimethyl sulfoxide (DMSO), trypsin replacement enzyme 1X, disulfiram, copper gluconate, celecoxib, temozolomide, ticlopidine, itraconazole and captopril were all purchased from Sigma Aldrich.

Collagenase, trypan blue solution 0.4%, minimum essential medium (MEM), antibiotic-antimycotic (containing penicillin, streptomycin and fungizone), neurobasal medium, N2

X100 supplement, B-27 X50 supplement, epidermal growth factor (EGF), fibroblast growth factor basic (bFGF) and hank's balanced salt solution (HBSS) were all purchased from Gibco.

1.077 +/- 0.001 g/mL Ficoll-Paque density gradient cushions was purchased from GE Healthcare Life Sciences. Pronase from Roche Diagnostics. Phosphate buffer saline (PBS) from Oxoid. Human plasma (HP) from Patricell. Dulbecco's modified eagle medium (DMEM-F12) was initially purchased from Sigma Aldrich, but due to the lack of availability, supply was replaced by Gibco.

2.3.2 Biopsy collection and dispersion

Unfixed TC and BAT tissues were collected immediately following craniotomies at Queen Elizabeth Hospital in accordance with ethical approval (application number: 11-029) from the Human Biomaterials Resource Centre (HBRC). Collected samples were immediately placed in collection fluid and transported to the laboratory for primary cell culture.

A total of 17 samples were collected from 12 patients, each assigned a patient number from 1 to 12 (Table 2.1). TC samples were collected from all 12 patients with an additional BAT samples collected from 5 of those patients.

Table 2.1: Summary of sample collection.

Patient	Sample
1	TC
2	TC
	BAT
3	TC
4	TC
	BAT
5	TC
	BAT
6	TC
7	TC
8	TC
9	TC
	BAT
10	TC
	BAT
11	TC
12	TC

For culturing, the tumour tissue was firstly immersed in HBSS then sliced into approximately 1-mm³ fragments using a scalpel and washed with HBSS to remove excess blood clots. Fragments were then suspended in 30 mL HBSS and digested with enzymes: collagenase (0.25 mg/mL), pronase (0.5 mg/mL) and DNase (0.4 mg/mL) for 30 minutes with constant stirring at 37 °C and 4 °C. Any undigested material was then sieved using 100 µm pore nylon mesh and the suspension layered onto 2 X 12 mL Ficoll-Paque density gradient cushions (Density: 1.077 +/- 0.001 g/mL) which were then centrifuged at 400 g for 30 minutes at room temperature. The tumour cells, settled as a band at the interphase and were siphoned off, while the red blood cells formed a pellet that was discarded. 15 mL of HBSS was then added and the solution centrifuged for 5 minutes at 1200g. The supernatant was removed, and the pellet re-suspended in 1 mL of HBSS to check for cell viability.

2.3.3 Histological evaluation and biopsy protein expression

Histological evaluation and IDH, ATRX, MGMT and P53 gene mutation screening were performed at the Queen Elizabeth Hospital, Birmingham. Biopsy from patients were collected and reviewed by the neuropathologists. Tumour grade was confirmed according to the WHO classification scheme [4-6, 288]. Tissue biopsies were also used to screen for some or all four of the most commonly mutated genes related to disease progression: IDH, ATRX, MGMT and P53.

2.3.4 Whole exome sequencing

A total of six glioma patients were used for this study. Whole exome sequencing of patient's tissue biopsy and corresponding tissue cultured cells in serum-based medium were performed. Exome sequencing data were extrapolated into FASTQ files. Data processing was then performed to filter of all variants most likely to be somatic.

2.3.5 Cell culture

Cells were seeded at 2x10⁵ cells/cm² in either serum based or serum free culture media and incubated at 37 °C, 5% CO₂.

For serum based culture; DMEM-F12 medium with L-glutamine and sodium bicarbonate (1:1 mixture) was supplemented with 10% FBS, 100 μ M sodium pyruvate, 0.05 mM MEM and 1% antibiotic-antimycotic solution.

For serum-free based media; tumour cells were cultured in neurobasal based medium consisting of N2, B27 supplements (0.5 \times each), human recombinant bFGF, EGF (50 ng/mL each) and 1% antibiotic-antimycotic solution. Or DMEM-F12 medium with L-glutamine and sodium bicarbonate (1:1 mixture) supplemented with 10% HP, 100 μ M sodium pyruvate, 0.05 mM MEM and 1% antibiotic-antimycotic solution.

Cell viability check

10 μ L of trypan blue solution was added to 10 μ L of a cell suspension, which was subsequently loaded onto a hemacytometer and examined under a microscope. Cells were counted and cell viability calculated. For newly sampled dispersed cells and trypsin detached cultured cells, viability scores were between 95-100 %. Following cryogen storage, the thawed cells had viability scores between 60-90 %.

Cell detachment and splitting

Once confluent, the cells were split by removing the culture medium, washing the cells with HBSS and incubating with 1X trypsin replacement enzyme (2.5 mL for 75 cm³ and 1.5 mL for 25 cm³ flasks) for 3 minutes at 37 °C, 5% CO₂. The cell suspension was then transferred into a centrifuge tube and 10 mL of fresh culture medium was added. The tube was then centrifuged for 3 minutes at 400 g. Following centrifugation, the supernatant was removed, and the pellet re-suspended in culture medium. Cell count and viability check were performed, and the cells were then seeded into new flasks and incubated at 37 °C, 5% CO₂. TC and BAT cells were grown up to passage number 10 and 20, respectively.

Cell storage and Cryopreservation

Following cellular count and viability check, cells were stored at 1-5 $\times 10^6$ cells/mL. 1 mL aliquots were placed into cryovials with 15 % FBS and 7 % DMSO. The cryovials were immediately transferred into Mr. Frosty™ and frozen at -80 °C for up to 30 days, the vials were then transferred to liquid nitrogen storage at -196 °C.

Thawing frozen cells

Once thawed, 10 mL of culture medium was added and centrifuged for 3 minutes at 400 g.

The supernatant was removed, and the pellet re-suspended in culture medium. This centrifugation and resuspension step was repeated twice. Following cell count and viability check, the cells were seeded into culture flask(s) and culture medium was added.

2.3.6 Drug solution

Drug solutions were produced in accordance to their solubility (Table 2.2). TMZ, IRN, CoGlu and CAP were dissolved in sterile distilled water (SDW) to make 1 mM stock solution. PTV, DSF, TCL and CXB were dissolved in DMSO, to make 100 mM solution, except for ITZ where a 50 mM solution was made.

Table 2.2: TMZ, IRN, PTV, DSF, CoGlu, CAP, TCL, CXB & ITZ stock solutions

Drug	Solvent	Concentration (mM) Made	Actual solubility (mg/mL)
TMZ	SDW	1	3.46 in SDW [289]
IRN	SDW	1	10-30 in SDW [216]
PTV	DMSO	100	20 in DMSO [290]
CoGlu	SDW	1	10-30 in SDW [179]
DSF	DMSO	100	15 in DMSO [290]
CAP	SDW	1	160 in SDW [291]
TCL	DMSO	100	10-30 in DMSO [290]
CXB	DMSO	100	16.6 in DMSO
ITZ	DMSO	50	10-20 in DMSO [290]

To minimise or eliminate DMSO toxicity to cells, these solutions were further diluted in culture medium to make 1 mM stock solutions. The stock solution of each drug was then serially diluted in culture media to make working solutions of the following concentrations: 100,000, 10,000, 1000, 500, 250, 125, 62.5, 31.25, 15.6 and 7.8 nM.

The working solutions were stored at 5 °C for up to 2 weeks. Or for drugs with known freeze thaw stability: TMZ, IRN, PTV, TCL, ITZ, CXB and CAP [292-298], at -20 °C for up to 1 month. Frozen solutions were only thawed once.

2.3.7 MTT cell metabolism and IncuCyte cell proliferation imaging assays

All MTT and IncuCyte assays were performed on TC and BAT tissue cultured samples below passage 10 and 20 respectively, to maintain original phenotypic population, as much as possible [299, 300].

Cells were seeded in 96 well plates at 4000 cells/well for MTT assay and 5000 cells/well for IncuCyte assay. For both assays control wells consisting of untreated cells were included, while for the MTT assay blank wells consisting of media only were also included. To allow for cellular attachment; plates were incubated for 24h at 37 °C, 5 % CO₂. Following incubation, the medium was aspirated and 200 µL of drug solution was added. For control and blank wells, 200 µL of culture medium was added, while for the test wells each drug concentration was added in triplicate. To reduce evaporation from the test and control wells over the extended incubation period, 250 µL of sterile distilled water was added to the perimeter wells (Figure 2.1).

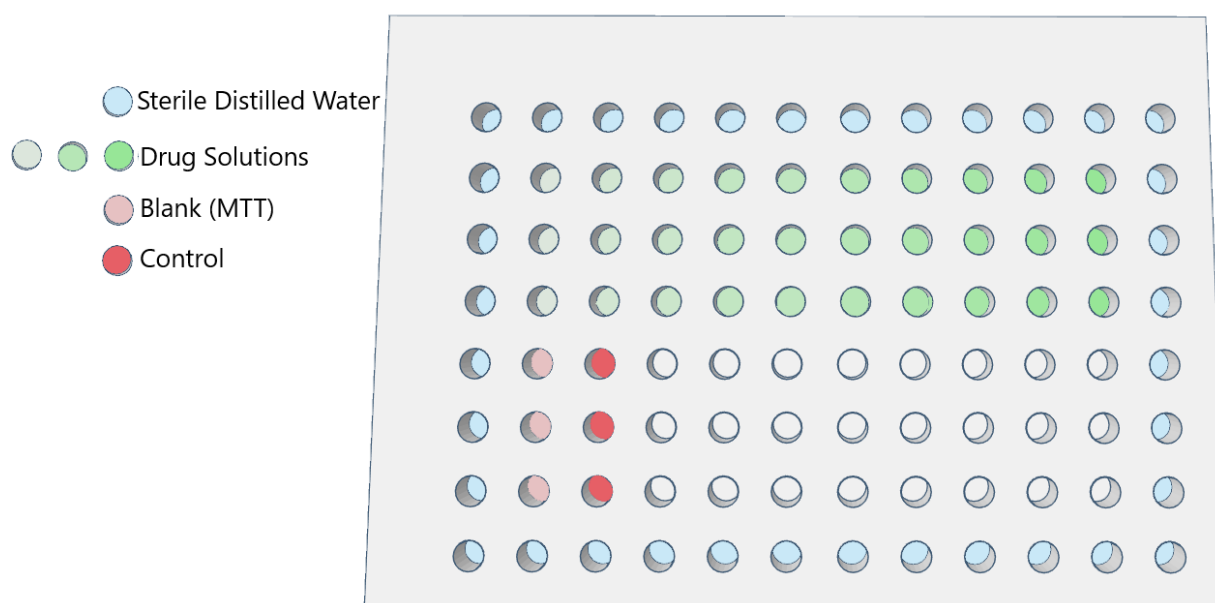


Figure 2.1: 96 well plate cytotoxicity assay layout.

For the MTT assay plates were incubated for 3 days. Following the incubation period, 20 µL of MTT solution (5 mg/mL in sterile PBS) was added to the test and control wells, the plates were then further incubated for 3 hours. The medium was then aspirated and replaced with 100 µL of DMSO to dissolve the formazan crystals formed. After 15 minutes, at room temperature a reading was performed using a FLUOstar Omega microplate reader (BMG Labtech, Durham, NC, USA) at 490 nM wavelength. Percentage viability of each drug solution was calculated, and a cytotoxicity graph was plotted.

For the IncuCyte assay the 96 well plates were transferred into an IncuCyte Zoom (Essen BioScience, Ann Arbor, Michigan, USA). Cells were then imaged at 3 hours intervals for 72 hours. The images were then analysed using IncuCyte zoom software (Essen BioScience, Ann Arbor, Michigan, USA); each image was masked, and the cell confluence data were used to calculate a % cell viability score (Equation 2-1).

For both MTT and IncuCyte assays cytotoxicity graphs were plotted and LogIC₅₀ values were determined.

Equation 2-1: Percentage cell viability

$$\% \text{ Cell Viability} = \frac{\text{Cell confluence score of drug treated wells}}{\text{Cell confluence score of control wells}} \times 100$$

2.3.8 Statistical Analysis

To determine the LogIC₅₀ and coefficient of determination (R²) values, Log inhibitor vs response analysis nonlinear regression (curve-fit) model with an upper limit set at Log 6 nM was performed by GraphPad Prism version 8.00 for Windows, GraphPad Software, La Jolla California USA, www.graphpad.com.

Statistical significance for the LogIC₅₀ data between the TC and BAT samples was assessed via unpaired student's *t* test method.

2.4 Results

2.4.1 Clinical demographics

The demographic characteristics of the glioma patient population are summarised in Figure

2.2. The cohort consisted of 8 males, 3 females and 1 unspecified with a median age at resection of 57.8 years. 8 of our glioma samples were grade IV GBM, 3 grade III glioma and 1 unspecified.

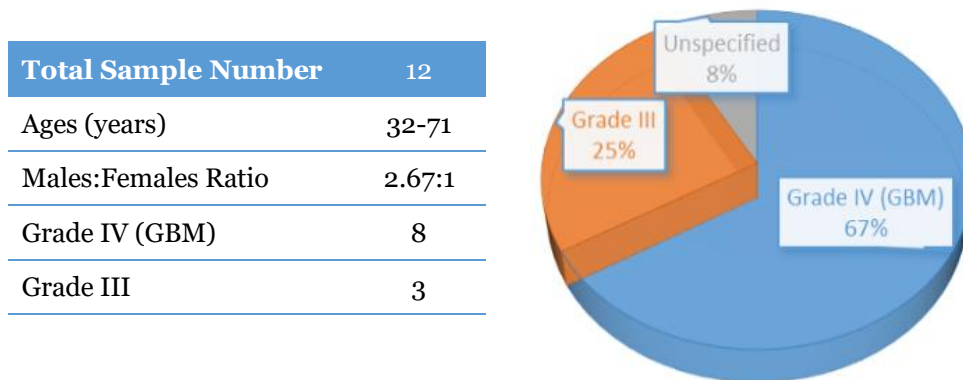


Figure 2.2: Summary of patient cohort and grade of GBM tumours.

The results of the genetic screening of aberrant protein expression status for IDH1, MGMT, ATRX and P53 in each glioma patient are shown in Table 2.3. IDH1, ATRX and p53 are all associated with growth control genes. Whereas MGMT is used to determine if treatment with DNA alkylating agents such as TMZ would be therapeutically beneficial. Recently groups have started to compare the molecular characterization of the tumour with patient response to treatment. Mutations in IDH1 and ATRX genes are associated with younger patients and usually result in a better response to treatment and improved OSR [5, 132, 301-303].

Discrepancy in the data for P53 mutation exists, with some studies reporting better survival in patients with P53 mutations while others have failed to find such correlation [132, 135, 304-306]. Also P-53 mutation impact on survival was often linked to other genetic phenotypes (e.g alternative lengthening of telomere) [304]. Hence within our study, data evaluation of P-53 mutation will not be discussed.

Table 2.3: The result of IDH1, ATRX, p53 and MGMT immunoexpression in tissue biopsy. N/A indicates that the data could not be determined

Patient	Tumour Grade	Mutation							
		IDH1		ATRX		P53		MGMT	
		Wild-type	Mutant	Wild-type	Mutant	Wild-type	Mutant	Methylated	Unmethylated
1	N/A	N/A		N/A		N/A		N/A	
2	IV	✓		✓		✓		✓	
3	IV	✓		✓		N/A		✓	
4	IV	✓		✓		N/A		Low level methylation	
5	III		✓	✓		N/A			✓
6	III		✓		✓		✓		✓
7	IV	N/A		✓		N/A			✓
8	IV	✓		✓		✓		N/A	
9	IV	✓		✓		✓		Low level methylation	
10	IV	✓		N/A		N/A			✓
11	IV	✓		✓			✓		✓
12	III	N/A			✓		✓		✓

2.4.2 Defining cell culture and test conditions

Optimisation of cell culture and drug screening assay test conditions was performed in order to generate reliable data that would represent clinical performance as accurately as possible, without compromising on efficiency in relation to cost, time and resources.

Culture media

Three culture media's were evaluated for their use in culturing the primary glioma cells: F-12 FBS serum based medium, F-12 serum-free based medium and neurobasal serum-free based medium. Culture medium suitability was examined in three test stages: 1) ability to sustain cellular viability 2) ability to support cellular growth at a feasible rate suitable for drug screening and 3) maintain the genetic profile of the original tumour cell population.

Immediately following tissue processing, glioma cells were cultured in flasks and growth medium was added. The culture mediums' ability to sustain the growth of primary glioma cells was assessed based on cell survival beyond passage two, or in the case of slow growing cells, survival for a one-month period. For each media the following cell survivals were demonstrated:

- F-12 serum-based medium: Twenty-two samples were grown in this media, of those, 21 samples survived beyond passage two.
- F-12 serum-free based medium: Three samples were grown and although very slow cellular growth was observed all three samples survived for a one-month incubation period.
- Neurobasal serum-free based medium: Seven samples were grown in this media and only four survived beyond passage two.

Based on the cell survival data, only F-12 serum-based and F-12 serum-free media were successful in sustaining the survival of the primary glioma cells. Therefore, it was decided to only assess cell growth in these two media types.

Cell growth was measured via cell counting. An equal number of primary cells from three TC samples were plated into two 75 cm³ flasks, with one flask grown in F-12 serum-based medium and the other in F-12 serum-free based medium. All other growth conditions were kept identical. The results demonstrated that cellular growth was 3 times faster in the F-12 serum based medium than the F-12 serum-free based medium (Figure 2.3). This growth rate deviation between the two media was observed across all three glioma samples which consist of different tumour grade and mutation status. In conclusion, the slow cellular growth demonstrated for the F-12 serum-free medium would not be suitable for cell cytotoxicity analysis as it would result in a significant waste of research resources, effort, time and money.

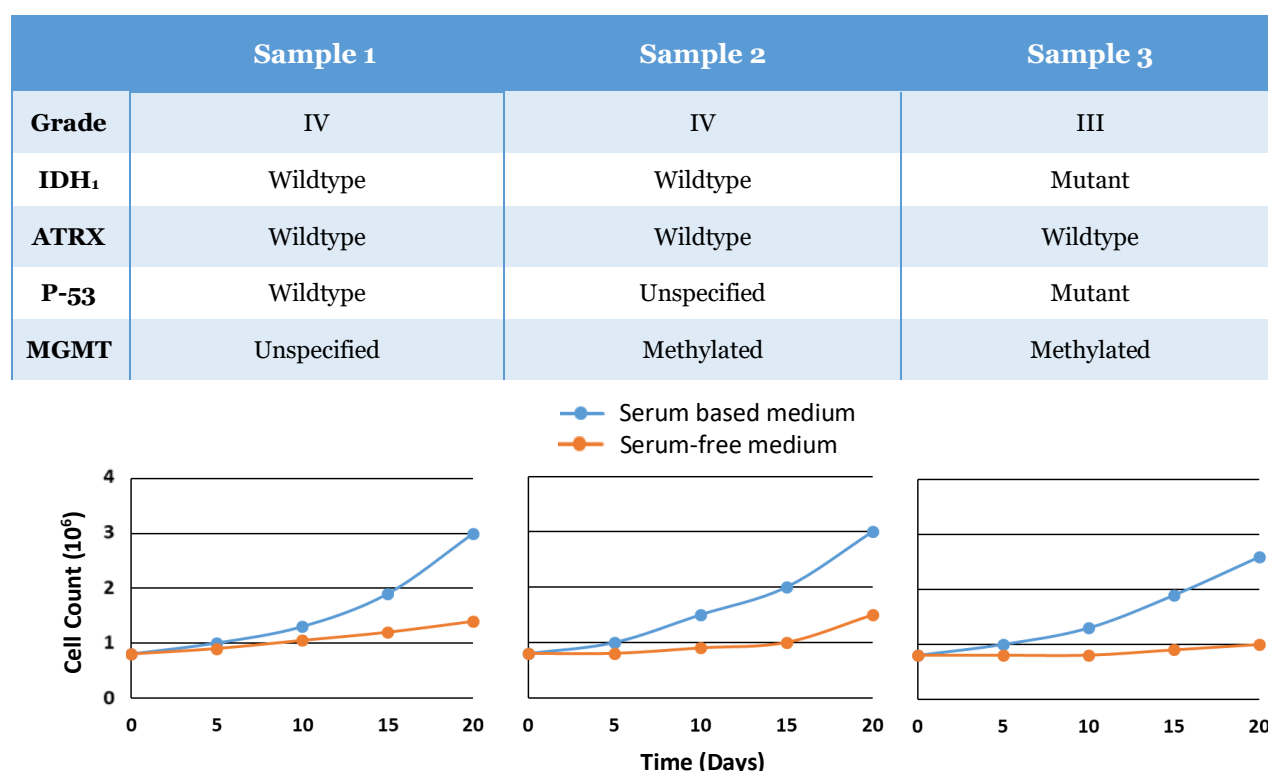


Figure 2.3: Cellular growth measurement of three glioma primary cells under either F-12 serum or F-12 serum-free culture medium.

To ensure that the F-12 serum-based medium maintained the genetic profile of the original tumour cell population, whole exome sequencing was performed on the patient's biopsy tissue and the cultured cells. The results demonstrate that the cultured cells share 93-98 % of the genomic variants from the original tumour tissue, thus this supports the clinical relevance of the cells cultured in serum based media (Table 2.4).

Table 2.4: Summary of whole exome sequencing of all non-somatic variants for patient's tissue biopsy and corresponding tissue cultured cells grown in serum-based medium.

Patient	Glioma Grade	Non-Somatic Tissue Biopsy Variants	Non-Somatic Tissue Cultured Cells Variants	Percentage Common-Post Filtration
2	IV	408	401	98.3
4	IV	429	420	98.0
5	III	404	376	93.1
6	III	463	470	98.5
7	IV	414	407	98.3
8	IV	450	427	94.9

Optimising cell culture cytotoxicity assay

Initial method refinement was performed to ensure the accurate measurement of drug effectiveness on killing the cancer cells. This was important because many different aspects in tissue culture could lead to cell death such as nutrient depletion, excessive release of cellular metabolites and media evaporation, all of which can prevent accurate assessment of drug cytotoxicity.

In a 24 hour cell cytotoxicity assay, it is common practice to plate cells at 10,000 cells/well density. However, because of IRN's S-phase specific cancer targeting mechanism of action (Chapter one, 1.4.1 Irinotecan) longer incubation period is required for the cells to reach S-phase [200, 201, 307]. Hence for an extended incubation period assay a high initial cell density may lead to growth plateau and cellular death during the assay. To assess this, a cell survival/growth assay was performed. Cells were plated at 2000, 4,000, 10,000 and 20,000 cells/well, in triplicate, within a 96 well plate (Figure 2.4). For each well cellular confluence and medium colour change were observed. Following a 16 day incubation period all plated wells reached growth plateau and medium colour changed from red to pale orange,

indicating nutrient depletion and release of cellular metabolites [308]. However, the 10,000 and 20,000 cells/well, reached growth plateau within less than 7-days conveying that both are not suitable for the extended period assay. The 2,000 and 4,000 cells/well exhibited a more extended growth period with an initial cell confluence of 20 and 40% respectively. From this result the 4000 cells/well initial seed density was selected.

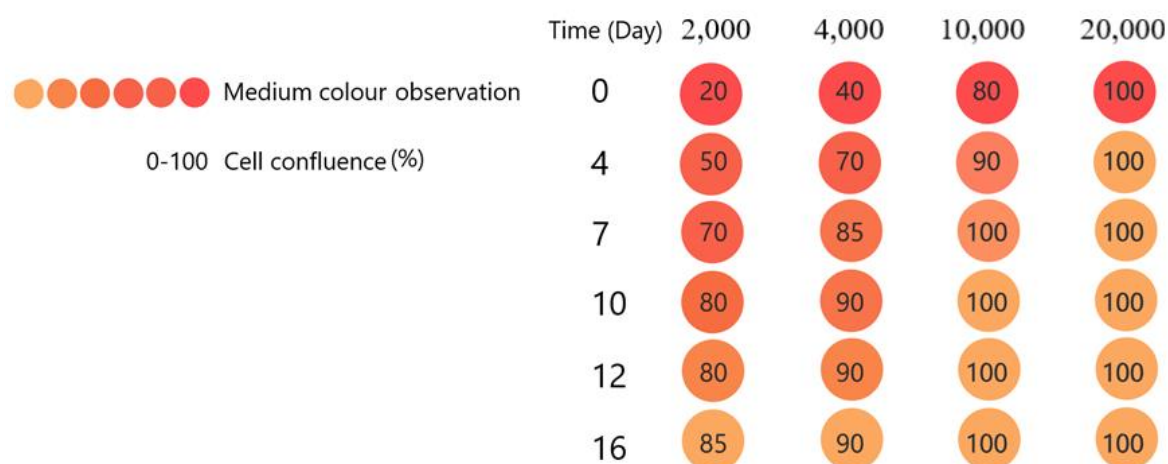


Figure 2.4: Summary of cell survival assay for MTT method validation. Glioma cells were seeded in a 96-well plate at 2000, 4,000, 10,000 and 20,000 cells/well density. Cellular confluence and medium colour change are observed over a 16-day incubation period.

Another concern during the extended incubation period is fluid evaporation. Media evaporation during the assay could lead to cell death affecting the accuracy of the cytotoxicity results [309]. To reduce media evaporation only non-perimeter wells were used as working wells for the assay. 250 μ L of SDW was added to the perimeter wells to reduce evaporation. Figure 2.5 shows the effect of this method on increasing the correlation of determination values (R^2) for the LogIC₅₀ curve, indicating a better fit for the log inhibitor vs response nonlinear regression analysis model.

During pre-method development the working wells suffered from significant media evaporation which resulted in higher cell viability data variability. For both day 3 and 5 analysis, the pre-method development assay had data with wide error bars and R^2 values, resulting in a cytotoxicity profile that was too ambiguous for an accurate measurement of the LogIC₅₀ values. In an effort to minimize these variations the MTT assay was refined resulting in lower media evaporation and improved results.

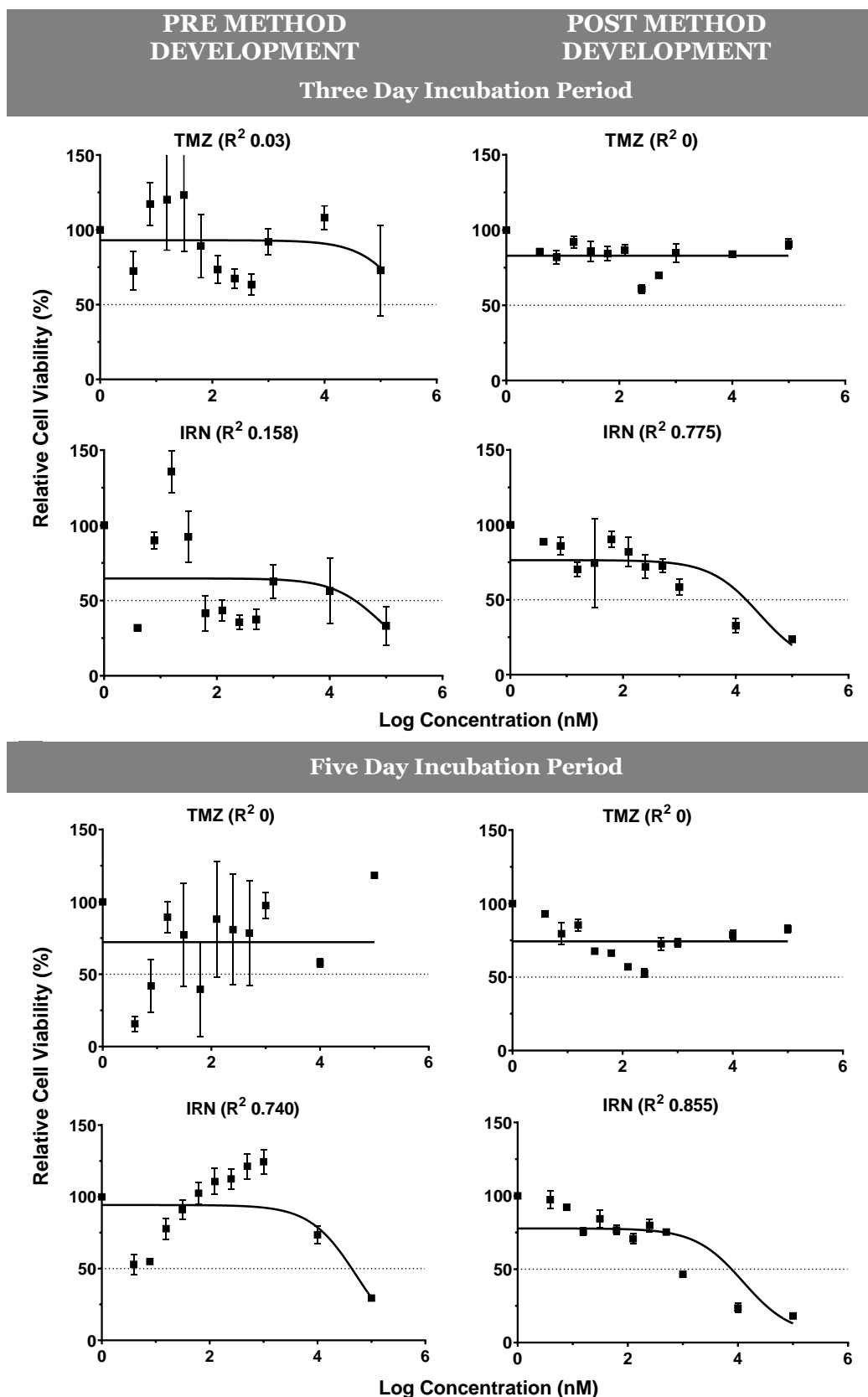


Figure 2.5: Patient 1 TC sample MTT cell viability graphs prior to and following method development. In pre-method development all wells within a 96 well-plate were used for the assay. In post-method development only non-perimeter wells were used, perimeter wells were filled with 250 μ L SDW. \pm SEM is indicated as error bars

2.4.3 Cell metabolism assay (MTT)

To investigate whether single drug treatment would be effective against gliomas, ten patient derived primary cells were used to perform a 3-day MTT assay. A total of nine drugs were investigated: TMZ, IRN, PTV, DSF, CoGlu, CAP, CXB, ITZ and TCL. For simplicity and clinical relevance, patient samples were grouped into their distinct tumour grade (IV, III). The cytotoxicity data was presented for each drug individually and the patients collectively. For each drug a cytotoxicity graph was plotted and LogIC₅₀ values calculated. Drug effectiveness was ranked into four distinctive categories; high (LogIC₅₀= 0-3 nM), medium (LogIC₅₀= 3-4 nM), low (LogIC₅₀= 4-5 nM) and ineffective if no LogIC₅₀ value was achieved, these four categories were chosen arbitrary to reduce ambiguity during data discussion and simplify comparison between different dataset. An overview of results from the 10 patient samples is provided within section 2.5.3 MTT Data analysis and visualisation. Furthermore, a full LogIC₅₀ data summary is presented in thesis appendix A.

Patients' drug response- tumour core (TC)

Within this section the cytotoxicity data for each drug against the TC samples were assessed. Those drugs that demonstrate enhanced potency were discussed in more detail.

Grade IV (glioblastoma)

Temozolomide

No grade IV patients responded to TMZ (Figure 2.6), although half of the tested samples had methylated MGMT: patients 2, 3, 4 & 9. This could be due to the development of chemoresistance from previous alkylating drug therapy or that for TMZ to be effective higher dosage of drug is needed. Within the literature TMZ IC₅₀ values for 24-72 hour cytotoxicity assay are often reported within the range of 200-900 μ M, i.e at least double our tested drug concentration [310-313]. Hence for TMZ to be effective higher dosage would be required, way beyond our assessed concentration. As we are aiming to develop a localised chemotherapeutic treatment that is safe, with minimal local toxicity, we have not assessed the cytotoxicity of the drugs at greater than 100 μ M.

Two cytotoxicity profiles that are worth noting are patient 9 and 10 (Figure 2.6). At low concentrations, less than Log 3 nM, low percentage cell viability values were achieved.

However, with poor LogIC₅₀ curve R² values the cytotoxicity profile was too ambiguous for an accurate measurement of a LogIC₅₀ value, thus TMZ was deemed to be ineffective for both patient samples.

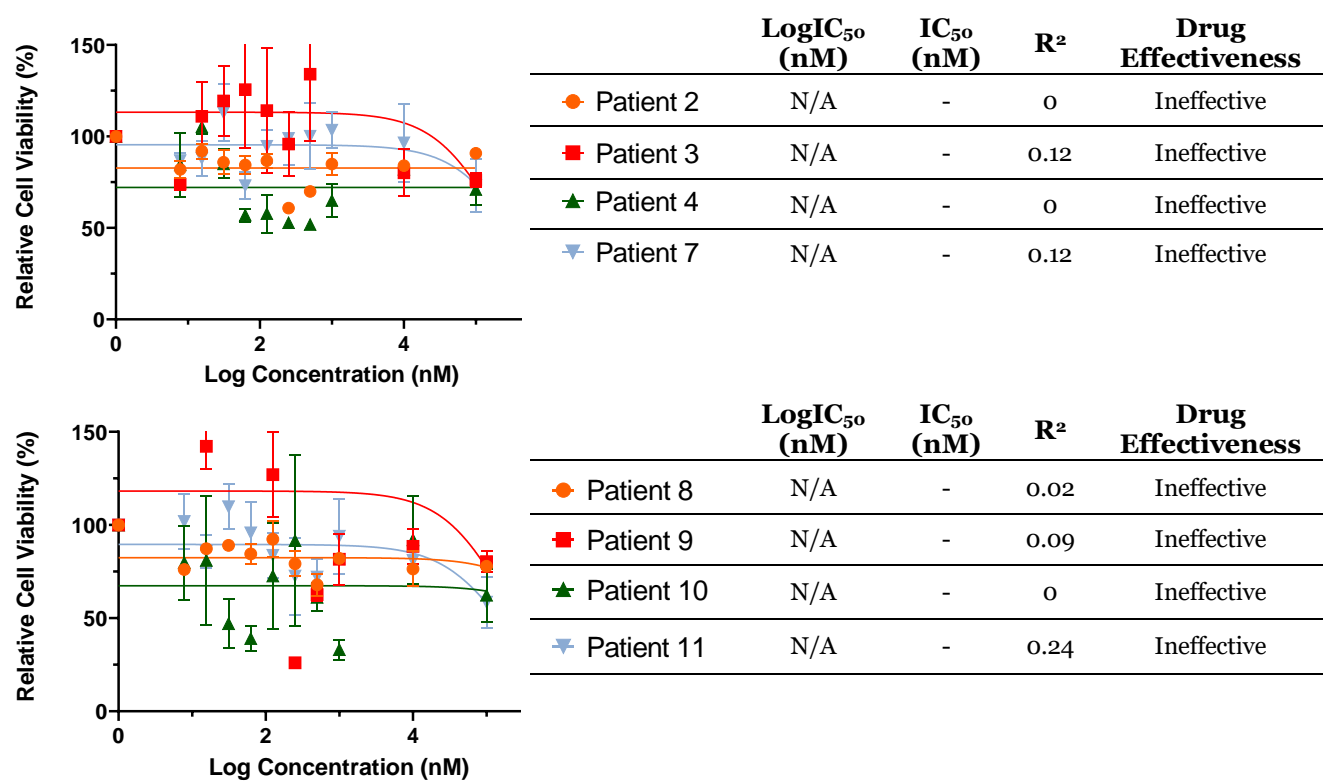


Figure 2.6: LogIC₅₀ cytotoxicity curves and data table of TMZ chemotherapy tested against primary cells. Eight number assigned grade IV TC samples were evaluated using MTT assay. ± SEM is indicated as error bars.

Irinotecan

Seven out of the eight grade IV patient samples demonstrated effectiveness at high drug concentration with LogIC_{50} values between 4.24 and 4.87 nM (Figure 2.7). Only patient 3 was ineffective as although its cell viability value at Log 5 nM was 40%, low R^2 (0.2) value was achieved demonstrating poor goodness of fit for the Log inhibitor (drug concentration) vs response (cell viability) nonlinear regression analysis model, making it difficult to estimate the LogIC_{50} (Figure 2.7). Hence, IRN monotherapy was effective for the majority of patients, however high doses are required.

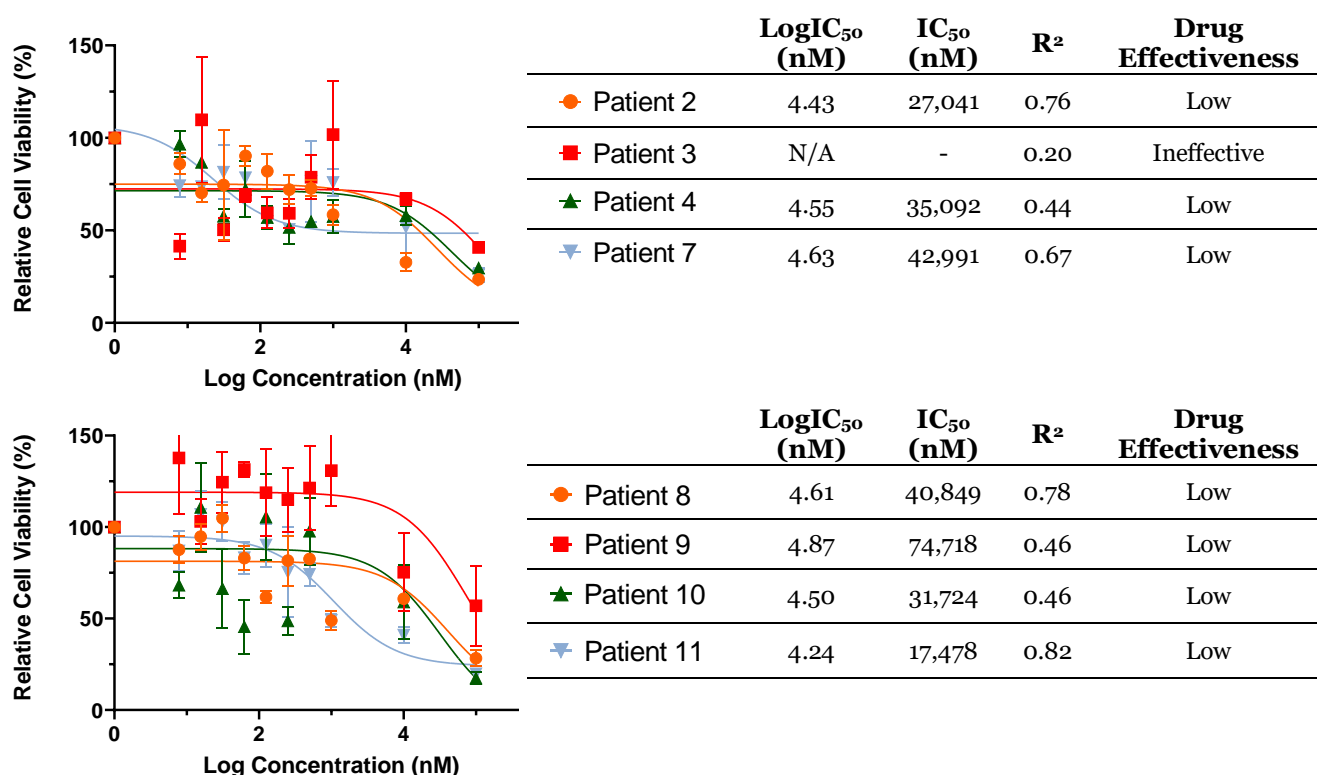


Figure 2.7: LogIC_{50} cytotoxicity curves and data table of IRN drug tested against primary cells. Eight number assigned grade IV TC samples were evaluated using MTT assay. \pm SEM is indicated as error bars.

Pitavastatin

All grade IV patient samples responded to PTV (Figure 2.8). Compared to other drug treatments, PTV achieved the best response with drug effectiveness ranging from high to low. Patients 10 and 11 demonstrated high drug effectiveness with LogIC_{50} values of 2.67 and 1.98 nM, respectively, whilst patients 7 and 8 achieved medium effectiveness with LogIC_{50} values of 3.20 and 3.22 nM, respectively (Figure 2.8). Finally, patient samples 3, 4 and 9, demonstrated low drug effectiveness with LogIC_{50} values between 4.72 and 4.99 nM (Figure 2.8).

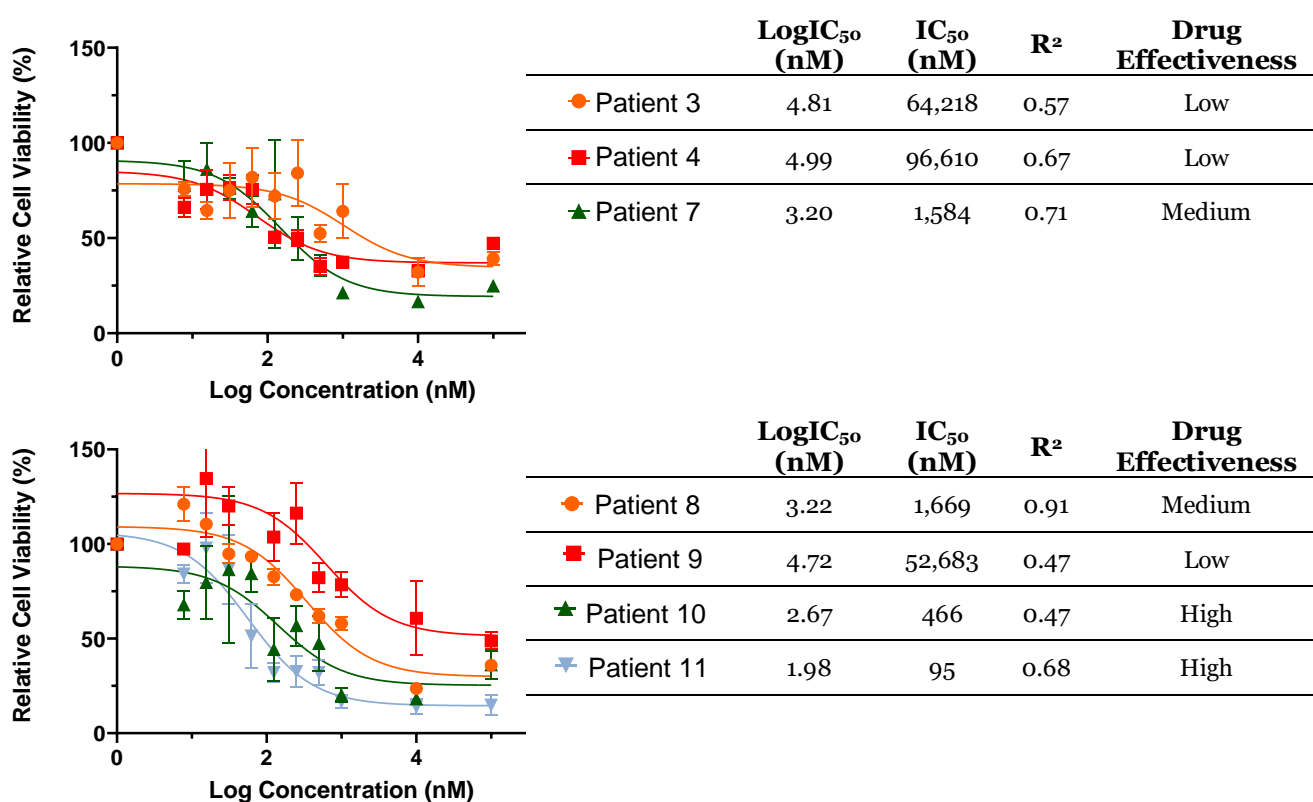


Figure 2.8: LogIC_{50} cytotoxicity curves and data table of PTV drug tested against primary cells. Seven number assigned grade IV TC samples were evaluated using MTT assay. \pm SEM is indicated as error bars.

Disulfiram

DSF was effective against two grade IV patient samples, 8 and 9, with LogIC₅₀ values of 4.83 and 3.54 nM, respectively (Figure 2.9). Additionally, both samples achieved high R² values (> 0.7) demonstrating that the cell viability data is tightly clustered around the cytotoxicity curve, enabling to predict the LogIC₅₀ values more precisely (Figure 2.9).

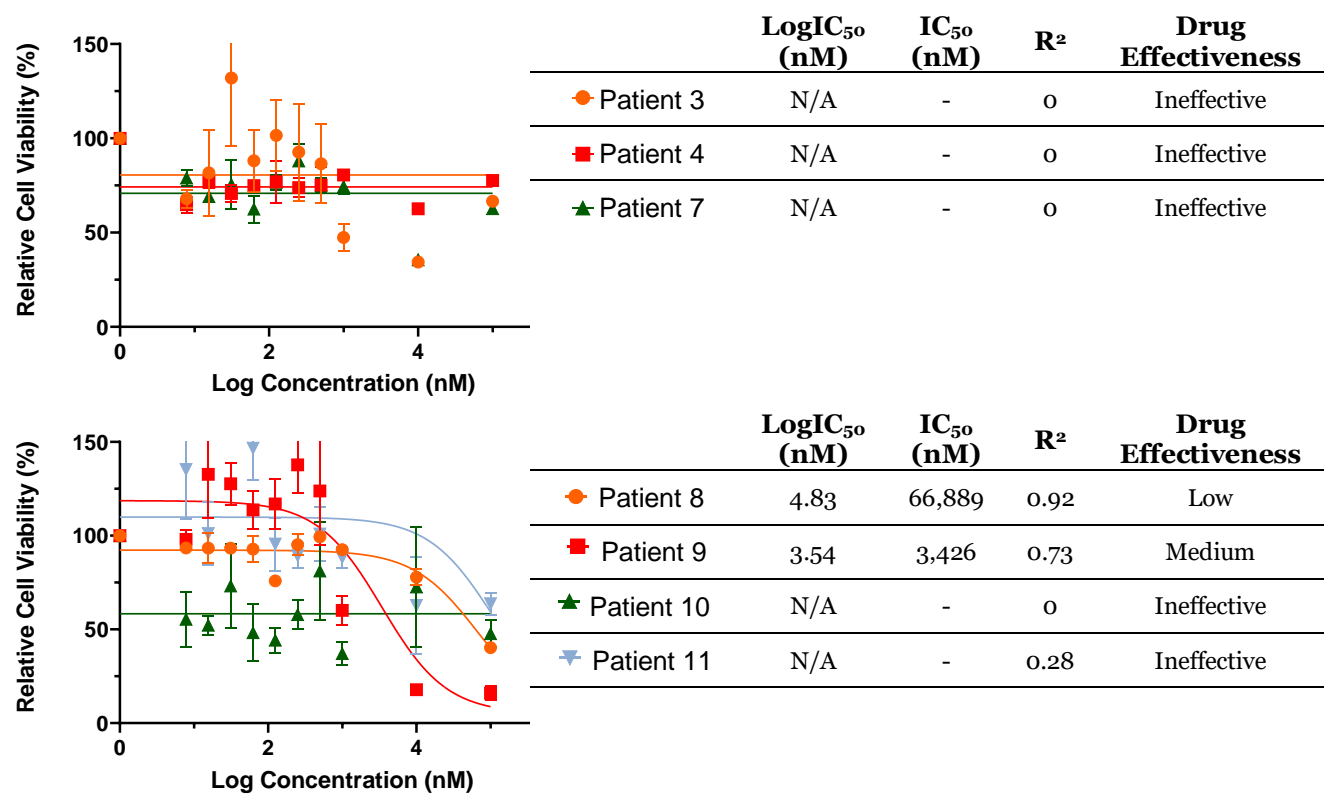


Figure 2.9: LogIC₅₀ cytotoxicity curves and data table of DSF drug tested against primary cells. Seven number assigned grade IV TC samples were evaluated using MTT assay. ± SEM is indicated as error bars.

Copper Gluconate

CoGlu was shown to be largely ineffective against grade IV tumours, with only one sample, patient 4, responding at high drug concentration with a LogIC_{50} value of 4.95 nM (Figure 2.10).

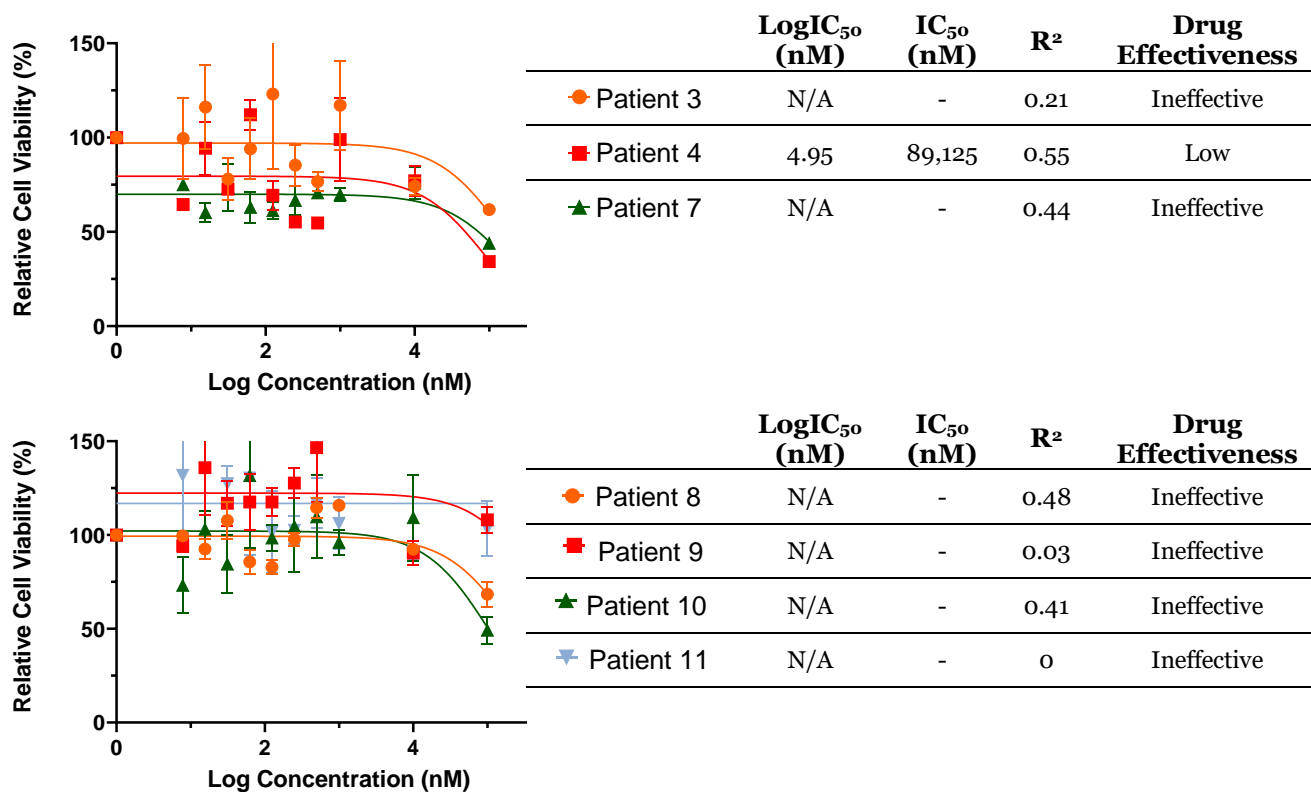


Figure 2.10: LogIC_{50} cytotoxicity curves and data table of CoGlu drug tested against primary cells. Seven number assigned grade IV TC samples were evaluated using MTT assay. \pm SEM is indicated as error bars.

Captopril

None of the seven grade IV patient samples evaluated were effective against CAP treatment

(Figure 2.11).

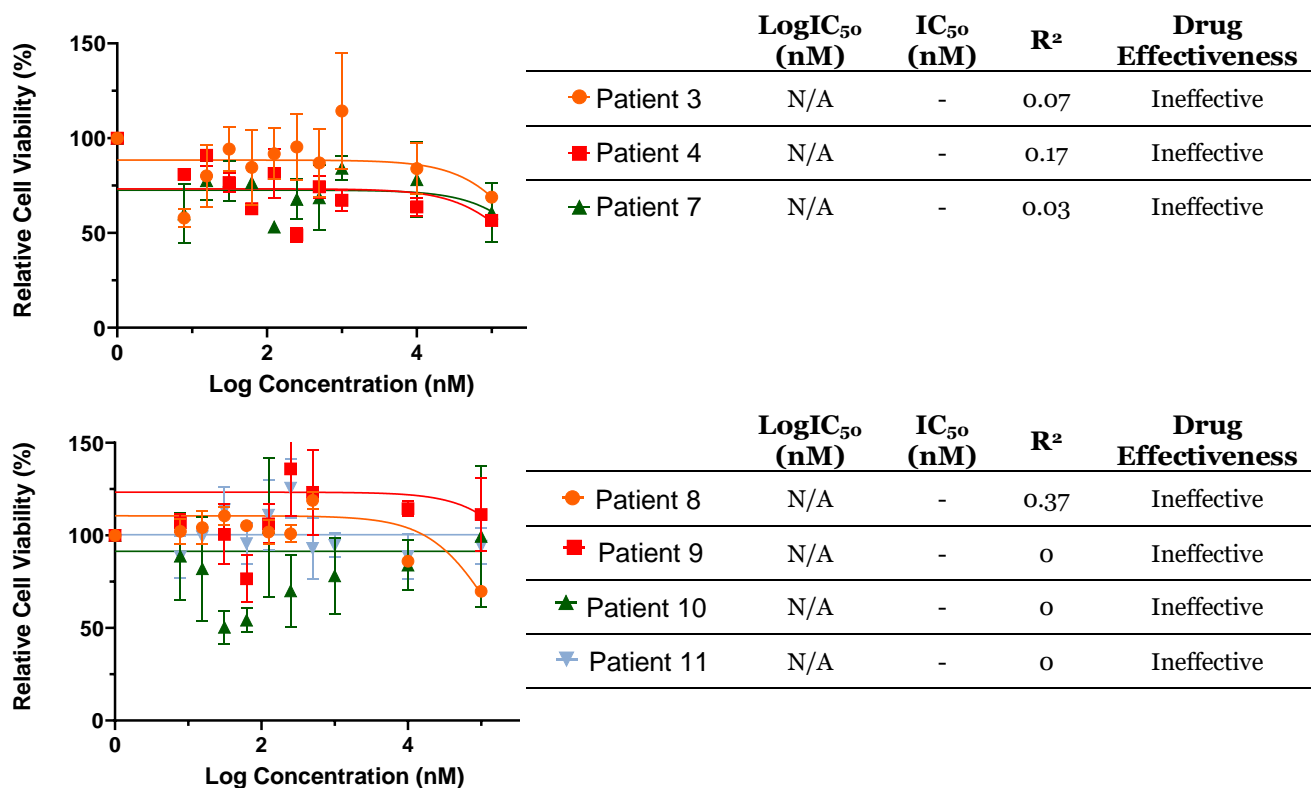


Figure 2.11: LogIC₅₀ cytotoxicity curves and data table of CAP drug tested against primary cells. Seven number assigned grade IV TC samples were evaluated using MTT assay. ± SEM is indicated as error bars.

Celecoxib

Six out of the seven grade IV patient samples responded to CXB treatment at high drug concentrations with LogIC_{50} values between 4.17 and 4.87 nM (Figure 2.12). At Log 5 nM all samples had a large decrease in the cell viability value suggesting that at high dose CXB is highly effective (Figure 2.12). Additionally, the LogIC_{50} vs response curves were consistent in shape, with relatively good R^2 values (> 0.7), demonstrating that CXB induced a consistent response across all samples.

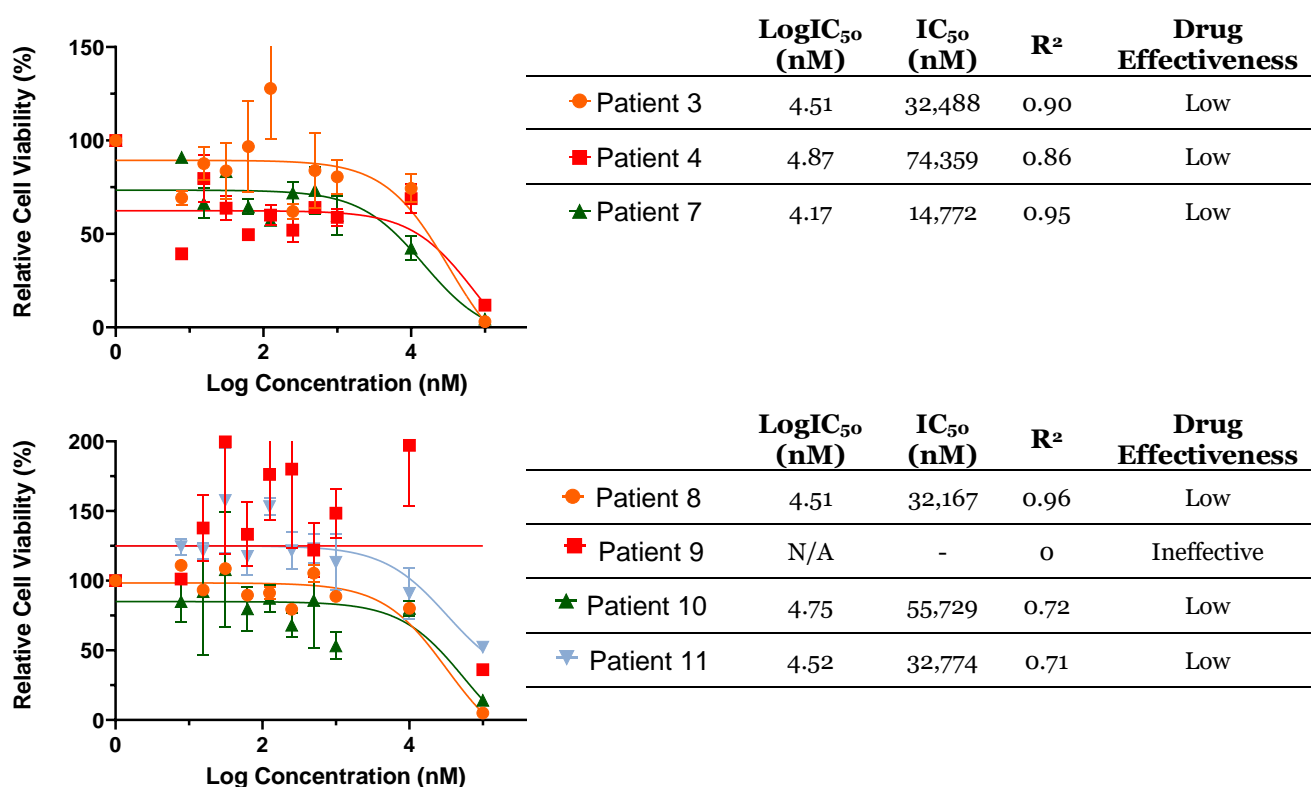


Figure 2.12: LogIC_{50} cytotoxicity curves and data table of CXB drug tested against primary cells. Seven number assigned grade IV TC samples were evaluated using MTT assay. \pm SEM is indicated as error bars.

Ticlopidine

None of the grade IV samples responded to TCL treatment (Figure 2.13).

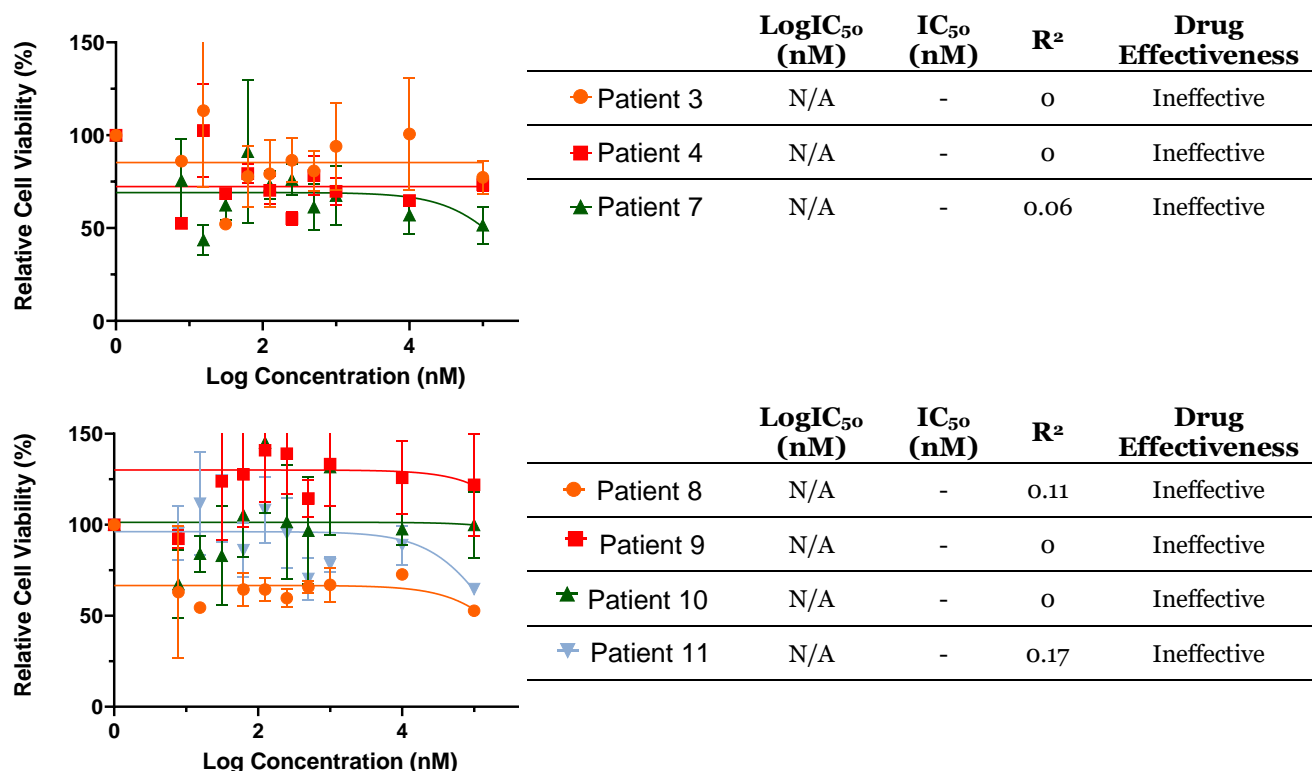


Figure 2.13: LogIC₅₀ cytotoxicity curves and data table of TCL drug tested against primary cells. Seven number assigned grade IV TC samples were evaluated using MTT assay. ± SEM is indicated as error bars.

Itraconazole

Only two grade IV samples were effective against ITZ, patients 7 and 8, with LogIC₅₀ values of 4.29 and 4.33 nM, respectively (Figure 2.14).

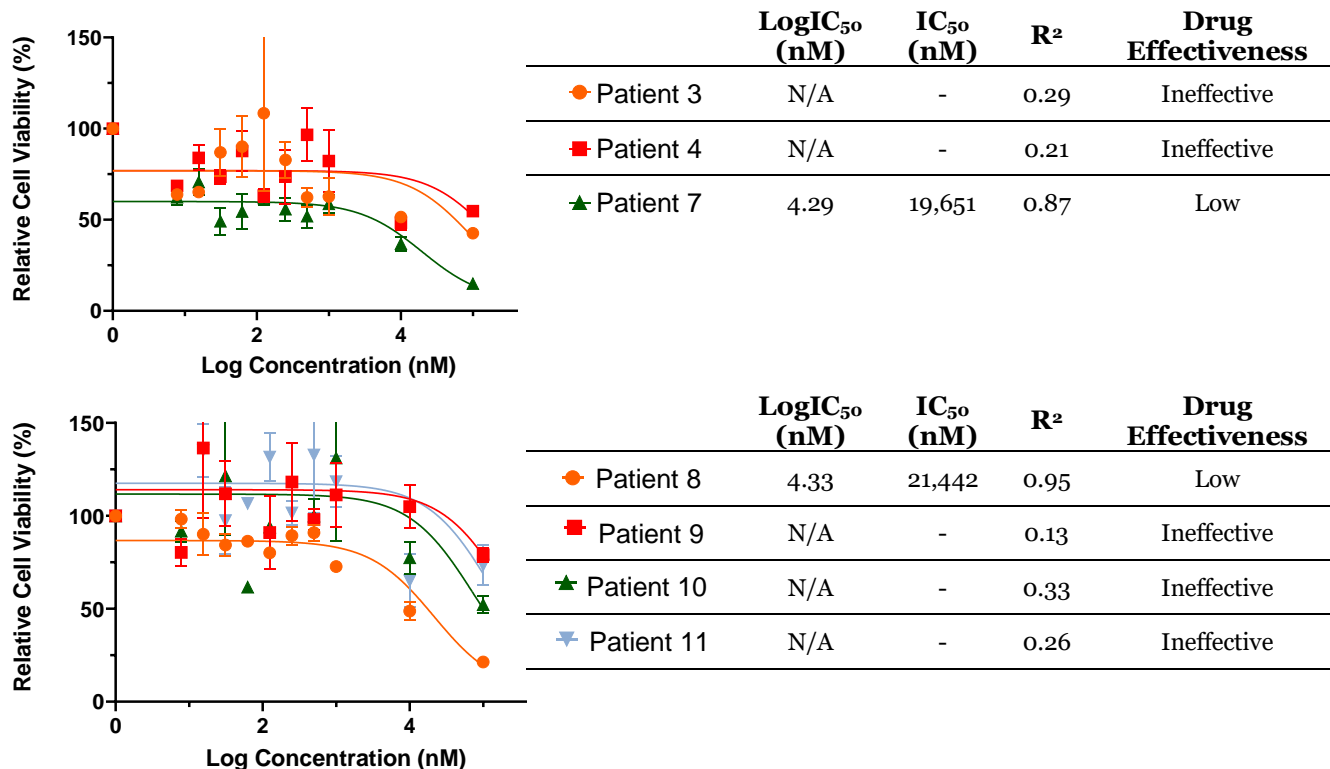


Figure 2.14: LogIC₅₀ cytotoxicity curves and data table of ITZ drug tested against primary cells. Seven number assigned grade IV TC samples were evaluated using MTT assay. ± SEM is indicated as error bars.

Grade III Temozolomide

TMZ demonstrated no response against both grade III samples (Figure 2.15). it is noteworthy however that both samples are MGMT unmethylated, hence resistance to TMZ treatment was anticipated (2.4.1 clinical demographics, Table 2.3)

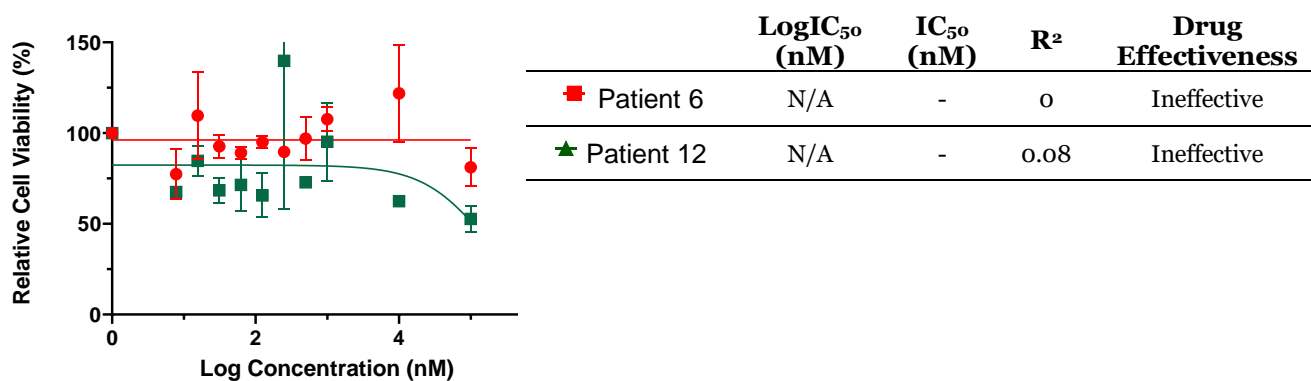


Figure 2.15: LogIC₅₀ cytotoxicity curves and data table of TMZ chemotherapy tested against primary cells. Two number assigned grade III TC samples were evaluated using MTT assay. ± SEM is indicated as error bars.

Irinotecan

IRN was effective against both grade III glioma samples with LogIC_{50} values of 4.51 and 4.64 nM for patient 6 and 12, respectively. The cytotoxicity curves were also highly correlated with R^2 values above 0.7 demonstrating good goodness of fit for the Log inhibitor (drug concentration) vs response (cell viability) nonlinear regression analysis model (Figure 2.16) .

Both patient 6 and 12 tumour samples, as specified by their IDH1 and ATRX protein expression status as well as tumour grade (2.4.1 Clinical demographics, Table 2.3), are known to be less aggressive than our other tested patient derived samples. However according to our data, response to treatment between both grade III and IV sample groups were equivalent (LogIC_{50} values between 4 and 5 nM), demonstrating no variation in response to IRN treatment between the different tumour grades and protein expression status.

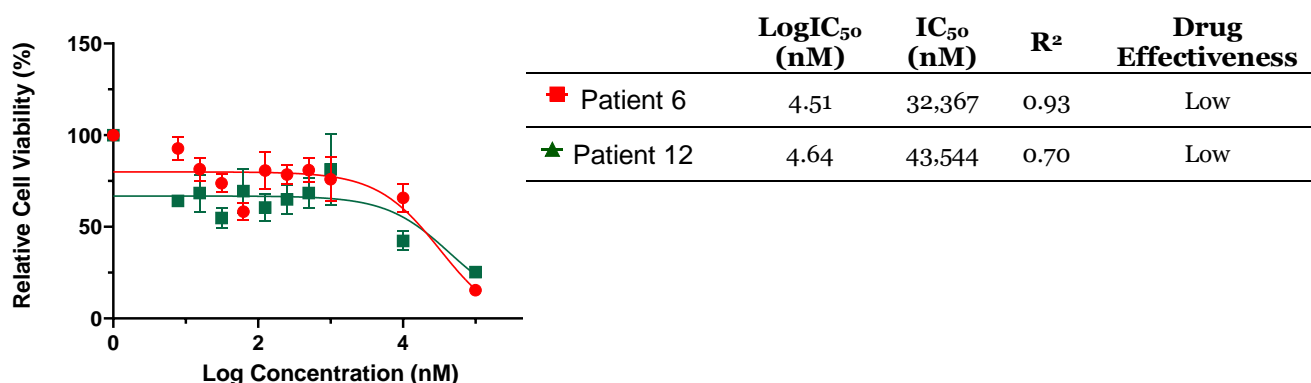


Figure 2.16: LogIC_{50} cytotoxicity curves and data table of IRN drug tested against primary cells. Two number assigned grade III TC samples were evaluated using MTT assay. \pm SEM is indicated as error bars.

Pitavastatin

Both grade III patient samples, 6 and 12, responded to PTV with LogIC_{50} values of 4.75 and 2.63 nM, respectively (Figure 2.17). Grade III cytotoxicity data were consistent to that of grade IV as PTV was shown to be effective across both sample groups. Moreover, although both tumour grade III and IV consisted of opposing IDH1 and ATRX protein expression status (2.4.1 Clinical demographics, Table 2.3), no variation in drug response was detected.

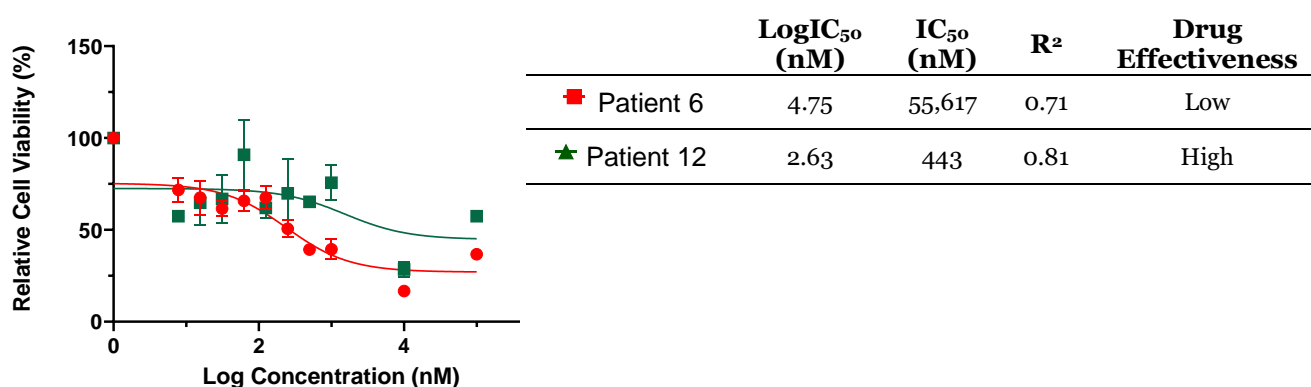


Figure 2.17: LogIC_{50} cytotoxicity curves and data table of PTV drug tested against primary cells. Two number assigned grade III TC samples were evaluated using MTT assay. \pm SEM is indicated as error bars.

Disulfiram

Both patient 6 and 12 samples achieved low cell viability scores (< 28 %) at Log 4 nM, however the LogIC₅₀ curves R² values were zero, demonstrating poor goodness of fit for the Log inhibitor (drug concentration) vs response (cell viability) nonlinear regression analysis model. Therefore, DSF was deemed ineffective as the cytotoxicity profiles were too ambiguous for an accurate measurement of a LogIC₅₀ value (Figure 2.18).

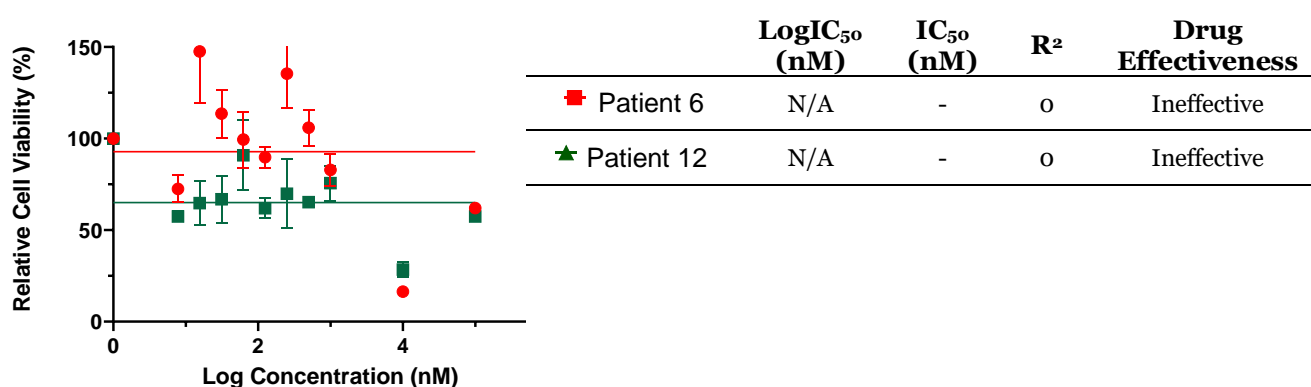


Figure 2.18: LogIC₅₀ cytotoxicity curves and data table of DSF drug tested against primary cells. Two number assigned grade III TC samples were evaluated using MTT assay. ± SEM is indicated as error bars.

Copper Gluconate

Two grade III patient samples were evaluated, CoGlu was effective against one, patient 6 with a LogIC₅₀ value of 4.51 nM (Figure 2.19). Across the majority of both Grade III and IV samples cytotoxicity data, a slight decrease in the cell viability values were observed at Log 5 nM. This demonstrates that although CoGlu was generally ineffective, a small response was achieved at high dose with comparable results between the different tumour grades.

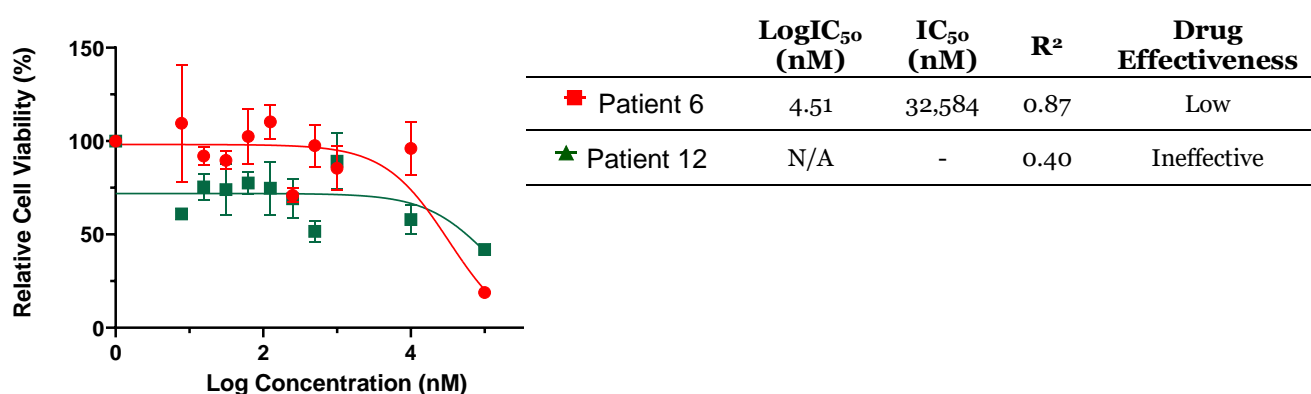


Figure 2.19: LogIC₅₀ cytotoxicity curves and data table of CoGlu drug tested against primary cells. Two number assigned grade III TC samples were evaluated using MTT assay; Patient 6 and 12. ± SD is indicated as error bars.

Captopril

Two grade III patient samples were evaluated and neither responded to CAP (Figure 2.20).

Both grade III and IV LogIC₅₀ curves data were similar even though both sample groups consist of opposing IDH1 and ATRX protein expression status (2.4.1 Clinical demographics, Table 2.3).

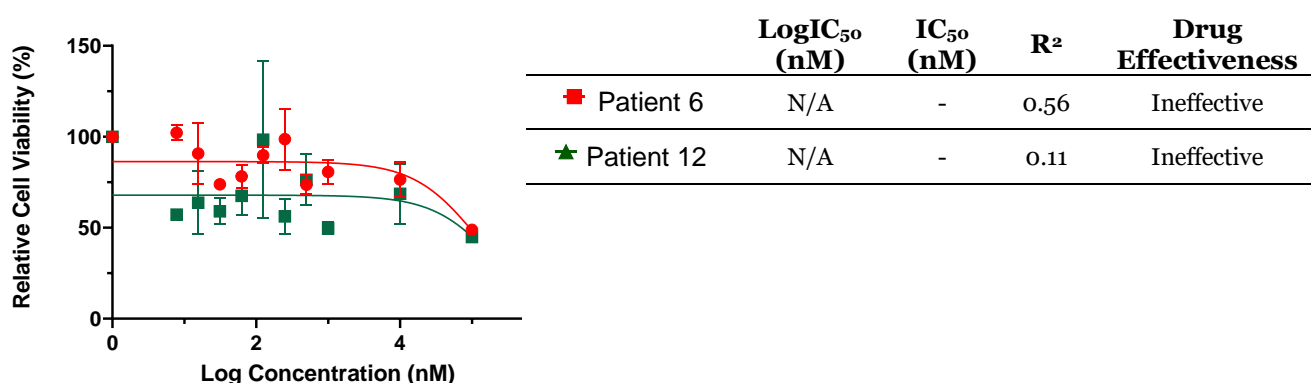


Figure 2.20: LogIC₅₀ cytotoxicity curves and data table of CAP drug tested against primary cells. Two number assigned grade III TC samples were evaluated using MTT assay. \pm SEM is indicated as error bars.

Celecoxib

Both grade III patient samples, 6 and 12, demonstrated effectiveness at high drug concentration with LogIC₅₀ values of 4.69 and 4.72 nM, respectively (Figure 2.21). This response to CXB treatment is consistent to that of grade IV samples, as at Log 5 nM a large decrease in the cell viability values were observed across both tumour grades (Figure 2.21). Thus, CXB drug treatment has proven to be highly effective at Log 5 nM.

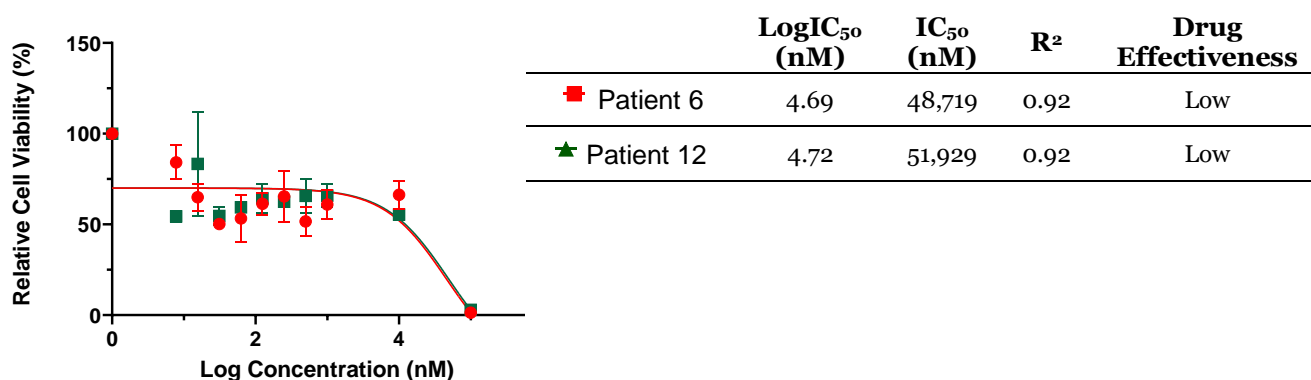


Figure 2.21: LogIC₅₀ cytotoxicity curves and data table of CXB drug tested against primary cells. Two number assigned grade III TC samples were evaluated using MTT assay. \pm SEM is indicated as error bars.

Ticlopidine

None of the grade III patient samples responded to TCL treatment. (Figure 2.22).

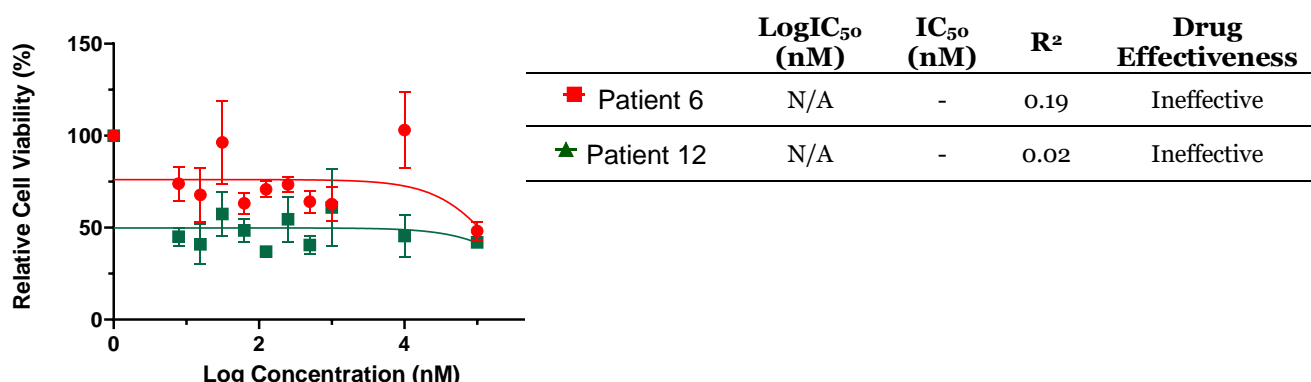


Figure 2.22: LogIC₅₀ cytotoxicity curves and data table of TCL drug tested against primary cells. Two number assigned grade III TC samples were evaluated using MTT assay. ± SEM is indicated as error bars.

Itraconazole

None of the grade III patient samples were potent against ITZ (Figure 2.23). similar to the grade IV samples, a slight decrease in the cell viability values occurred at the higher Log 4 and 5 nM drug concentrations. This shows that although ITZ was generally ineffective, a small response was achieved at high dose.

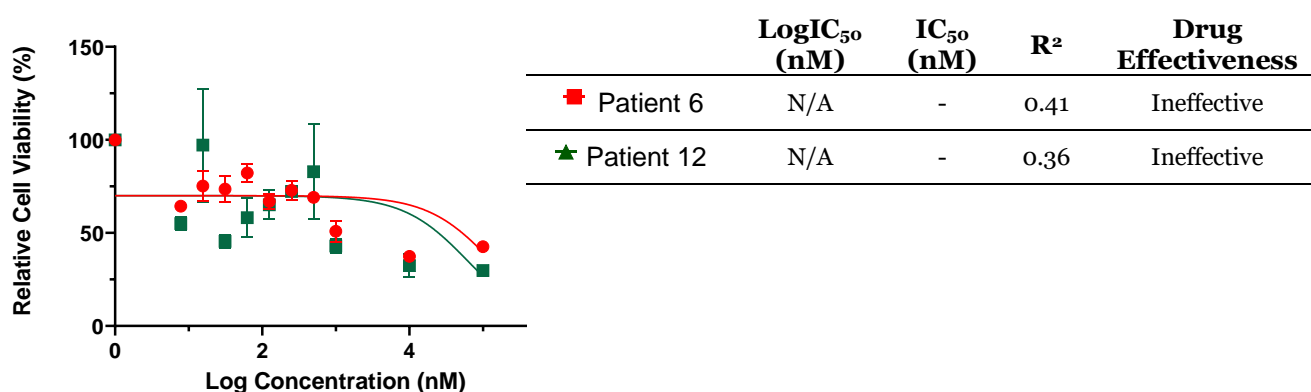


Figure 2.23: LogIC₅₀ cytotoxicity curves and data table of ITZ drug tested against primary cells. Two number assigned grade III TC samples were evaluated using MTT assay. ± SEM is indicated as error bars.

Patients' drug response- brain around tumour (BAT)

Following a craniotomy, the TC is often completely removed but the BAT is left behind. This residual tumour is subsequently targeted via chemotherapy and radiation; however, it eventually forms resistance resulting in recurrence of a chemo resistant tumour. To investigate whether a low dose single drug treatment (< 100 μM) would be effective against residual tumour, four patients derived BAT cells were used to perform a 3-day MTT assay.

Within this section the cytotoxicity data of each drug against the BAT samples were evaluated. Due to the difficulty in culturing grade III BAT samples up to a sufficient cell number for MTT assay use, only grade IV samples were used.

Grade IV (glioblastoma)

Temozolomide

Four patient derived BAT samples were assessed and only one, patient 8, demonstrated a response at high drug concentration with LogIC₅₀ value of 2.86 nM (Figure 2.24).

Compared to the same patients TC samples, equivalent response to TMZ treatment were obtained for patients 4 and 9, however, patient 8 differed, with TMZ being ineffective against the TC but highly effective against the BAT (Figure 2.24). This difference could be due to intratumour heterogeneity between the separate tumour fragments [146, 161, 283, 314, 315].

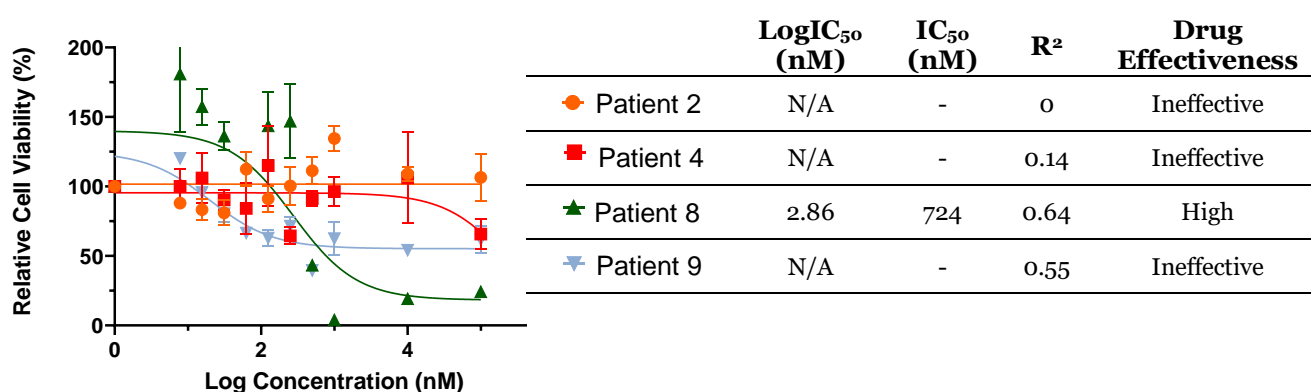


Figure 2.24: LogIC₅₀ cytotoxicity curves and data table of TMZ chemotherapy tested against primary cells. Four number assigned grade IV BAT samples were evaluated using MTT assay. ± SEM is indicated as error bars.

Irinotecan

No grade IV BAT samples responded to IRN (Figure 2.25). This cytotoxicity data was inconsistent to that of the same patient's TC samples, because for the TC IRN was effective at high dose with LogIC_{50} values between 4.43 and 4.87 nM. This demonstrates that IRN was less potent against the BAT, which is surprising as IRN works during the S phase of the cell cycle and should thus be equally effective across the different tumour fragments. Furthermore, as the BAT tissue is the part of the tumour that is growing and proliferating we would expect those drugs that target the cell cycle to be more effective [200, 201, 316].

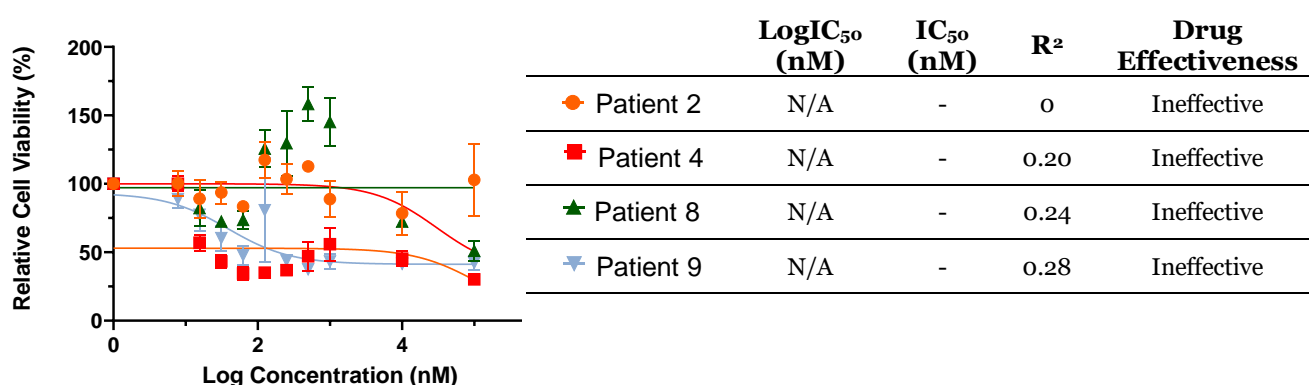


Figure 2.25: LogIC_{50} cytotoxicity curves and data table of IRN drug tested against primary cells. Four number assigned grade IV BAT samples were evaluated using MTT assay. \pm SEM is indicated as error bars.

Pitavastatin

Four patient derived BAT samples were assessed and only two were effective with a LogIC_{50} value of 4.61 and 4.84 nM for patients 8 and 9, respectively (Figure 2.26).

When compared to the corresponding TC samples, PTV was less effective against the BAT because the TC had LogIC_{50} values of 4.99, 3.22 and 4.72 nM, while the BAT's were >5, 4.61 and 4.84 nM for patients 4, 8 and 9, respectively.

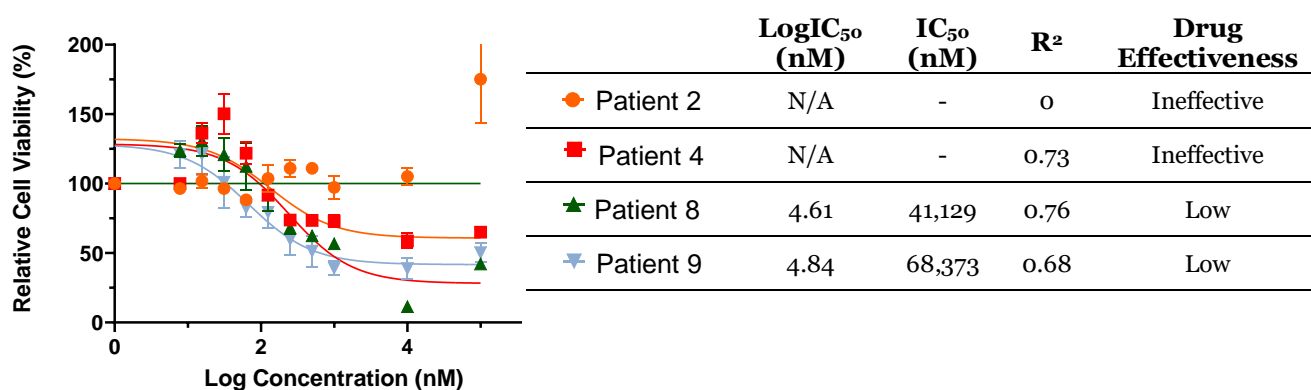


Figure 2.26: LogIC_{50} cytotoxicity curves and data table of PTV drug tested against primary cells. Four number assigned grade IV BAT samples were evaluated using MTT assay. \pm SEM is indicated as error bars.

Disulfiram

Four patient samples were evaluated and only one, patient 9, was effective with a LogIC_{50} value of 3.30 nM (Figure 2.27). Comparing this data to the corresponding TC samples reveal that for patients 4 and 9 equivalent drug response were obtained, while for patient 8, a difference was found as DSF was effective at high dose against the TC, with a LogIC_{50} value of 4.83 nM, but was ineffective against the BAT. Nevertheless, at high drug concentrations a reduction in the cell viability values were detected with Log 4 and 5 nM cell viabilities reaching 57 and 89 %, respectively (Figure 2.27).

Thus, the overall drug cytotoxicity data demonstrates that variation in the response between the different tumour fragments was small.

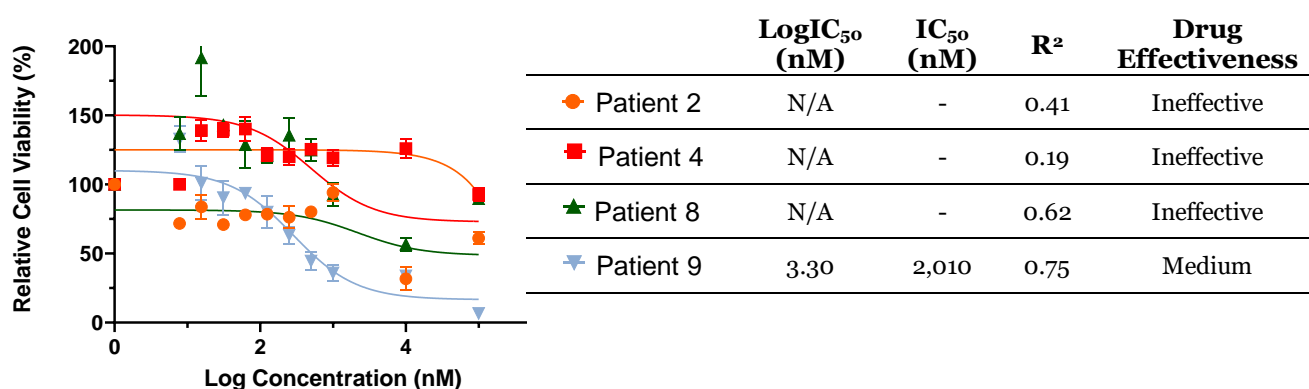


Figure 2.27: LogIC_{50} cytotoxicity curves and data table of DSF drug tested against primary cells. Four number assigned grade IV BAT samples were evaluated using MTT assay. \pm SEM is indicated as error bars.

Copper Gluconate

Only one, patient 8, BAT sample was effective at high drug concentration with a LogIC_{50} value of 4.92 nM (Figure 2.28). Comparing this data to the corresponding TC fragments reveal that equivalent response to CoGlu treatment was obtained for patient 9, while variations were found for patients 4 and 8. As patient 4 demonstrated low effectiveness against the TC but it was ineffective against the BAT (LogIC_{50} (nM): TC = 4.95 : BAT = >5), while for patient 8 CoGlu was ineffective against the TC but demonstrated low drug effectiveness against the BAT (LogIC_{50} (nM): TC = >5 : BAT = 4.92). Hence, although there appears to be a slight variation in cytotoxicity data between the different tumour fragments, overall the drug cytotoxicity data was very consistent and as a treatment for gliomas CoGlu was ineffective.

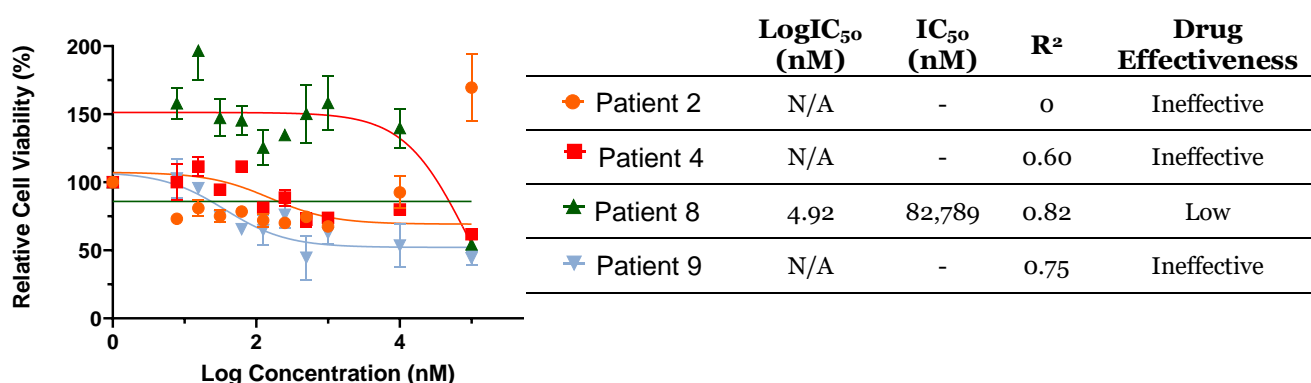


Figure 2.28: LogIC_{50} cytotoxicity curves and data table of CoGlu drug tested against primary cells. Four number assigned grade IV BAT samples were evaluated using MTT assay. \pm SEM is indicated as error bars.

Captopril

Four BAT samples were evaluated, with none of them responding to CAP (Figure 2.29). This data is consistent with that of the TC samples, therefore as a monotherapy CAP is ineffective.

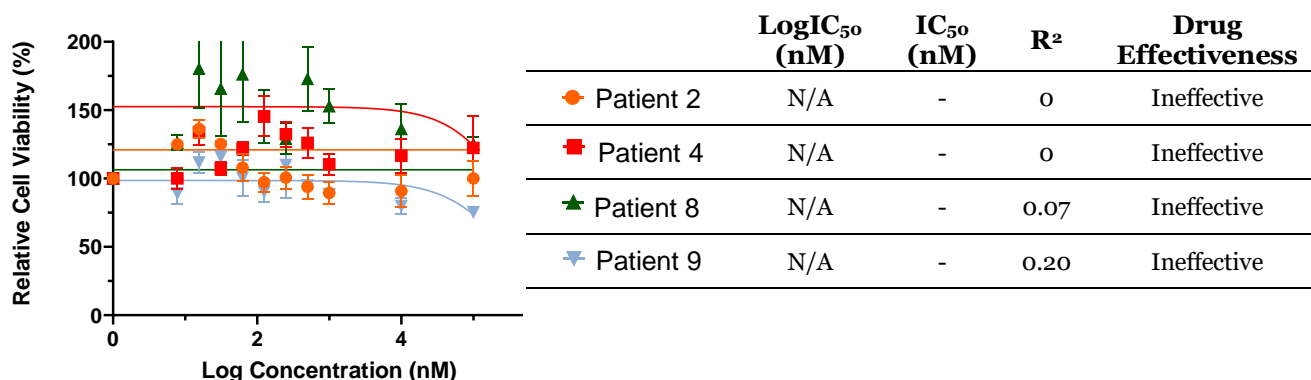


Figure 2.29: LogIC₅₀ cytotoxicity curves and data table of CAP drug tested against primary cells. Four number assigned grade IV BAT samples were evaluated using MTT assay. \pm SEM is indicated as error bars.

Celecoxib

Three out of the four tested BAT samples demonstrated effectiveness at high drug concentrations with LogIC₅₀ values between 4.47 and 4.96 nM (Figure 2.30). When compared to the corresponding TC samples equivalent cytotoxicity data were obtained. However, the dose vs response curves were inconsistent, to illustrate, at log 5 nM there was a large decrease in the cell viability values across all of the TC samples, here this was only observed for one sample, patient 8 (Figure 2.30). Thus, although the overall LogIC₅₀ values were consistent, there was a noticeable variation in CXB response at 100 μ M drug concentration.

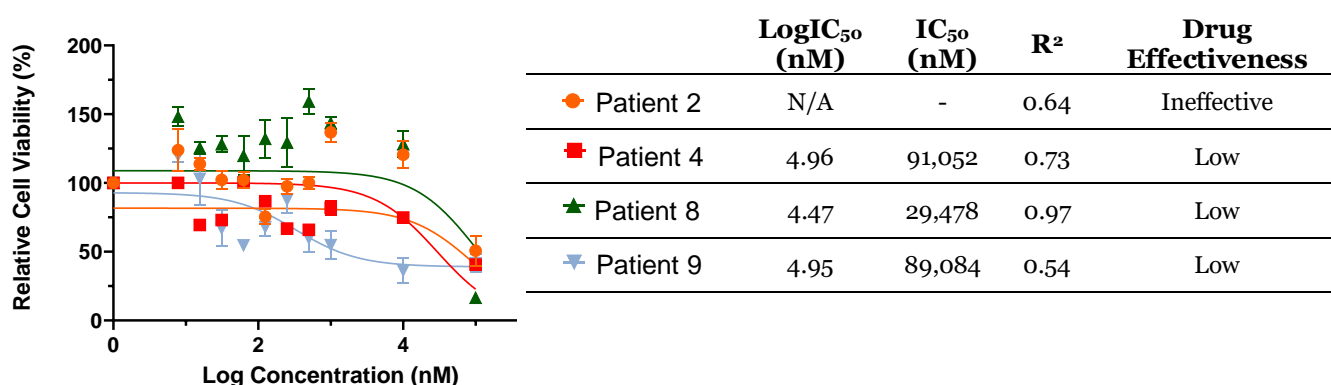


Figure 2.30: LogIC₅₀ cytotoxicity curves and data table of CXB drug tested against primary cells. Four number assigned grade IV BAT samples were evaluated using MTT assay. \pm SEM is indicated as error bars.

Ticlopidine

Four BAT samples were evaluated with none responding to TCL treatment (Figure 2.31).

Compared to the same patients TC samples, the drug cytotoxicity data were consistent.

Hence TCL was proven to be ineffective as a treatment for glioma.

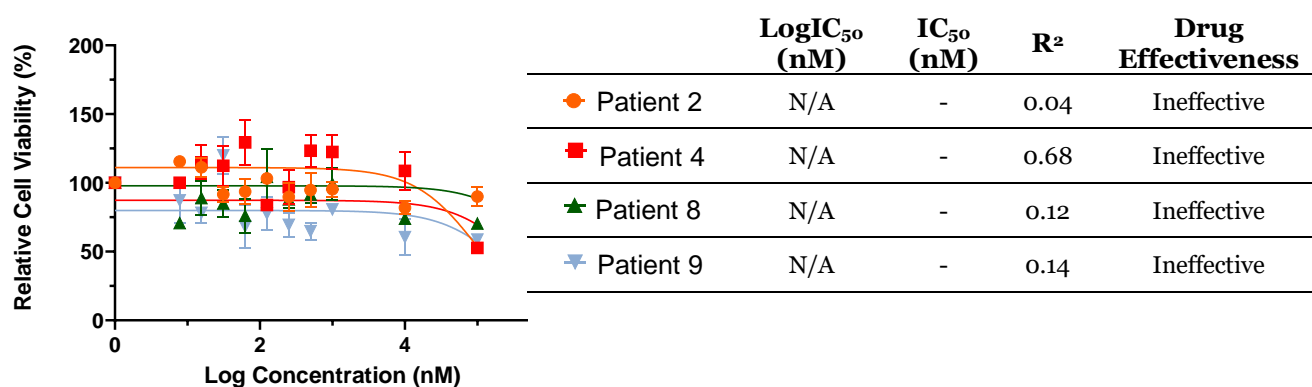


Figure 2.31: LogIC₅₀ cytotoxicity curves and data table of TCL drug tested against primary cells. Four number assigned grade IV BAT samples were evaluated using MTT assay. \pm SEM is indicated as error bars.

Itraconazole

Four patient BAT samples were evaluated and only one, patient 4, achieved low drug effectiveness with a LogIC_{50} value of 4.77 nM (Figure 2.32).

Comparing this data to the corresponding TC fragment reveal that against patient 9 ITZ treatment was ineffective across both TC and BAT, whilst for patient 4 and 8 variations were demonstrated. For patient 4 ITZ treatment was ineffective against the TC but demonstrated low drug effectiveness against the BAT (LogIC_{50} (nM): TC = >5 : BAT = 4.77), while for patient 8 ITZ demonstrated low effectiveness against the TC sample but was ineffective against the BAT (LogIC_{50} (nM): TC= 4.33 : BAT = >5). Hence, although there appears to be a slight variation in cytotoxicity data between the sperate tumour fragments, the overall drug cytotoxicity data was consistent and as a therapy ITZ was ineffective across the majority of patients.

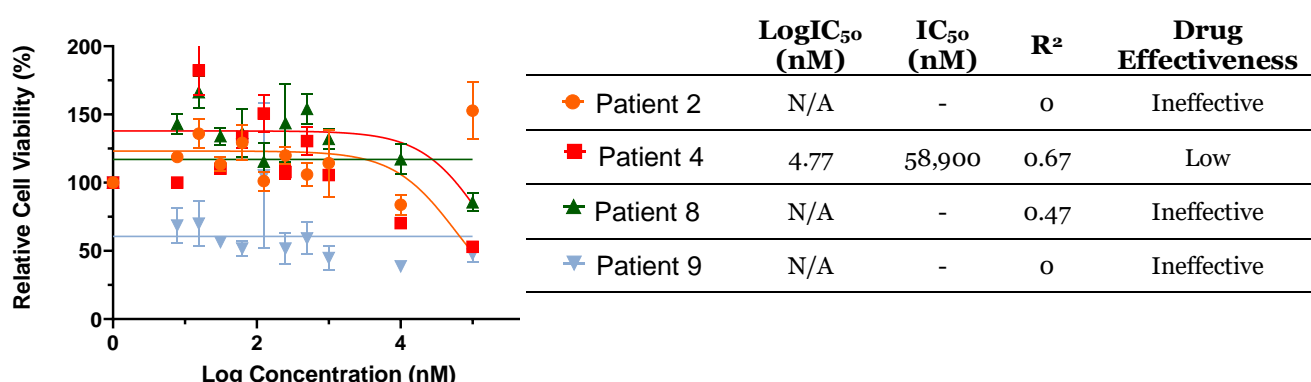


Figure 2.32: LogIC_{50} cytotoxicity curves and data table of ITZ drug tested against primary cells. Four number assigned grade IV BAT samples were evaluated using MTT assay. \pm SEM is indicated as error bars.

2.4.4 IncuCyte cell proliferation imaging assay

Cell metabolism assays such as MTT rely on cell metabolic activity as a measure of cellular viability, thus indirectly assessing cytotoxicity. Within this study direct measurement of cellular viability via cell imaging assay was performed on patient 4 TC and BAT samples, to ensure the accuracy of the drug cytotoxicity data and as a comparison between end-point MTT and real-time IncuCyte assay.

Same as the experimental configuration for the MTT assay, a total of nine drugs were investigated: TMZ, IRN, PTV, DSF, CoGlu, CAP, CXB, ITZ & TCL. For each sample, a

cytotoxicity graph was plotted and LogIC_{50} values calculated. Drug effectiveness was ranked into four distinctive categories; high (LogIC_{50} = 0-3 nM), medium (LogIC_{50} = 3-4 nM), low (LogIC_{50} = 4-5 nM) and ineffective if no LogIC_{50} value was achieved, these four categories were chosen arbitrary to reduce ambiguity during data discussion and simplify comparison between different dataset.

Additionally, for each drug cellular confluence measurement and observation of cellular morphological changes at 0.1 μM , 1 μM and 100 μM drug dose, over a 3-day treatment period were performed. For the BAT data the contrast phase images were less resolved, as a result cellular shape could not be seen thus data evaluation of cellular morphology change will not be discussed for this sample.

Patient 4 TC

The Log concentration vs cell viability curve data demonstrate that TMZ, CAP, TCL and ITZ were ineffective against the TC sample, whilst IRN, PTV, DSF and CXB were effective with LogIC_{50} values of 4.52, 5.00, 4.27 and 4.99 nM, respectively (Figure 2.33). The highest response against TC sample was achieved by CoGlu with a LogIC_{50} value of 3.80 nM (Figure 2.33).

Compared to the same patient TC cytotoxicity data from the MTT assay, results were comparable with consistent drug potency values obtained for TMZ, IRN, PTV, CAP, CXB, TCL and ITZ. The only inconsistency was with DSF and CoGlu, as both were shown to be more effective when tested using the IncuCyte assay (DSF LogIC_{50} (nM): MTT= >5, IncuCyte= 5.0 and CoGlu LogIC_{50} (nM): MTT= 5.0 , IncuCyte= 3.8 nM).

Thus, although there appears to be a variation in DSF and CoGlu cytotoxicity data for most drugs the cytotoxicity values were equivalent between the MTT and IncuCyte assays.

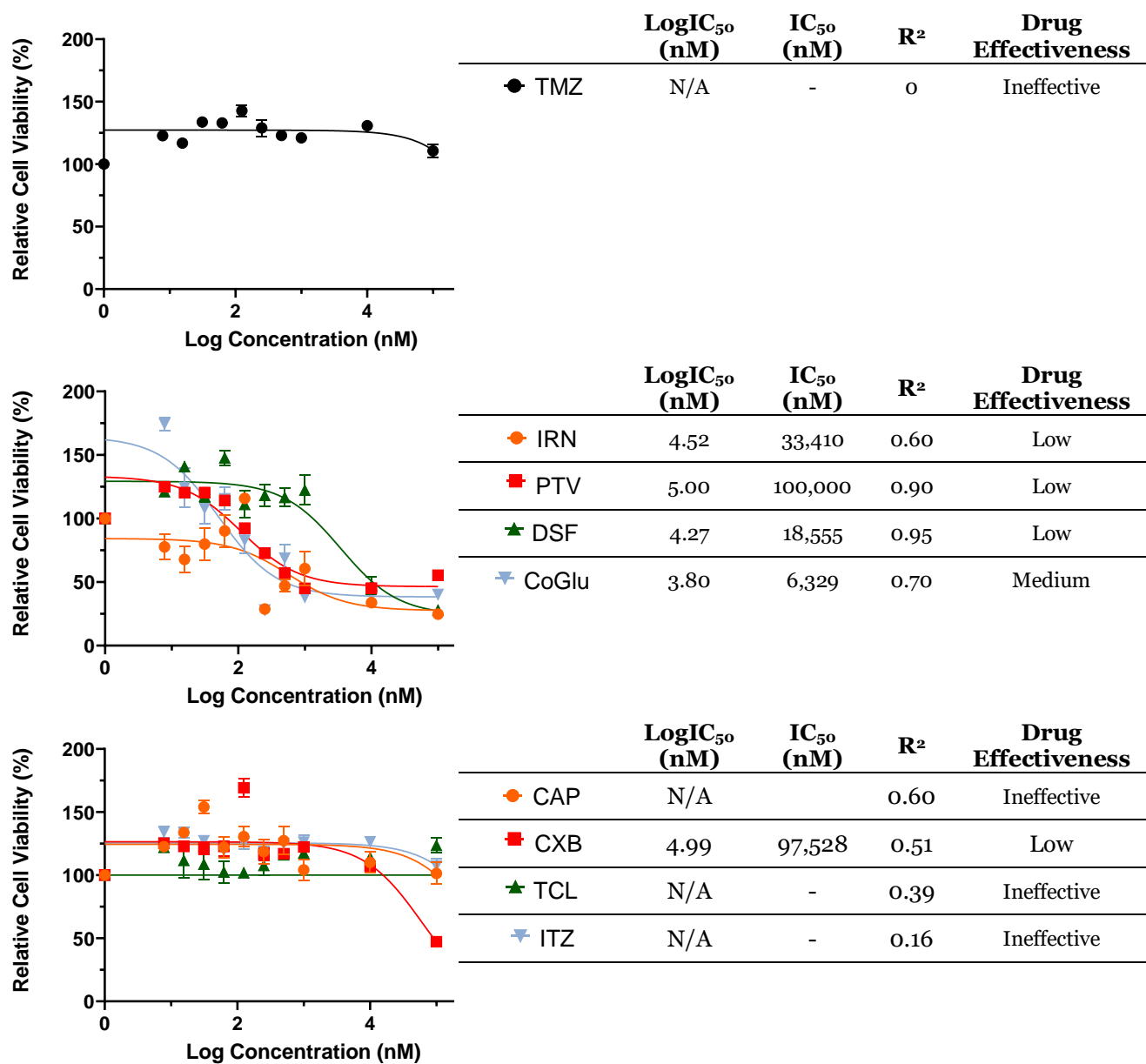


Figure 2.33: LogIC₅₀ cytotoxicity curves and data table of mono-therapeutic drug treatments tested against patient 4 TC cells using IncuCyte assay. ± SEM is indicated as error bars.

Temozolomide

TMZ demonstrated no efficacy across all doses, with exponential tumour growth observed over the 72 hour incubation period and no cellular morphological changes detected (Figure 2.34). At 100 μM dose, a slowdown in tumour growth was observed but not at a significant rate with cellular confluence value reaching 32 % at 72 hour incubation period compared to 40 % for the 0.1 μM dose treatment (Figure 2.34). Therefore, TMZ was deemed to be ineffective as a treatment for glioma as although the high 100 μM dose did demonstrate some response, fast cellular growth sustained throughout the treatment period continuing the development of tumour.

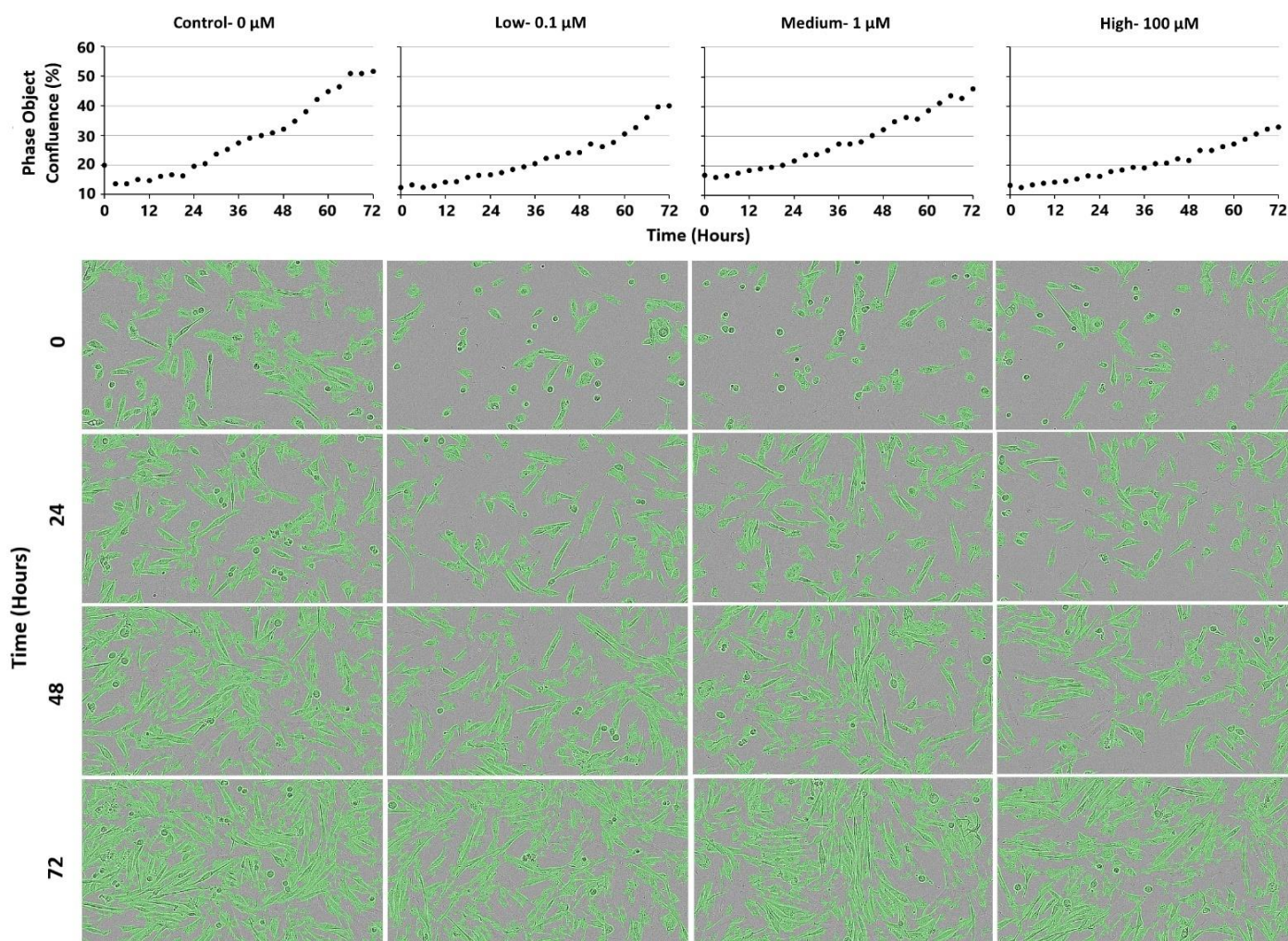


Figure 2.34: IncuCyte cell confluence and representative images data of patient 4 derived TC cells treated with TMZ. Drug concentration from left to right: control, 0.1 μM low, 1 μM medium and 100 μM high.

Irinotecan

At 0.1 μM dose IRN demonstrated no efficacy, with exponential tumour growth over time (Figure 2.35), while at 1 μM dose tumour growth slowed. The most substantial reduction in tumour confluence (7 %) occurred with the 100 μM IRN dose. Cellular morphological changes were also observed with cells appearing more spherical, smaller in size and their margins were unclear when compared to the control group. Therefore, IncuCyte analysis has demonstrated that IRN potency against patient 4 TC sample is dose dependent, requiring a high 100 μM dose for any potency or morphological change to be seen. This confirms the MTT assay data as all of the other grade IV samples required high IRN dose to achieve a response.

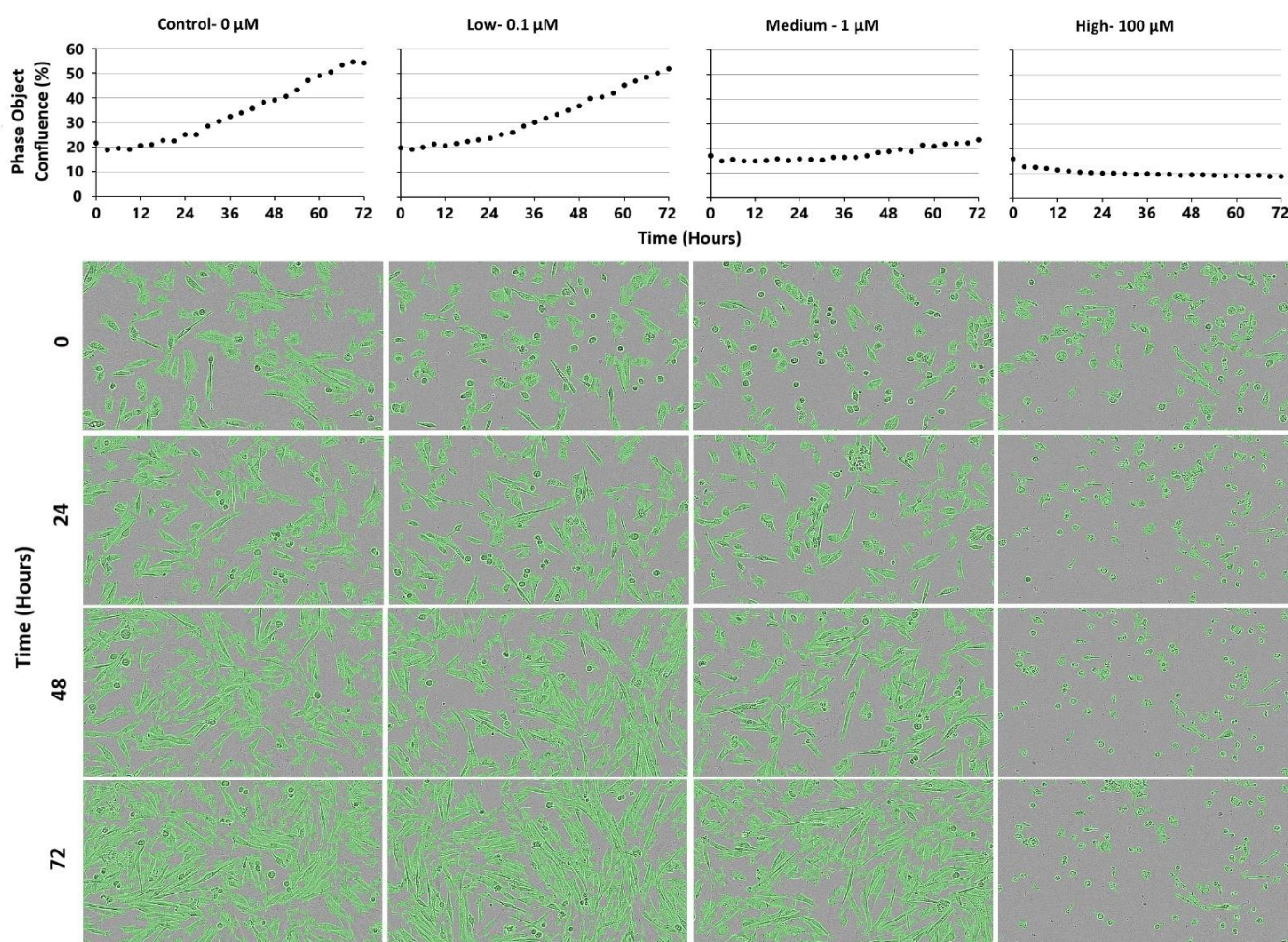


Figure 2.35: IncuCyte cell confluence and representative images data of patient 4 derived TC cells treated with IRN. Drug concentration from left to right: control, 0.1 μM low, 1 μM medium and 100 μM high.

Pitavastatin

At low 0.1 μM exponential tumour growth was observed over the 72-hour treatment period with no changes in cellular morphology (Figure 2.36). At 1 and 100 μM dose, a similar growth pattern was observed; initially, fast exponential tumour growth was established but by day one the cellular growth ceased and a reduction in tumour confluence followed (Figure 2.36). Unlike other effective drug treatments where an instant shape transformation of cells occurred, PTV induced a slow and gradual response. Initially cells transformed from highly infiltrating elongated structures to less infiltrating elongated cells with an enhanced spherical core which gradually decreased in size to form a small ball (Figure 2.36). PTV cell arrest is predicted to occur within the G₀/G₁ of the cell cycle [142, 221], although the precise mechanism of action remains unknown, this could provide an explanation for the gradual change in morphology as it takes place within the growth stage of the cell cycle which is known to be slow and gradual. Here the data correlate well to the MTT assay results as the majority of GBM tested samples required 1-100 μM of PTV dose (Log 3-5 nM) to achieve a response.

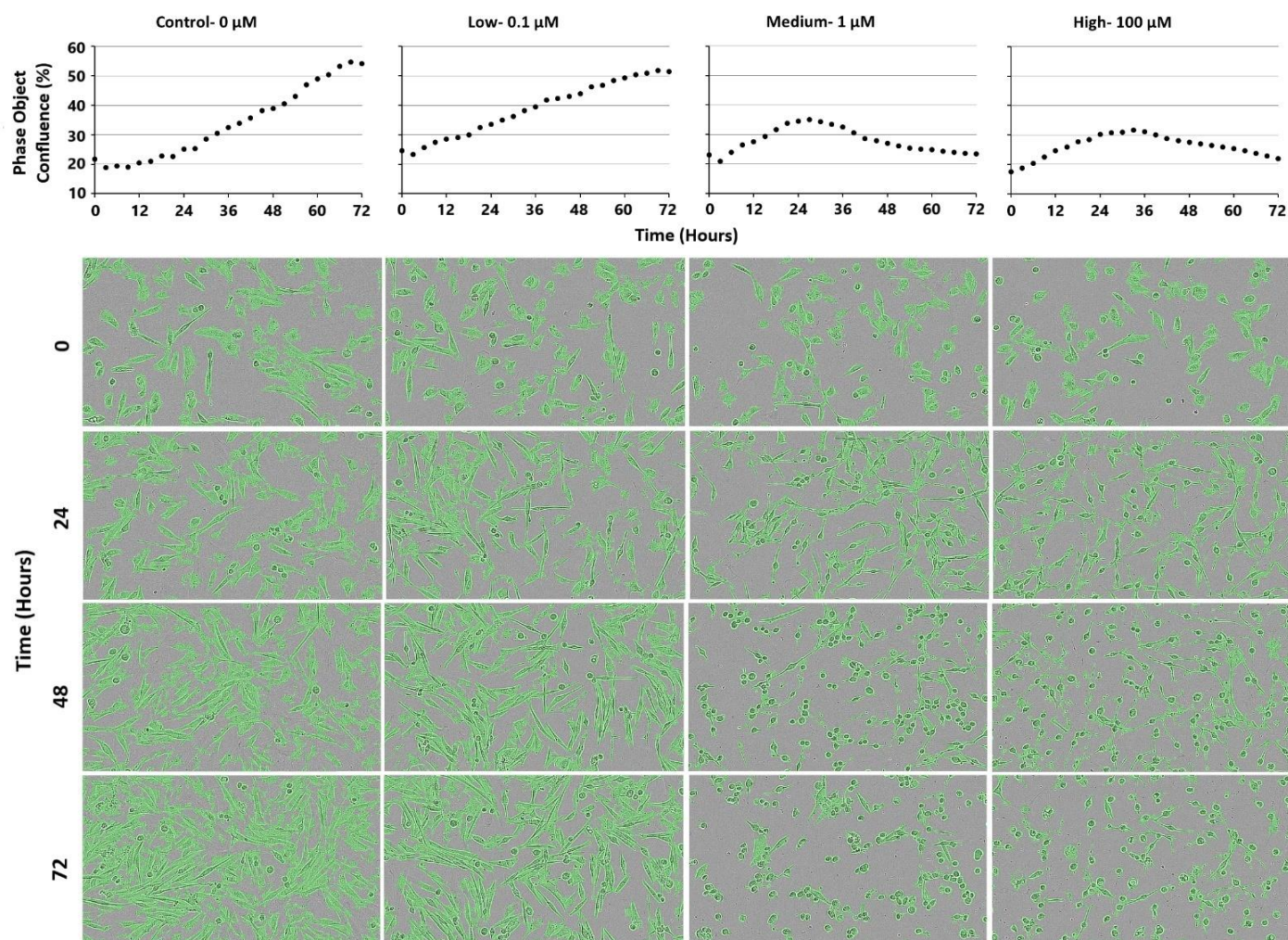


Figure 2.36: IncuCyte cell confluence and representative images data of patient 4 derived TC cells treated with PTV. Drug concentration from left to right: control, 0.1 μM low, 1 μM medium and 100 μM high.

Disulfiram

At 0.1-1 dose exponential tumour growth occurred over the 72-hour treatment period, while at 100 μM drug concentration a small 4 % reduction in tumour confluence was detected (Figure 2.37). A change in cellular morphology was also observed with an increase in dose and incubation period, for instance, at 0.1 μM dose cells were elongated, highly infiltrating, with irregular margins but as dosing and incubation time increased, cells appeared smaller and developed a spherical shaped morphology with clear margins (Figure 2.37).

Compared to the MTT assay cytotoxicity data for the same patient sample, DSF is demonstrated to be more effective when tested using the IncuCyte assay.

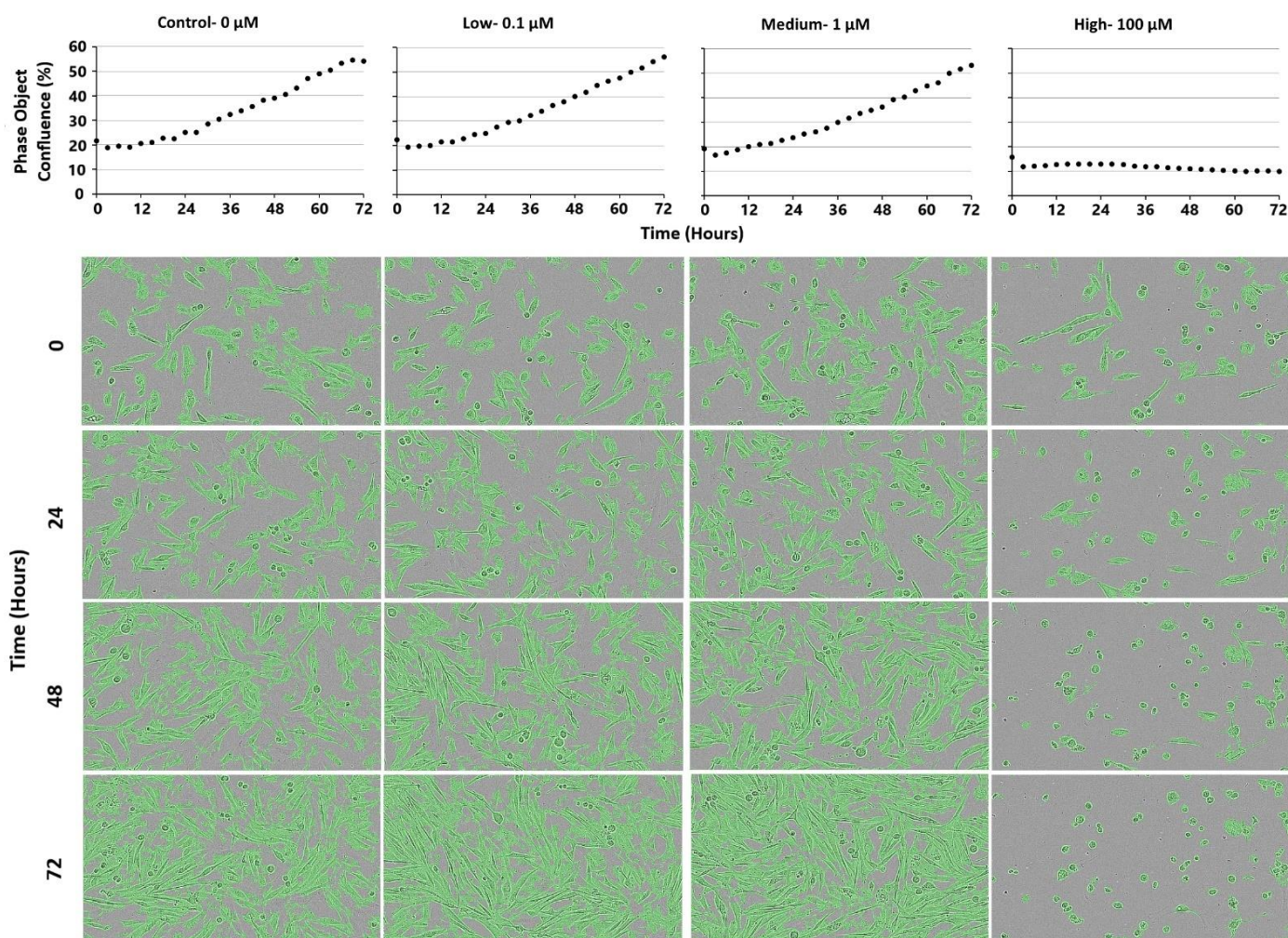


Figure 2.37: IncuCyte cell confluence and representative images data of patient 4 derived TC cells treated with DSF. Drug concentration from left to right: control, 0.1 μM low, 1 μM medium and 100 μM high.

Copper Gluconate

At 0.1 μM dose exponential but slow tumour growth was observed over the 72-hour treatment period, while at 1-100 μM dose cellular growth stopped (Figure 2.38). Cellular morphology change was also observed, as growth ceased, cells shrunk and retreated to a less elongated structure (Figure 2.38).

Similar to the DSF cytotoxicity data, CoGlu was shown to be more potent when tested via the IncuCyte assay where a response against the tumour was observed even at 0.1 μM dose (Log 2 nM) (Figure 2.38).

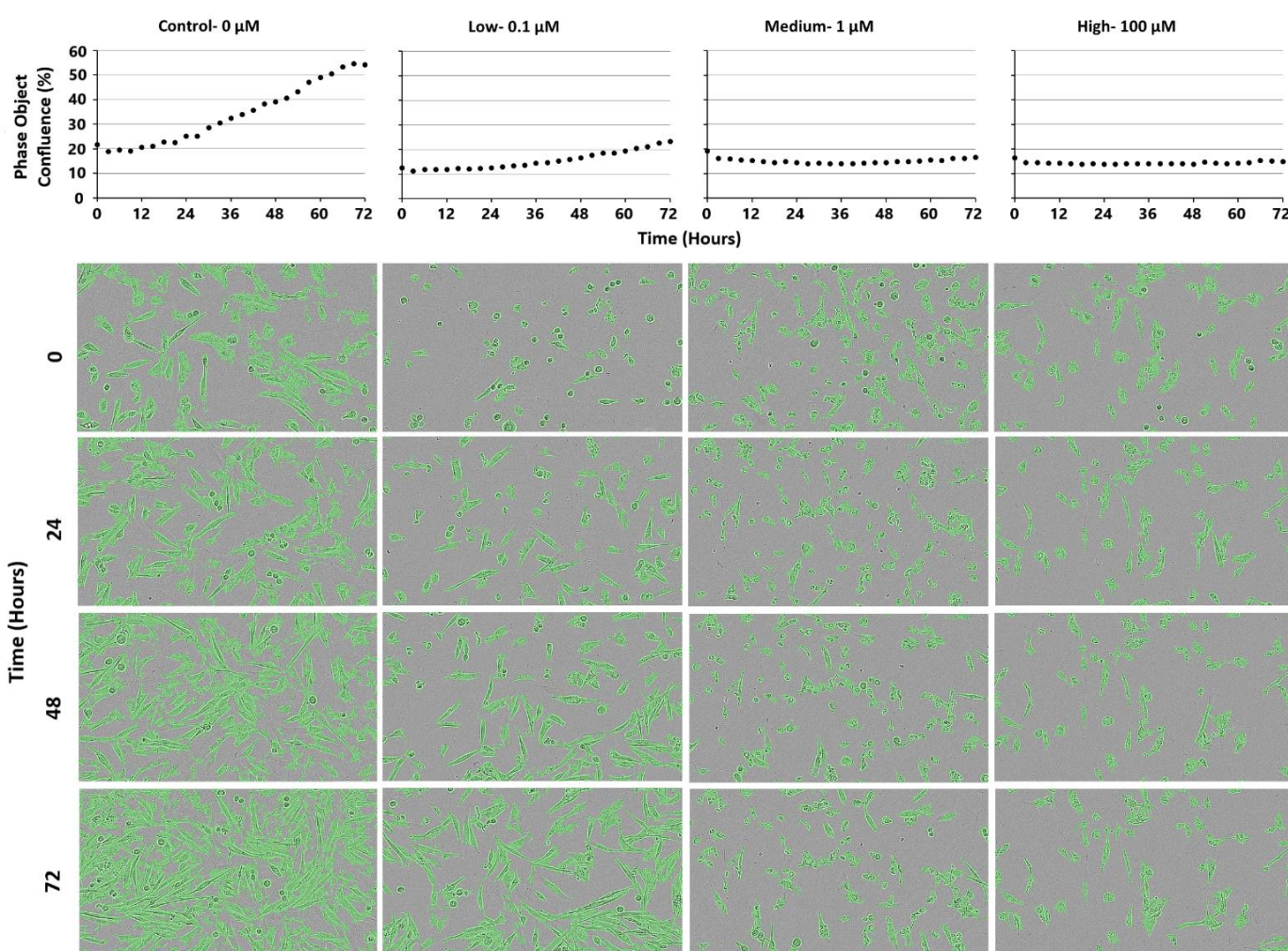


Figure 2.38: IncuCyte cell confluence and representative images data of patient 4 derived TC cells treated with CoGlu. Drug concentration from left to right: control, 0.1 μM low, 1 μM medium and 100 μM high.

Captopril

CAP was shown to be ineffective against the tumour even at high 100 μM drug dose. Across all dosages exponential tumour growth was obtained with no observed cellular morphology change over the 72-hour treatment period (Figure 2.39). This validates our MTT assay cytotoxicity data as all of the grade IV glioma samples did not respond to CAP treatment.

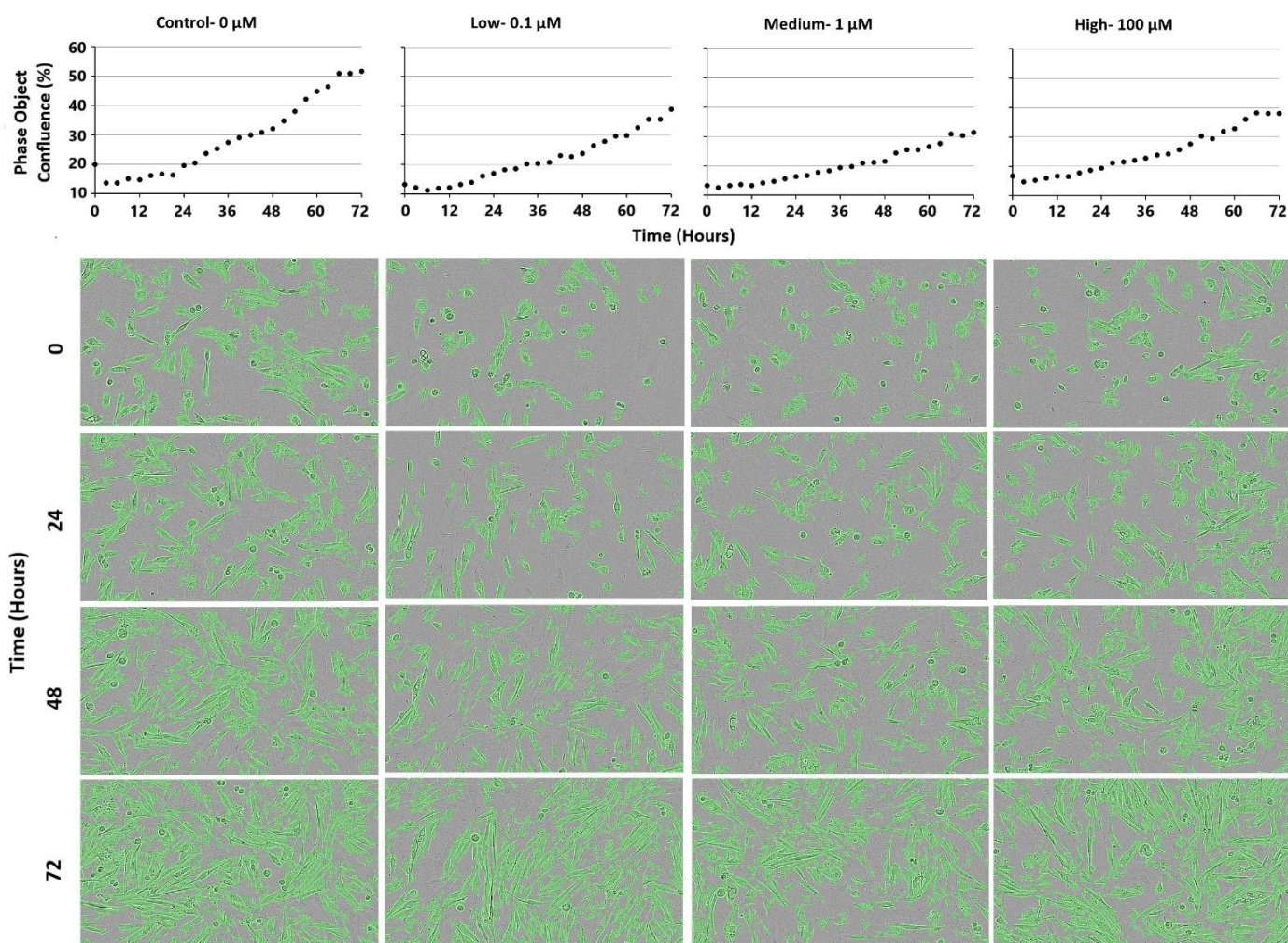


Figure 2.39: IncuCyte cell confluence and representative images data of patient 4 derived TC cells treated with CAP. Drug concentration from left to right: control, 0.1 μM low, 1 μM medium and 100 μM high.

Celecoxib

At 0.1 to 1 μM dose exponential tumour growth was observed over the 72-hour treatment period, whilst at 100 μM dose cellular growth stopped with cellular confluence remaining relatively constant ($\pm 4\%$). However, unlike other drugs, CXB provoked no cellular morphological change with cells possessing the same morphology across all doses (Figure 2.40). This confirms the MTT cytotoxicity data, as most of the MTT tested samples required 100 μM dose (Log 5 nM) for any response to be observed.

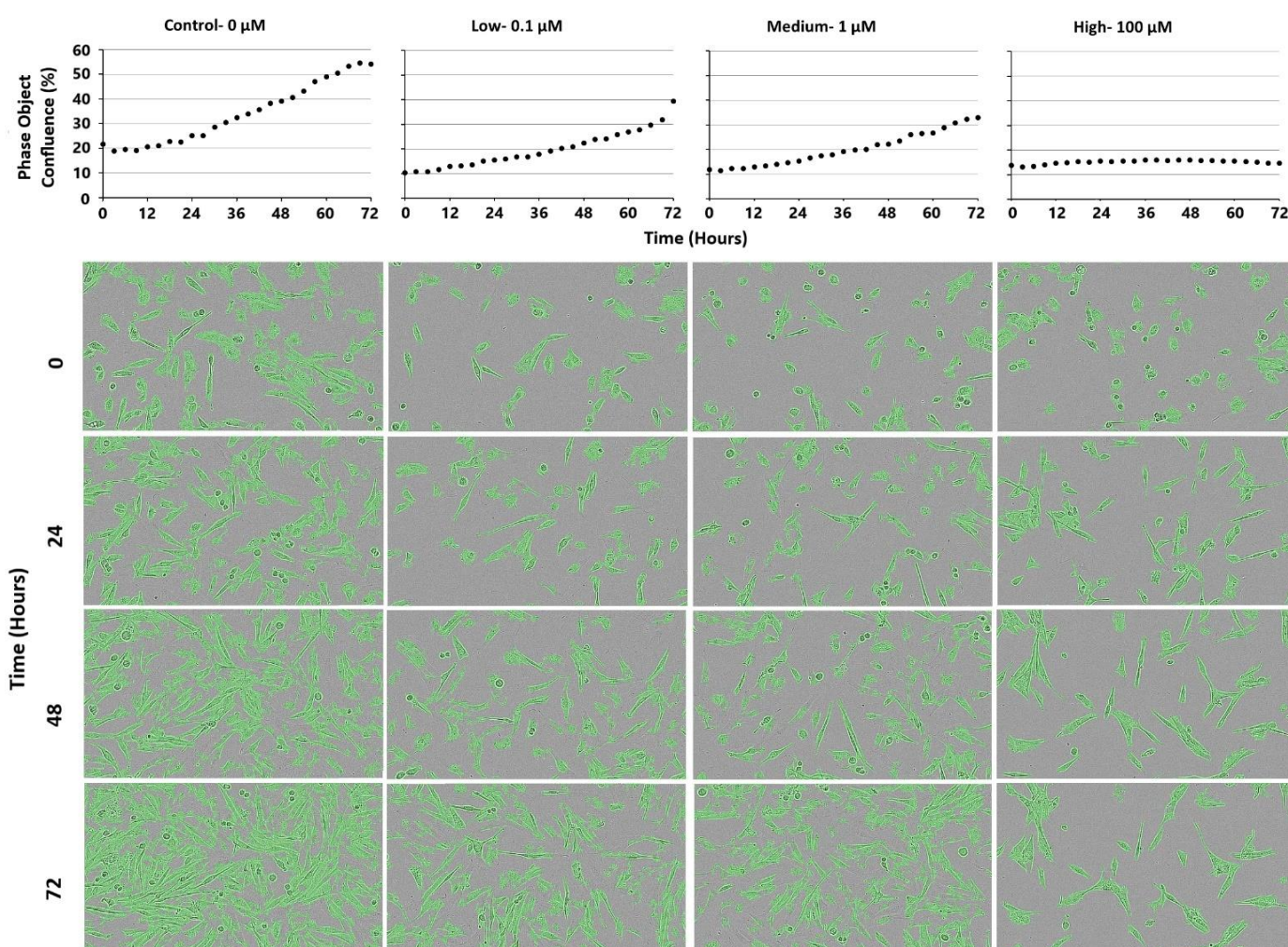


Figure 2.40: IncuCyte cell confluence and representative images data of patient 4 derived TC cells treated with CXB. Drug concentration from left to right: control, 0.1 μM low, 1 μM medium and 100 μM high.

Ticlopidine

There was no variation in response between the drug treatment and control. Across all doses exponential tumour growth was demonstrated and no change in cellular morphology was observed over the 72-hour treatment period (Figure 2.41). This data was consistent to the MTT assay results and confirmed that TCL is ineffective against gliomas.

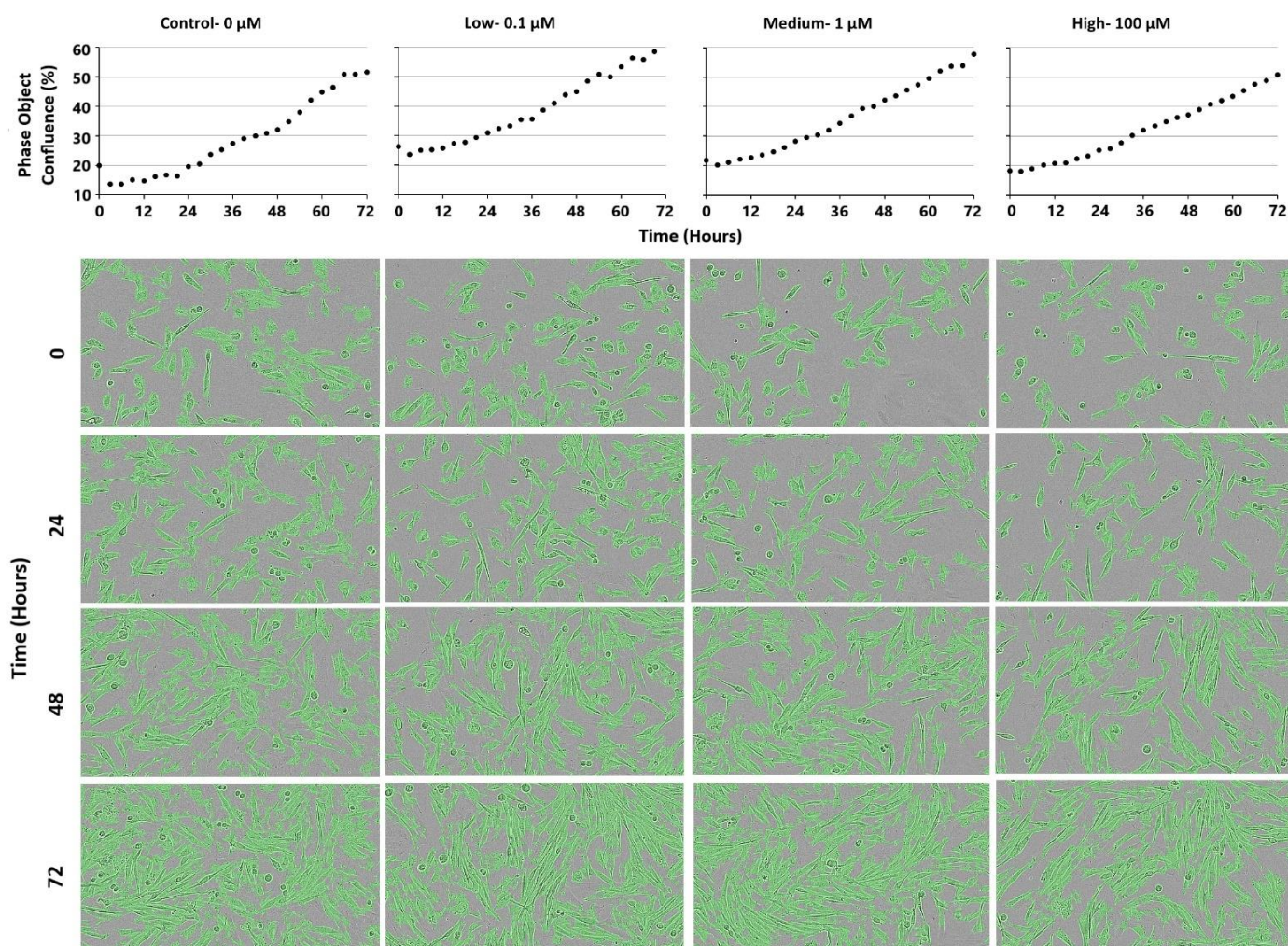


Figure 2.41: IncuCyte cell confluence and representative images data of patient 4 derived TC cells treated with TCL. Drug concentration from left to right: control, 0.1 µM low, 1 µM medium and 100 µM high.

Itraconazole

ITZ was demonstrated to be ineffective across all doses, with exponential tumour growth observed over the 72 hour incubation period (Figure 2.42). Similar to TMZ, CAP, CXB and TCL treatments, it provoked no cellular morphological change with cells appearing to possess the same morphology across all doses. This result was consistent to the MTT cytotoxicity assay data.

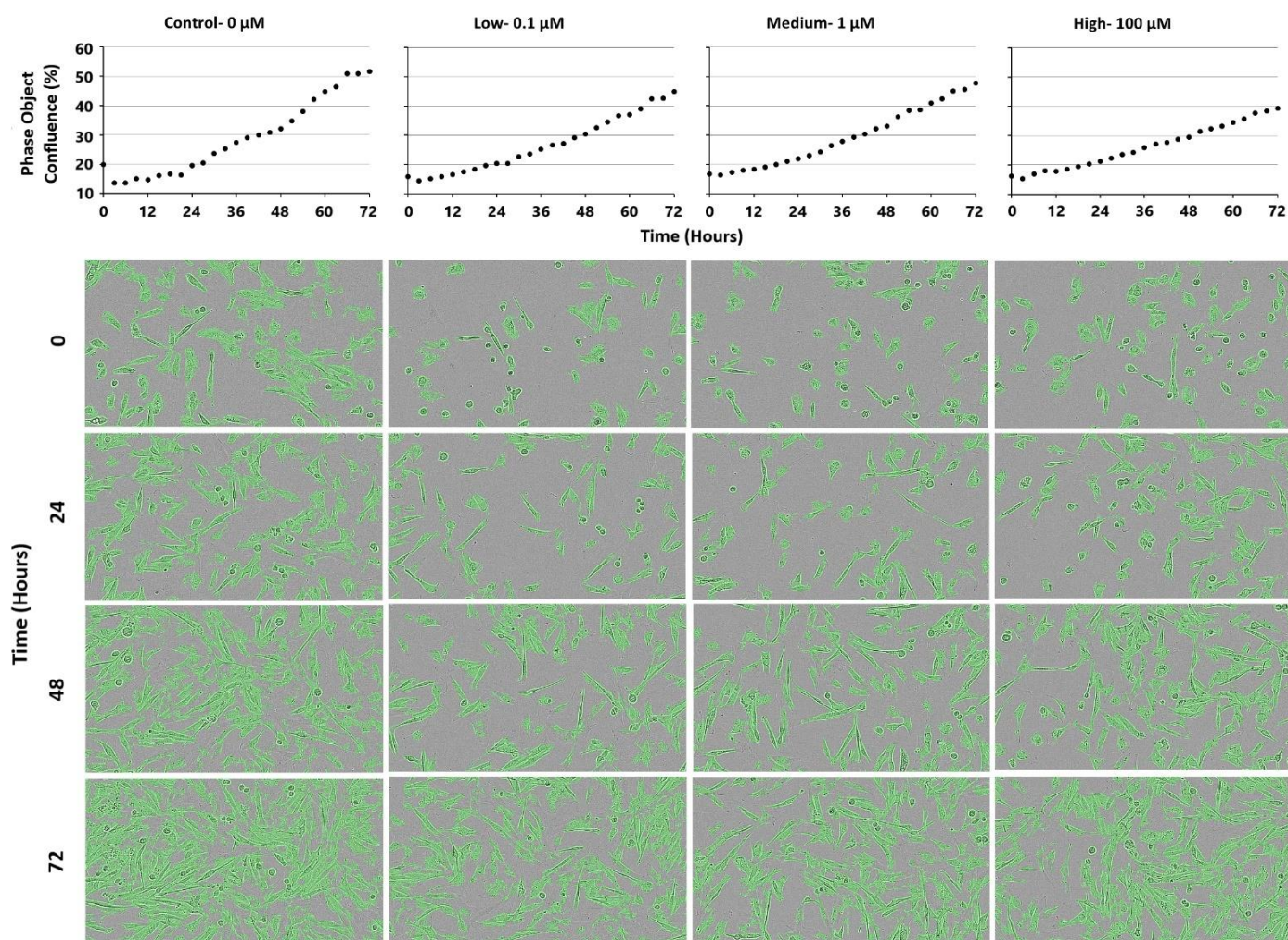


Figure 2.42: InCuCyte cell confluence and representative images data of patient 4 derived TC cells treated with ITZ. Drug concentration from left to right: control, 0.1 µM low, 1 µM medium and 100 µM high.

Patient 4 BAT

The drug cytotoxicity data shows that TMZ, DSF, CoGlu, CAP, ITZ and TCL were ineffective against patient 4 BAT sample, while IRN and CXB demonstrated low effectiveness with LogIC_{50} values of 4.60 and 4.66 nM, respectively (Figure 2.43). The highest response against BAT sample was achieved by PTV with a LogIC_{50} value of 4.0 nM, however the cell viability curve was atypical as with increasing drug concentration there was no decrease in cell viability.

Compared to the MTT cytotoxicity results, similar LogIC_{50} values were achieved for TMZ, DSF, CoGlu, CAP, CXB and TCL. Whilst IRN, PTV and ITZ drug treatment differed, as according to the MTT assay IRN and PTV were ineffective however when tested using IncuCyte they achieved a LogIC_{50} values of 4.60 and 4.0 nM, respectively. Inversely, ITZ was ineffective when tested using the IncuCyte but demonstrated low effectiveness by the MTT assay with a LogIC_{50} value of 4.77 nM. Hence, with the exception for IRN, PTV and ITZ, most tested drugs achieved equivalent cytotoxicity response across the two assays.

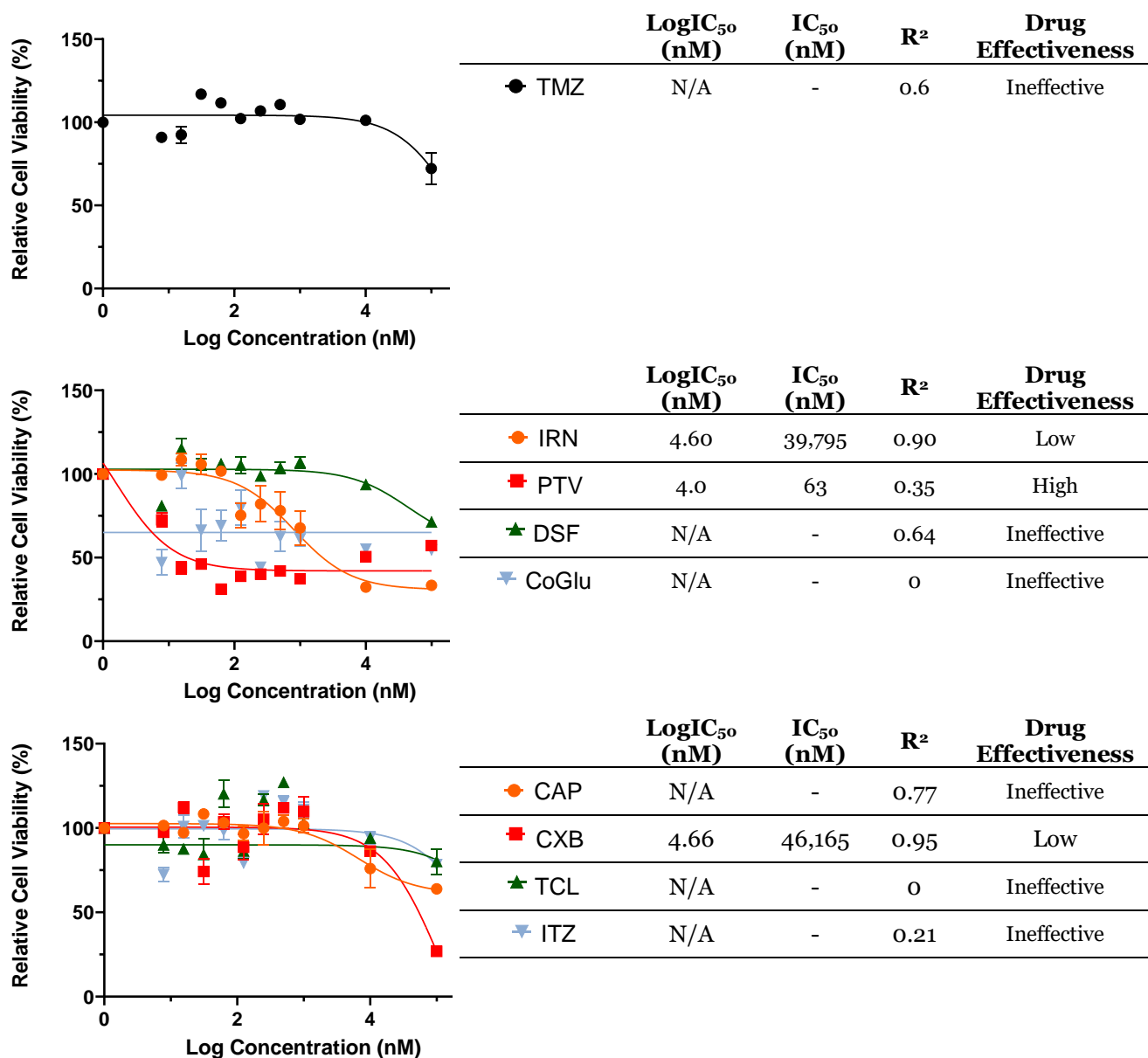


Figure 2.43: LogIC₅₀ cytotoxicity curves and data table of mono-therapeutic drug treatments tested against patient 4 BAT cells using IncuCyte assay. ± SEM is indicated as error bars.

Temozolomide

Similar to the TC sample exponential tumour growth was observed over the 72 hour incubation period across all doses (Figure 2.44). However, at 100 μM dose, a slowdown in tumour growth was observed with cellular confluence value reaching 40 % at 72 hour incubation period compared to 53 % for the control (Figure 2.44). Hence TMZ was deemed to be ineffective as a treatment for glioma as although the high 100 μM dose did demonstrate some response, fast cellular growth sustained throughout the treatment period continuing the development of tumour.

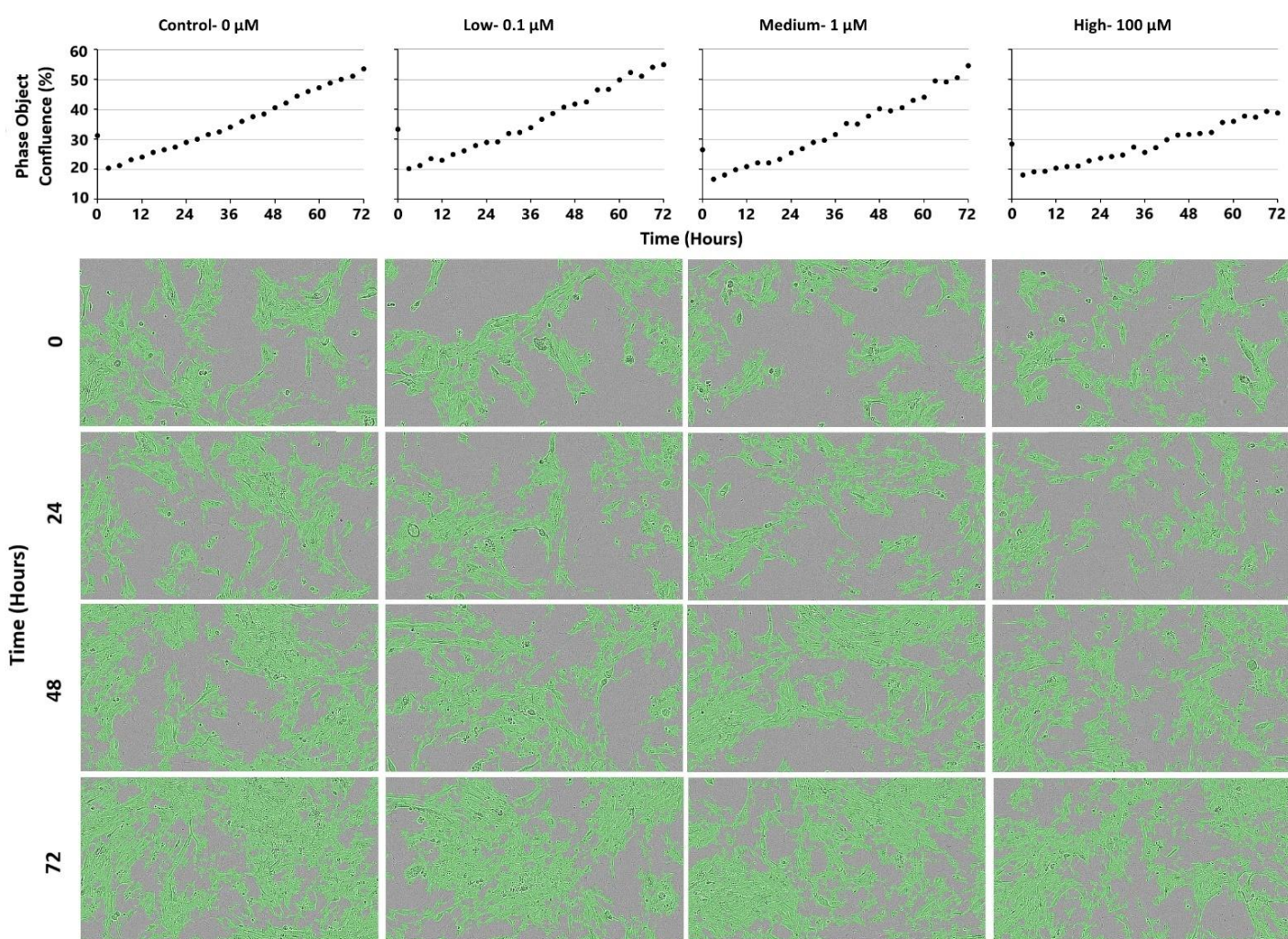


Figure 2.44: IncuCyte cell confluence and representative images data of patient 4 derived BAT cells treated with TMZ. Drug concentration from left to right: control, 0.1 μM low, 1 μM medium and 100 μM high.

Irinotecan

For IRN drug treatment a dose dependent response was demonstrated. Compared to control, the 0.1 and 1 μM dose treatments slowed tumour growth by 1.25 and 1.4 folds, respectively while at 100 μM dose, cellular growth stopped, and confluence decreased by 11 % following a 72 hour treatment period (Figure 2.45).

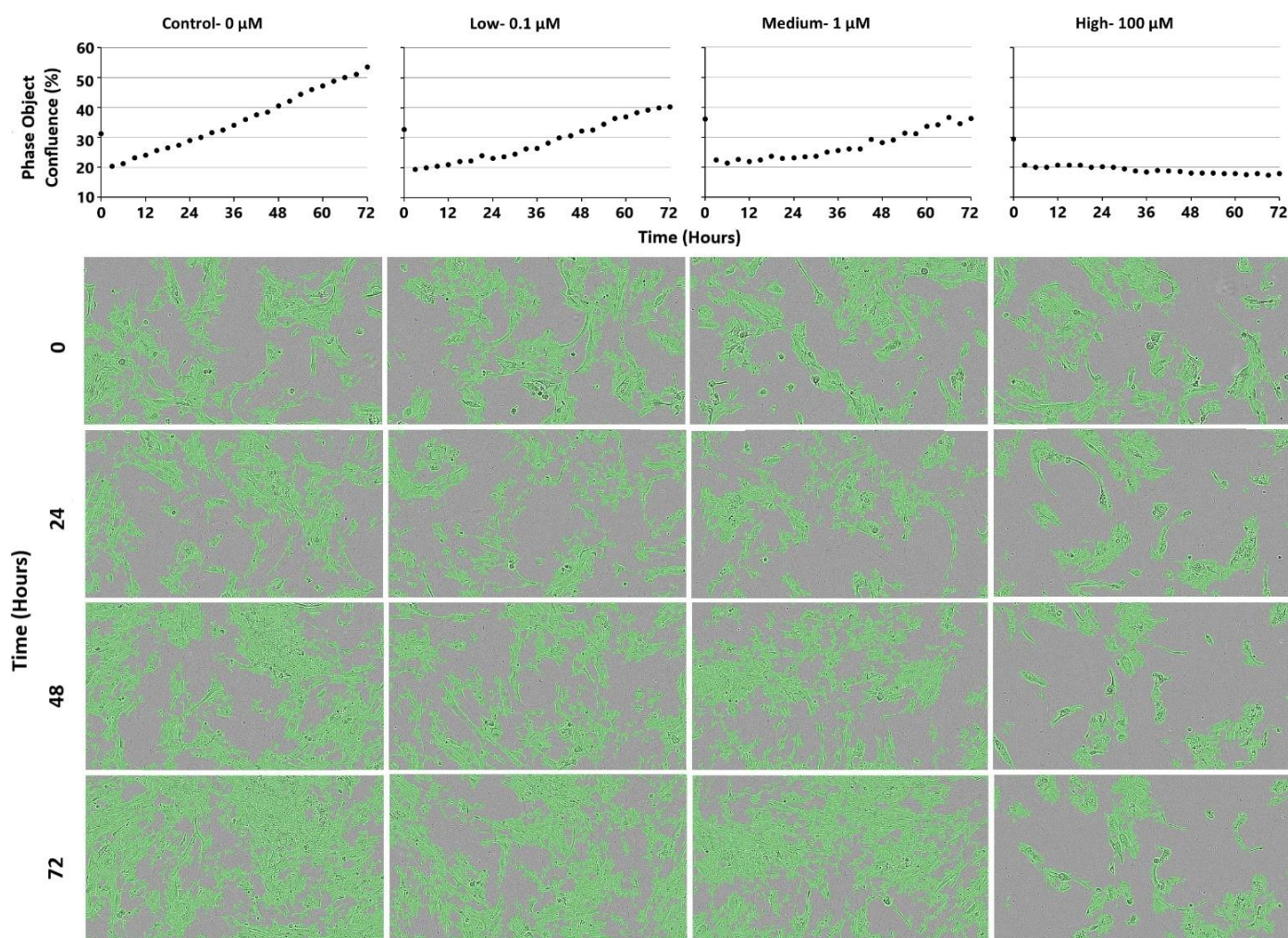


Figure 2.45: IncuCyte cell confluence and representative images data of patient 4 derived BAT cells treated with IRN. Drug concentration from left to right: control, 0.1 μM low, 1 μM medium and 100 μM high.

Pitavastatin

Following a 72-hour treatment period PTV achieved a 20, 12 and 8 % decrease in cell confluence for the 0.1, 1 and 100 μM dose, respectively. (Figure 2.46). Compared to control, PTV was proven to be effective even at low 0.1 μM dose, however with increasing drug concentration there was no improvement in response to PTV treatment as following a 72-hour treatment cell confluence remained relatively constant across all doses.

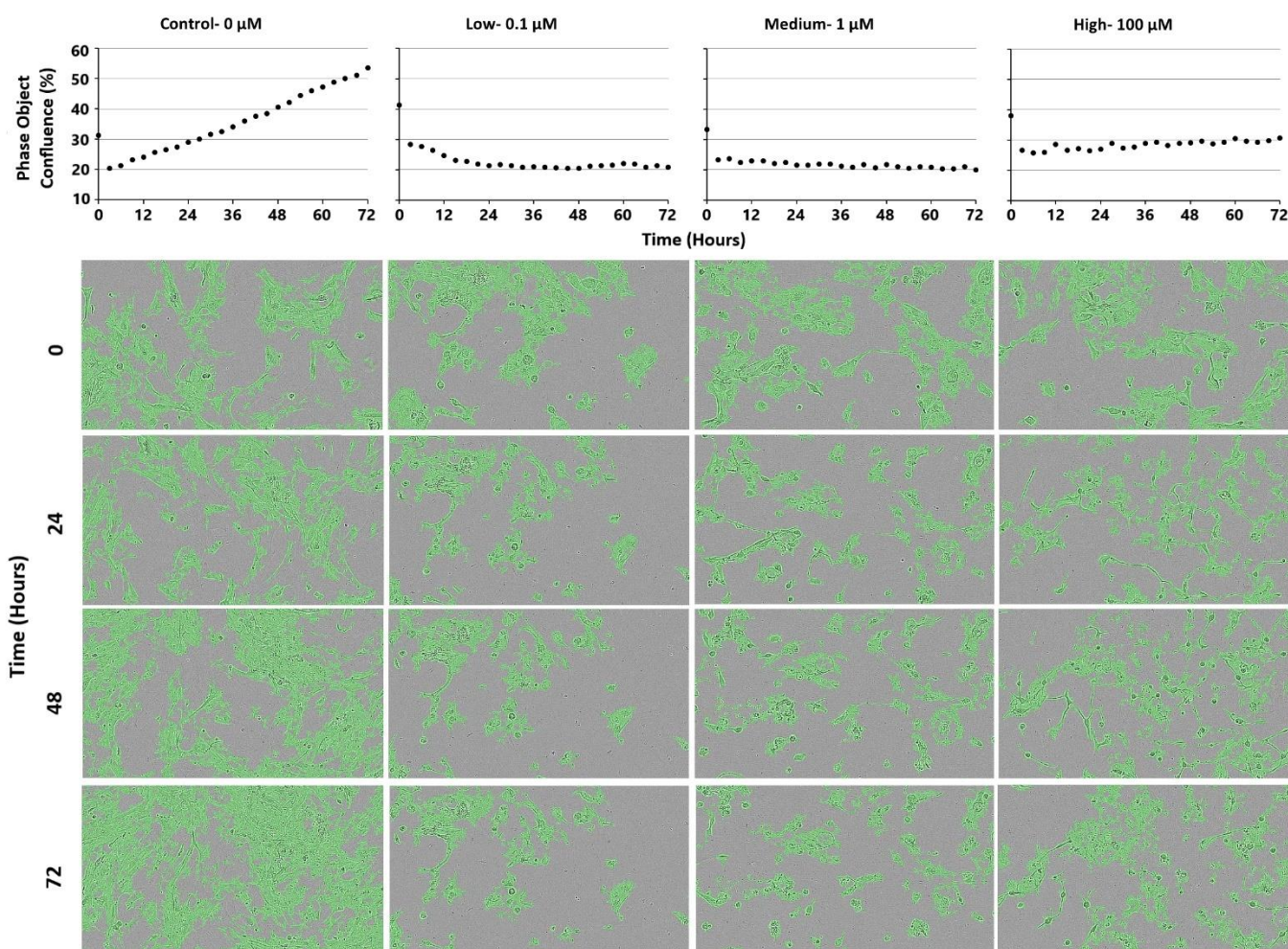


Figure 2.46: IncuCyte cell confluence and representative images data of patient 4 derived BAT cells treated with PTV. Drug concentration from left to right: control, 0.1 μM low, 1 μM medium and 100 μM high.

Disulfiram

DSF demonstrated no efficacy across all doses with exponential tumour growth observed over the 72 hour incubation period (Figure 2.47). At 100 μM dose, a slight slowdown in tumour growth was observed, with cellular confluence value reaching 39 % at 72 hour incubation period compared to 53 % for the control (Figure 2.47). Hence DSF was deemed to be ineffective as a treatment for glioma as although the high 100 μM dose did demonstrate some response, fast cellular growth sustained throughout the treatment period continuing the progress of tumour.

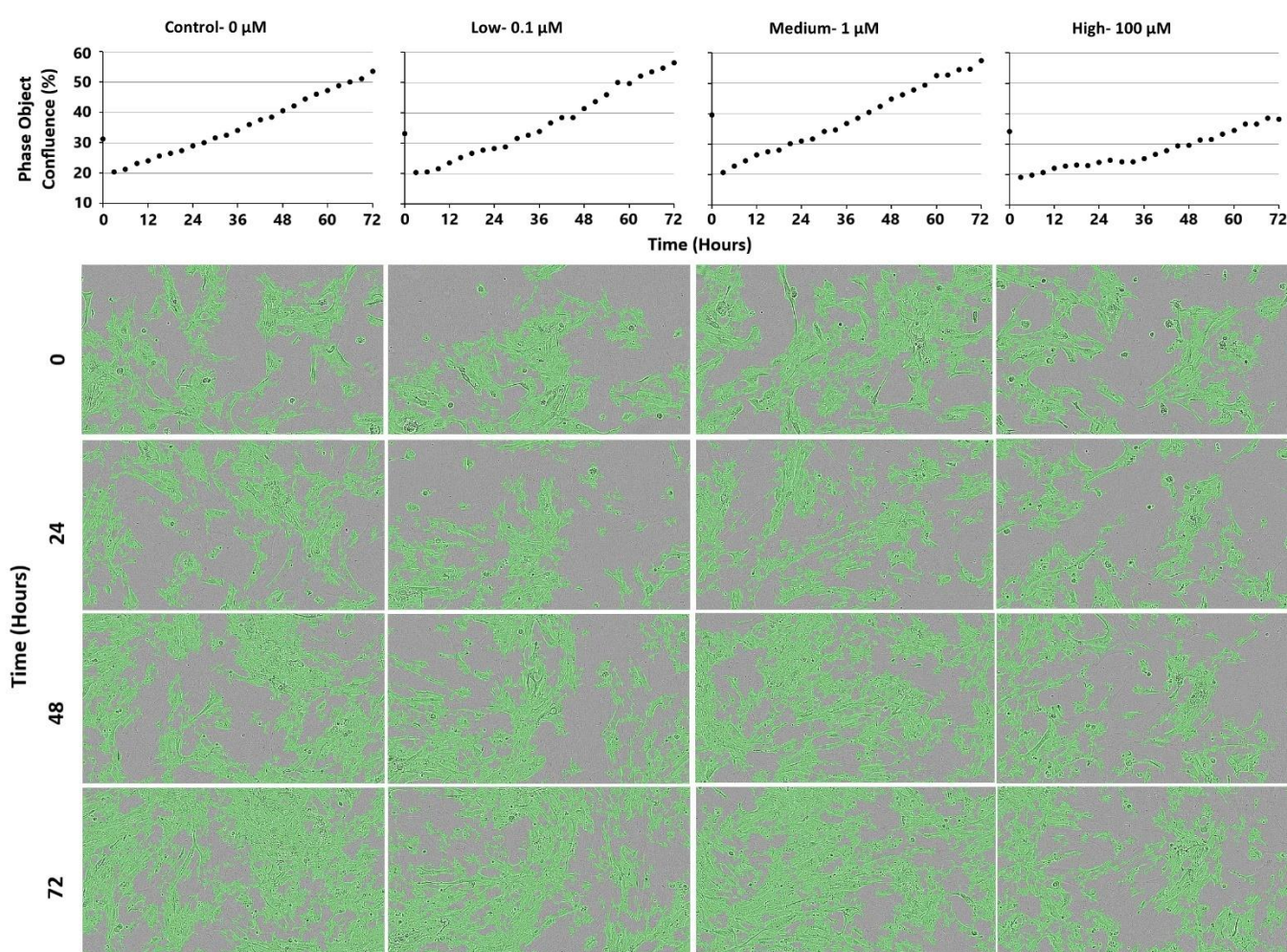


Figure 2.47: IncuCyte cell confluence and representative images data of patient 4 derived BAT cells treated with DSF. Drug concentration from left to right: control, 0.1 μM low, 1 μM medium and 100 μM high.

Copper Gluconate

Response against CoGlu was dose dependent as at 0.1 μM and 1 μM dose tumour growth slowed by 1.25 and 1.65 folds, respectively, while at 100 μM dose tumour growth reached a plateau, with no change in tumour confluence observed over the 72-hour treatment period (Figure 2.48).

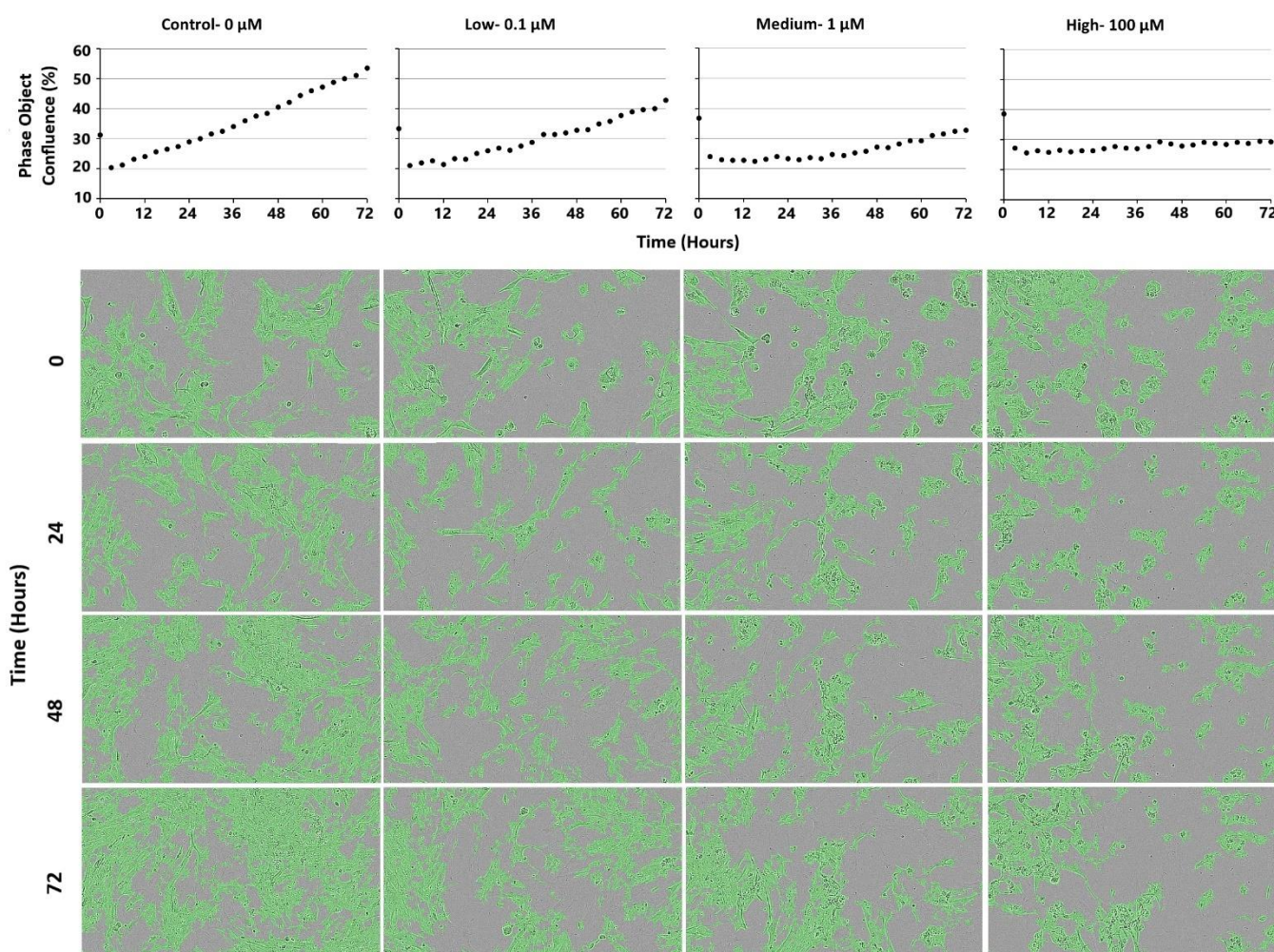


Figure 2.48: IncuCyte cell confluence and representative images data of patient 4 derived BAT cells treated with CoGlu. Drug concentration from left to right: control, 0.1 μM low, 1 μM medium and 100 μM high.

Captopril

At 0.1 and 1 μM dose CAP demonstrated no efficacy, with exponential tumour growth observed over the 72 hour incubation period (Figure 2.49). At 100 μM dose, a slowdown in tumour growth was observed with cellular confluence value reaching 34 % at 72 hour incubation period compared to 54 % for the control (Figure 2.49). Hence CAP was deemed to be ineffective as a treatment for glioma as although the high 100 μM dose did demonstrate some response, fast cellular growth sustained throughout the treatment period continuing the development of tumour.

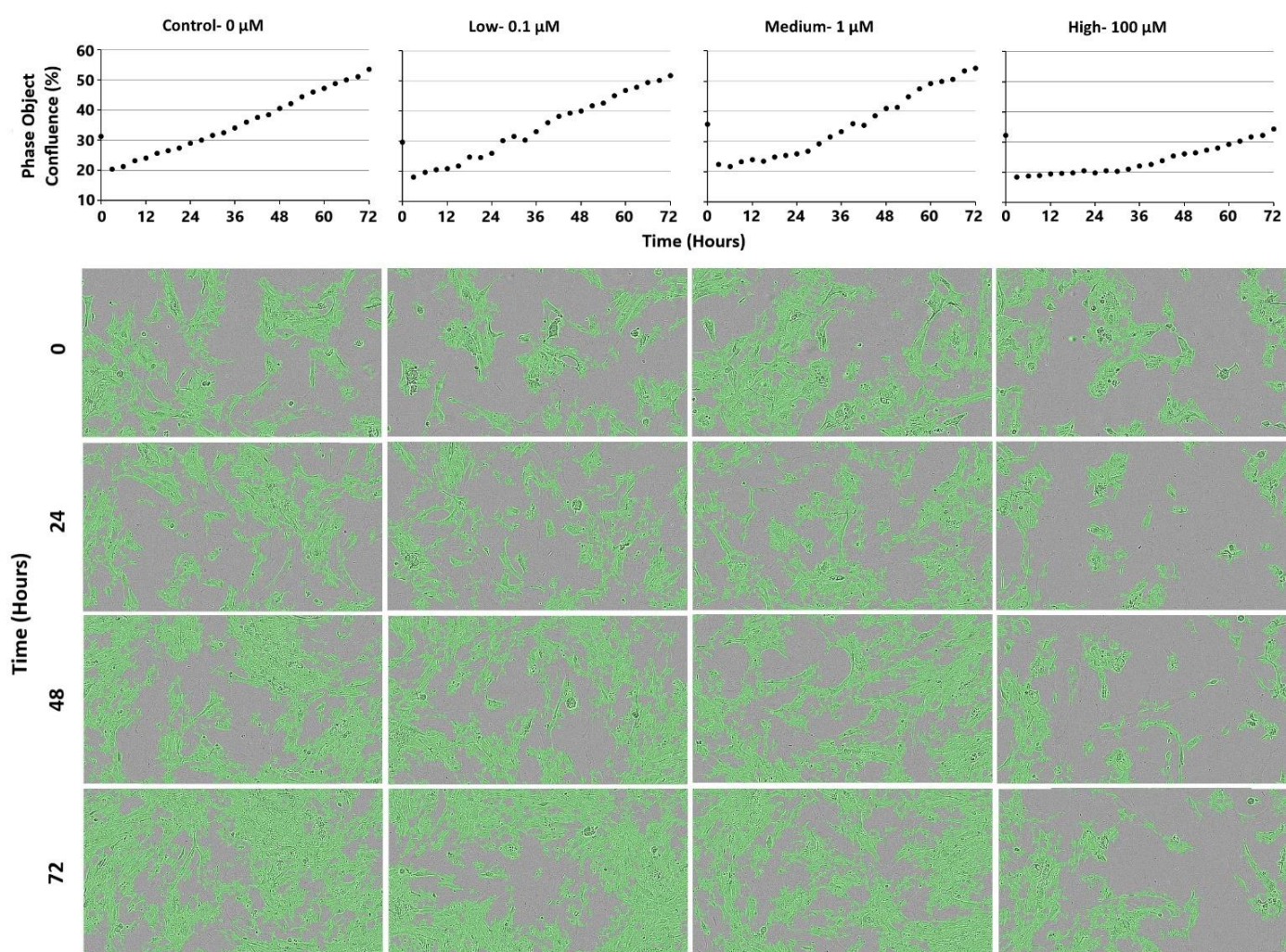


Figure 2.49: IncuCyte cell confluence and representative images data of patient 4 derived BAT cells treated with CAP. Drug concentration from left to right: control, 0.1 μM low, 1 μM medium and 100 μM high.

Celecoxib

Similar to the TC sample, at 0.1 and 1 μM dose no response to CXB treatment was demonstrated, however at 100 μM dose an 11 % reduction in tumour confluence was observed (Figure 2.50). Therefore, CXB was proven to be effective at high 100 μM drug concentration, this was consistent with the MTT assay data as all grade IV samples required 100 μM dose (Log 5 nM) for a cytotoxic response.

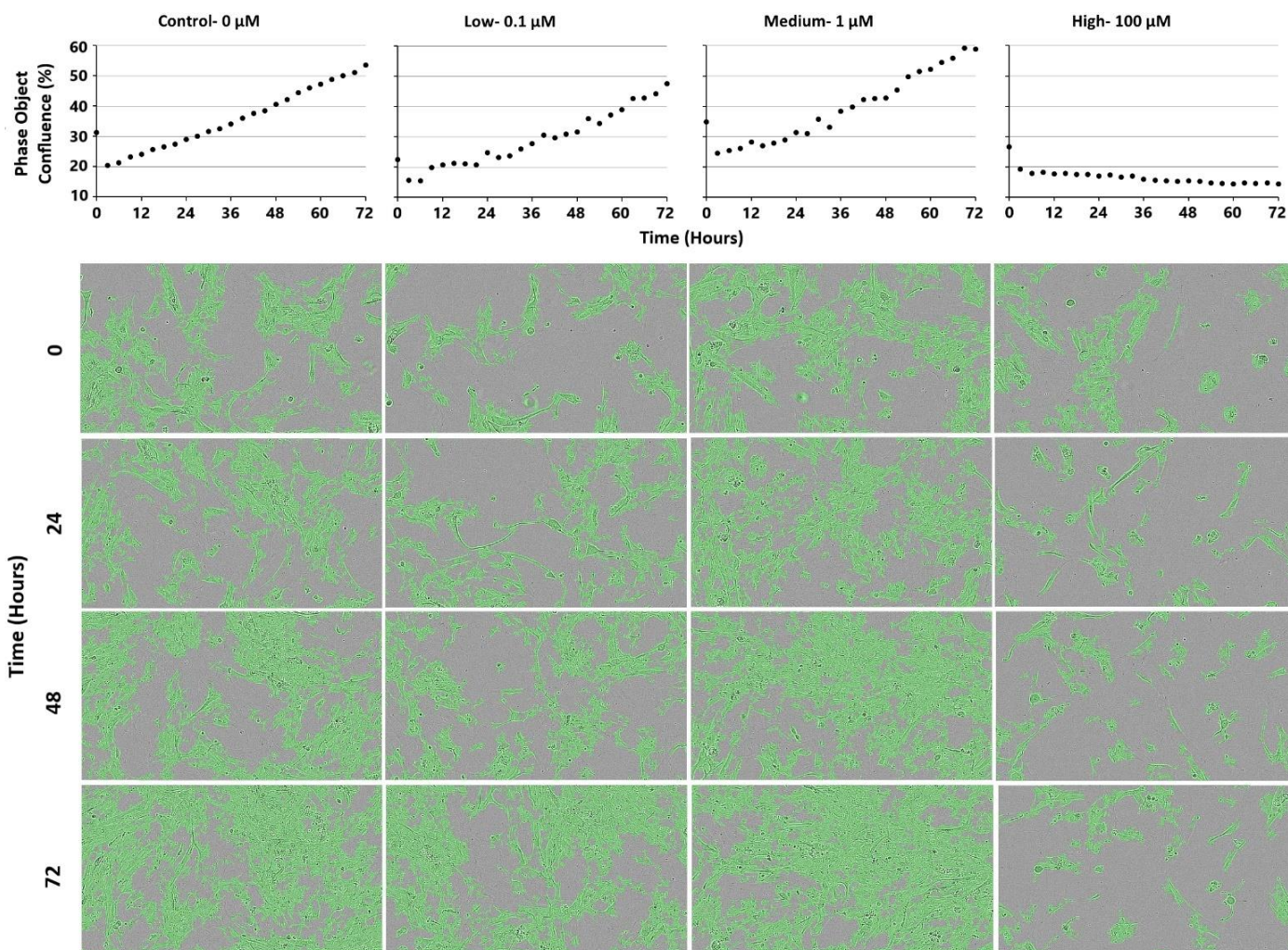


Figure 2.50: IncuCyte cell confluence and representative images data of patient 4 derived BAT cells treated with CXB. Drug concentration from left to right: control, 0.1 μM low, 1 μM medium and 100 μM high.

Ticlopidine

At 0.1 to 100 μM dose TCL demonstrated no efficacy against patient 4 BAT sample, with exponential tumour growth observed over the 72-hour treatment period (Figure 2.51).

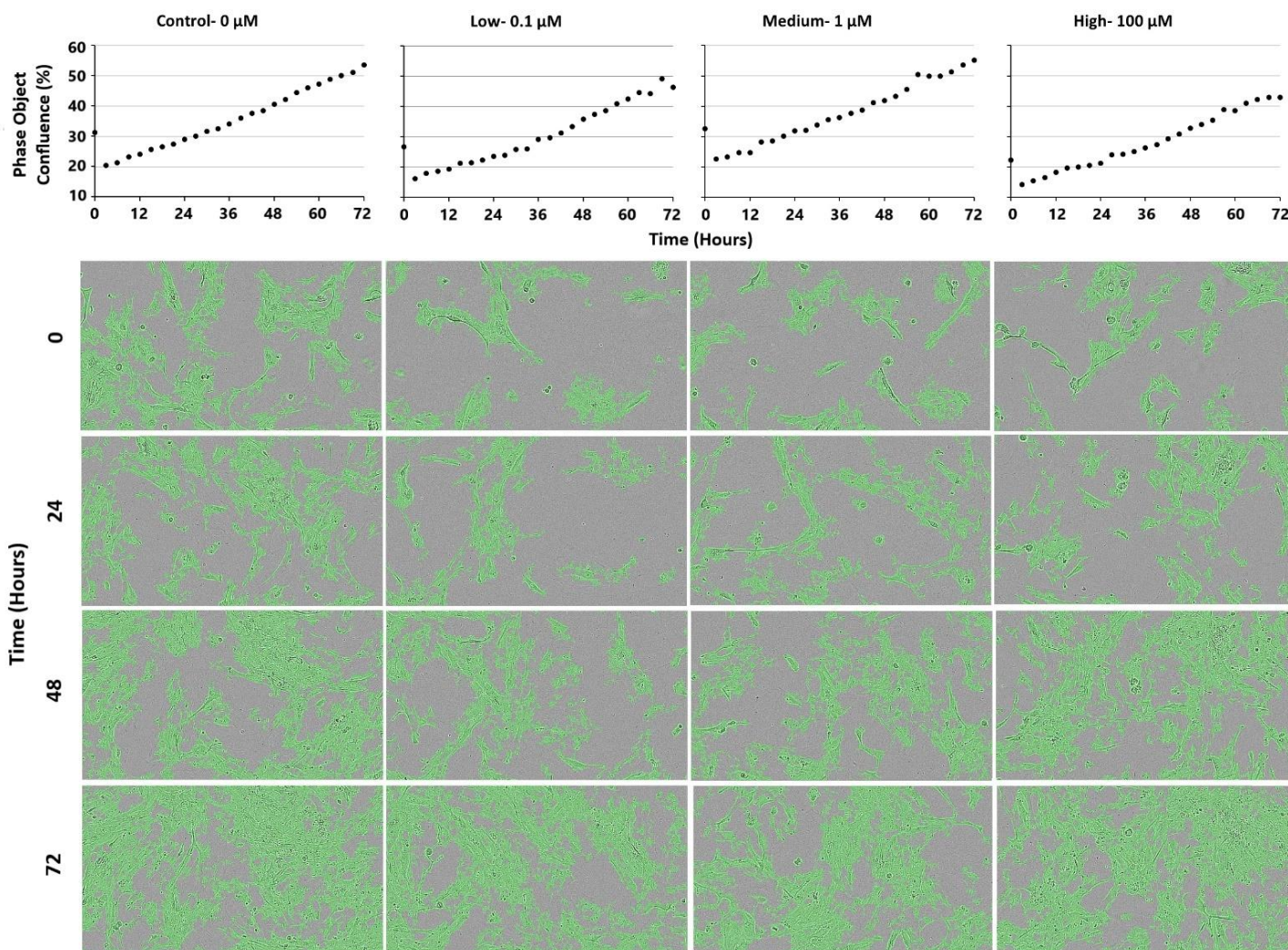


Figure 2.51: IncuCyte cell confluence and representative images data of patient 4 derived BAT cells treated with TCL. Drug concentration from left to right: control, 0.1 μM low, 1 μM medium and 100 μM high.

Itraconazole

ITZ demonstrated no efficacy against all 0.1 to 100 μM doses, with exponential tumour growth observed over the 72 hour incubation period (Figure 2.52).

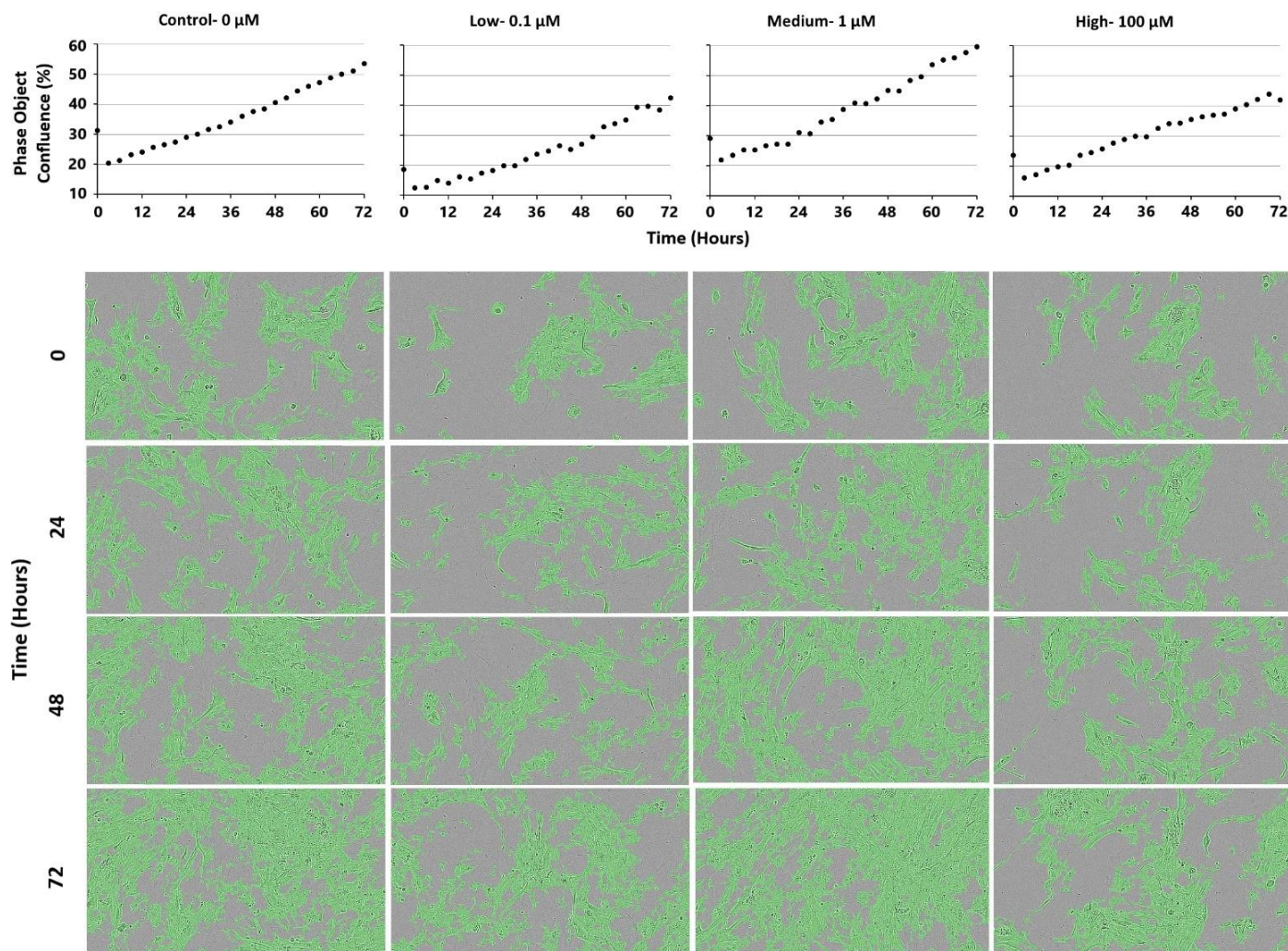


Figure 2.52: IncuCyte cell confluence and representative images data of patient 4 derived BAT cells treated with ITZ. Drug concentration from left to right: control, 0.1 μM low, 1 μM medium and 100 μM high.

2.5 Discussion

2.5.1 Patient demographic vs cytotoxicity drug response

The demographic of the glioma patient population for the samples mainly consist of older age and high-grade (III and IV) tumours. These particular demographic features often correlate with high resistance to treatment and lower survival rate (Chapter one, Figure 1.1) [8]. The use of a more aggressive sample population to assess drug cytotoxicity will add additional validity to any positive data.

2.5.2 Patient abrupt protein expression vs tumour growth and drug response

During pathological testing IDH1, P53, and ATRX, which are all associated with growth control genes, are used to determine the grade and aggressiveness of a tumour. Whereas MGMT is used to determine if treatment with DNA alkylating agents such as TMZ would be worthwhile.

A study undertaken by A Chaurasia et.al assessed ATRX, IDH1 and P53 biomarkers mutation analysis and their correlation to patient survival [132]. Data from 163 patients revealed that patients with mutant IDH and ATRX genes have improved prognosis, while P53 mutation lead to a worse prognosis. Hence a combination of ATRX mutant, IDH mutant and P53 wildtype genes lead to significant improvement in both OSR and PFS [51, 132, 134]. Within our study patient sample population an IDH and ATRX mutations mainly correlated with the lower grade III samples (Table 2.3). Hence any variation between tumour grade IV and III cytotoxicity data could be due to variation in those specified genes, which are known to correlate with the OSR of patients [5, 132, 301-303].

The TC MTT assay data demonstrated little variation between the tumour grade and drug response, with drug effectiveness being consistent between the two grades (Figure 2.53). This is of significance because within a clinical setting lower tumour grade is associated with a more favourable prognosis. Our data demonstrate that this survival benefit could be as a result of a slower rate of cell proliferation rather than drug activity against the tumour. A slow proliferation rate was observed across all grade III samples. The sample from patient 5 with an IDH mutant and ATRX wildtype combination was the slowest. The patient 5 TC

sample did not proliferate at all, with cell number remaining constant over a 3-month incubation period, while the BAT only proliferated during the first month of incubation and then completely stopped.

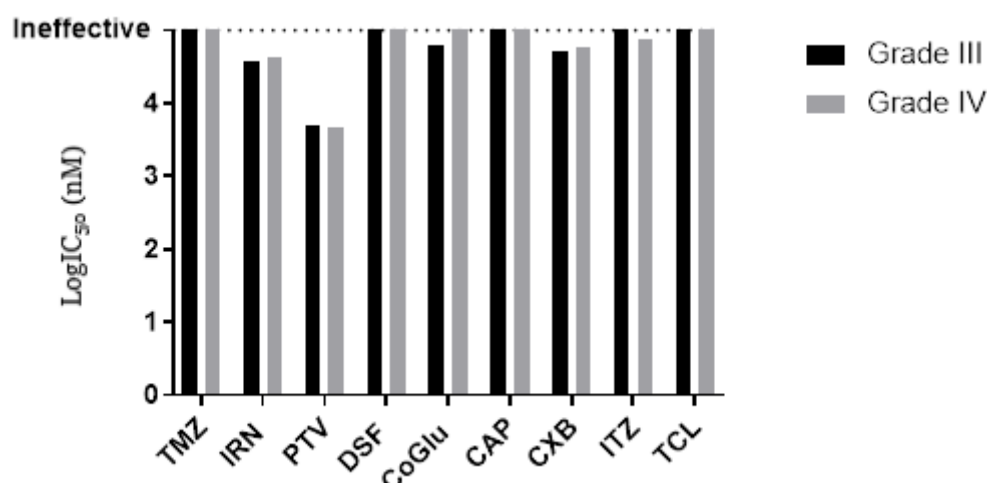


Figure 2.53: MTT LogIC₅₀ cytotoxicity data of, grade IV patients 2-4, 7-11 and grade III patients 6 and 12, TC sample population. For ineffective drug treatments predicted Graphpad Prism LogIC₅₀ values were used.

MGMT methylation is well known to correlate to a favourable prognosis for patients. Many studies have confirmed a correlation between MGMT methylation and OSR benefit in patients treated with TMZ [317-319]. A study undertaken by M. E. Hegi found that the MGMT promotor was methylated in 45 % of 206 cases [317]. Gliomas are also well known for their ability to recur following chemo and radiation treatment. New growth is often composed of a new genetic strain that is resistant to the previous therapy [150, 155, 156]. Hence within our study it would be anticipated that some of the samples are resistant to TMZ treatment because of a combination of two factors: 1) MGMT un-methylation and 2) previous TMZ treatment.

2.5.3 MTT Data analysis and visualisation

A wide variety of *de-novo* treatment options for gliomas have been developed and tested within clinical settings without producing any positive results. These include; newly synthesised drugs, radiation therapy, immunotherapy, advanced surgical treatments and a combination of these [320-326]. Since no effective treatment has been found following the

large investment in developing new treatments, repurposing of already FDA approved drugs is gaining a new interest (Chapter one, 1.4 Drugs that may be suitable for repurposing to treat Glioblastoma).

For this study IRN, PTV, DSF, CoGlu, CAP, CXB, TCL and ITZ have been chosen because they have proven to be pharmacologically well characterized, have a low likelihood of either inducing local toxicity or adding to patient side effect burden and have evidence for interfering with a recognized, well-characterized growth promoting element of glioma (Chapter one, 1.4 Drugs that may be suitable for repurposing to treat Glioblastoma, Table 1.2).

10 TC and 4 BAT glioma samples were used to perform the MTT assay cytotoxic screen of the repurposed drugs. The results reveal that when tested at $<100\ \mu\text{M}$ dose on average PTV was more effective than any other single drug, including TMZ, with LogIC_{50} values of $< 3.5\ \text{nM}$ across a large proportion of the tested samples. (Table 2.5). IRN and CXB monotherapies were also effective against a large proportion of the patient samples but at higher Log 4-5 nM doses (Table 2.5). For the remaining drugs, DSF, CoGlu and ITZ demonstrated some level of efficacy but only for a small proportion of the TC and BAT samples and usually at higher Log 4-5 nM doses (Table 2.5). Finally, CAP and TCL were ineffective across all samples (Table 2.5).

Table 2.5: Colour coded MTT assay logIC₅₀ data chart of patients 1-12 derived TC and BAT cells treated with TMZ, IRN, PTV, DSF, CoGlu, CAP, CXB, TCL and ITZ.

TC

Patient	TMZ	IRN	PTV	DSF	CoGlu	CAP	CXB	TCL	ITZ	Drug Effectiveness	LogIC ₅₀ (nM)
2	Ineffective	4.43								High	1
3	Ineffective	Ineffective	4.81	Ineffective	Ineffective	Ineffective	4.51	Ineffective	Ineffective		1.5
4	Ineffective	4.55	4.99	Ineffective	4.95	Ineffective	4.87	Ineffective	Ineffective		2
6	Ineffective	4.85	4.75	Ineffective	4.51	Ineffective	4.69	Ineffective	Ineffective		2.5
7	Ineffective	4.63	3.20	Ineffective	Ineffective	Ineffective	4.17	Ineffective	4.29		3
8	Ineffective	4.61	3.22	4.83	Ineffective	Ineffective	4.51	Ineffective	4.33	Medium	3.5
9	Ineffective	4.87	4.72	3.54	Ineffective	Ineffective	Ineffective	Ineffective	Ineffective		4
10	Ineffective	4.50	2.67	Ineffective	Ineffective	Ineffective	4.75	Ineffective	Ineffective	Low	4.5
11	Ineffective	4.24	1.98	Ineffective	Ineffective	Ineffective	4.52	Ineffective	Ineffective		5
12	Ineffective	4.64	2.63	Ineffective	Ineffective	Ineffective	4.72	Ineffective	Ineffective	Ineffective	>5

BAT

Patient	TMZ	IRN	PTV	DSF	CoGlu	CAP	CXB	TCL	ITZ
2	Ineffective	Ineffective	Ineffective	Ineffective	Ineffective	Ineffective	Ineffective	Ineffective	Ineffective
4	Ineffective	Ineffective	Ineffective	Ineffective	Ineffective	Ineffective	4.96	Ineffective	4.77
8	2.86	Ineffective	4.61	Ineffective	4.92	Ineffective	4.47	Ineffective	Ineffective
9	Ineffective	Ineffective	4.84	3.30	Ineffective	Ineffective	4.95	Ineffective	Ineffective

Although the current chemotherapeutic treatment TMZ ineffectiveness at <100 μM doses may seem surprising, within the literature TMZ IC_{50} values are often reported within the range of 200-900 μM for a 24-72 hour cytotoxicity assay [310-313]. Hence supporting our results that below 100 μM concentration TMZ is ineffective.

Compared to other studies assessing drug cytotoxicity against glioma cell lines, our LogIC_{50} values are slightly higher (Table 2.6) [142, 173-175, 253, 262, 327, 328]. Since we are using cells directly derived from patients this is expected because primary cells are known to be more heterogenous and more resistant against treatment [147, 148, 161, 280-283].

Table 2.6: IC_{50} and LogIC_{50} cytotoxicity data of ITZ, PTV, IRN, DSF, CAP, CoGlu+DSF and CXB, tested against glioma cell lines. [142, 173-175, 253, 262, 327, 328]

Drug	IC_{50} (nM)	LogIC_{50} (nM)
ITZ	390	2.59
PTV	5760	3.76
IRN	8025	3.90
DSF	>10,000	>4
CAP	50,000-25,000	4.70-4.40
DSF+ 1 μM CoGlu	119-460	2.08-2.67
CXB	1250-4490	3.10-3.65

A study undertaken by Sottoriva et.al revealed that genetic variation between different tumour fragments taken a short distance apart is a result of intra-tumour heterogeneity [146]. In this study, the difference in tissue response due to intra-tumour heterogeneity was evaluated. Two separate tumour fragments, TC and BAT, were tested for their response to treatment. For effective and partially effective drugs IRN, PTV, DSF, CXB and ITZ, a statistical student t-test was performed. Results show that there is a statistically significant variation in cytotoxic response between TC and BAT samples for IRN, PTV and ITZ ($P=0.001$, 0.003 and 0.03 , respectively), with all three treatments demonstrating lower effectiveness against the BAT sample (Figure 2.54).

Hence, intra-tumour heterogeneity can result in a significant variation in response to treatment. This is of clinical importance because TC samples are completely removed during

resection surgery and any residual tumour left behind is that of the BAT sample. Therefore, performing cytotoxicity drug screening against the BAT could be more clinically relevant as our data reveals significant variation in response between the different tumour fragments.

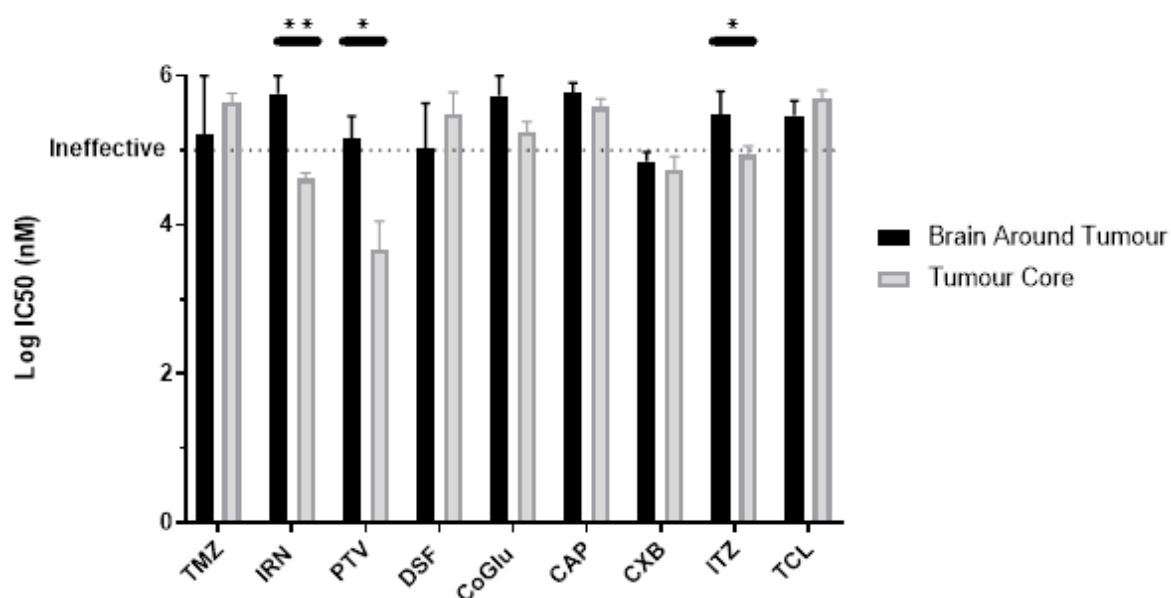


Figure 2.54 Average LogIC₅₀ data for 10 TC and 4 BAT samples tested against mono-therapeutic drug treatments. To plot data for ineffective drug treatments predicted Graphpad Prism LogIC₅₀ values were used. \pm SD is indicated as error bars. Significance between groups is denoted by * $P < 0.05$, ** $P < 0.01$, *** $P < 0.001$, if no line is drawn $P > 0.05$.

2.5.6 IncuCyte data analysis and visualisation

MTT assays are commonly used on glioma primary cells to assess the cytotoxicity of anticancer drugs. However previous reports have been contradicting in regard to the accuracy of results [329]. Within this study the IncuCyte cell imaging proliferation assay was used to confirm the reliability and accuracy of the MTT cytotoxicity data. The IncuCyte assay has the ability to acquire real-time phase contrast images and cell confluence metric over the length of the incubation period [287, 330]. This is useful because along with cell proliferation measurements, it can provide additional information on any change in cellular growth curve and morphology, without the need to interfere with the experiment.

Using both MTT and IncuCyte assays, patient 4 TC and BAT samples were assessed for their response to TMZ, IRN, PTV, DSF, CoGlu, CAP, CXB, ITZ and TCL. The data demonstrates

that although there appears to be some variation between MTT and IncuCyte cytotoxicity data, specifically for TC: DSF and CoGlu and BAT: IRN and PTV, for the vast majority of tested samples, the LogIC₅₀ data were comparable and equivalent drug response values were obtained across the two assays (Figure 2.55). The low variation between the MTT and IncuCyte data validate the accuracy of our drug cytotoxicity data.

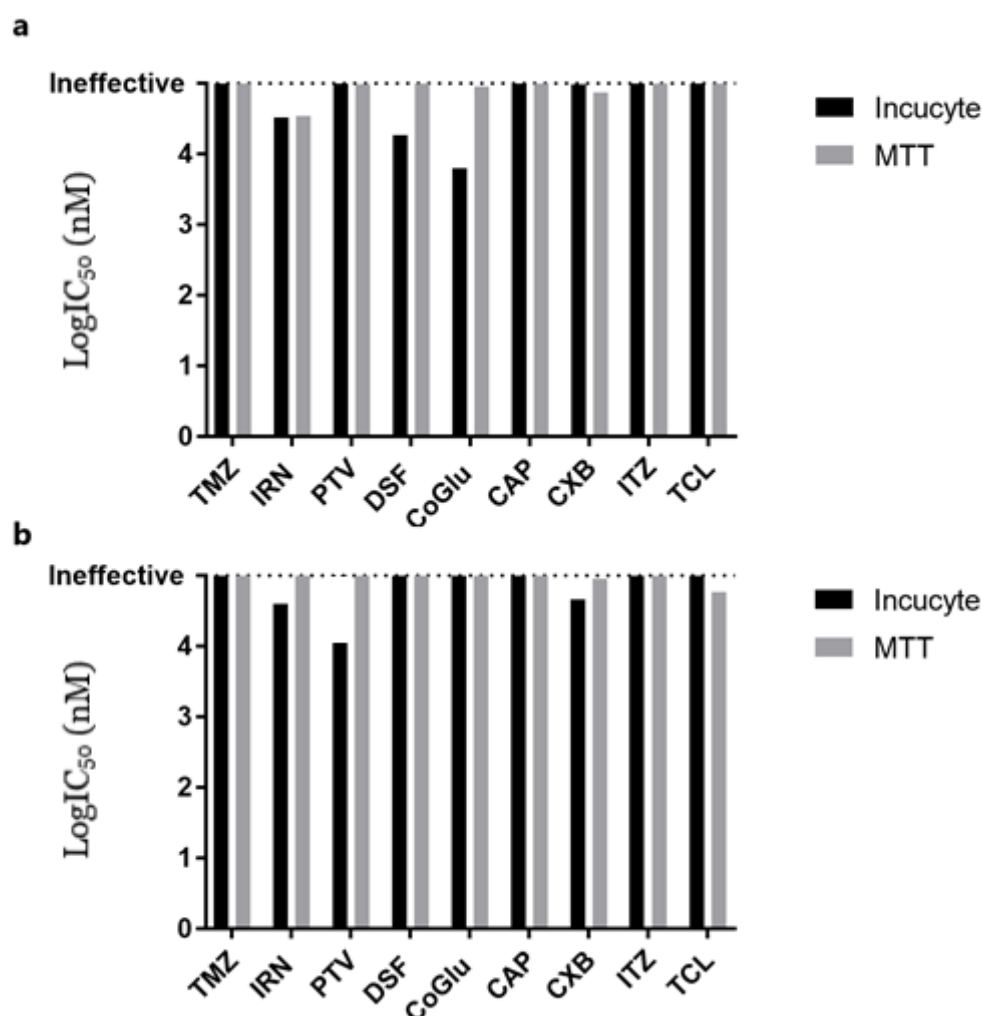


Figure 2.55: MTT vs IncuCyte LogIC₅₀ cell viability data for patient 4 tumour fragments **a)** Tumour Core **b)** Brain around tumour.

As well as the LogIC₅₀ data for each drug, low (0.1 μ M), medium (1 μ M) and high (100 μ M) dose evaluation were performed. Cellular confluence measurements and live images were taken at 24, 48 and 72 hours post treatment; cellular growth curves were used to determine proliferation rate and cellular images were used to track changes in cell confluence and morphology.

With the exception for PTV all the drugs evaluated demonstrated a dose dependant inhibition pattern against both patient 4 TC and BAT samples. Furthermore, with IRN, PTV, DSF and CoGlu, an increase in dose and incubation period induced an alternation in cellular morphology, with cells appearing smaller in size and possessing a spherical shaped morphology compared to the larger, more elongated shape normally observed with glioma cells [382, 383].

For the PTV treated BAT sample the drug dose versus response data did not fit the 'normal' trend, as an increase in PTV dose did not correlate with a decrease in cell confluence. One hypothesis for this trend is the initiation of dormant cells (also sometimes referred to as stem cells); where cells cease to divide but survive in an inactive state while waiting for the appropriate environmental conditions to begin proliferation again. This cell survival mechanism is known to facilitate tumour survival and progression for gliomas [331].

2.6 Conclusion

To ensure our data is reliable and would represent clinical performance as accurately as possible both cellular culture media and cytotoxicity screen test conditions were initially refined, to generate more reliable data that would represent clinical performance as accurately as possible, without compromising on efficiency in relation to cost, time and resources. Once our test conditions were chosen, we performed drug cytotoxicity screen of 8 repurposed drugs: IRN, PTV, DSF, CoGlu, CAP, CXB, TCL and ITZ, and compared those to the current standard chemotherapeutic treatment, TMZ. The cytotoxicity data generated from 12 patient derived tumour samples revealed that at $<100\text{ }\mu\text{M}$ dose IRN, PTV and CXB drug treatments were more effective than TMZ, with PTV being the most potent.

Drug response variation between different tumour fragments were also assessed by performing our drug cytotoxicity screen against both TC and BAT samples. The data demonstrated that significant variation in drug response were found for IRN, PTV and ITZ treatments providing evidence for the existence of intra-tumour heterogeneity.

Moreover, to confirm the reliability and accuracy of our cytotoxicity data, patient 4 LogIC₅₀ results were compared across two separate cytotoxicity assays (MTT and IncuCyte). Between the two assays similar drug effectiveness values were obtained demonstrating our data to be reliable and represents an accurate measure of drug efficacy against gliomas.

Acknowledgment

This work uses samples provided by patients in the NHS. Special thanks to all tissue donors and Queen Elizabeth Hospital staff involved.

For whole exome sequence analysis samples were initially processed and prepared, these were then sent to the University of Birmingham functional genomics laboratory for sequencing. Subsequent data analysis was then performed by Anne Marie Garrett.

IncuCyte assay experimental procedure was performed by Mary Olaloko, subsequent data analysis was then carried out separately.

3. CHAPTER THREE: TISSUE CULTURE COMBINATION DRUG TREATMENT

3.1 Abstract

Background: GBM consist of a diverse collection of genetically heterogeneous clones, with resistance to therapy developing overtime as a result of the more aggressive and less responsive clones being left behind after each treatment cycle. This genetic diversity explains current therapeutic treatments failures and the need for targeting multi genetic cancer pathways simultaneously to kill the different collection of genetic clones.

Method: To address this, four combination drug treatments were chosen to target multiple growth promoting pathways found within a single tumour and/or form synergistic drug activity: i) IRN-PTV-DSF-CoGlu ii) IRN-CAP-CXB-ITZ iii) IRN-CAP-DSF iv) IRN-PTV-CAP-TCL. We used two distinct patient derived tumour fragments (TC and BAT) to generate heterogeneous cell culture. We then tested the efficacy of each combination therapy against culture derived from patients with different MGMT promoter methylation status, phenotypic/ genotypic background and tumour grade. Furthermore, to ensure accuracy of our drug cytotoxicity data, the cell viability results were compared across two distinct cytotoxicity assays (MTT and IncuCyte).

Results: The results demonstrate that multidrug treatment approach was more efficacious than treatment with a single drug, with data validated across different assays. Furthermore, those treatments were also effective across different tumour fragments despite their varying phenotypic characteristics.

Conclusion: Repurposed multi-drug treatments are effective against more glioma patients and at lower dose than single drug. This data was confirmed across separate tumour fragments and cytotoxicity assays, ensuring the accuracy of our drug cytotoxicity data.

3.2 Introduction

Within a single tumour fragment glioma consist of a diverse collection of genetically heterogeneous cellular clones [146, 148, 281, 332-334]. Resistance to treatment naturally develops due to the aggressive and less responsive cancer cells being left behind following each treatment cycle, clinically this is presented as therapeutic treatments failure and

reoccurrence. Since TMZ FDA approval many other single drug treatments have been trialled with no improvement to therapeutic outcome. We thus sought to create a new low dose multidrug treatments that better target the key clinical challenges arising from intratumoral heterogeneity of glioma tumours. Combination drug treatment can enhance efficacy through targeting multiple genetic cancer pathways and eradicating increased number of the cancer cell population, this outcome has been supported by clinical trial data which compare prognosis of patients treated with either single or combination treatment [66, 213, 214, 234, 235, 335-337]. Here we have investigated a list of promising repurposed drugs that have previously been proven to exhibit activity against glioma, are pharmacologically well characterized and hold low likelihood of adding to a patient's side effect burden (Chapter one, 1.4 Drugs that may be suitable for repurposing to treat Glioblastoma). Each drug used in this study classifies into one of the following drug categories that have previously been proposed for use together in combination treatment [66, 213, 214, 234, 235, 335-337]:

Group 1 - Statins

Statins (e.g. PTV) have been proposed as a potential treatment for cancer initially because they have been linked to a lower mortality rate (but not diagnosis) for various cancers [338-342]. For glioma, data has been contradictory, both significant and non-significant associations between statin use and rate of diagnosis as well as survival of glioma patients are reported [343-346]. This could be because of disease location and the requirement to surpass the BBB which is difficult to achieve for many drug molecules. It is thought however that statins could impact glioma via targeting cell signalling pathways and cell permeability poly-glycoprotein pump preventing cell proliferation and active transport of cytotoxic substances, such as IRN, out of the cell [228, 229, 347]. Hence forming a synergistic activity when combined.

Group 2 - Non-Steroidal Anti-Inflammatory Drugs

A high rate of neo-angiogenesis is associated with glioma tumour, providing fast growing tumour cells with a continuous supply of nutrients and toxic waste removal [348]. Anti-

angiogenesis substances, such as CXB have been associated with antineoplastic properties [348-351]. Metronomic therapy of CXB in combination with TMZ have previously been proposed for the treatment of gliomas but no influence on patient survival was found when compared to the current standard [348, 352]. Other than metronomic treatment, no patient survival data after treatment with non-steroidal anti-inflammatory drugs (NSAID) was found. However a recent meta-analysis found a decreasing risk of glioma with increasing NSAID's use, when considering both dosage and length of treatment [353]. Hence the angiogenesis properties of NSAIDs may enhance therapeutic activity when used in combination with other drug treatments.

Group 3- Other antiangiogenic agents

Other angiogenesis and vascularization inhibitors such as Bevacizumab and CAP may slow glioma progression [354]. When combined with other growth and invasion inhibitory agents enhanced potency could be achieved [185].

Group 4 - Oxidative Stress inducing agents

Increasing the reactive oxygen species within cells has been proven to potentiate apoptosis in cancer cells [355, 356]. This mechanism of action is already utilized within radiation and chemotherapy [355]. For cancer cells to reach oxidative stress levels required to induce cancer cell death, a combination of oxidative agents may be needed. DSF, in addition to its other anticancer mechanisms (Chapter one, 1.4 Drugs that may be suitable for repurposing to treat Glioblastoma), has been proven to increase glioma cellular oxidative stress due to its derivative diamide structure [354]. When combined with copper, synergistic oxidative activity and enhanced potency against glioma is predicted [178, 233].

Within this chapter each of the above four drug groups were utilised to develop low dose multidrug treatments that are effective against glioma cells. The multidrug treatments ability to kill glioma cells were compared against both their single drug counterparts and the current standard of care TMZ.

This chapter is a progression from the preliminary work in chapter two, where nine mono-therapeutic drug treatments were evaluated against ten primary glioma cells. Here the same ten primary glioma cells were utilized to assess four combinational drug treatments: i) IRN-PTV-DSF-CoGlu ii) IRN-CAP-CXB-ITZ iii) IRN-CAP-DSF iv) IRN-PTV-CAP-TCL. The chapter presents a full discussion of patient samples clinical demographics, cytotoxicity data, response variation due to intra-tumour heterogeneity and disease re-occurrence following an extended treatment period.

3.3 Materials and methods

All materials and patient samples used were the same as chapter two. Therefore list of materials, sample collection, histological evaluation and cell culture methods are all identical to those listed within chapter two, 2.3 Materials and methods.

3.1 Drug solution

Drug solutions were made according to their solubility (Chapter two, 2.3.6 Drug solution, Table 2.2). TMZ, IRN, CoGlu and CAP were dissolved in sterile distilled water to make a 1 mM stock solution. PTV, DSF, CXB, TCL and ITZ were dissolved in DMSO, to make a 100 mM solution, except for ITZ a 50 mM solution was made. Then to reduce or eliminate DMSO toxicity to cells, these solutions were further diluted in culture medium to make a 1 mM single drug solutions.

Each 1 mM single drug solution was then diluted further in culture medium and combined to produce a 100,000 nM stock solution as per method shown in Figure 3.1.

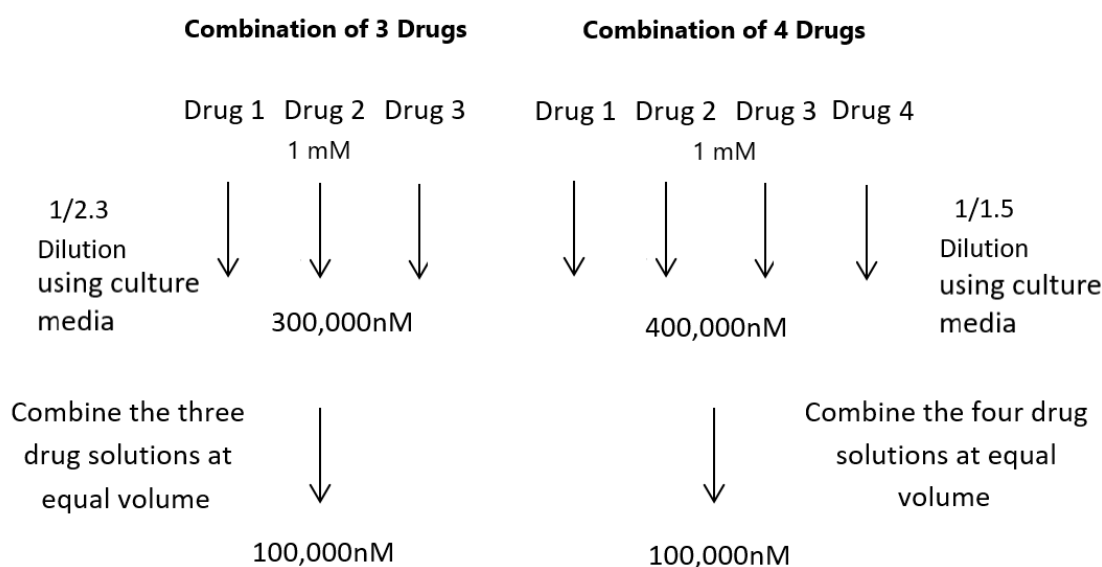


Figure 3.1: Protocol for making 3 and 4 drug combination assay solutions.

Stock solution of each drug combination were then serially diluted in culture media to make the following working concentrations: 100,000, 10,000, 1000, 500, 250, 125, 62.5, 31.25, 15.6 and 7.8 nM. Working solutions were then stored at 5 °C for up to 2 weeks.

3.2 MTT cell metabolism and Incucyte cell proliferation assay

All MTT and IncuCyte assays were performed on TC and BAT tissue cultured samples below passage 10 and 20 respectively, to maintain as much as possible original phenotypic population [299, 300].

Cells were seeded in 96 well plates at 4000 cells/well for MTT assay and 5000 cells/well for IncuCyte assay. For both assays control wells consisting of untreated cells were included, while for the MTT assay blank wells consisting of media only were also included. To allow for cellular attachment; plates were incubated for 24h at 37 °C, 5 % CO₂. Following incubation, medium was aspirated and 200 µL of treatment solution was added. For control and blank wells, 200 µL of culture medium was added, while for the test wells each combination drugs concentration was added in triplicate. Due to the extended incubation period, 250 µL of sterile distilled water was added to perimeter wells to reduce evaporation of medium from test and control wells.

MTT assay:

Plates were incubated for 3, 6, 8, 10 or 14 days. Following incubation period, 20 µL of MTT solution (5 mg/mL in sterile PBS) was added and plates were further incubated for 3 hours. Medium was then aspirated and replaced with 100 µL of DMSO to dissolve the formazan crystals formed. After 15 minutes, at room temperature a reading was performed using FLUOstar Omega microplate reader (BMG Labtech, Durham, NC, USA) at 490 nM wavelength. Percentage viability of each test well was then calculated, and cytotoxicity graph was plotted.

IncuCyte life cell imaging assay:

The 96 well test plate was transferred into IncuCyte Zoom (Essen BioScience, Ann Arbor, Michigan, USA). Cells were then imaged at 3 hours intervals for up to 20 days. Obtained images were then analysed using IncuCyte zoom software (Essen BioScience, Ann Arbor, Michigan, USA); each image was masked, and the cell confluence data was used to calculate

the cell viability score (Chapter two, 2.3.7 MTT cell metabolism and IncuCyte cell proliferation imaging assays, equation 2-1: percentage cell viability).

3.3 Statistical analysis

To determine the LogIC₅₀ and coefficient of determination (R²) values, Log inhibitor vs response analysis nonlinear regression (curve-fit) model with an upper limit set at Log 6 nM was performed by GraphPad Prism version 8.00 for Windows, GraphPad Software, La Jolla California USA, www.graphpad.com.

Statistical significance for the LogIC₅₀ data between the TC and BAT samples was assessed via unpaired student's *t* test method.

To compare equivalent sample population, a 0.05 statistical paired t-test method was used. Specifically, this was used to compare the LogIC₅₀ values of single drug vs combination treatments (e.g PTV vs IRN-PTV-CAP-TCL). The measurements for the two different treatments were applied to the same patients' sample group. Tests were also done simultaneously (i.e same time point) and under identical test conditions.

3.4 Results

3.4.1 clinical demographics

Because this chapter is a progression from chapter two preliminary work, the same patient derived cell-lines were used. The demographic characteristics of the glioma patient population are summarised in chapter two, 2.4.1 Clinical demographics, Table 2.3: patients 2-4, 6-12. The cohort consisted of 7 males and 3 females with a median age at resection surgery of 56 years. Eight of our glioma samples were grade IV and two were grade III.

The genetic screening of aberrant protein expression status for IDH1, MGMT, ATRX and P53 were also performed (chapter two, 2.4.1, Table 2.3). Grade IV patient samples consisted mainly of wildtype IDH1 and ATRX genes, whereas grade III samples were mainly mutant. Patient samples with mutant IDH1 and ATRX genes are often associated with a slower growing tumour, in clinical setting, this corresponds to a better response to treatment [5, 132, 301-303]. For MGMT genetic expression, samples consisted of 6 unmethylated and 4 methylated. Alkylating drugs such as TMZ are known to respond better against glioma tumour with methylated MGMT.

3.4.2 Cell metabolism assay (MTT)

To investigate whether a low dose combination drug treatment would be more effective than a single therapy against glioma, nine patient derived primary cells were used to perform a 3-day MTT assay. A total of four drug combinations were investigated: i) IRN-PTV-DSF-CoGlu ii) IRN-CAP-CXB-ITZ iii) IRN-CAP-DSF iv) IRN-PTV-CAP-TCL. For simplicity and clinical relevance, patient samples were grouped into their distinct tumour grade (IV, III). The cytotoxicity data was presented for each drug combination individually and the patients collectively. For each drug combination a cytotoxicity graph was plotted and LogIC_{50} values calculated. Drug effectiveness was ranked into four distinctive categories; high ($\text{LogIC}_{50} = 0-3$ nM), medium ($\text{LogIC}_{50} = 3-4$ nM), low ($\text{LogIC}_{50} = 4-5$ nM) and ineffective if no LogIC_{50} value was achieved, these four categories were chosen arbitrary to reduce ambiguity during data discussion and simplify comparison between different dataset. When relevant data was compared against individual patient's aberrant protein expression status and single drug cytotoxicity data from chapter two. An overview of the results from the nine patient samples was carried out within the discussion 3.5.3 MTT data analysis and visualisation section. Furthermore, a full LogIC_{50} data summary is presented in thesis appendix B.

Patients' drug response- tumour core (TC)

Within this section a full discussion of each drug combination effectiveness against the TC was constructed.

Grade IV (glioblastoma)

IRN-PTV-DSF-CoGlu

The cytotoxicity profile of IRN-PTV-DSF-CoGlu drug combination reveal that it is highly effective. All samples reached a low, <10 % relative cell viability values at Log 4 nM (Figure 3.2). In addition, low and highly predictable LogIC_{50} values ($\text{LogIC}_{50} < 3 \text{ nM}$ and $R^2 > 0.5$) were obtained for all of the tested samples. Compared to the single drug treatments cytotoxicity curves, this therapy was proven to be more potent.

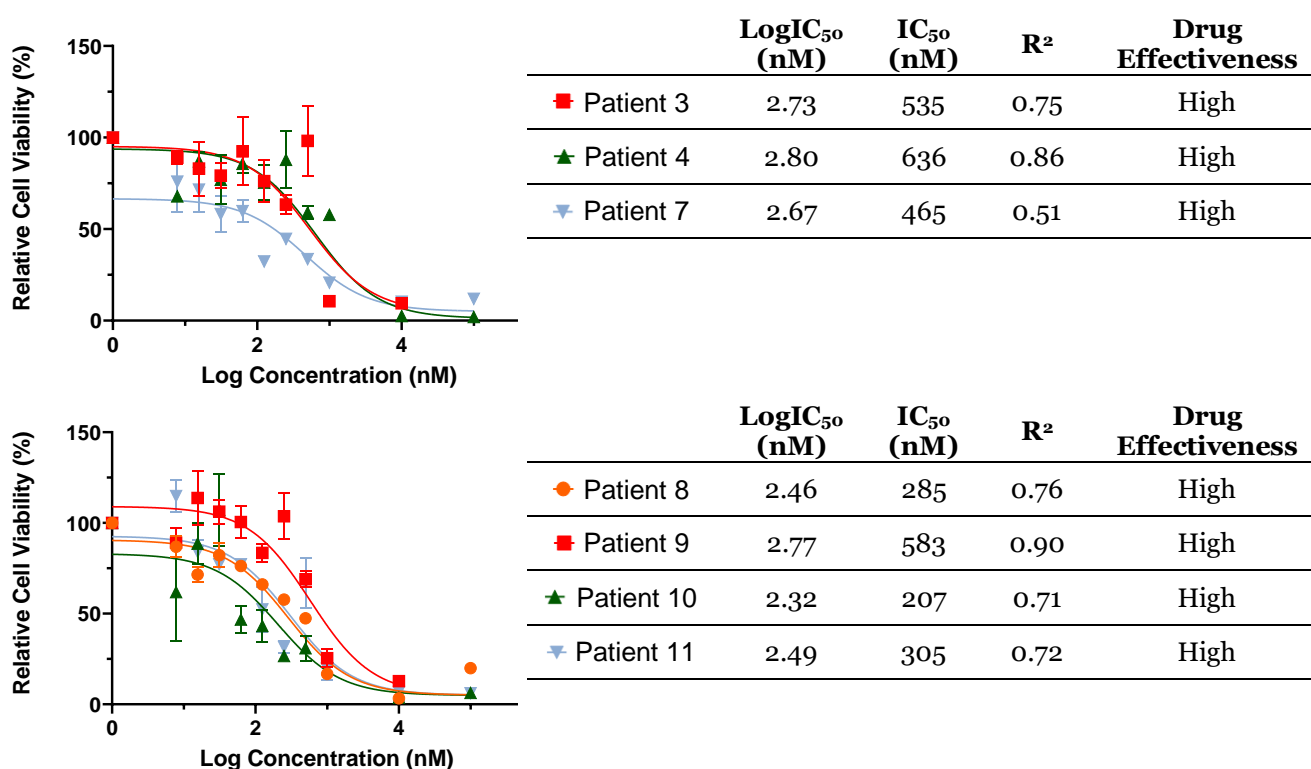


Figure 3.2: LogIC_{50} cytotoxicity curves and data table of IRN-PTV-DSF-CoGlu drug combination tested against primary cells. Seven number assigned grade IV TC samples were evaluated using MTT assay. \pm SEM is indicated as error bars.

IRN-CAP-CXB-ITZ

All Grade IV samples responded to IRN-CAP-CXB-ITZ combination drug treatment (Figure 3.3). Drug effectiveness ranged between low to medium; patients 3, 4, 7, 8 and 9 were low with LogIC_{50} values ranging between 4.15 and 4.59 nM, while patients 10 and 11 were medium with LogIC_{50} values of 3.62 and 3.86 nM, respectively (Figure 3.3). In addition, the LogIC_{50} curves were all consistent in shape and achieved high correlation of determination values ($R^2 > 0.5$) enabling the dose vs response relationship pattern of treatment to be predicted.

Compared to the single drug treatments, the cytotoxicity curves highly resembled IRN and CXB (Chapter two, 2.4.3 Cell metabolism assay (MTT)), this could indicate that response against treatment is achieved mainly from the individual drugs targeting different genetic cancer pathways rather than a synergistic activity of the drug combination.

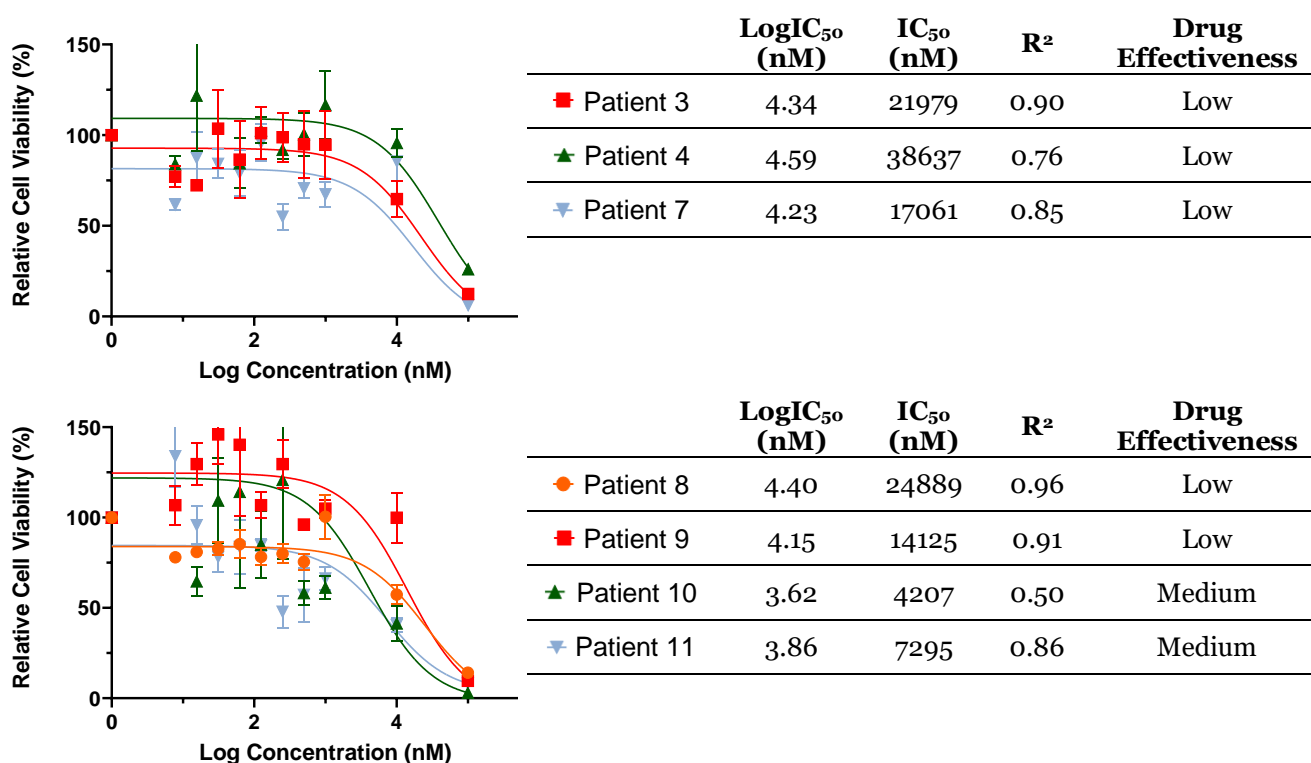


Figure 3.3: LogIC_{50} cytotoxicity curves and data table of IRN-CAP-CXB-ITZ drug combination tested against primary cells. Seven number assigned grade IV TC samples were evaluated using MTT assay. \pm SEM is indicated as error bars.

IRN-CAP-DSF

This drug combination was potent against all tested grade IV samples (Figure 3.4). Patients 3 and 11 achieved medium drug effectiveness with LogIC_{50} values of 3.90 and 3.51 nM, respectively, whilst patients 4, 7, 8, 9 and 10 were low with a LogIC_{50} value range between 4.01 and 4.34 nM (Figure 3.4). When compared to other combination drug treatment, this therapy achieved the lowest variation in LogIC_{50} data and the highest correlation of determination values across all samples, $R^2 > 0.75$. Hence although this combination was not highly effective, a consistency in response to treatment was achieved across different patients.

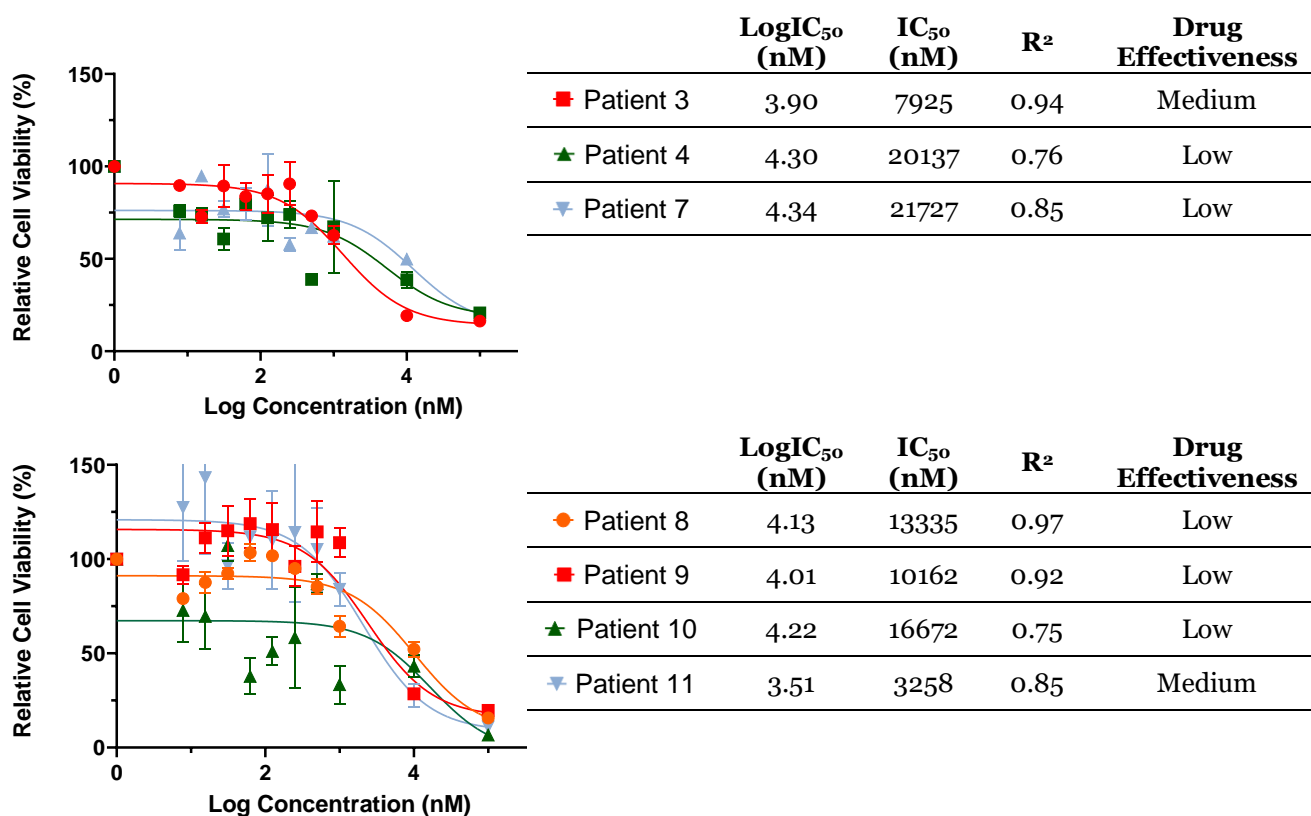


Figure 3.4: LogIC_{50} cytotoxicity curves and data table of IRN-CAP-DSF drug combination tested against primary cells. Seven number assigned grade IV TC samples were evaluated using MTT assay. \pm SEM is indicated as error bars.

IRN-PTV-CAP-TCL

Drug effectiveness for this combination ranged between low to high. Patients 3, 4 and 8 were low with a LogIC_{50} value range between 4.42 and 4.93 nM, whilst patient 11 was medium, with a LogIC_{50} value of 3.58 nM, and patients 7 and 10 were high with LogIC_{50} values of 2.46 and 2.81 nM, respectively (Figure 3.5). Although this drug combination was effective against all patient samples and on average achieved good LogIC_{50} values, when compared to PTV single drug treatment there was no variation in therapeutic response between the LogIC_{50} values of the two therapeutic drug groups ($p = 0.331$) (chapter two, 2.4.3 Cell metabolism assay (MTT)). This suggests that PTV is the dominant drug in this combination with the other drugs contributing very little. Particularly since when comparing this combination treatment to single drug IRN, CAP and TCL, significant variation in therapeutic response were found ($p = 0.017$, 2×10^{-6} , 2×10^{-6} for IRN, CAP and DSF, respectively).

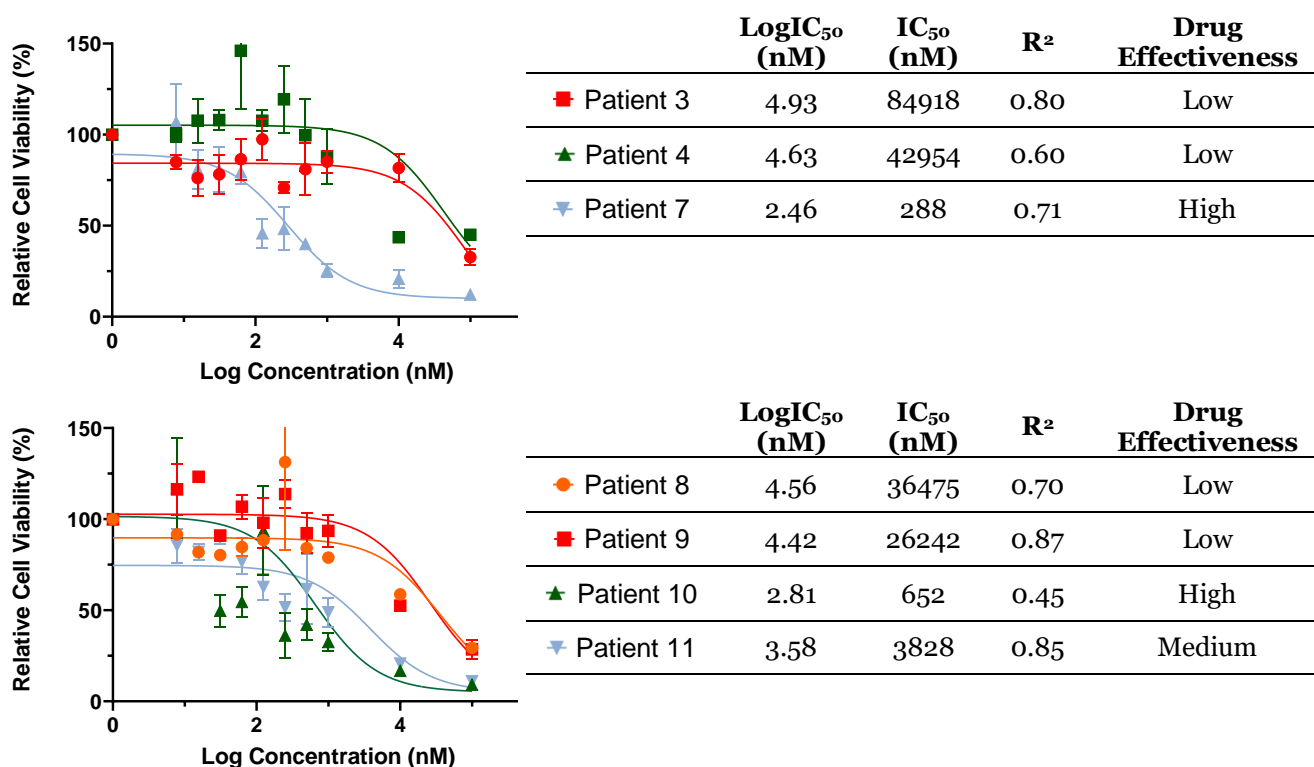


Figure 3.5: LogIC_{50} cytotoxicity curves and data table of IRN-PTV-CAP-TCL drug combination tested against primary cells. Seven number assigned grade IV TC samples were evaluated using MTT assay. \pm SEM is indicated as error bars.

Grade III IRN-PTV-DSF-CoGlu

This drug combination achieved high drug effectiveness against patients 6 and 12 TC

samples with LogIC₅₀ values of 2.38 and 2.41 nM, respectively (Figure 3.6). The LogIC₅₀ curves of both samples were sigmoidal in shape with good correlation, $R^2 > 0.5$ confirming that this drug combination is potent at low dose, < 700 nM. Although grade III samples IDH1 and ATRX protein expression status (3.4.1) are known to be less aggressive than grade IV tested samples, according to our data, response to treatment of both sample groups are equivalent.

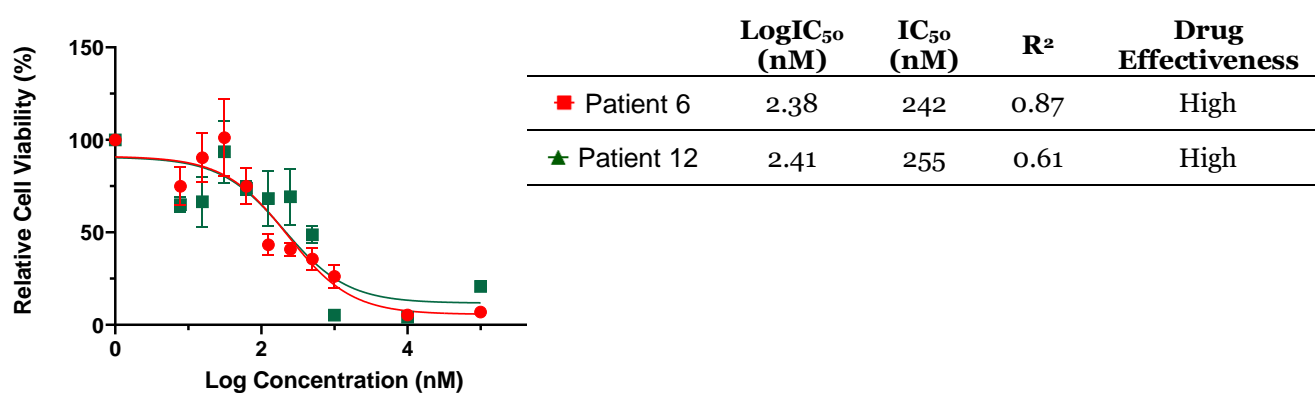


Figure 3.6: LogIC₅₀ cytotoxicity curves and data table of IRN-PTV-DSF-CoGlu drug combination tested against primary cells. Two number assigned grade III TC samples were evaluated using MTT assay. \pm SEM is indicated as error bars.

IRN-CAP-CXB-ITZ

Similar to grade IV cytotoxicity data, IRN-CAP-CXB-ITZ drug combination was effective at high dosage with LogIC₅₀ values of 4.14 and 4.49 nM for patient 6 and 12, respectively (Figure 3.7). High correlation of determination values were also achieved ($R^2 > 0.75$) enabling to predict the dose vs response relationship more reliably. Moreover, when compared to IRN and CXB single drug treatments, the LogIC₅₀ curves were comparable. At Log 5 nM a large decrease in the cell viability scores were observed across both treatment groups confirming that response against treatment could have been achieved from the individual drugs targeting different genetic cancer pathways rather than an enhanced synergic activity of the drug combination.

Therefore, the drug cytotoxicity data was found to be highly consistent between the different tumour grades, III and IV, and this drug combination was confirmed to be highly effective at Log 5 nM.

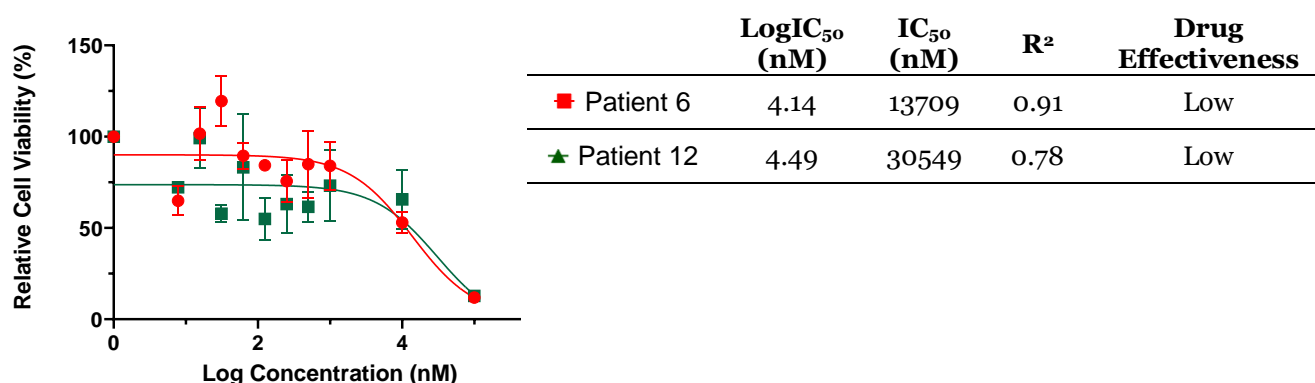


Figure 3.7: LogIC₅₀ cytotoxicity curves and data table of IRN-CAP-CXB-ITZ drug combination tested against primary cells. Two number assigned grade III TC samples were evaluated using MTT assay. \pm SEM is indicated as error bars.

IRN-CAP-DSF

Both grade III patient samples, 6 and 12, responded at medium drug concentration with LogIC_{50} values of 3.55 and 3.81 nM, respectively (Figure 3.8). When compared to the grade IV tested samples, drug cytotoxicity data were consistent. Both sample groups demonstrated that IRN-CAP-DSF drug combination was effective at medium dose, this was supported by a high correlation of determination values for the LogIC_{50} curves, $R^2 > 0.75$.

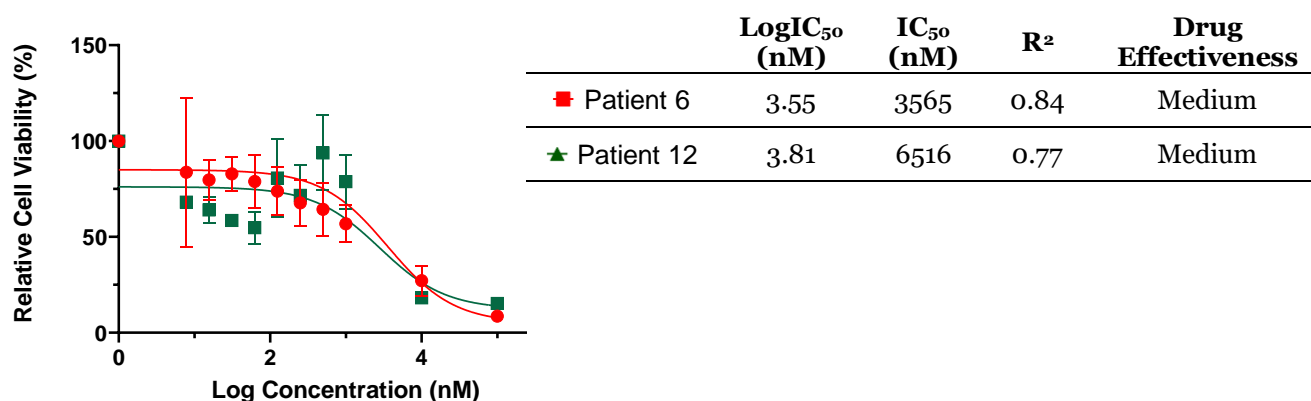


Figure 3.8: LogIC_{50} cytotoxicity curves and data table of IRN-CAP-DSF drug combination tested against primary cells. Two number assigned grade III TC samples were evaluated using MTT assay. \pm SEM is indicated as error bars.

IRN-PTV-CAP-TCL

Patient 6 and 12 achieved LogIC₅₀ values of 4.60 and 4.63 nM, respectively (Figure 3.9). This cytotoxicity data was consistent to that of the grade IV tested samples, even though their tumour grade (III) IDH1 and ATRX protein expression status were of a less aggressive tumour (2.4.1 Clinical demographics, Table 2.3).

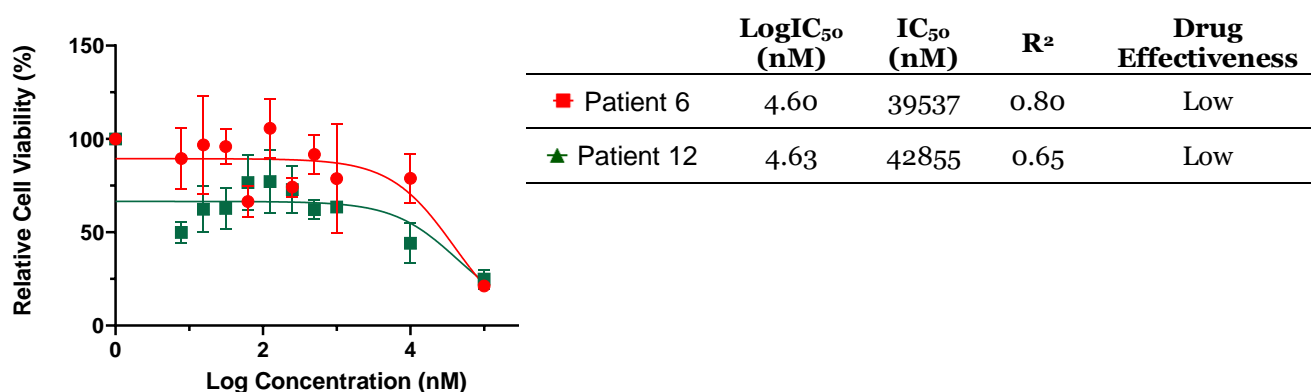


Figure 3.9: LogIC₅₀ cytotoxicity curves and data table of IRN-PTV-CAP-TCL drug combination tested against primary cells. Two number assigned grade III TC samples were evaluated using MTT assay. \pm SEM is indicated as error bars.

Patients' drug response- brain around tumour (BAT)

Following a craniotomy, the TC is often completely removed but the BAT is left behind. This residual tumour is subsequently targeted via chemotherapy and radiation; however, it eventually forms resistance resulting in recurrence of a chemo resistant tumour. To investigate whether a low dose combination drug treatment would be more effective against residual tumour than a single drug treatment, four patients derived BAT cells were used to perform a 3-day MTT assay. Within this section a full discussion of each drug combination effectiveness against the BAT was carried out. When relevant, the data was compared against the individual patient's aberrant protein expression status and single drug cytotoxicity data from chapter two.

Due to the difficulty in culturing grade III BAT samples up to a sufficient cell number for use in an MTT assay, only grade IV samples were used.

Grade IV (glioblastoma)

IRN-PTV-DSF-CoGlu

All grade IV patient BAT samples responded to IRN-PTV-DSF-CoGlu combination drug treatment. Drug effectiveness ranged between low to high; patient 1 and 9 achieved low and medium therapeutic response with LogIC_{50} values of 4 and 3.64 nM, respectively, while patients 4 and 8 were high with LogIC_{50} values of 2.63 and 2.25 nM, respectively (Figure 3.10).

When compared to the same patients TC samples (patients 4, 8 and 9) there was no significant variation in response to treatment ($P=0.74$). In addition, the cell viability data and LogIC_{50} curves were comparable between the two tumour fragments. Thus, the overall drug cytotoxicity data demonstrates that variation in the response between the different tumour fragments was small.

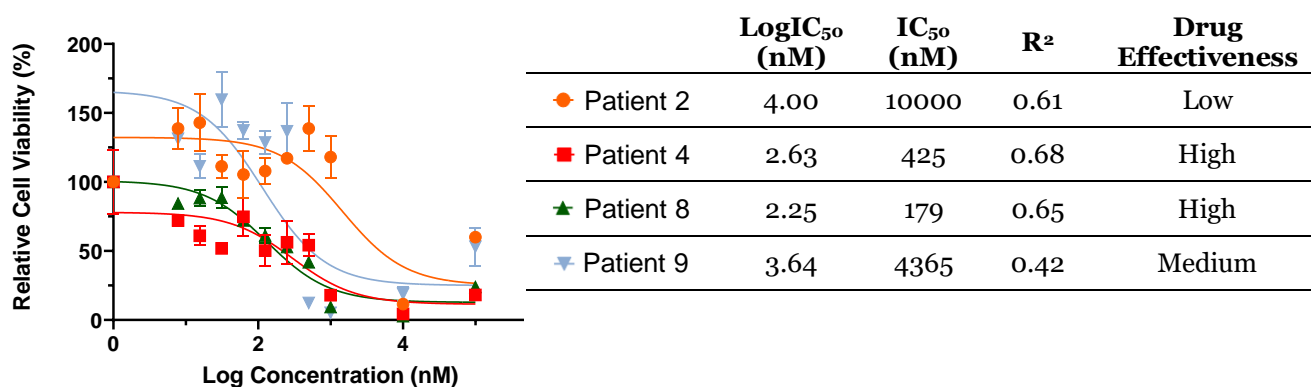


Figure 3.10: LogIC_{50} cytotoxicity curves and data table of IRN-PTV-DSF-CoGlu drug combination tested against primary cells. Four number assigned grade IV BAT samples were evaluated using MTT assay. \pm SEM is indicated as error bars.

IRN-CAP-CXB-ITZ

Two out of the four patient tested samples responded against IRN-CAP-CXB-ITZ combination drug treatment; patients 8 and 9 with LogIC_{50} values of 4.30 and 3.76 nM, respectively (Figure 3.11). Comparing this data to the corresponding TC fragments (for patients 4, 8 and 9) reveal that there was statistically no significant variation between the cytotoxic response of the two groups, $P = 0.32$. In addition, at Log 5 nM there was a large decrease in the cell viability scores, particularly for patients 8 and 9, which typically resembled IRN and CXB single drug treatment data, confirming that response against treatment could be from the individual drugs targeting different genetic cancer pathways rather than a synergistic activity of the drug combination.

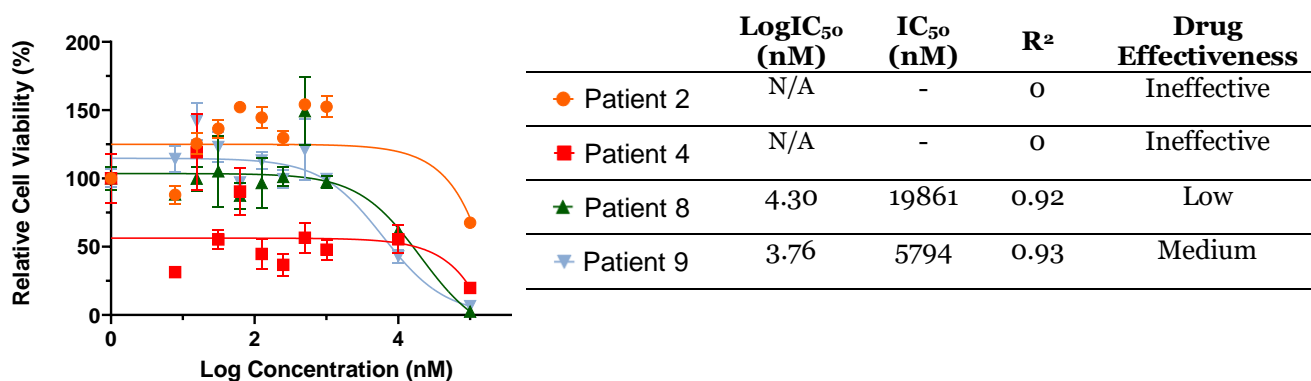


Figure 3.11: LogIC_{50} cytotoxicity curves and data table of IRN-CAP-CXB-ITZ drug combination tested against primary cells. Four number assigned grade IV BAT samples were evaluated using MTT assay. \pm SEM is indicated as error.

IRN-CAP-DSF

Three out of the four grade IV BAT tested samples responded against IRN-CAP-DSF combination drug treatment; patients 4 and 8 with LogIC_{50} values of 4.42 and 4.44 nM, respectively, whilst patient 9 was effective at medium dose with LogIC_{50} value of 3.33 nM (Figure 3.12). When compared to the same patients TC samples (patients 4, 8 and 9) there was statistically no significant variation in drug response ($P=0.41$).

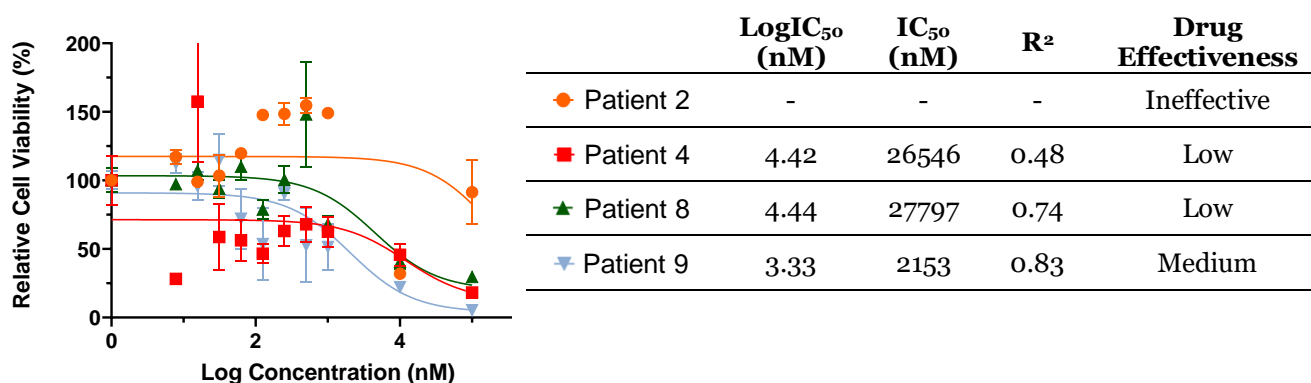


Figure 3.12: LogIC_{50} cytotoxicity curves and data table of IRN-CAP-DSF drug combination tested against primary cells. Four number assigned grade IV BAT samples were evaluated using MTT assay. \pm SEM is indicated as error.

IRN-PTV-CAP-TCL

Three out of the four patient tested samples responded against IRN-PTV-CAP-TCL combination drug treatment; patient 4 achieved a LogIC_{50} value of 4.74 nM while patients 8 and 9 demonstrated high effectiveness with LogIC_{50} values of 2.55 and 2.58 nM, respectively (Figure 3.13). Comparing this data to the corresponding TC fragments reveal that for patients 4, 8 and 9 there was statistically no significant variation between the cytotoxic response of the two groups ($P = 0.10$).

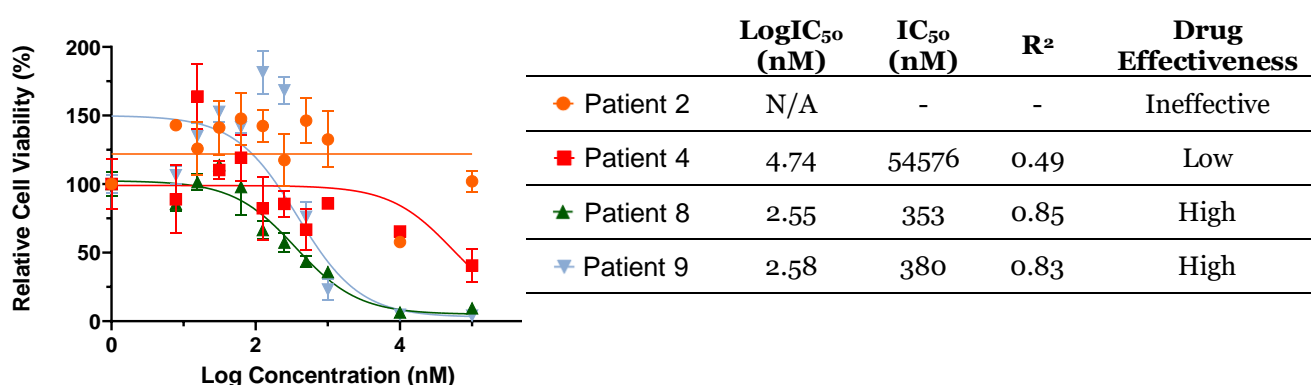


Figure 3.13: LogIC_{50} cytotoxicity curves and data table of IRN-PTV-CAP-TCL drug combination tested against primary cells. Four number assigned grade IV BAT samples were evaluated using MTT assay. \pm SEM is indicated as error.

3.4.3 IncuCyte cell proliferation assay

Cell metabolism assays such as MTT rely on the cell metabolic activity as a measure of cellular viability, thus indirectly assessing cytotoxicity. Within this study direct measurement of the cellular viability via cell imaging assay was performed on patient 4 TC and BAT samples, to ensure the accuracy of the drug cytotoxicity data and as a comparison between end-point MTT and real-time IncuCyte assays.

Same as the experimental configuration of the MTT assay, a total of four drug combinations were investigated: i) IRN-PTV-DSF-CoGlu ii) IRN-CAP-CXB-ITZ iii) IRN-CAP-DSF iv) IRN-PTV-CAP-TCL. For each sample, a cytotoxicity graph was plotted and LogIC_{50} values calculated. Drug effectiveness was ranked into four distinctive categories; high ($\text{LogIC}_{50} = 0-3$ nM), medium ($\text{LogIC}_{50} = 3-4$ nM), low ($\text{LogIC}_{50} = 4-5$ nM) and ineffective if no LogIC_{50} value was achieved, these four categories were chosen arbitrary to reduce ambiguity during data discussion and simplify comparison between different dataset.

Additionally, for each therapy cellular confluence measurement and observation of cellular morphological changes at 0.1 μM , 1 μM and 100 μM dose were performed, over a 3-day treatment period for the TC and up to 20 days for the BAT. For the BAT data the contrast phase images were less resolved, as a result cellular shape could not be determined, thus data evaluation of cellular morphology change will not be discussed for this sample.

Patient 4 TC

IRN-PTV-DSF-CoGlu, IRN-CAP-CXB-ITZ, IRN-CAP-DSF and IRN-PTV-CAP-TCL

combination drug treatments were all effective against patient 4 TC sample with LogIC_{50} values of 3.13, 4.59, 4.25 and 4.67 nM, respectively (Figure 3.14). Additionally, high R^2 values (> 0.84) were achieved across all combination drug treatments demonstrating that the cell viability data is tightly clustered around the cytotoxicity curve, enabling to predict the LogIC_{50} values more precisely (Figure 3.14). Compared to other single drug treatments and the current standard therapy (TMZ) improved logIC_{50} values were achieved (Chapter two, 2.4.3 Cell metabolism assay (MTT)).

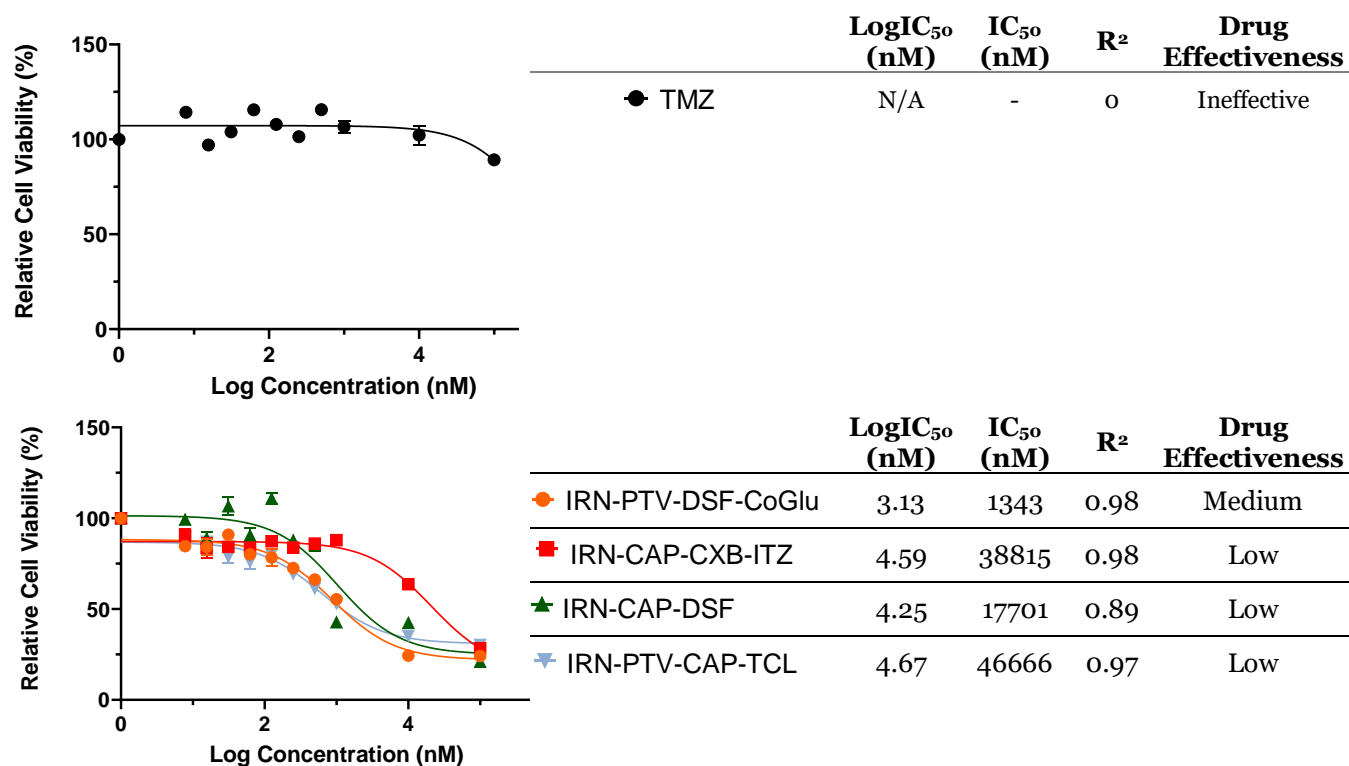


Figure 3.14: IncuCyte 3-day cytotoxicity assay, LogIC_{50} curves and data table of combination drug treatments tested against patient 4 TC cells. \pm SEM is indicated as error.

To ensure the accuracy of the drug cytotoxicity data and as a comparison between end-point MTT and real-time IncuCyte assays, the LogIC₅₀ values of both cytotoxicity assays were compared and the therapeutic dose response data were shown to be comparable (Table 3.1).

Table 3.1: Combination drug treatment LogIC₅₀ values comparison between MTT and IncuCyte assays for the TC samples.

Treatment	LogIC ₅₀ (nM)	
	MTT	IncuCyte
IRN-PTV-DSF-CoGlu	2.803	3.128
IRN-CAP-CXB-ITZ	4.587	4.589
IRN-CAP-DSF	4.304	4.248
IRN-PTV-CAP-TCL	4.633	4.669

IRN-PTV-DSF-CoGlu

Both cellular confluence and morphological data confirmed a dose-response relationship for this combination. Compared to the control, at low dose IRN-PTV-DSF-CoGlu drug combination was proven to be ineffective with exponential tumour growth over time (Figure 3.15). At medium dose slow tumour growth was observed during the initial 24 hours of treatment followed by a plateau (Figure 3.15). At high dose, cellular confluence declined, and morphological changes were observed; cellular structure changed from highly elongated to a small, ball shaped morphology (Figure 3.15). This data confirms the MTT cytotoxicity results as most samples responded against treatment at medium dose.

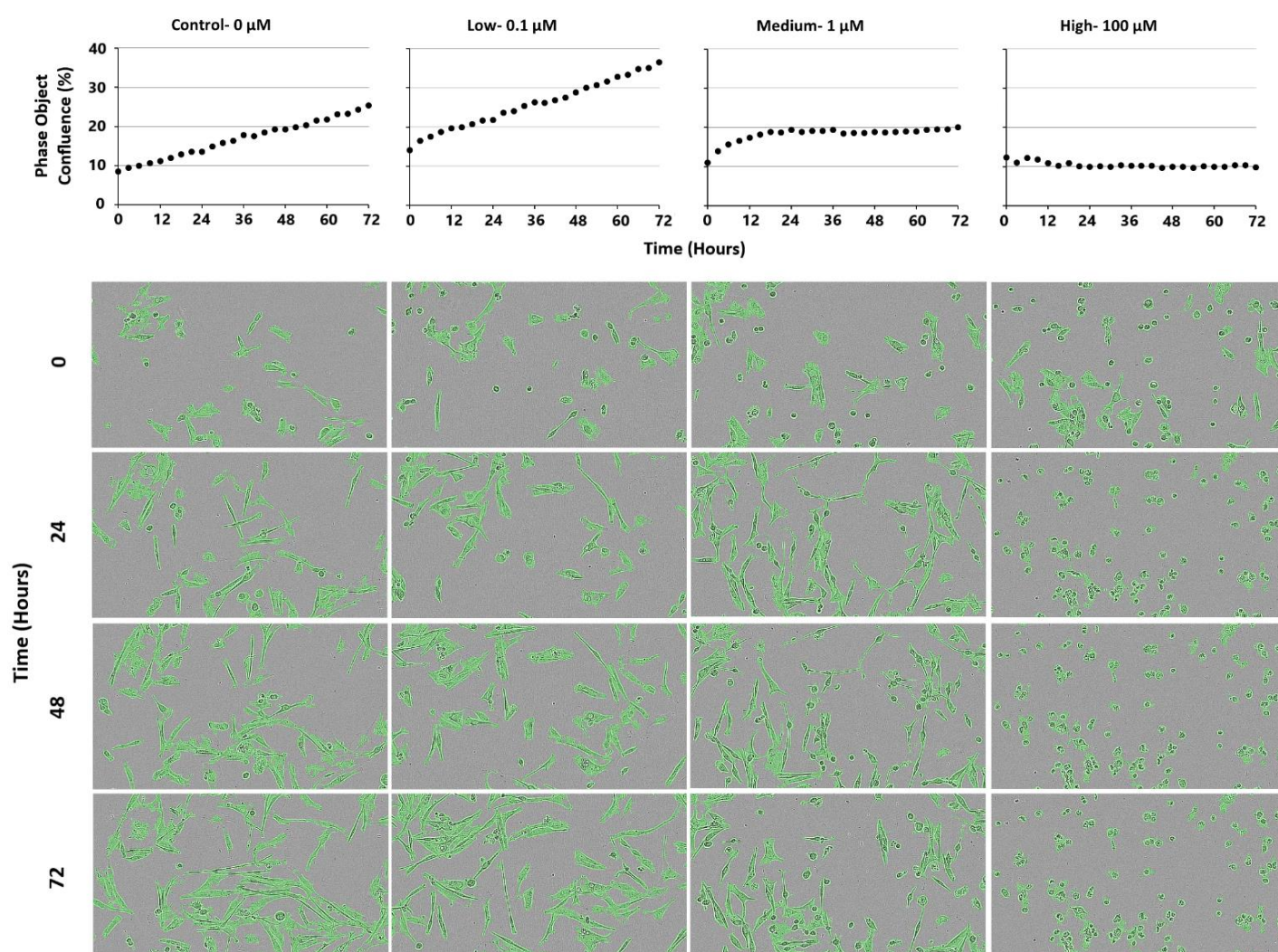


Figure 3.15: IncuCyte cell confluence and representative images data of patient 4 derived TC cells treated with IRN-PTV-DSF-CoGlu drug combination. Drug concentration from left to right: control, 0.1 μ M low, 1 μ M medium and 100 μ M high.

IRN-CAP-CXB-ITZ

Both low and medium dose treatments exhibited a similar cellular growth pattern as the control; exponential tumour growth was observed with cells developing into elongated shaped interconnected cell culture over time (Figure 3.16). At high dose, no growth was observed, and cellular confluence remained constant with cells appearing to form a small irregular shaped structure following a 72 hour treatment (Figure 3.16). This data confirms our MTT cytotoxicity results as most of the patient samples responded against IRN-CAP-CXB-ITZ treatment at high dose.

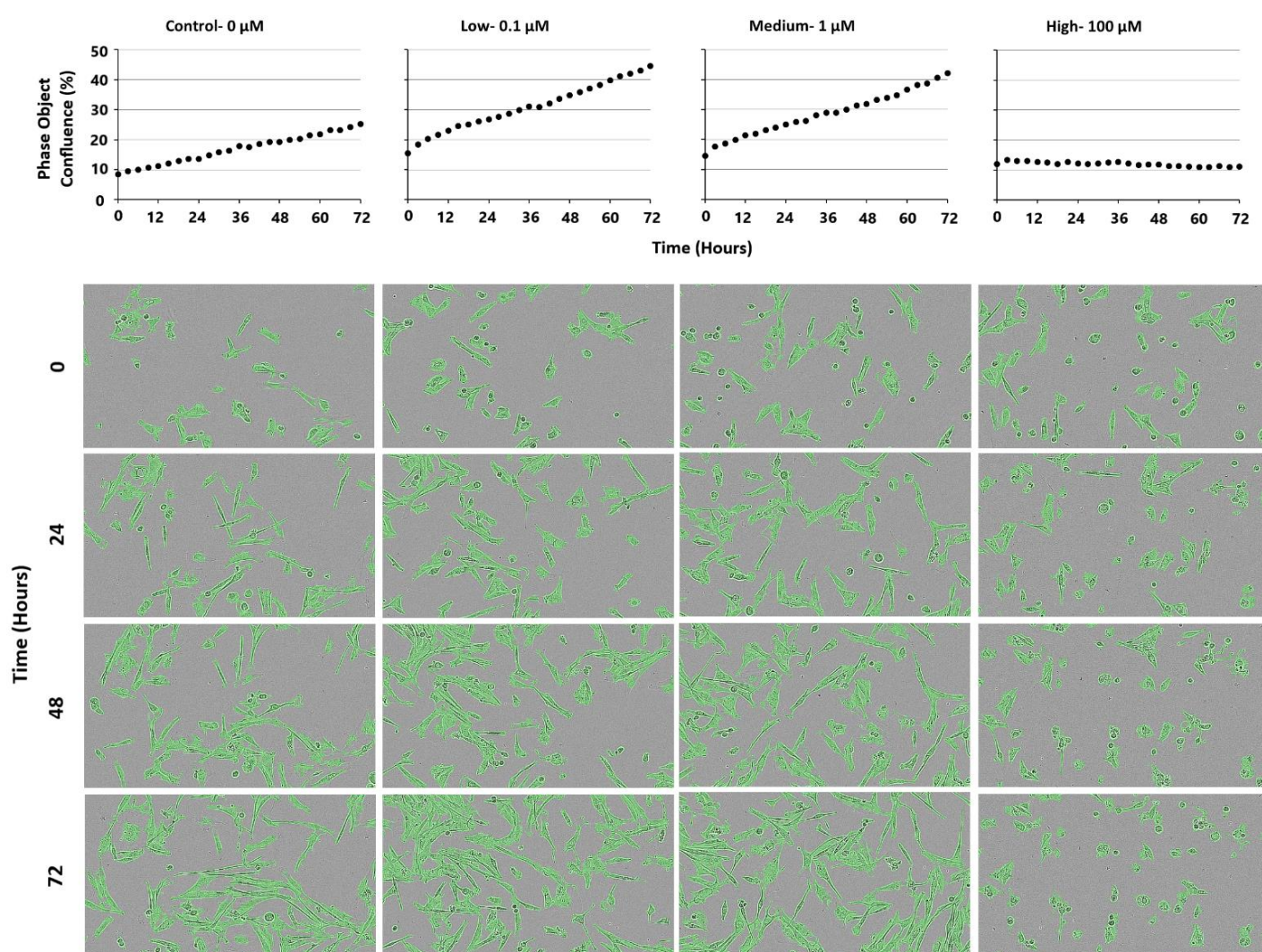


Figure 3.16: IncuCyte cell confluence and representative images data of patient 4 derived TC cells treated with IRN-CAP-CXB-ITZ drug combination. Drug concentration from left to right: control, 0.1 µM low, 1 µM medium and 100 µM high.

IRN-CAP-DSF

At low dose IRN-CAP-DSF drug combination demonstrated no efficacy with exponential tumour growth over time, while at medium and high dose treatments, tumour growth ceased and cellular confluence remained relatively constant over the 72 hour treatment period. Cellular morphology was also effected with cells appearing smaller and less elongated compared to control (Figure 3.17). Thus, this data validates our IRN-CAP-DSF drug combination MTT cytotoxicity results as most patient tested samples responded against treatment at medium or high dose.

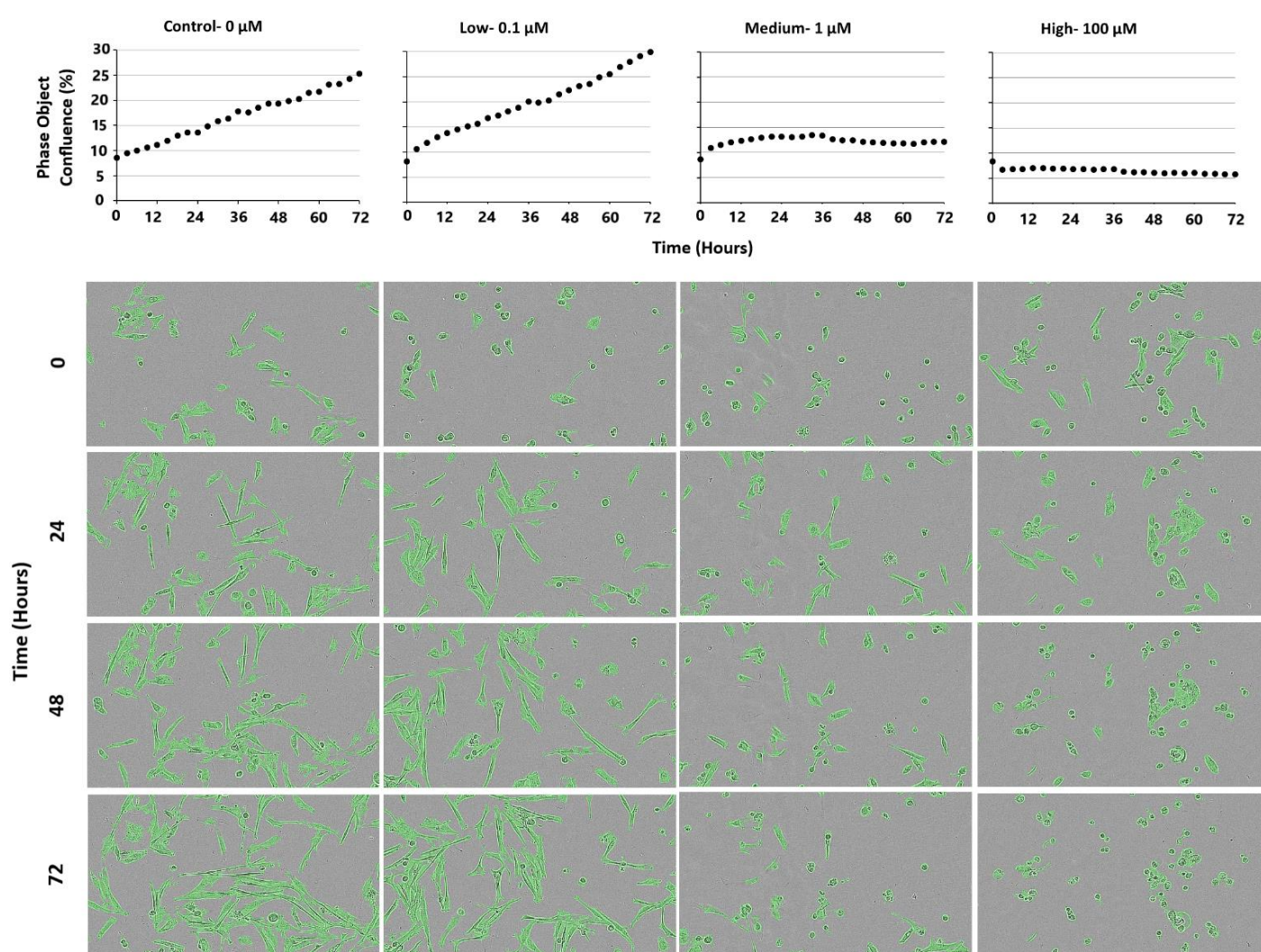


Figure 3.17: IncuCyte cell confluence and representative images data of patient 4 derived TC cells treated with IRN-DSF-CAP drug combination. Drug concentration from left to right: control, 0.1 μM low, 1 μM medium and 100 μM high.

IRN-PTV-CAP-TCL

IRN-PTV-CAP-TCL drug combination cell confluence and morphology data were extremely similar to the PTV single drug treatment (Chapter two, 2.4.3 Cell metabolism assay (MTT)).

At low dose, exponential tumour growth was observed with cells developing into a large elongated network of cell culture (Figure 3.18). At medium dose, fast exponential tumour growth was initially established followed by a plateau, cellular morphology remained as elongated structure but with an enhanced spherical core (Figure 3.18). Similar but a more strengthened response was observed at high dose; initially fast exponential tumour growth was established followed by a decline, cellular morphology changed from highly elongated to a small ball shaped structure (Figure 3.18).

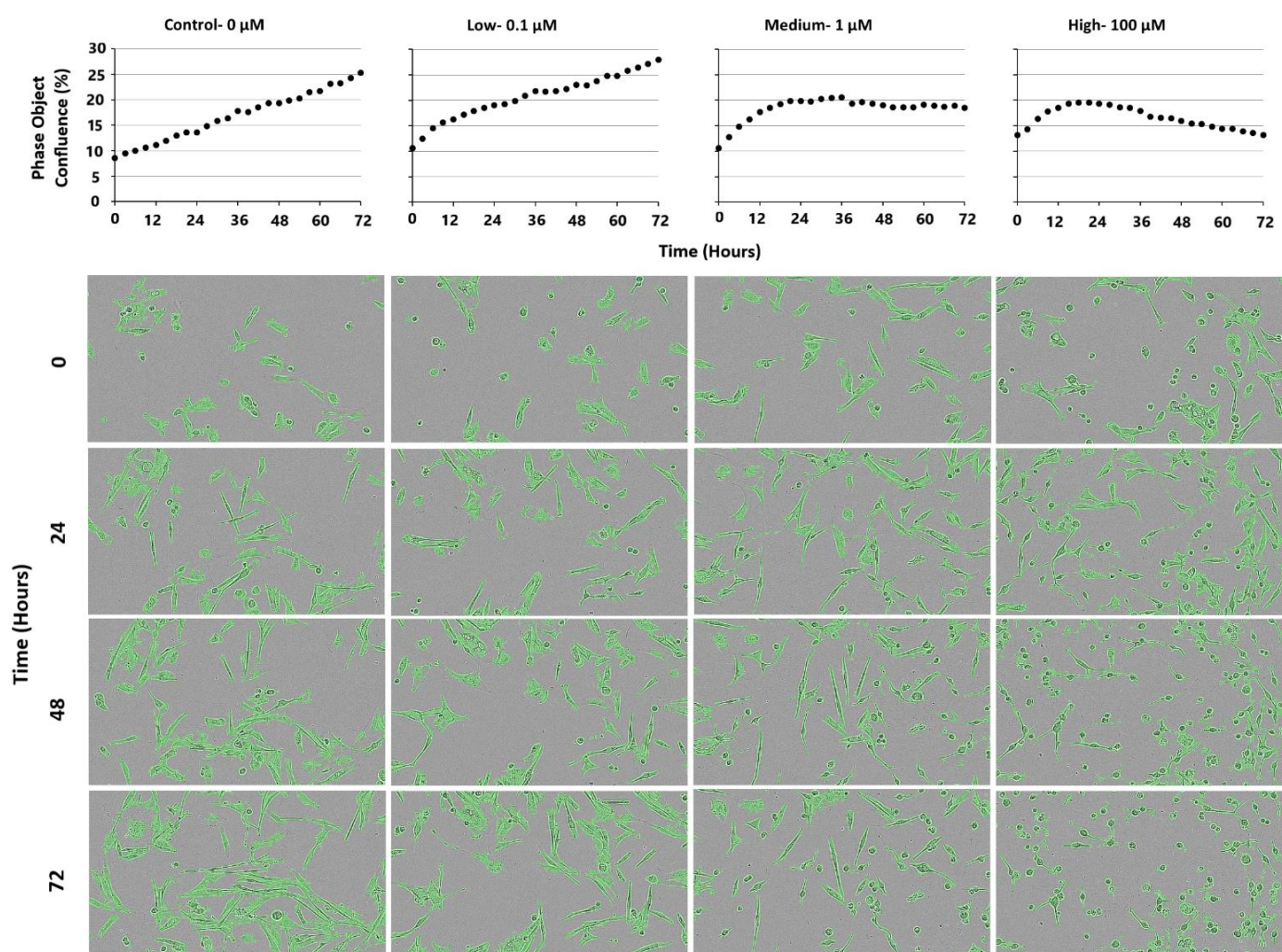


Figure 3.18: IncuCyte cell confluence and representative images data of patient 4 derived TC cells treated with IRN-PTV-CAP-TCL drug combination. Drug concentration from left to right: control, 0.1 μM low, 1 μM medium and 100 μM high.

Patient 4 BAT

IRN-CAP-CXB-ITZ, IRN-CAP-DSF and IRN-PTV-CAP-TCL drug combinations were

effective with LogIC_{50} values of 4.71, 4.64 and 4.44 nM, respectively (Figure 3.19), while

IRN-PTV-DSF-CoGlu was ineffective. Compared to other single drug treatments including

the current standard, TMZ improved cytotoxic response were observed (Chapter two, 2.4.3

Cell metabolism assay (MTT)).

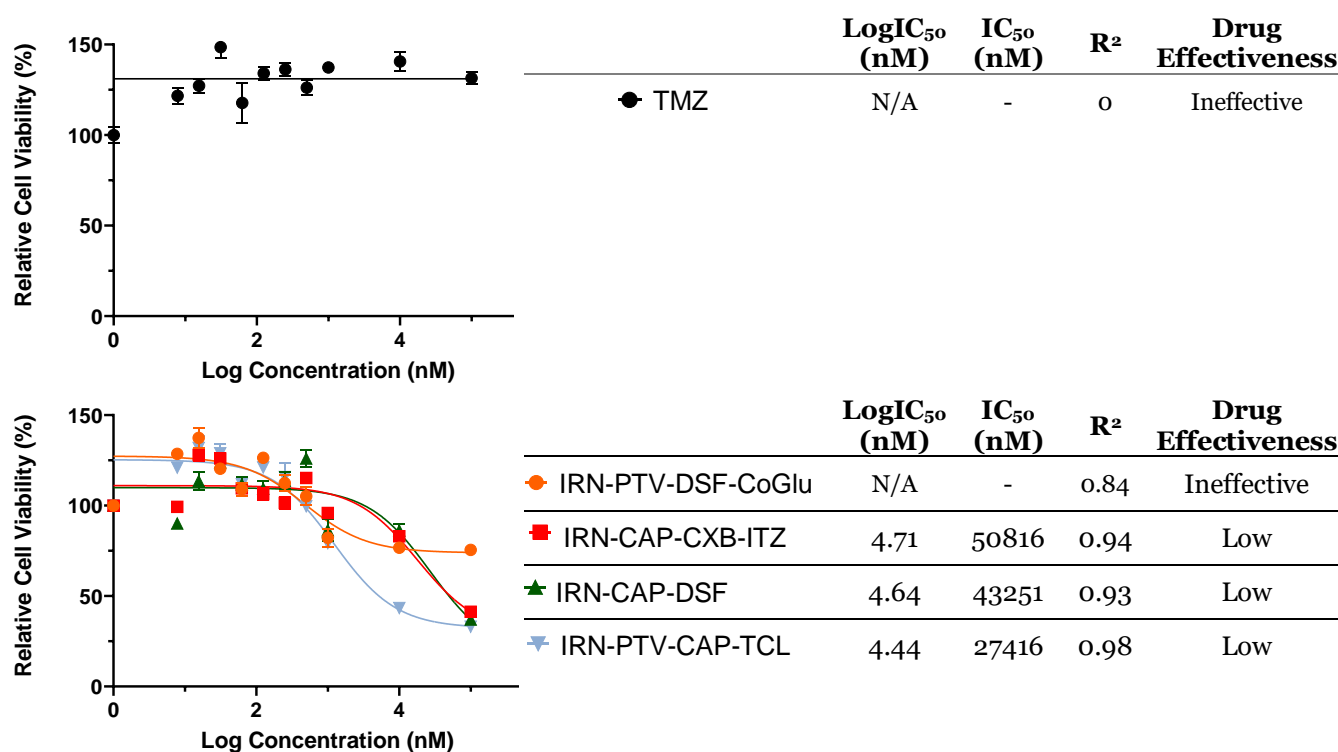


Figure 3.19: IncuCyte 3-day cytotoxicity assay, LogIC_{50} curves and data table of combination drug treatments tested against patient 4 BAT cells. \pm SEM is indicated as error.

To ensure the accuracy of the drug cytotoxicity data and as a comparison between end-point MTT and real-time IncuCyte assays, the LogIC₅₀ values of both cytotoxicity assays were compared and comparable therapeutic response data were obtained for IRN-CAP-DSF and IRN-PTV-CAP-TCL but variability in therapeutic response were demonstrated for IRN-PTV-DSF-CoGlu and IRN-CAP-CXB-ITZ (Table 3.2).

Table 3.2: Combination drug treatment LogIC₅₀ values comparison between MTT and IncuCyte assays for the BAT samples.

Treatment	LogIC ₅₀ (nM)	
	MTT	IncuCyte
IRN-PTV-DSF-CoGlu	2.628	ineffective
IRN-CAP-CXB-ITZ	ineffective	4.707
IRN-CAP-DSF	4.424	4.636
IRN-PTV-CAP-TCL	4.737	4.438

TMZ

During the initial 3-days of treatment TMZ was proven to be ineffective across all doses with exponential tumour growth observed over time (Figure 3.20). Beyond this period, at low dose cellular confluence peaked at 78 % during day 10, this then declined to 65 % by day 20 (Figure 3.20). At medium dose, cellular confluence reached the maximum that the environment can sustain, 80 % by day 11, this then decreased to 55 % by day 20 (Figure 3.20). At high dose, growth oscillation was observed; initially exponential tumour growth was demonstrated, this was then followed by a decline at day 8, but by day 13 fast exponential tumour growth was re-initiated (Figure 3.20). Overall, the data demonstrate that during the first week of treatment fast exponential tumour growth was observed across all doses. By week two, tumour growth ceased but for the low and medium dose treatments this was likely to have occurred because of environmental constrain rather than a drug response, for the high dose treatment a drug response was demonstrated but by week three tumour re-occurrence happened. Hence extended period TMZ treatment was proven to be ineffective.

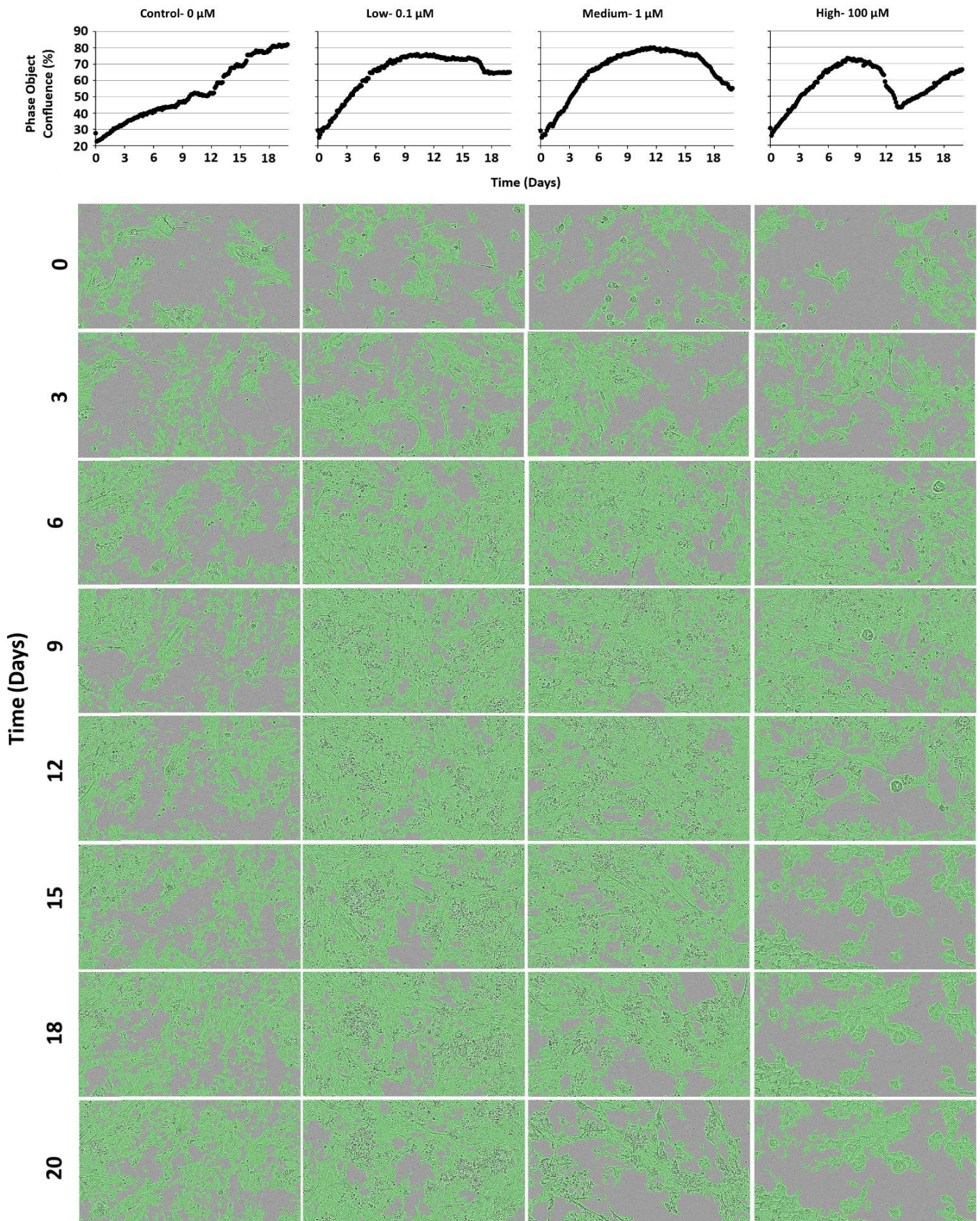


Figure 3.20: IncuCyte cell confluence and representative images data of patient 4 derived BAT cells treated with TMZ monotherapy. Drug concentration from left to right: control, 0.1 μ M low, 1 μ M medium and 100 μ M high.

IRN-PTV-DSF-CoGlu

During the initial 3 days of assay, only medium and high dose treatments demonstrated a response against tumour, as compared to control a slower cellular proliferation rate was observed (Figure 3.21). This does confirm the MTT cytotoxicity assay data as most of the tested BAT samples required medium dose for a response.

Following day 3, a response was achieved across all doses; at low dose, cellular confluence reached a 53 % peak at day 9 and then decreased to 49% by day 20 (Figure 3.21). At medium and high dose, cellular confluence peaked at 39 and 30 %, respectively during the first week of treatment and then slowly declined to 21 and 29 %, respectively by day 20 (Figure 3.21). When compared to the control treatment, IRN-PTV-DSF-CoGlu drug combination achieved good efficacy even at low dose.

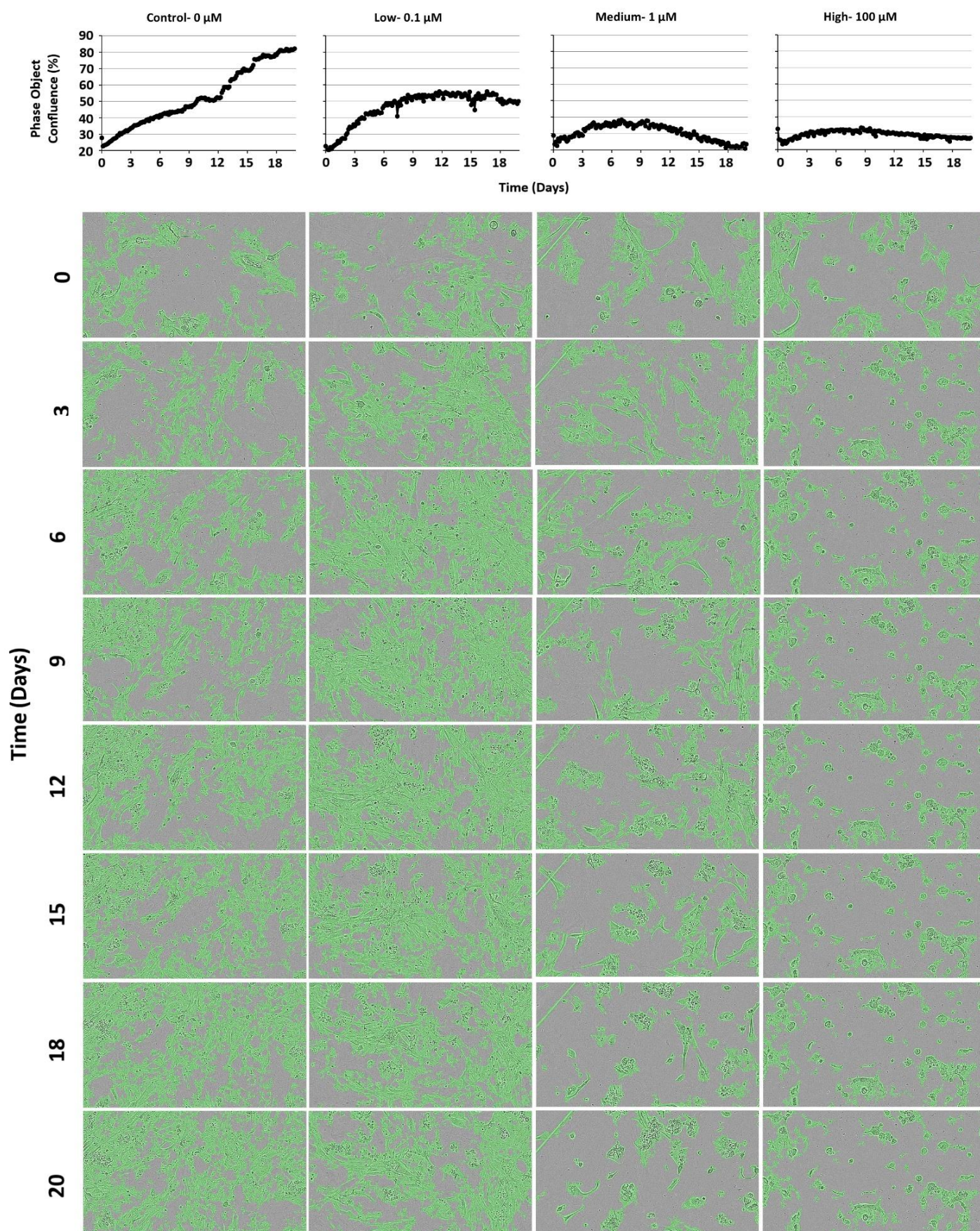


Figure 3.21: IncuCyte cell confluence and representative images data of patient 4 derived BAT cells treated with IRN-PTV-DSF-CoGlu drug combination. Drug concentration from left to right: control, 0.1 μM low, 1 μM medium and 100 μM high.

IRN-CAP-CXB-ITZ

This combinational treatment was only assessed for 9 days due to IncuCyte instrumental issues that occurred during analysis. Within the initial 3 days of analysis; the low and medium dose treatments were comparable to control as exponential tumour growth was observed over the 72-hour treatment period, while at high dose, a reduction in tumour confluence was detected (Figure 3.22). This confirms the MTT cytotoxicity data as most of the tested BAT samples were effective at high drug concentration. Beyond day 3, a response was obtained across all doses; at low and medium dose following accelerated growth cellular confluence reached a plateau by day 7 and 5 respectively, while at high dose, cellular confluence continued to decrease until reaching a plateau was reached at day 5 (Figure 3.22). Therefore IRN-CAP-CXB-ITZ drug combination was proven to be effective against tumour even at low dose.

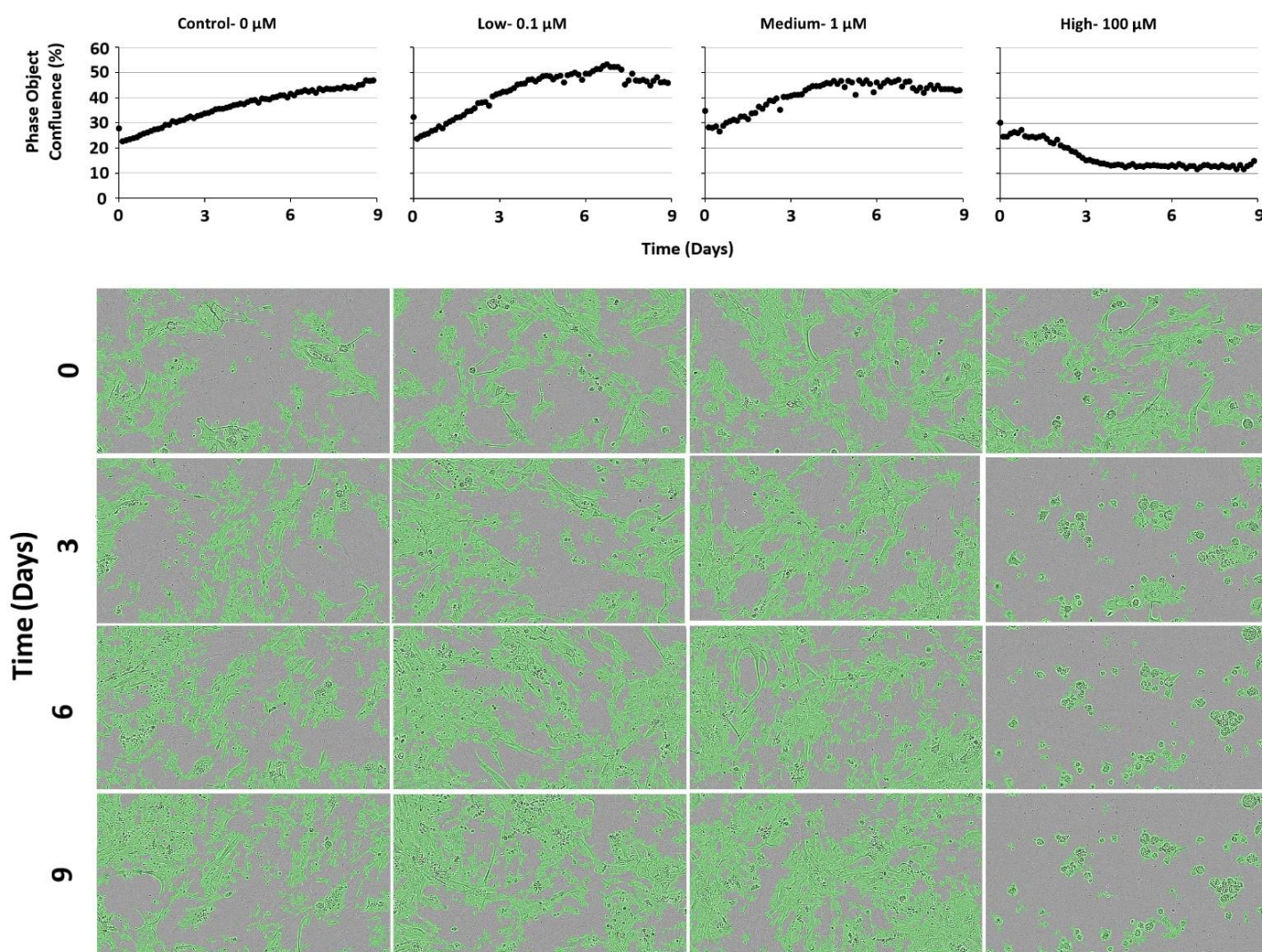


Figure 3.22: IncuCyte cell confluence and representative images data of patient 4 derived BAT cells treated with IRN-CAP-CXB-ITZ drug combination. Drug concentration from left to right: control, 0.1 μM low, 1 μM medium and 100 μM high.

IRN-CAP-DSF

At low dose IRN-CAP-DSF combination drug treatment produced no cytotoxic response with exponential tumour growth over time and cellular confluence reaching 80 %, which was the maximum confluence that the environment can sustain (Figure 3.23). At medium dose initially a slow cellular proliferation was observed, but by day 14 growth ceased and cellular confluence reached a plateau (Figure 3.23). At high dose, during the initial 24 hours of treatment cellular confluence declined by 20% and then remained constant over the rest of the treatment period (Figure 3.23). This validates our IRN-CAP-DSF drug combination cytotoxicity MTT data as most of the patient tested BAT samples were potent at medium or high dose.

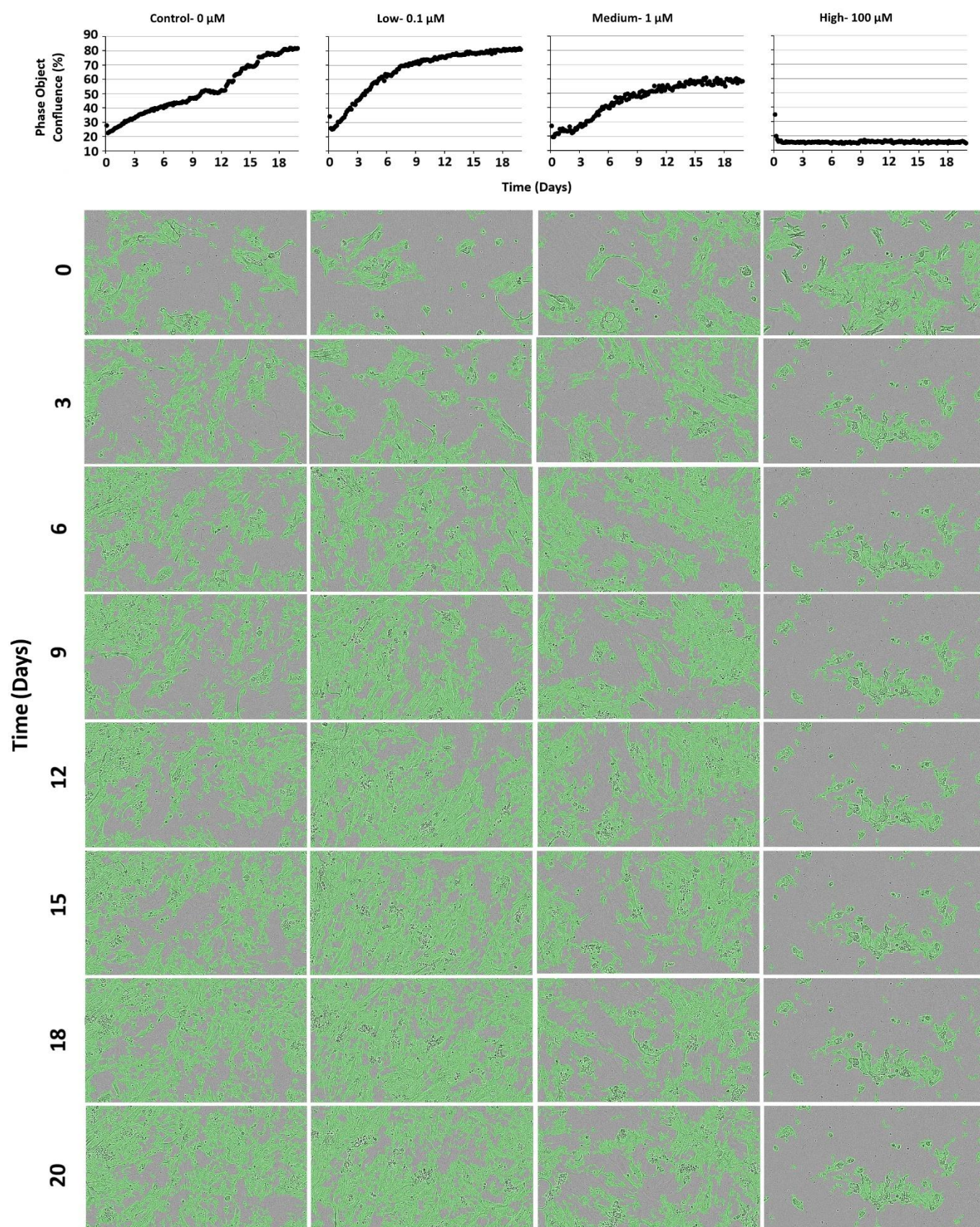


Figure 3.23: IncuCyte cell confluence and representative images data of patient 4 derived BAT cells treated with IRN-CAP-DSF drug combination. Drug concentration from left to right: control, 0.1 μ M low, 1 μ M medium and 100 μ M high.

IRN-PTV-CAP-TCL

An equivalent therapeutic response was obtained for IRN-CAP-DSF and IRN-PTV-CAP-TCL drug combinations. At low dose, IRN-PTV-CAP-TCL combination demonstrated no response against tumour, with cellular confluence reaching 80% by day 20, which was the maximum confluence that the environment can sustain (Figure 3.24). At medium dose, the cellular confluence reached a 49 % peak by day 10 and then slowly declined to 31 % by day 20 (Figure 3.24). At high dose, cellular confluence declined to 9 % within the initial 3 days of treatment and then remained relatively constant throughout the rest of the treatment period (Figure 3.24). This confirms the MTT cytotoxicity data as most of the tested BAT samples were effective at medium dose.

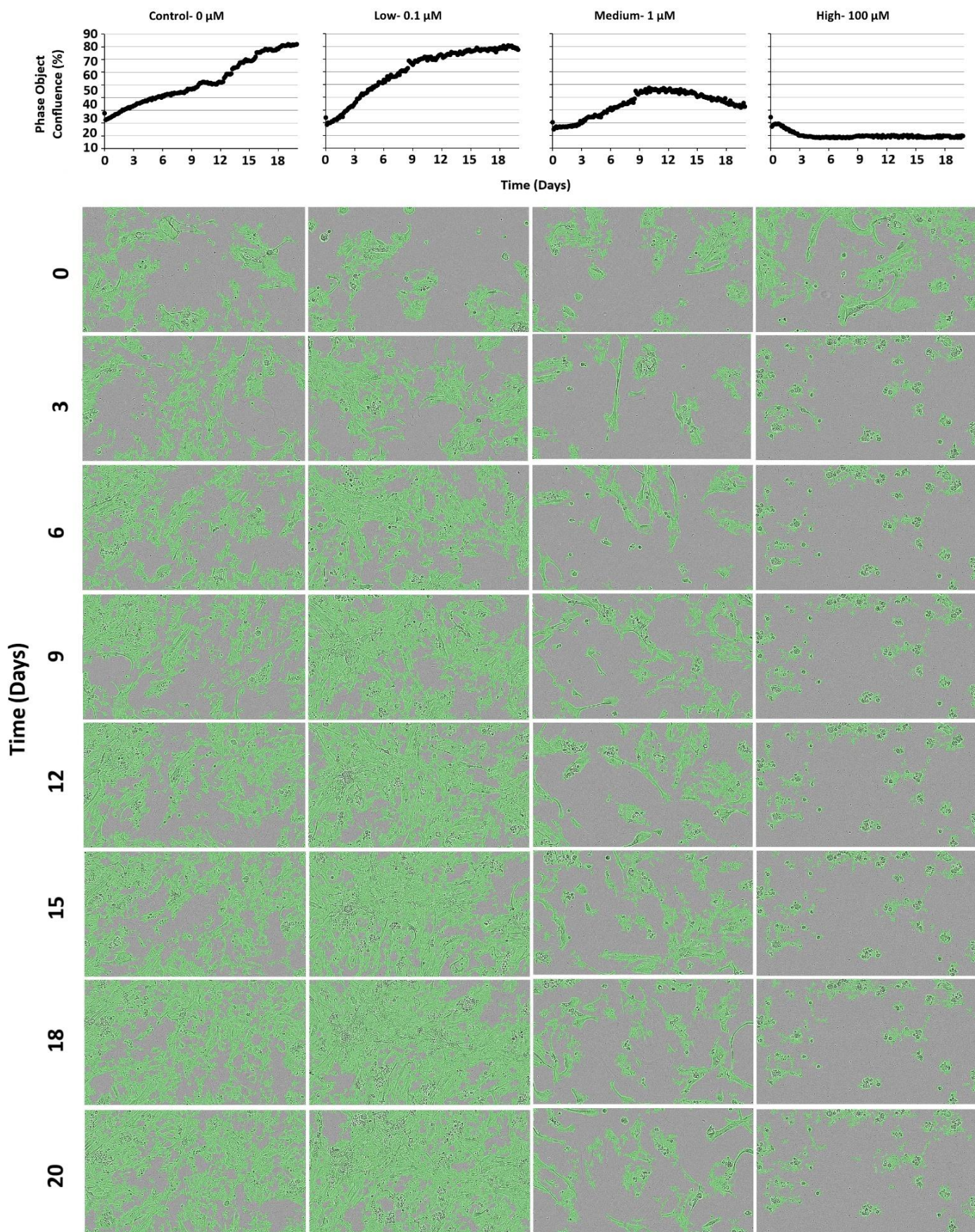


Figure 3.24: IncuCyte cell confluence and representative images data of patient 4 derived BAT cells treated with IRN-PTV-CAP-TCL drug combination. Drug concentration from left to right: control, 0.1 μ M low, 1 μ M medium and 100 μ M high.

2.4.4 Re-occurrence of residual BAT tumour

Following surgical and chemotherapeutic treatment, reoccurrence in the form of a local continuous growth develops in almost all glioma patients. Thus, to investigate tumour resistance against our combination drug treatments an extended cytotoxicity assay was performed using two separate methods: MTT and IncuCyte. Using MTT assay, each of our four drug combinations as well as the current standard treatment, TMZ were analysed for up to two weeks against five patient BAT samples. Whereas for the IncuCyte assay, each therapy was analysed for up to 20 days against the patient 4 BAT sample.

The MTT cytotoxicity results reveal that across the treatment period all four drug combinations were more potent than TMZ. Initially all tested treatments demonstrated a similar therapeutic response progression, whereas at day 6 a significant decrease in the LogIC_{50} values were obtained followed by a small increase on day 8 (Figure 3.25, a). Following this, on days 10 and 14 TMZ LogIC_{50} values continued to increase whereas the IRN-PTV-DSF-CoGlu and IRN-DSF-CAP drug combinations continued to decrease. For the remaining drug combinations: IRN-PTV-CAP-TCL potency remained relatively stable and IRN-CAP-CXB-ITZ was slightly more potent on day 14. By day 14, lower LogIC_{50} values were obtained across all combination drug treatments than the initial day 3 analysis. Thus, confirming no tumour re-occurrence as no rapid increase in LogIC_{50} values were detected following 14 days of treatment (Figure 3.25, a).

Using IncuCyte, only one BAT sample was assessed but for a more prolonged period of 20 days, except for IRN-CAP-CXB-ITZ which was only assessed up to day 9. For TMZ, the data demonstrates that it was ineffective even after 20 days of analysis (Figure 3.25, b). For the combination drug treatments, no evidence of tumour relapse was obtained, IRN-PTV-DSF-CoGlu and IRN-PTV-CAP-TCL drug combinations achieved lower LogIC_{50} values during the latter days of treatment, while a relatively stable drug response was obtained for IRN-CAP-DSF and IRN-CAP-CXB-ITZ drug combinations (Figure 3.25, b).

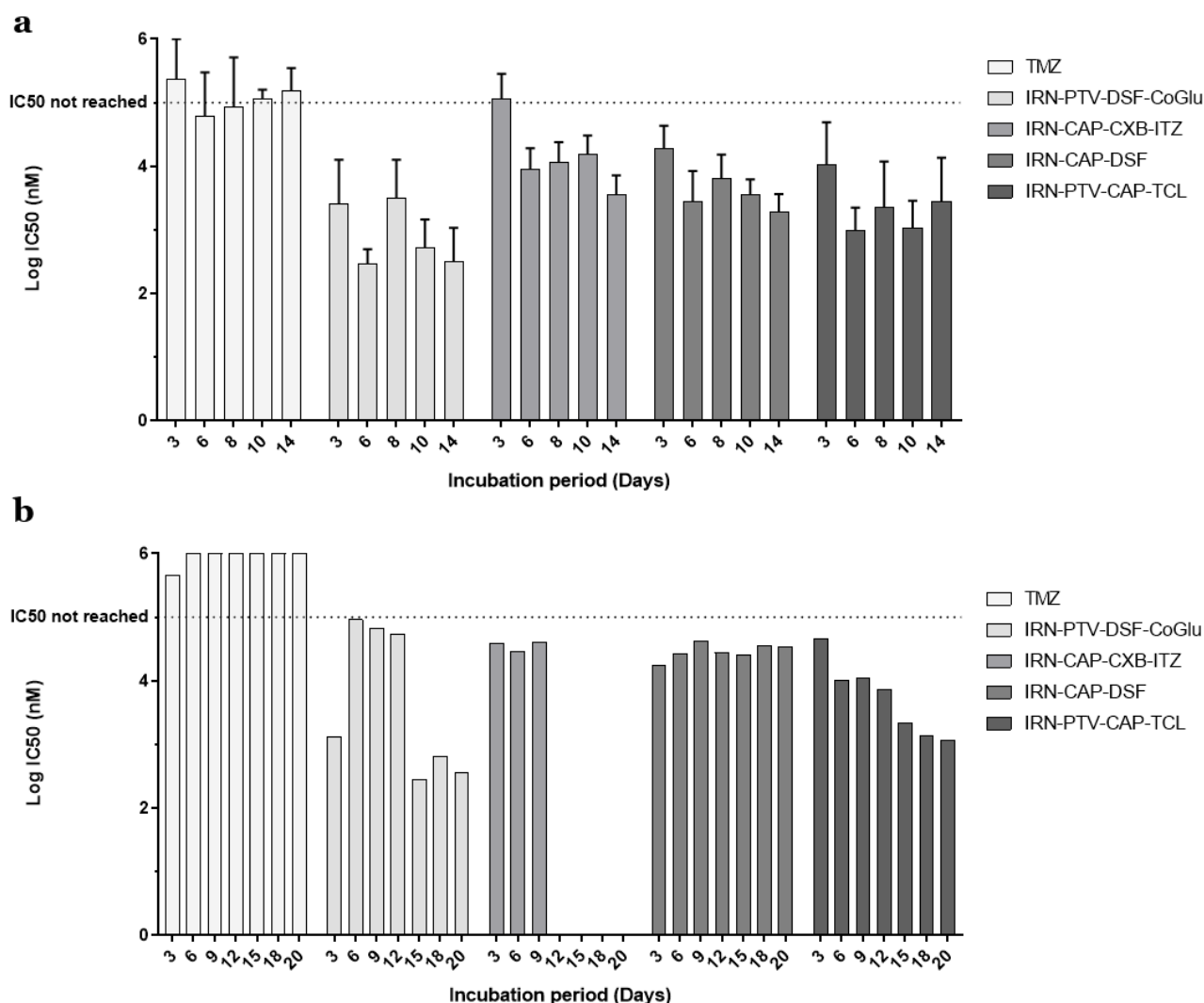


Figure 3.25: Tumour relapse assessment of current standard treatment, TMZ and four combination drug treatment; i) IRN-PTV-DSF-CoGlu ii) IRN-CAP-CXB-ITZ iii) IRN-CAP-DSF iv) IRN-PTV-CAP-TCL tested against residual tumour BAT cells via two distinct cytotoxicity assay: **a)** MTT, average LogIC_{50} data of patient 2, 4, 5, 8 and 9 \pm SEM is indicated as error bars **b)** IncuCyte, LogIC_{50} data of patient 4 only.

3.5 Discussion

3.5.1 Patient demographic vs cytotoxicity drug response

The demographic of the glioma patient population for the samples mainly consist of older patients and high-grade (III and IV) tumours, which often correlate with more highly resistance tumours (Chapter one, 1.1 Introduction, Figure 1). Cytotoxicity analysis using a known 'hard to treat' sample population provides a more robust therapeutic screening method for the combination drug treatments.

3.5.2 Tumour protein expression vs tumour growth and drug response

Within our sample population wildtype IDH1 and ATRX protein expression status were more prevalent with the higher grade IV tumours, whereas mutant status was more prevalent for grade III. Hence any variation between tumour grade III and IV cytotoxicity data can be due to variation in those specified genes, which are known to affect the OSR of patients (Chapter two, 2.5.2 Patient abrupt protein expression vs tumour growth and drug response).

Our data demonstrate that although some variation was observed, particularly for IRN-PTV-DSF-CoGlu and IRN-PTV-CAP-TCL drug combinations, the overall trend of data was consistent between the two tumour grades (Figure 3.26). To illustrate this, across both grade III and IV patient samples IRN-PTV-DSF-CoGlu drug combination was proven to be the most potent followed by IRN-CAP-DSF, IRN-CAP-CXB-ITZ and IRN-PTV-CAP-TCL (Figure 3.26). Additionally, there was no evidence of either grade having a superior response with any particular treatment (Figure 3.26). Those results are comparable to the mono-therapeutic cytotoxicity data obtained in chapter two, providing additional proof that wildtype IDH1 and ATRX abrupt protein expressions as well as a lower tumour grade does not result in a better response to treatment (Figure 3.26).

Although clinically lower tumour grade is associated with a more favourable prognosis [5, 132, 301-303], this could be because of a slower rate of tumour growth rather than enhanced therapeutic activity against the tumour. Our evidence for this is that during the tissue culture stage and with all samples grown under the same conditions, it took a significantly longer incubation period for the grade III cells to achieve a cellular confluence above 70 %.

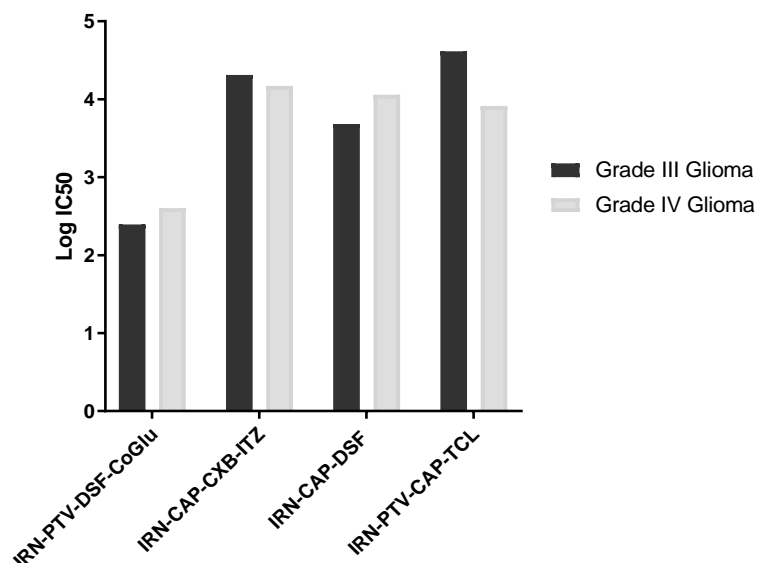


Figure 3.26: MTT LogIC₅₀ cytotoxicity data of, grade IV patients 3, 4, 7-11 and grade III patients 6 and 12, TC sample population. For ineffective drug treatments predicted Graphpad Prism LogIC₅₀ values were used.

3.5.3 MTT data analysis and visualisation

Many combination drug regimens have previously been proposed to overcome the heterogenic nature of glioma tumours, with many innovative combinations being tested in preclinical and clinical trials [234, 357-360]. So far, this idea has been met with limited success, often due to either high toxicity, inability of the drugs to cross the BBB or rapid systemic drug degradation [29, 361-363]. A good example of this is DSF and CoGlu combination, in a study undertaken by Senger DL *et al*, DSF-CoGlu combination was screened against patient derived tumour cells, the results showed that the combination can functionally impairs DNA repair pathways and enhances the effects of DNA alkylating agents like TMZ [178] . Since this study, the treatment was tested in several clinical trials using current systemic administration methods without producing any positive results (Chapter one, 1.4.3 Disulfiram/Copper Gluconate, Table 1.3) [235, 364]. Due to DSF extreme instability under physiological conditions, DSF is known to rapidly degrades and so orally administered DSF does not reach the tumour tissue at therapeutic concentrations.

Here, we assessed four carefully selected drug combinations for their use to enhance therapeutic outcome via complementary mechanisms of action. If successful, this can reduce the dose required to obtain a therapeutic response, consequently minimising toxic side effects and tumour cells developing resistance. Developing those treatments for local administration would further minimise dosage requirement by limiting the drug at the target site and minimizing the exposure of total body to the drug [64, 362, 365].

9 TC and 4 BAT glioma samples were used to perform a cytotoxicity screen of the combination drug treatments via MTT assay. On average IRN-PTV-DSF-CoGlu drug combination was the most potent, with LogIC₅₀ values < 2.8 nM, across a large proportion of the tested samples (Table 3.3, Figure 3.27). IRN-CAP-CXB-ITZ, IRN-CAP-DSF and IRN-PTV-CAP-TCL drug combinations were also effective but at higher doses, achieving medium or low potency values (Table 3.3). In comparison to our mono-therapeutic drug treatment data from chapter two, at $\leq 100 \mu\text{M}$ dose the combination drug treatments achieved lower LogIC₅₀ values and were effective across more patients' samples.

Table 3.3: Colour coded MTT assay logIC₅₀ data chart. Listing patients 3-4, 6-12 derived TC and BAT cells treated with IRN-PTV-DSF-CoGlu, IRN-CAP-CXB-ITZ, IRN-CAP-DSF, IRN-PTV-CAP-TCL.

Tumour Core						Drug Effectiveness	logIC ₅₀ (nM)
Patient Sample	TMZ	IRN-PTV-DSF-CoGlu	IRN-CAP-CXB-ITZ	IRN-CAP-DSF	IRN-PTV-CAP-TCL	High	1
3	Ineffective	2.73	4.34	3.90	4.93		1.5
4	Ineffective	2.80	4.59	4.30	4.63		2
6	Ineffective	2.38	4.14	3.55	4.60		2.5
7	Ineffective	2.67	4.23	4.34	2.46		3
8	Ineffective	2.46	4.40	4.13	4.56	Medium	3.5
9	Ineffective	2.77	4.15	4.01	4.42		4
10	Ineffective	2.32	3.62	4.22	3.49	Low	4.5
11	Ineffective	2.49	3.86	3.51	3.58		5
12	Ineffective	2.41	4.49	3.81	4.63	Ineffective	>5
BAT							
Patient Sample	TMZ	IRN-PTV-DSF-CoGlu	IRN-CAP-CXB-ITZ	IRN-CAP-DSF	IRN-PTV-CAP-TCL		
2	Ineffective	4.00	Ineffective	Ineffective	Ineffective		
4	Ineffective	2.63	Ineffective	4.42	4.74		
8	2.86	2.25	4.30	4.44	2.55		
9	Ineffective	3.64	3.76	3.33	2.58		

To assess the difference in therapeutic response due to intra-tumour heterogeneity, two separate tumour fragments; the TC and BAT were tested against the combination drug treatment (Figure 3.27). For all four combinations: IRN-PTV-DSF-CoGlu, IRN-CAP-CXB-ITZ, IRN-CAP-DSF and IRN-PTV-CAP-TCL, a statistical student t-test was performed. Results show that there was no statistically significant variation in cytotoxic response between the TC and the BAT samples ($p = 0.26, 0.29, 0.37, 0.91$) (Figure 3.27). Therefore, our multi drug therapies have the potential to overcome the issue of intra-tumour heterogeneity, which is a major cause of treatment failure and recurrence in high grade brain tumours [146, 314]. Previously within chapter two, IRN, PTV and ITZ mono-therapeutic treatments were not capable of inducing equivalent cytotoxic response across different tumour fragments (Chapter two, 2.5.3 MTT Data analysis and visualisation). Hence utilizing our combination drug treatments in the clinic may yield higher efficacy by targeting a more diverse population of the cancer cells.

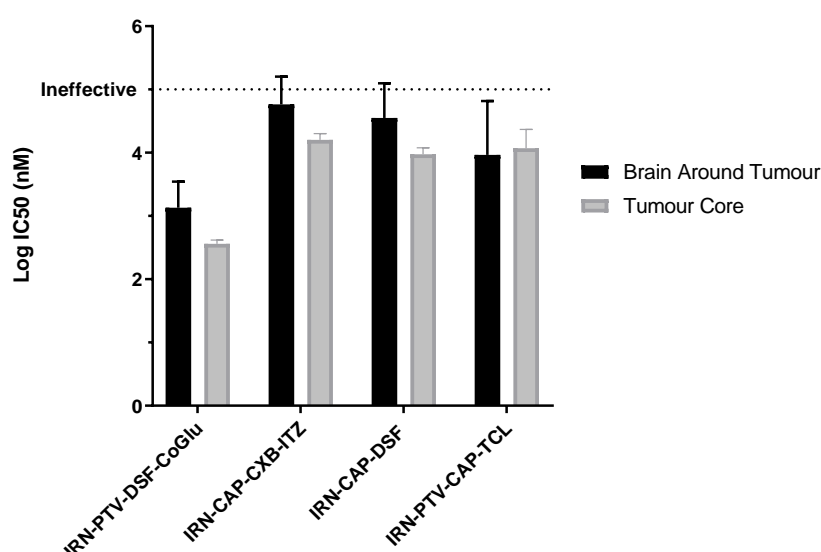


Figure 3.27: Average LogIC₅₀ data for 9 TC and 4 BAT samples tested against combination drug treatments. To plot data for ineffective drug treatments predicted Graphpad Prism LogIC₅₀ values were used. \pm SD is indicated as error bars

3.5.4 IncuCyte data analysis and visualisation

To assess the reliability and accuracy of the drug combinations cytotoxicity data, we compared end point MTT assay to the real-time IncuCyte assay. Using both assays, patient 4 TC and BAT samples were assessed for their response to IRN-PTV-DSF-CoGlu, IRN-CAP-

CXB-ITZ, IRN-CAP-DSF and IRN-PTV-CAP-TCL drug combinations. The data demonstrated that although there appears to be some variation between MTT and IncuCyte cytotoxicity data, for the vast majority of tested samples, the drug LogIC₅₀ data were equivalent.

As well as the LogIC₅₀ data for each drug combination, low (0.1 µM), medium (1 µM) and high (100 µM) dose evaluation were performed. Cellular confluence measurements and snapshot images were taken at 24, 48 and 72 hour post treatment; cellular growth curves were used to determine proliferation rate and cellular images were used to track changes in cell confluence and morphology. All four drug combinations demonstrated a dose dependant inhibition pattern against both patient 4 TC and BAT samples. Compared to TMZ, improved tumour growth inhibition was demonstrated by all four drug combinations. When the combination drug treatments were evaluated at a dose of 100 µM the tumour growth ceased, whereas with 100 µM TMZ tumour growth continued. Furthermore, with all combinations an increase in dose and incubation period induced an alternation in cellular morphology, with cells appearing smaller in size and possessing a spherical shape compared to the larger, more elongated shape normally observed with glioma cells [366, 367].

3.5.5 Resistance against multidrug treatment

One of the main reasons for current treatment failure is tumour resistance which develops during treatment [161, 315]. As an initial preclinical assessment of our combinational drug treatments an extended cytotoxicity screen was performed using both MTT and IncuCyte assays.

The MTT assay was performed on five glioma patient BAT samples, providing a good estimation for the data variability across different patients. Following a 14 day analysis, there was no evidence of tumour reoccurrence across all tested combination drug treatments with the initial day 3 LogIC₅₀ values for IRN-PTV-DSF-CoGlu, IRN-CAP-CXB-ITZ, IRN-CAP-DSF and IRN-PTV-CAP-TCL being 3.42, 5.05, 4.29 and 4.04 nM, respectively, while the final 14 day analysis LogIC₅₀ values were 2.51, 3.56, 3.29 and 3.45 nM, respectively. For the

combination drug treatments on average the best LogIC₅₀ values were achieved on day 14, except for IRN-PTV-CAP-TCL combination, which achieved a relatively stable cytotoxic results between days 6 and 14. TMZ was also assessed and on average it achieved the best cytotoxicity response on days 6 and 8, with LogIC₅₀ values of 4.79 and 4.93 nM respectively, but it was proven to be ineffective across most patient samples. Additionally, on day 3 and 14 analysis, TMZ was ineffective across all patient samples with LogIC₅₀ values above 5 nM. Therefore, across a two weeks treatment period at $\leq 100 \mu\text{M}$ dose our drug combinations were proven to be more potent than the current standard, TMZ. Additionally, no evidence for tumour resistance was demonstrated for IRN-PTV-DSF-CoGlu, IRN-CAP-CXB-ITZ, IRN-CAP-DSF and IRN-PTV-CAP-TCL combination drug treatments.

Using IncuCyte assay, only one patient BAT sample was assessed against TMZ and our drug combinations. IRN-PTV-DSF-CoGlu, IRN-CAP-DSF and IRN-PTV-CAP-TCL were evaluated for 20 days, while IRN-CAP-CXB-ITZ was assessed for 9 days. All four combination drug treatments demonstrated either improved or stable therapeutic response during the assay. TMZ was proven to be ineffective throughout the treatment period with LogIC₅₀ values above 5 nM. Thus, for up to 20 days of treatment our drug combinations were proven to be more potent than the current standard, TMZ. In addition, no evidence for tumour resistance occurred for IRN-PTV-DSF-CoGlu, IRN-CAP-DSF and IRN-PTV-CAP-TCL combination drug treatments following 20 days of analysis.

3.6 Conclusion

Within this chapter we performed a cytotoxicity screen for IRN-PTV-DSF-CoGlu, IRN-CAP-CXB-ITZ, IRN-CAP-DSF and IRN-PTV-CAP-TCL combination drug treatments against 10 patient derived glioma samples. Our data demonstrate that compared to the single drug treatments tested in chapter two, the combinational therapies were potent across more patients and at lower dose. Furthermore, on average the IRN-PTV-DSF-CoGlu multi drug treatment was the most potent with IC₅₀ values below 630 nM, demonstrating that this treatment is far more effective than the current standard treatment TMZ, as its IC₅₀ value is much higher, usually between 200-900 μM [301-304].

Furthermore, unlike single drug treatments, our multi drug therapies were less influenced by intratumour heterogeneity as no significant variation in the LogIC₅₀ values were obtained between the TC and BAT samples. In addition, the extended cytotoxicity assay revealed no signs of increased cellular proliferation following 20 days of treatment, suggesting that the cells did not develop resistance to our combinational therapies. This is important as drug resistance is a major cause of recurrence in brain tumours.

Finally, to ensure the reliability of our cytotoxic data, we compared the MTT assay results with the IncuCyte results and equivalent drug cytotoxicity values were obtained for the vast majority of samples. Therefore, our MTT cytotoxicity data is reliable and represents an accurate measurement of drug efficacy against gliomas.

Acknowledgment

This work uses samples provided by patients in the NHS. Special thanks to all tissue donors and Queen Elizabeth Hospital staff involved.

IncuCyte assay experimental procedure was performed by Mary Olaloko, subsequent data analysis was then carried out separately.

4. CHAPTER FOUR: HPLC METHOD DEVELOPMENT AND VALIDATION

4.1 Abstract

Two reversed-phase high-performance liquid chromatography (RP-HPLC) methods for the quantification of each individual drug in the IRN-PTV-DSF-DDC_Cu and IRN-CAP-DSF combinations were developed and subsequently validated. The analysis was performed using a Thermo Scientific Synchronis-C18 column (150 × 4.6 mm, 5 µm, 16 % carbon loading) with a mobile phase consisting of a water:acetonitrile:acetic acid mixture (30:70:0.1, v/v/v for IRN-PTV-DSF-DDC_Cu and 30:70:0.2, v/v/v for IRN-CAP-DSF). The flow rate was 1.0 ml/min, with an injection volume of 10 µL and UV detection performed at 245 and 270 nm wavelengths. The column temperature was kept stable at 27 °C (+/- 1.5 °C). For both drug combinations, the method showed linearity ($R > 0.997$), good precision ($RSD\% < 10$), recovery (90–110%), limits of detection ($\leq 20 \mu\text{g/mL}$) and limits of quantification ($\leq 80 \mu\text{g/mL}$). This is the first HPLC method used to separate these drug combinations.

4.2 Introduction

Combination drug therapy is routinely prescribed for GBM, this treatment approach is either used to combat tumour growing at accelerated speed or unpleasant side effects from the cancer treatment itself [368]. Few standard single drug regimens are licenced, but in practice a combination therapies are prescribed for patients via conventional administration routes. The most recognized example of this is the oral and intravenous administration of two or three small molecules such as TMZ and the corticosteroid drug dexamethasone and/or the antiepileptic drug levetiracetam. While such treatments have certainly shown improved patient outcomes [369-371], the development of more sophisticated drug combinations that target the different GBM clones is needed to improve survival or be curative.

Within previous chapters IRN-PTV-DSF-CoGlu and IRN-CAP-DSF drug combinations were proven to be superior in targeting glioma tumours when compared to any other tested therapeutic drug regimens. Prescribing those drug combination treatments using current

systemic administration methods would be unsuitable as most of those drugs either cannot pass the BBB due to their chemical properties or suffer from high hepatic first pass metabolism (Chapter one, 1.4 Drugs that may be suitable for repurposing to treat Glioblastoma). Therefore, high doses would be required for the drugs to reach the tumour site at therapeutic dosage, increasing the risk of toxic side effects.

Drug delivery systems (DDS) such as Gliadal® implants have been commonly used to deliver single drugs such as Carmustine, but further development is needed to enable multidrug delivery. A DDS capable of delivering multiple drugs could be developed to deliver each active pharmaceutical ingredient (API) independently at a control release rate. Such a device could concentrate the drug at the tumour location, minimising dosage requirement and reducing the risk of toxic side effects for patients. Because of cancers heterogeneous nature, many such as breast and melanoma will require combination drug therapy and could therefore benefit from DDSs to delivery combination drug treatments [372, 373].

Unfortunately for drug formulation combination drug therapy presents an analytical challenge. While single-component systems have been routinely analysed using methods such as spectrometry. Multidrug analysis method development is extremely extensive with considerable knowledge of analytical techniques required. Nevertheless, to develop IRN-PTV-DSF-CoGlu and IRN-CAP-DSF drug combinations into a formulation it is important to be able to analyse them without having to resort to complicated multi analytical methods to measure each drug individually. High performance liquid chromatography (HPLC) was selected as it can separate drug components prior to detection, allowing for a single analytical method to be used. Prior to method development only CoGlu was anticipated to present a major difficulty because it cannot be detected via UV-Vis based detection methods due to it having a very broad and weak absorption band between 550 and 1000 nm [374]. Using Refractive Index Detector (RID) was initially trialled but no signal was observed across all water and acetonitrile based mobile phases. Hence CoGlu was considered to be unsuitable for HPLC diode-array detector (DAD) and RID based analysis.

DSF when combined with CoGlu is known to quickly breakdown then react to form bis(N,N-diethyl dithiocarbamato)copper(II) (DDC_Cu) complex (Figure 4.1). From previous studies DDC_Cu was demonstrated to be a major secondary component obtained from DSF and CoGlu drug combination [375, 376]. Because of this it is necessary to detect and quantify DDC_Cu during our formulation development studies, and unlike CoGlu, DDC_Cu has a strong UV-Vis absorption band and can be detected by HPLC-DAD [377].

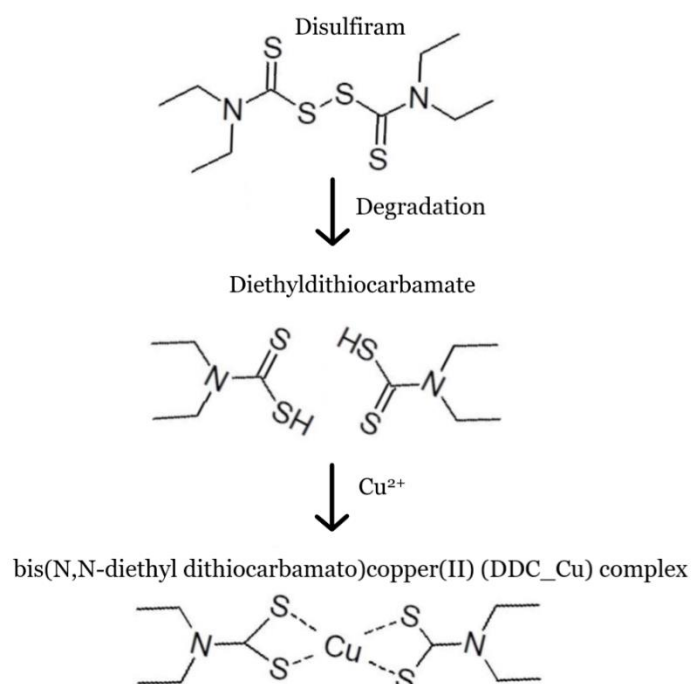


Figure 4.1: Disulfiram and copper gluconate reaction scheme to form a bis(N,N-diethyl dithiocarbamato)copper(II) complex.

Within this chapter we describe the development and subsequent validation of two reversed-phase HPLC methods for simultaneous determination of IRN-PTV-DSF-DDC_Cu and IRN-CAP-DSF drug combinations.

4.3 Materials and methods

4.3.1 Materials and reagents

Irinotecan hydrochloride, pitavastatin calcium, and bis(N,N-diethyl

dithiocarbamato)copper(II) complex were purchased from Jiangsu Hengrui Medicine Co

Ltd, LGM Pharma and Combi-Blocks respectively. Disulfiram and captopril were purchased

from Sigma Aldrich, while PLGA and Kolliphor® P188 were purchased from Corbion Purac and BASF respectively.

Acetonitrile, water, 1M acetic acid and acetone used were of HPLC grade and supplied by Sigma Aldrich. Dichloromethane (DCM) used for matrix extraction was reagent grade from Sigma Aldrich.

4.3.2 Placebo extraction procedure

Placebo implants were placed in a glass vial containing 5 mL of DCM to dissolve. The DCM was then evaporated off in a water bath set at 65°C. Once evaporated, 10 mL of mobile phase was added to make a matrix solution that was used for spiking drug solutions. Following spiking, this solution was then filtered using a 0.2 µm pore sized syringe filter, which was then analysed by HPLC to determine the content of each drug.

4.3.3 Instrument and chromatographic condition

For IRN-PTV-DSF-DDC_Cu drug combination, analyses was performed using a Dionex Ultimate 3000 LC system (Thermo Scientific, Loughborough, United Kingdom) equipped with pump, autosampler and a diode array detector – DAD. Data collection and analyses was performed using Chromeleon software (Thermo Scientific, Loughborough, United Kingdom).

For IRN-CAP-DSF drug combination, analyses was performed using Agilent LC System (Agilent Technologies, Santa Clara, California, United States) equipped with pump, autosampler and a diode array detector – DAD. Data collection and analyses was performed using Agilent ChemStation software (Agilent Technologies, Santa Clara, California, United States).

For both drug combinations, the chromatographic column used was Thermo Scientific Synchronis, C18 (150 mm × 4.6 mm; 5 µm, 100 Å, 16 % carbon loading). The mobile phase consisted of water:acetonitrile:acetic acid mixture (30:70:0.1, v/v/v for IRN-PTV-DSF-DDC_Cu and 30:70:0.2, v/v/v for IRN-CAP-DSF), with a flow rate of 1 mL/min. The injection volume was 10 µL and UV detection wavelength was performed at 245 nm for IRN,

PTV, CAP and DSF, and 270 nm for DDC-Cu. Using IRN-PTV-DSF-DDC_Cu method's mobile phase the retention times of IRN, PTV, DSF and DDC_Cu were 1.0, 2.4, 6.5 and 14 minutes, respectively. Using IRN-CAP-DSF method's mobile phase the retention times of IRN, CAP and DSF were 1.1, 2.5 and 8.0 minutes, respectively. All experiments were performed at 27 °C and the total peak area was used to quantify each drug. Prior to sample injection the column was purged and equilibrated with mobile phase for 30 minutes.

4.3.4 Methods development

The methods were optimized by investigating the influence of changing the composition of the mobile phases, flow rate, column and temperature. From these test conditions, an adequate peak symmetry (symmetry factor between 0.8 to 1.5) and short run time (< 20 minutes) was achieved.

4.3.5 Preparation of solutions

Drugs stock solution

IRN-PTV-DSF-DDC_Cu

IRN-PTV-DSF combination drug solution was prepared by dissolving 100 mg of each drug together in 100 mL of mobile phase (Final concentration, 1000 µg/mL). Separately, DDC_Cu solution was prepared by dissolving accurately weighed 66 mg of the drug in 100 mL of acetone (Final concentration, 660 µg/ml). The IRN-PTV-DSF and DDC-Cu solutions were subsequently combined (4:6, v/v) to make a final 400 µg/mL stock solution of IRN-PTV-DSF-DDC_Cu drug combination.

IRN-CAP-DSF

A stock solution was prepared by dissolving 60 mg of IRN, CAP & DSF together in 100 mL of mobile phase (Final concentration, 600 µg/mL).

Both stock solutions were stored at 4 °C and protected from light for up to 72 hours. On the day of analysis, the stock solutions were allowed to accumulate to room temperature, sonicated at 30°C for 1 minute and fresh working solutions were prepared from the stock solutions.

4.3.6 Methods validation

Specificity

Specificity of the assay was investigated by the injection of drug combinations with extracted placebo to demonstrate the absent of interference.

Each of the combination drug stock solutions were spiked with the matrix (4.3.2 Placebo extraction procedure) at 25:75 v/v for the IRN-PTV-DSF-DDC-Cu drug combination and 50:50 v/v for the IRN-CAP-DSF combination.

Linearity

For the IRN-PTV-DSF-DDC_Cu drug combination, standard solutions were prepared at seven concentrations, covering 20, 40, 60, 80, 100, 200 & 400 % of the target concentration. For the IRN-CAP-DSF drug combination, standard solutions were prepared at seven concentrations, covering 27, 33, 66, 100, 133, 166 & 200 % of the target concentration. In both assays three individually prepared replicates at each concentration were analysed and the area under the peak was used to quantify each drug. A plot of concentration (x-axis) versus mean response (y-axis) was used to determine linearity. Additionally, for each drug the relative standard deviation (RSD %), equation for regression line and R^2 values were determined.

Range

The range for both methods was determined from the linearity and accuracy studies.

Accuracy

Spiked placebo solutions were prepared at three concentration levels over the target concentration range of 60 to 200 % for IRN-PTV-DSF-DDC_Cu and 66 to 133 % for IRN-CAP-DSF drug combinations. At each concentration, three individually prepared replicates were analysed, the mean, standard deviation (SD), RSD% and percentage recoveries were calculated.

Precision- Repeatability

Chromatographic precision was determined by injecting 10 replicates of the target analyte.

The retention time, peak area and peak height were recorded with the mean, SD and RSD% calculated.

Precision- Intermediate precision

Intermediate precision was determined by using two HPLC instruments to assess Inter day precision at three concentration levels. IRN-PTV-DSF-DDC_Cu drug combination was evaluated over the range of 60 to 200 % of target concentration and IRN-CAP-DSF was evaluated over the range of 66 to 133 % of target concentration. The results were expressed as relative % purity with the mean, SD, RSD% calculated.

Limit of detection and Limit of quantitation

Both the LOD and LOQ were estimated, the lowest concentration in the standard curve was used as the LOQ value and a slightly lower concentration was used as the LOD. For each test, 6 replicates were injected with the RSD% value for the peak area calculated.

System suitability

System suitability was performed in accordance with the European pharmacopeia (EP) [378]. Six injections containing analyte at 100% of test concentration was used, the following parameters were determined: plates, resolution, symmetry and reproducibility (RSD% of retention time, peak area and height for six replicates).

4.4 Results and discussion

4.4.1 Scope and applicability

The intended scope of both methods is to separate, detect and quantify the concentration of IRN, PTV, DSF, DDC_Cu and CAP found in and released from a PLGA polymer based implantable DDS. The predicted average concentration of each drug normally found in formulated implant is 300 µg/mg, with each implant weighing 6-10 mg, both methods are appropriate for use to measure implant drug content and dissolution. The methods can also be extended to measure drug concentrations in any other PLGA polymer based formulation such as nanoparticles and gels [110, 379-381].

4.4.2 Method development and optimization

PTV, DSF and DDC_Cu are all hydrophobic with PTV and DDC_Cu being almost insoluble in aqueous solutions [382-385]. During the development stage a reverse phase C18 column was considered due to the hydrophobic nature of the compounds and because it has previously been utilized to analyse IRN, PTV, CAP, DSF and DDC_Cu compounds individually [386-390]. Within previous studies the most common reagents used for the mobile phase were methanol, acetonitrile, water and phosphate buffer, therefore a mixture of those reagents were initially trialled to separate a IRN and PTV drug mixture, as they were considered to be the most closely related molecules, being similar in chemical structure and polarity. The use of phosphate buffer and acetonitrile mobile phase at different ratios resulted in either poor peak symmetry (< 0.8 or > 1.5) or theoretical plate number (< 2000) for either of those drugs. Use of a water and methanol mobile phase also resulted in poor peak symmetry (< 0.8 or > 1.5), resolution (< 1.5) or plate number depending on the v/v ratio. Finally, the use of water and acetonitrile based mobile phase with 0.1 % acetic acid resulted in good separation, peak symmetry and theoretical plate number. Both drug combinations IRN-PTV-DSF-DDC_Cu and IRN-CAP-DSF were then trialled using this mobile phase with good separation achieved. Additionally, a UV wavelength absorption scan was performed for each drug and a wavelength of 245 nM was chosen for IRN, PTV, CAP and DSF as it achieved a balance of good absorption across all four drugs. Only DDC_Cu was analysed close to its lambda max value of 270 nM.

IRN-PTV-DSF-DDC_Cu Drug combination

To optimise the method, different compositions of the mobile phase, flow rates and columns were trialled. The best drug separation was observed at 30:70:0.1, v/v/v of water:acetonitrile:acetic acid ratio. Using a column with higher carbon loading content (19%) resulted in broader peaks. Using a longer column (250 mm) improved the retention time of IRN (1.7 minutes) but resulted in poor peaks symmetry (> 1.5 for IRN, PTV and DSF). Reducing the flow rate of the method (0.5 mL/min), again improved IRN retention time (2.0 minutes) but resulted in poor peak symmetry (< 0.8 for IRN, DSF and DDC_Cu) and

increased the overall analysis length of the method quite considerably (50 minutes).

Therefore, a 150 X 4.6 mm column with a low carbon loading and a mobile phase consisting of water:acetonitrile:acetic acid (30:70:0.1 v/v/v) achieved the best overall drug separation, run time, peak symmetry and plate number for IRN-PTV-DSF-DDC_Cu drug combinations. Maintaining a stable column temperature also ensured consistent retention times for DSF and DDC_Cu (8 and 19 minutes, respectively at 20 °C and 6.5 and 14 minutes, respectively at 27 °C).

IRN-CAP-DSF

The method developed for IRN-PTV-DSF-DDC_Cu was initially trialled, and it provided good drug separation, run time and plate number for the IRN-CAP-DSF combination. However, it resulted in poor peak symmetry (0.7) for CAP and thus method optimisation was performed. Initially the acetic acid concentration was increased to 0.2 % v/v, as captopril is known to be most stable at pH 4 [391], which did improve peak symmetry (0.8) for CAP while maintaining good peaks for IRN and DSF. To further optimise the method, the column temperature was adjusted, however, at temperatures below 20 °C the method suffered from poor precision for CAP as the drug was often presented as multiple peaks. These additional non-dominant peaks were originally classified as contamination or degradation products but following a literature review and multiple batch testing they were discovered to be peaks belonging to stereoisomers of CAP (Figure 4.2) [392]. CAP can exist in four conformational isomers, in solution CAP can undergo reversible trans-cis isomerism in minutes, which can occur during chromatographic separation.

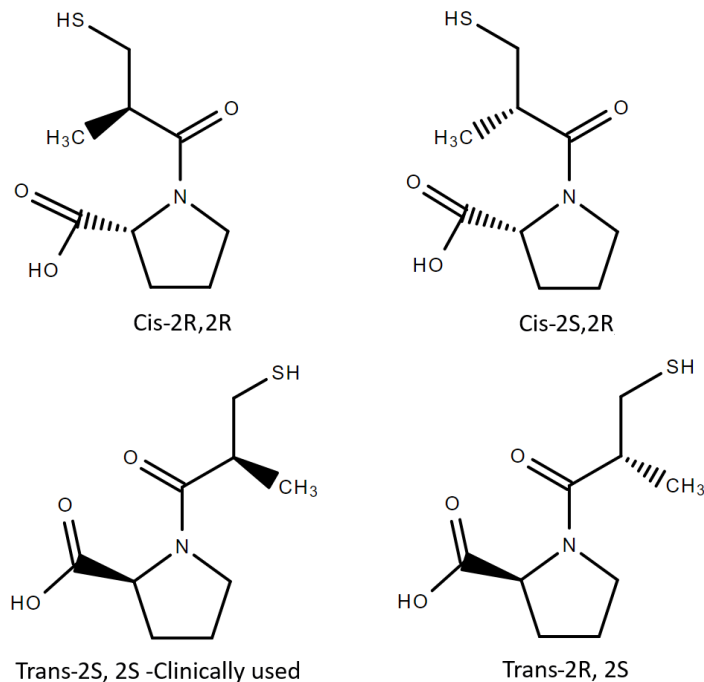


Figure 4.2: Structures of the four captopril stereoisomers (2R,2R, 2S,2R, 2S,2S, and 2R,2S)

Within the literature this was widely recognised to present as either separated peaks, split peaks or a fronting peak depending on the chromatographic conditions [392, 393]. To

eliminate poor peak elution and enhance precision for CAP, column temperature was increased. At temperature above 32 °C the method suffered from poor precision for DSF (RSD above 15 %). Hence the method was stabilised at 27 °C as this achieved the best linearity and precision for the IRN-CAP-DSF drug combination. This slight increase above ambient temperature ensured that CAP eluted as a single peak, which is likely to be all stereoisomers of CAP eluting as one peak due to frequent isomerisation. Other interpretation could be that the multiple isomers coalesce into one form at high temperature, but this is less likely to be the case, though conclusive stereoisomer identification would require other studies such as NMR. For the purpose of the current study a 27 °C column temperature was selected as it allowed for the separation, detection and quantification of the IRN-CAP-DSF drug combination.

4.4.3 Specificity

The chromatograph for both the IRN-PTV-DSF-DDC-Cu and IRN-CAP-DSF drug combinations spiked with extracted placebo implant reveal that each drug was well separated from any potential interfering peaks (Figure 4.3). No interfering peaks were observed at 245 and 270 nm absorption wavelengths for both IRN-PTV-DSF-DDC_Cu and IRN-CAP-DSF drug combinations (Figure 4.3).

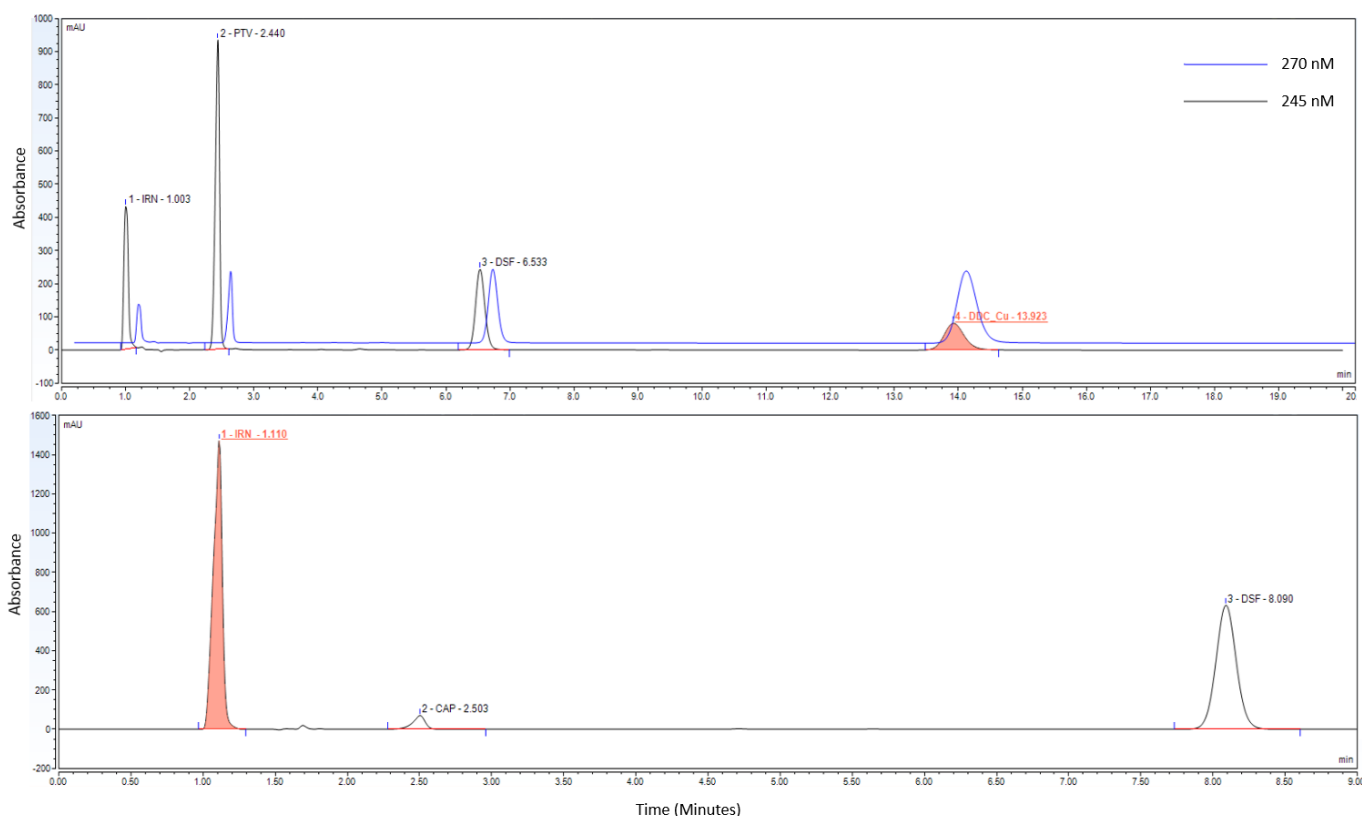


Figure 4.3: Chromatograms depicting the specificity of each drug combinations. The top chromatogram is of IRN-PTV-DSF-DDC_Cu combination measured at 245 and 270 nM wavelengths. Whereas the bottom chromatogram shows IRN-CAP-DSF combination measured at 245 nM wavelength.

4.4.4 Linearity

IRN-PTV-DSF-DDC_Cu

The regression analysis data for the IRN_PTV-DSF-DDC_Cu combination is presented in Table 4.1. The linear regression R^2 values for IRN, PTV, DSF and DDC_Cu analysis were all ≥ 0.997 , confirming a linear relationship between drug concentration and peak area. Additionally, the average peak area RSD% values for all drugs were $> 10\%$ demonstrating that the data is tightly clustered around the mean.

Table 4.1: Results of regression analysis for the linearity data of IRN, PTV, DSF and DDC_Cu.

Irinotecan			
Concentration (µg/mL)	Concentration as % of analyte target	Peak area (mAU) (mean of three injection)	Peak area RSD (%)
20	20	7.85	0.98
40	40	16.48	7.70
60	60	23.39	2.15
80	80	31.23	0.79
100	100	39.21	1.13
200	200	76.47	1.32
400	400	148.72	1.53
Equation for regression line Y= 0.3695x + 1.5386		Correlation Coefficient (R ²) 0.9998	
Pitavastatin			
Concentration (µg/mL)	Concentration as % of analyte target	Peak area (mAU) (mean of three injection)	Peak area RSD (%)
20	20	16.94	1.33
40	40	34.07	1.07
60	60	50.53	1.17
80	80	67.83	0.93
100	100	84.91	1.50
200	200	164.15	0.53
400	400	294.65	0.93
Equation for regression line Y= 0.7307x + 7.9256		Correlation Coefficient (R ²) 0.9966	
Disulfiram			
Concentration (µg/mL)	Concentration as % of analyte target	Peak area (mAU) (mean of three injection)	Peak area RSD (%)
20	20	8.92	0.38
40	40	17.99	1.16
60	60	26.88	0.12
80	80	36.35	1.72
100	100	47.21	8.12
200	200	89.03	0.64
400	400	176.98	0.21
Equation for regression line Y=0.441x + 0.9166		Correlation Coefficient (R ²) 0.9999	
Bis(N,N-diethyl dithiocarbamato)copper(II) complex			
Concentration (µg/mL)	Concentration as % of analyte target	Peak area (mAU) (mean of three injection)	Peak area RSD (%)
20	20	15.81	10.00
40	40	30.97	7.60
60	60	46.27	5.97
80	80	63.05	7.90
100	100	79.87	5.86
200	200	159.88	7.99
400	400	320.04	8.04
Equation for regression line Y= 0.8027x - 0.9286		Correlation Coefficient (R ²) 1	

IRN-CAP-DSF

The regression analysis data for IRN-CAP-DSF is presented in Table 4.2. The linear regression R^2 values for IRN, CAP and DSF analysis were all ≥ 0.997 . The average peak area RSD% values for IRN, CAP and DSF were mostly below 10 %, demonstrating that our IRN-CAP-DSF data is linear and tightly clustered around the mean.

Table 4.2 Results of regression analysis for the linearity data of IRN, CAP and DSF.

Irinotecan			
Concentration (µg/mL)	Concentration as % of analyte target	Peak area (mAU) (mean of three injection)	Peak area RSD (%)
80	27	2084.76	8.59
100	33	2481.97	0.44
200	66	5005.89	0.10
300	100	7293.82	0.62
400	133	9582.13	0.79
500	166	11474.02	0.27
600	200	13722.17	7.00
Equation for regression line y = 22.417x + 396.4		Correlation Coefficient (R ²) 0.999	
Captopril			
Concentration (µg/mL)	Concentration as % of analyte target	Peak area (mAU) (mean of three injection)	Peak area RSD (%)
80	27	117.00	10.0
100	33	149.13	7.10
200	66	425.26	10.95
300	100	684.67	3.67
400	133	975.42	2.05
500	166	1292.80	2.93
600	200	1525.52	16.28
Equation for regression line y = 2.7647x - 122.47		Correlation Coefficient (R ²) 0.999	
Disulfiram			
Concentration (µg/mL)	Concentration as % of analyte target	Peak area (mAU) (mean of three injection)	Peak area RSD (%)
80	27	2108.59	8.77
100	33	2499.26	0.43
200	66	4797.45	2.06
300	100	6782.17	1.27
400	133	8629.46	0.32
500	166	10088.90	0.00
600	200	12627.10	8.74
Equation for regression line y = 19.715x + 650.46		Correlation Coefficient (R ²) 0.997	

4.4.5 Range

The recorded range for the IRN-PTV-DSF-DDC_Cu and IRN-CAP-DSF drug combination HPLC methods were 20-400 and 80-600 $\mu\text{g/mL}$ respectively.

4.4.6 Accuracy

IRN-PTV-DSF-DDC_Cu

The mean recovery values for each of the individual drugs ranged between 90 to 110 % of the theoretical value (Table 4.3) indicating that the method is accurate [394].

Table 4.3: Intra-day accuracy measurements of HPLC assay for IRN-PTV-DSF-DDC_Cu combination.

IRN	% of nominal	Peak area (mAU) (Mean of 3 injections)	SD	RSD%	Amount of standard (µg/mL)		Recovery (%)
Sample					Spiked	Found	
1	60	24.18	0.11	0.45	60	63.91	106.52
2	100	39.88	0.35	0.88	100	106.39	106.39
3	200	80.50	0.01	0.01	200	216.33	108.16
PTV	% of nominal	Peak area (mAU) (Mean of 3 injections)	SD	RSD%	Amount of standard (µg/mL)		Recovery (%)
Sample					Spiked	Found	
1	60	48.33	0.18	0.38	60	58.21	97.02
2	100	79.97	0.71	0.89	100	101.51	101.51
3	200	159.79	0.08	0.05	200	210.76	105.38
DSF	% of nominal	Peak area (mAU) (Mean of 3 injections)	SD	RSD%	Amount of standard (µg/mL)		Recovery (%)
Sample					Spiked	Found	
1	60	27.03	0.07	0.27	60	60.33	100.55
2	100	44.98	0.37	0.83	100	100.95	100.95
3	200	91.24	0.04	0.05	200	205.59	102.79
DDC_Cu	% of nominal	Peak area (mAU) (Mean of 3 injections)	SD	RSD%	Amount of standard (µg/mL)		Recovery (%)
Sample					Spiked	Found	
1	60	48.31	0.12	0.24	60	61.35	102.24
2	100	79.50	0.08	0.10	100	100.20	100.20
3	200	154.40	0.92	0.59	200	193.51	96.75

IRN-CAP-DSF

The mean recovery values for each of the individual drugs ranged between 90 to 110 % of the theoretical value (Table 4.4) indicating good method accuracy.

Table 4.4 Intra-day accuracy measurements of HPLC assay for IRN-CAP-DSF combination.

IRN	% of nominal	Peak area (mAU) (Mean of 3 injections)	SD	RSD%	Amount of standard (µg/mL)		Recovery (%)
Sample					Spiked	Found	
1	66	4777.38	12.86	0.27	200	195.43	97.72
2	100	7150.36	220.63	3.09	300	301.29	100.43
3	133	9224.47	43.30	0.47	400	393.81	98.45
CAP	% of nominal	Peak area (mAU) (Mean of 3 injections)	SD	RSD%	Amount of standard (µg/mL)		Recovery (%)
Sample					Spiked	Found	
1	66	455.62	37.17	8.16	200	209.10	104.55
2	100	717.94	29.69	4.14	300	303.98	101.33
3	133	1016.52	50.50	12.04	400	411.98	102.99
DSF	% of nominal	Peak area (mAU) (Mean of 3 injections)	SD	RSD%	Amount of standard (µg/mL)		Recovery (%)
Sample					Spiked	Found	
1	66	4350.39	85.97	1.98	200	187.67	93.84
2	100	6235.46	56.20	0.90	300	283.29	94.43
3	133	9305.10	291.26	3.00	400	438.99	109.75

4.4.7 Precision- Repeatability

IRN-PTV-DSF-DDC_Cu

The RSD% values for the retention time, peak area and peak height for IRN, PTV, DSF and DDC_Cu were all $\leq 3.8\%$ indicating that the method is precise (Table 4.5).

Table 4.5 Intra-day precision of HPLC assay for IRN-PTV-DSF-DDC_Cu combination.

Irinotecan 100 µg/mL			
Injection no	RT (min)	Peak area (mAU)	Peak height
1	1.15	39.02	688.19
2	1.15	38.94	675.34
3	1.15	39.23	688.93
4	1.15	39.00	666.35
5	1.15	38.78	679.68
6	1.15	38.90	670.74
7	1.15	39.09	680.27
8	1.15	39.10	689.74
9	1.15	38.92	689.26
10	1.15	39.06	687.27
Mean	1.1524	39.0031	681.5769
SD	0.001264911	0.127142	8.496273
RSD%	0.109763195	0.325978	1.246561
Pitavastatin 100 µg/mL			
Injection no	RT (min)	Peak area (mAU)	Peak height
1	2.72	85.70	1167.74
2	2.72	85.53	1163.60
3	2.72	86.25	1170.30
4	2.72	85.64	1161.31
5	2.72	84.85	1152.56
6	2.72	85.45	1161.45
7	2.72	85.64	1162.58
8	2.72	85.81	1164.78
9	2.72	85.35	1161.77
10	2.72	85.76	1163.12
Mean	2.7188	85.5982	1162.92
SD	0.001549193	0.358977	4.655917
RSD%	0.056980776	0.419374	0.400364
Disulfiram 100 µg/mL			
Injection no	RT (min)	Peak area (mAU)	Peak height
1	8.07	45.56	285.12
2	8.07	45.45	283.99
3	8.08	45.82	286.21
4	8.09	45.47	284.27
5	8.09	44.83	280.32
6	8.07	45.35	283.30
7	8.09	45.27	282.53
8	8.08	45.47	284.30
9	8.07	45.13	282.28
10	8.09	45.43	283.21
Mean	8.0788	45.3765	283.5533
SD	0.009053	0.264777	1.635595
RSD%	0.112058	0.583512	0.576821

Bis(N,N-diethyl dithiocarbamato)copper(II) complex 100 µg/mL			
Injection no	RT (min)	Peak area (mAU)	Peak height
1	13.80	76.56	195.97
2	13.62	79.06	210.57
3	13.63	84.91	224.57
4	13.63	78.17	200.64
5	13.63	79.68	211.44
6	13.65	79.20	210.92
7	13.66	81.91	213.97
8	13.67	81.76	205.98
9	13.67	82.10	215.46
10	13.68	79.10	212.66
Mean	13.6640	80.2446	210.2172
SD	0.05096622	2.409639685	7.94616806
RSD%	0.372996339	3.002867868	3.779979973

IRN-CAP-DSF

The RSD% values for retention time, peak area and peak height for IRN, CAP and DSF were all ≤ 4.5 % indicating that the method is precise (Table 4.6).

Table 4.6: Intra-day precision of HPLC assay for IRN-CAP-DSF combination.

Irinotecan 300 µg/mL			
Injection no	RT (min)	Peak area (mAU)	Peak height
1	1.20	7363.58	1600.94
2	1.18	7189.96	1550.79
3	1.20	7201.81	1564.51
4	1.21	7370.53	1672.10
5	1.23	7405.55	1608.64
6	1.25	7188.49	1563.16
7	1.25	7236.19	1571.93
8	1.17	7229.44	1551.92
9	1.17	7301.70	1592.01
10	1.19	7262.95	1572.26
Mean	1.205	7279.682577	1584.202451
SD	0.027313001	78.05188809	34.62071672
RSD%	2.266639051	1.07218807	2.185371995

Captopril 300 µg/mL			
Injection no	RT (min)	Peak area (mAU)	Peak height
1	2.55	742.08	116.70
2	2.52	697.40	108.93
3	2.51	694.94	107.61
4	2.50	709.84	110.37
5	2.50	742.63	115.67
6	2.51	758.37	121.28
7	2.50	726.65	113.19
8	2.50	771.53	120.54
9	2.50	697.78	108.20
10	2.50	722.64	107.41
Mean	2.506181818	726.2977996	112.9528536
SD	0.014455575	25.50832597	5.034380568
RSD%	0.576796722	3.512102885	4.457063642

Disulfiram 300 µg/mL			
Injection no	RT (min)	Peak area (mAU)	Peak height
1	7.96	6738.55	680.70
2	7.87	6627.78	669.04
3	7.87	6656.41	670.49
4	7.83	7155.86	720.38
5	7.81	6813.37	686.91
6	7.83	6543.37	658.34
7	7.83	6648.54	669.16
8	7.82	6304.52	633.34
9	7.82	6764.43	675.78
10	7.80	6815.57	683.69
Mean	7.838545455	6712.263202	674.6835022
SD	0.046759734	208.1164756	21.00808497
RSD%	0.596535854	3.100541045	3.113768887

4.4.8 Precision- Intermediate precision

IRN-PTV-DSF-DDC_Cu

The RSD% values obtained using two different instruments on two different days were all \leq 3.6 % demonstrating good intermediate precision and that the method can be replicated across different instruments and days. (Table 4.7)

Table 4.7: Intermediate precision of HPLC assay for IRN-PTV-DSF-DDC_Cu combination. Instrument 1 was Dionex Ultimate 3000 LC system and instrument 2 was Agilent LC system.

Irinotecan						
Relative % purity (% area)						
	Instrument 1			Instrument 2		
	Sample 1 60%	Sample 2 100 %	Sample 3 200 %	Sample 1 60%	Sample 2 100 %	Sample 3 200 %
Operator 1. Day 1	104.62	102.44	101.16	103.50	101.69	101.99
Operator 1, day 2	106.61	104.75	101.10	101.68	105.16	102.14
Mean Interday	105.615	103.595	101.13	102.59	103.425	102.065
RSD % Interday	1.33233205	1.576733	0.041952	1.25444424	2.372406	0.10392
Mean (Instrument)	104.1025	103.51	101.5975			
RSD % (Instrument)	1.98317219	1.646837	0.535285			
Pitavastatin						
Relative % purity (% area)						
	Instrument 1			Instrument 2		
	Sample 1 60%	Sample 2 100 %	Sample 3 200 %	Sample 1 60%	Sample 2 100 %	Sample 3 200 %
Operator 1. Day 1	99.76	99.86	99.93	99.15	99.64	100.22
Operator 1, day 2	99.76	99.86	99.93	98.49	99.43	100.15
Mean Interday	99.76	99.86	99.93	98.82	99.535	100.185
RSD % Interday	0	0	0	0.47226318	0.149186	0.049406
Mean (Instrument)	99.29	99.6975	100.0575			
RSD % (Instrument)	0.61024805	0.206923	0.149886			
Disulfiram						
Relative % purity (% area)						
	Instrument 1			Instrument 2		
	Sample 1 60%	Sample 2 100 %	Sample 3 200 %	Sample 1 60%	Sample 2 100 %	Sample 3 200 %
Operator 1. Day 1	93.54	95.97	98.01	99.86	98.60	99.64
Operator 1, day 2	93.23	95.98	97.97	98.64	97.99	99.65
Mean Interday	93.385	95.975	97.99	99.25	98.295	99.645
RSD % Interday	0.23473053	0.007368	0.028864	0.86918919	0.438817	0.007096
Mean (Instrument)	96.3175	97.135	98.8175			
RSD % (Instrument)	3.55587704	1.402596	0.967099			
Bis(N,N-diethyl dithiocarbamato)copper(II) complex						
Relative % purity (% area)						
	Instrument 1			Instrument 2		
	Sample 1 60%	Sample 2 100 %	Sample 3 200 %	Sample 1 60%	Sample 2 100 %	Sample 3 200 %
Operator 1. Day 1	102.45	101.47	100.75	99.46	100.47	101.21
Operator 1, day 2	102.49	101.46	100.75	99.47	100.50	100.98
Mean Interday	102.47	101.465	100.75	99.465	100.485	101.095
RSD % Interday	0.02760249	0.006969	0	0.0071091	0.021111	0.160873
Mean (Instrument)	100.9675	100.975	100.9225			
RSD % (Instrument)	1.71839375	0.560486	0.218195			

IRN-CAP-DSF

The RSD% values obtained by two different instruments on two different days were all ≤ 6.4 % demonstrating good intermediate precision so the method can be replicated across different instruments and days (Table 4.8)

Table 4.8: Intermediate precision of HPLC assay for IRN-CAP-DSF combination. Instrument 1 was Agilent LC system and instrument 2 was Dionex Ultimate 3000 LC system.

Irinotecan						
Relative % purity (% area)						
	Instrument 1			Instrument 2		
	Sample 1 66%	Sample 2 100 %	Sample 3 133 %	Sample 1 66%	Sample 2 100 %	Sample 3 133 %
Operator 1. Day 1	110.4636	110.8638	110.0815	105.20	103.59	110.99
Operator 1, day 2	110.7691	111.7299	109.489	101.78	109.15	108.14
Mean Interday	110.61635	111.29685	109.7853	103.49	106.37	109.565
RSD % Interday	0.216021122	0.61242518	0.418961	2.418305192	3.9315137	2.015254
Mean (Instrument)	107.053175	108.833425	109.6751			
RSD % (Instrument)	4.346635843	3.65630576	1.195169			
Captopril						
Relative % purity (% area)						
	Instrument 1			Instrument 2		
	Sample 1 66%	Sample 2 100 %	Sample 3 133 %	Sample 1 66%	Sample 2 100 %	Sample 3 133 %
Operator 1. Day 1	107.3231	109.4782	109.0618	101.52	108.50	105.70
Operator 1, day 2	103.5564	100.3922	100.094	107.89	106.43	110.15
Mean Interday	105.43975	104.9352	104.5779	104.705	107.465	107.925
RSD % Interday	2.663459113	6.424772214	6.341192	4.50427	1.463711	3.146625
Mean (Instrument)	105.072375	106.2001	106.2515			
RSD % (Instrument)	3.050809838	4.075129284	4.520879			
Disulfiram						
Relative % purity (% area)						
	Instrument 1			Instrument 2		
	Sample 1 66%	Sample 2 100 %	Sample 3 133 %	Sample 1 66%	Sample 2 100 %	Sample 3 133 %
Operator 1. Day 1	108.0299	104.3328	98.02026	107.29	97.40	102.45
Operator 1, day 2	107.8083	103.0763	98.54229	109.45	99.99	101.52
Mean Interday	107.9191	103.7046	98.28128	108.37	98.695	101.985
RSD % Interday	0.156695	0.88848	0.369131	1.527351	1.831407	0.657609
Mean (Instrument)	108.1446	101.1998	100.1331			
RSD % (Instrument)	0.92388	3.121914	2.182223			

4.4.9 Limit of detection and quantitation

IRN-PTV-DSF-DDC_Cu

The LOD and LOQ were set at 10 and 20 µg/mL, respectively with both achieving RSD% values of ≤ 2.5 % (Table 4.9).

Table 4.9 LOD and LOQ data of HPLC assay for IRN-PTV-DSF-DDC_Cu combination.

LOD: 10 µg/mL				
Sample	IRN Peak area (mAU)	PTV Peak area (mAU)	DSF peak area (mAU)	DDC_Cu peak area (mAU)
1	4.309	8.429	4.7034	6.4399
2	4.2853	8.3976	4.6879	6.8741
3	4.3051	8.4227	4.6899	6.8915
4	4.3	8.4327	4.7156	6.7826
5	4.3263	8.4498	4.694	6.7358
6	4.3072	8.4201	4.7016	6.8641
RSD %	0.31	0.20	0.22	2.51
LOQ=20 µg/mL				
Sample	IRN Peak area (mAU)	PTV Peak area (mAU)	DSF peak area (mAU)	DDC_Cu peak area (mAU)
1	7.869	16.2112	8.99	15.131
2	7.836	16.1083	9.011	15.140
3	8.164	16.2332	9.052	15.110
4	8.182	16.2436	9.018	15.114
5	8.15	16.2057	9.013	15.107
6	8.163	16.2233	9.027	15.100
RSD %	2.01	0.30	0.23	0.10

IRN-CAP-DSF

The LOD and LOQ were set at 20 and 80 µg/mL, respectively with both achieving RSD% values of ≤ 1.5 % (Table 4.10).

Table 4.10: LOD and LOQ data of HPLC assay for IRN-CAP-DSF combination.

LOD: 20 µg/mL			
Sample	IRN Peak area (mAU)	CAP Peak area (mAU)	DSF peak area (mAU)
1	475.50	26.18	441.46
2	470.35	26.79	441.88
3	473.05	26.87	438.97
4	479.31	26.88	441.76
5	477.77	26.81	442.70
6	470.07	25.97	440.01
RSD %	0.808996513	1.507646	0.311701
LOQ: 80 µg/mL			
Sample	IRN Peak area (mAU)	CAP Peak area (mAU)	DSF peak area (mAU)
1	2217.41	127.88	1970.26
2	1876.08	98.58	1946.70
3	1880.06	124.55	1918.91
4	1977.07	105.03	2320.66
5	1956.20	105.85	2023.73
6	1952.27	116.87	1981.37
RSD %	0.000633618	0.001040148	0.000730701

4.4.10 System suitability

For both the IRN-PTV-DSF-DDC_Cu and IRN-CAP-DSF chromatographic methods all peaks were proven to be well resolved, symmetrical and sharp with resolution values, peak symmetry and plate numbers all within the acceptable criteria (Table 4.11 & Table 4.12). Reproducibility of the method was also evaluated via injecting the target level of analyte 6 times, the RSD% values for retention time, peak area and peak height were calculated (Table 4.11 & Table 4.12). Only peak area was proven to be reproducible for both method across all drugs. Variations in retention times and peak height were obtained but as the resolution and peak area reproducibility were unaffected by this, it does not cause any potential disadvantage concerning the applicability of method.

Table 4.11 system suitability data of HPLC assay for IRN-PTV-DSF-DDC_Cu combination.

Irinotecan				
System suitability parameters	Acceptance criteria (EP)	Results		Criteria Met/Not met
		HPLC 1	HPLC 2	
Precision for retention time (n=6)	RSD ≤ 1 %	0.004	2.6	Not met
Precision for peak area (n=6)	RSD ≤ 1 %	0.1621	0.021	Met
Precision for peak height (n=6)	RSD ≤ 1 %	5.83	0.81	Not met
Resolution (n=6)	≥ 1.5	19.12	na	Met
Symmetry (n=6)	0.8 to 1.5	1.21	0.99	Met
Plates (n=6)	≥ 2000	5979	2008	Met
Pitavastatin				
System suitability parameters	Acceptance criteria (EP)	Results		Criteria Met/Not met
		HPLC 1	HPLC 2	
Precision for retention time (n=6)	RSD ≤ 1 %	0.003	2.1	Not met
Precision for peak area (n=6)	RSD ≤ 1 %	0.049	0.01	Met
Precision for peak height (n=6)	RSD ≤ 1 %	0.86	5.8	Not met
Resolution (n=6)	≥ 1.5	30.88	13.6	Met
Symmetry (n=6)	0.8 to 1.5	0.97	1.5	Met
Plates (n=6)	≥ 2000	10056	5251	Met
Disulfiram				
System suitability parameters	Acceptance criteria (EP)	Results		Criteria Met/Not met
		HPLC 1	HPLC 2	
Precision for retention time (n=6)	RSD ≤ 1 %	0.01	0.74	Met
Precision for peak area (n=6)	RSD ≤ 1 %	0.0206	0.001	Met
Precision for peak height (n=6)	RSD ≤ 1 %	0.1	0.001	Met
Resolution (n=6)	≥ 1.5	17.64	27	Met
Symmetry (n=6)	0.8 to 1.5	0.99	1.0	Met
Plates (n=6)	≥ 2000	16537	14000	Met

Bis(N,N-diethyl dithiocarbamato)copper(II) complex				
System suitability parameters	Acceptance criteria (EP)	Results		Criteria Met/Not met
		HPLC 1	HPLC 2	
Precision for retention time (n=6)	RSD ≤ 1 %	0.025	0.17	Met
Precision for peak area (n=6)	RSD ≤ 1 %	0.0998	0.001	Met
Precision for peak height (n=6)	RSD ≤ 1 %	0.19	2.56	Not met
Resolution (n=6)	≥ 1.5	n.a	30	Met
Symmetry (n=6)	0.8 to 1.5	0.98	1.0	Met
Plates (n=6)	≥ 2000	16524	8000	Met

Table 4.12 system suitability data of HPLC assay for IRN-CAP-DSF combination.

Irinotecan				
System suitability parameters	Acceptance criteria (EP)	Results		Criteria Met/Not met
		HPLC 1	HPLC 2	
Precision for retention time (n=6)	RSD ≤ 1 %	2.2	0.003	Not met
Precision for peak area (n=6)	RSD ≤ 1 %	0.001	0.14	Met
Precision for peak height (n=6)	RSD ≤ 1 %	0.002	5.00	Not met
Resolution (n=6)	≥ 1.5	Na	12.31	Met
Symmetry (n=6)	0.8 to 1.5	1.2	1.13	Met
Plates (n=6)	≥ 2000	2230	2050	Met

Captopril				
System suitability parameters	Acceptance criteria (EP)	Results		Criteria Met/Not met
		HPLC 1	HPLC 2	
Precision for retention time (n=6)	RSD ≤ 1 %	0.02	0.002	Met
Precision for peak area (n=6)	RSD ≤ 1 %	0.00	0.18	Met
Precision for peak height (n=6)	RSD ≤ 1 %	0.01	1.77	Not met
Resolution (n=6)	≥ 1.5	5.3	28.48	Met
Symmetry (n=6)	0.8 to 1.5	1.5	0.79	Met
Plates (n=6)	≥ 2000	3900	5500	Met

Disulfiram				
System suitability parameters	Acceptance criteria (EP)	Results		Criteria Met/Not met
		HPLC 1	HPLC 2	
Precision for retention time (n=6)	RSD ≤ 1 %	0.15	0.009	Met
Precision for peak area (n=6)	RSD ≤ 1 %	0.06	0.27	Met
Precision for peak height (n=6)	RSD ≤ 1 %	0.09	1.65	Not met
Resolution (n=6)	≥ 1.5	18.50	12.31	Met
Symmetry (n=6)	0.8 to 1.5	0.99	1.04	Met
Plates (n=6)	≥ 2000	14925	15899	Met

4.5 Conclusion

Two rapid, specific reverse-phase HPLC-DAD methods were developed for the determination of IRN-PTV-DSF-DDC_Cu and IRN-CAP-DSF drug combinations. The methods were validated and shown to be specific, linear, accurate, precise, and robust. Both

methods use a simple mobile phase composition, which is easy to prepare with little or no variation. With run time < 25 minutes large number of samples can be analysed with less mobile phase for a more eco-friendly and less time consuming analysis. Hence, this HPLC-DAD method can be used for routine analysis.

5. CHAPTER FIVE: FORMULATION AND DEVELOPMENT OF A MULT-DRUG IMPLANTABLE DRUG DELIVERY DEVICE

5.1 Abstract

The objective of this study was to formulate our previously selected drug combinations: IRN-PTV-DSF-CoGlu and IRN-CAP-DSF into an implantable drug delivery device. This was achieved in three stages 1) selection of excipients 2) profiling of drug and excipients thermal stability 3) characterisation of formulated implant.

Swelling and rheology tests were initially performed to select excipients that were both physically stable in *in-vitro* test conditions and had suitable melt-viscosity parameters for use in extrusion manufacture process. Stability of each drug at manufacture temperature was then investigated using HPLC and differential scanning calorimetry (DSC) analysis. Finally, the formulated implants were characterised for uniformity of mass, size and drug content, as well as drug release.

Our results demonstrate that a 50/50 PLGA polymer with a molecular weight of less than 20 kDa had melt-viscosity profile that is appropriate for use in low temperature (<120 °C) extrusion process. Furthermore, the inclusion of a plasticiser can lower the melt viscosity of polymer to eliminate some of the manufacturing problems associated with either injection moulding or extrusion manufacture process of the implantable device. To maintain the physical stability of implant in release media, swelling study was performed and P188 plasticiser was demonstrated to be the most suitable for use in formulation. Finally, DSC and thermal stability analysis demonstrated that all drugs and excipients were stable at the processing temperatures. Both IRN-PTV-DSF-CoGlu and IRN-CAP-DSF multidrug implantable device were formulated via a manual micro-extrusion process with data revealing good uniformity of size ($\pm 10\%$), weight ($\pm 10\%$) and drug content (20 %RSD). Sustained drug release of IRN, PTV, DSF and CAP treatments was also obtained under both bio relevant and sink *in-vitro* test conditions.

5.2 Introduction

Within any drug development procedure, it is important to develop a pharmaceutical formulation process ahead of clinical trials to ensure that the drug delivery device comply with good manufacturing practice (GMP). This may include but not limited to ensuring that the device is of high quality (e.g has good uniformity of weight, size, content), safe (e.g free from impurity and degradation products) and efficacious (e.g predict bioavailability due to known drug release profile) [395]. Implantable devices such as drug loaded polymeric implants are often composed of a therapeutic agent incorporated homogenously within either a polymer or polymer plus additives matrix. During the development procedure two main design processes are involved, first a formulation of drug into a pharmaceutical product with known stability and drug release characteristic followed by a scale-up manufacturing process. During the formulation phase, a polymer with known desired chemical and mechanical properties for its intended use is selected. For example, if long term drug delivery is required, then a polymer with a slow drug release profile can be selected. Additional additives, such as plasticisers, stabilisers and fillers can be included to enhance the implant's mechanical properties and reduce manufacturing costs. Currently a wide range of polymers are in use for pharmaceutical implants such as Ethylene-vinyl acetate (EVA), poly(lactic-co-glycolic acid) (PLGA), silicon elastomers and Polycaprolactone (PCL). Here we have selected PLGA for use to formulate a multi-drug delivery system because it is FDA approved and known to be safe, biodegradable in physiological environment without inducing adverse reactions and can be easily manufactured by a variety of techniques, such as extrusion, compression moulding, 3D printing and electrospinning [162, 163]. Additionally, the formulation of PLGA drug loaded implant into a defined geometric shape can result in a predictable and reproducible drug release and degradation profile [162]. All of this would contribute to ease in translating an implantable device from the lab into the clinic. For this study instead of individual drug delivery devices, a composite product was formed to ensure even drug distribution in the cavity and to make it easier for surgeons to implant. To develop the implantable drug delivery device a target product profile was prepared and

delivered in three study stages: 1) selection of excipients 2) thermal stability during manufacture for drug and excipients 3) characterisation of formulated implant (Table 5.1).

Table 5.1 Studies performed for drug delivery device development with target product profile.

Element	Study	Instrument measured with	Target product profile
Selection of excipients	Rheological assessment of polymer and plasticisers	Rheometer	At <120 °C, the formulation viscosity range within 10^3 - 10^4 Pa.s
	Influence of the plasticiser type and loading on the swelling of implants (n=4)	Digital Caliper	To eliminate or minimise
Thermal stability during manufacture	Drug stability at manufacture temperature (n=4)	HPLC	Drug recovery within ± 2 % deviation
	Crystallinity profile of formulation	DSC	Understand the amorphous and crystalline behaviour of drug + excipients following manufacture
Characterisation of Implant	Uniformity of mass (n=20)	Digital Caliper	Within ± 10 % deviation
	Uniformity of size (diameter x length) (n=20)	Digital Caliper	Within ± 10 % deviation
	Uniformity of drug Content (n=8)	HPLC	± 20 % from theoretical content
	Dissolution test (n=4)	HPLC	Controlled simultaneous drug release over the course of 1-4 weeks.

5.2.1 Selection of excipients

Rheology

Rheology is the science of the flow of materials [396]. A solid material, such as a rigid polymer, may behave more like a fluid with an increase in thermal and kinetic energy. When a polymer with viscoelastic properties such as PLGA is subjected to an applied stress, the response of that material would be composed of elastic deformation (which stores energy)

and viscous flow (which dissipates energy) [397]. In a pharmaceutical process such as extrusion or injection moulding applied heat, screw speed and pressure used to force a material through a shaping die all increase the applied thermal energy and shear rate onto the processed material, enhancing its flow properties. Since rheology studies can measure the flow of material when subjected to an applied shear, it can be utilized to predict the manufacturing processing parameters for a chosen material. For instance, in extrusion the viscosity of a material under applied force is useful to know since most polymers are only extrudable at viscosities between 10^2 and 10^5 Pa.s [398]. The viscosity measurement represents the resistance of material to flow and it is proportional to shear stress (Equation 5.1) [398, 399].

$$\eta \text{ (Viscosity)} = \frac{\tau \text{ (Shear Stress)}}{\gamma \text{ (Shear Rate)}} \quad \text{Equation: 5.1}$$

Additionally, the shear stress and shear rate applied may influence the overall mechanical properties and quality of extruded material. For a shear thinning material such as PLGA an increase in shear rate (i.e extrude faster through a die) reduces the viscosity, it also prevents potential hang-ups of the molten material. An increase in shear stress (applied torque), particularly above 0.14 MPa increases the chance of physical deformation of extruded material (e.g sharkskin and melt fracture) [398-400].

Hence rheology can provide information on the physical properties of material, enabling us to define the manufacturing processing parameters and develop a formulation that is capable of being manufactured by common techniques, such as extrusion.

Swelling of drug delivery device

The swelling of pharmaceutical systems containing a drug and a polymer in the brain can be predicted by measuring implant volume increase in release media overtime. Swelling occurs due to the absorbance of the cerebral spinal fluid (CSF) found in the brain [401, 402]. The entrapment of access CSF around the brain can lead to cerebral oedema which brain tumour patients are commonly susceptible to [403, 404]. Patients under localised Gliadel® wafer

treatment are commonly diagnosed with cerebral oedema, and although no study assessing the swelling of Gliadel® implant was found, one probable contributing factor to this could be because of its swelling as well as the relatively large size of Gliadel®, both contributing to a slight increase in entrapped CNS fluid volume (Figure 5.1) [403, 405]. Therefore, to ensure the safety of our drug delivery system (DDS), it is important to minimise fluid entrapment and swelling of the pharmaceutical formulation. Delivering a smaller sized implant should minimise the volume of CSF entrapped, while a swelling study ensure that the developed implant doesn't swell reducing the possibility of peritumoral brain oedema.

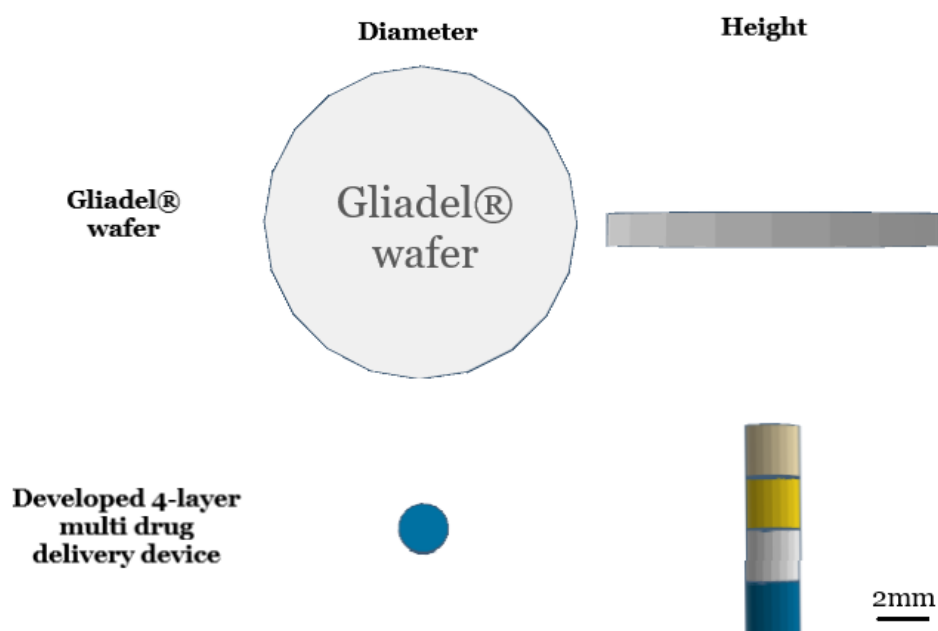


Figure 5.1: Dimensions (diameter x height) of Gliadel® wafer implant compared to our 4-layer multi-drug delivery device.

5.2.2 Thermal stability and interaction

Drug stability at manufacture temperature

In order to ensure safety and efficacy of a pharmaceutical product, it is important to determine any stability issues at an early stage of the product development process [406, 407]. Forced degradation of the drug at elevated temperatures can be performed to determine their thermal stability, ensuring that the manufactured product content is accurate, and more importantly safe to give to patients [408]. HPLC-UV analysis can be used

to determine drug degradation when compared to standard analyte of known purity by the by appearance, disappearance or sudden change in peak area and/or shape (e.g peak tailing, fronting, splitting, shouldering, etc.)

Differential scanning calorimetry (DSC)

DSC is an analytical technique where the sample is subjected to heating or cooling and the relative Gibbs free energy is calculated as a function of temperature [409, 410]. In pharmaceutical product development DSC can be a useful tool to assess drug degradation and interactions between the drug and excipients. A drug degradation or interaction often result in appearance, disappearance or shift of endothermic or exothermic peaks [411]. This allows for the characterisation of the physicochemical properties of the drug compound and to define the manufacturing processing parameters. For instance, if it is needed to deliver a stable pharmaceutical product in the amorphous form then it could be necessary to process the formulation at temperatures below those at which interactions and crystallization occur.

5.2.3 Drug release characteristics

Dissolution testing is a widely used technique for evaluating the drug release of pharmaceutical products [412]. The drug release profile of a dosage form can be used to predict its bioavailability and therapeutic effectiveness. Developing a drug delivery device with a predictable drug release profile is crucial to ensure that the device is safe and suitable for its intended use. During product development, dissolution can be performed under both biologically relevant and sink conditions. For biologically-relevant dissolution, water can be used, but for poorly water soluble drugs, dissolution under sink conditions must also be performed to assess how the device or formulation influences release by removing the issue of drug solubility [413]. To achieve sink conditions a media that is capable of dissolving 3x the drug concentration should be tested, this can be achieved by the addition of a suitable surfactant or co-solvent in the dissolution medium to enhance drug solubility [413]. If sink conditions are not met, then the rate of drug release will slow as the API nears saturation.

For an implantable device consisting of therapeutic agent incorporated homogeneously within either a polymer or polymer + additives matrix, the kinetics for drug release is highly

influenced by a number of factors such as implant geometry, loading ratio, implant microstructure, contact with the body fluid, implant location within the body, temperature, motion, molecular weight of components, the crystallinity of components and formulation. For biodegradable drug-loaded implants, the degradation rate of the implant must remain at a consistent rate to sustain a stable drug release profile. Two biodegradable drug delivery systems can be considered for drug release: i) a reservoir system, where drug release occurs prior to implant structure degradation. For this system the drug is released via diffusion through the implant matrix. Depending on the drug diffusion rate through the implant structure, the drug release profile will initially be a rapid release (burst effect) followed by either zero or first order release kinetic [414]. ii) Surface eroding system, where system degradation is proportional to drug release. This systems drug release profile will again initially be a rapid drug release (burst effect) followed by first order release kinetic [415, 416] (Figure 5.2).

Therefore, to predict the bioavailability and effectiveness of the IRN-PTV-DSF-Cu and IRN-CAP-DSF combinations therapy it is important to profile and understand their release from the drug delivery device.

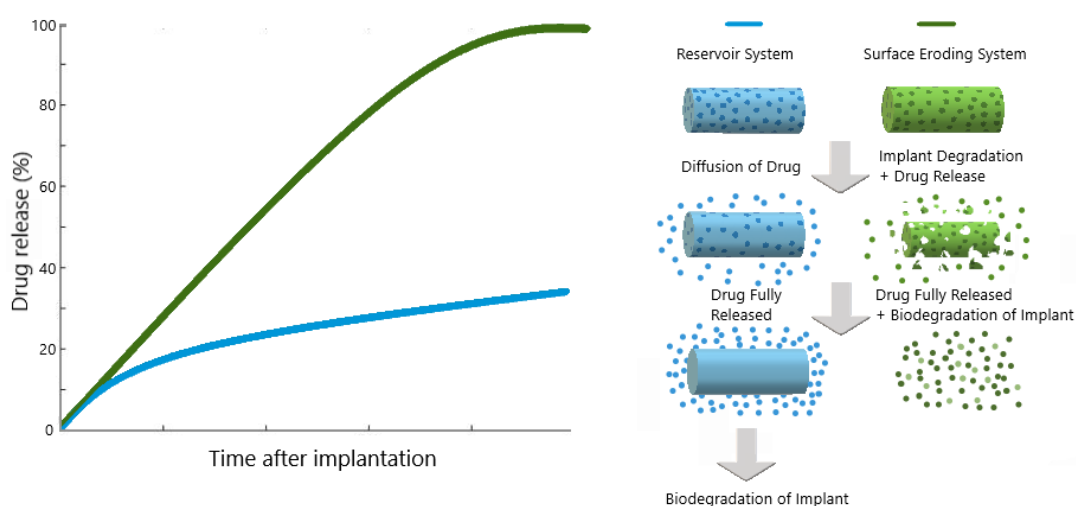


Figure 5.2: Drug release profile of reservoir and surface eroding biodegradable implants. With permission from [162].

5.3 Materials and methods

5.3.1 Materials and Reagents

Irinotecan hydrochloride and pitavastatin calcium were purchased from LGM Pharma respectively. Disulfiram, captopril, copper gluconate and sodium dodecyl sulphate (SDS) were from Sigma Aldrich. Polymers (PLGA 5002/5004/5010) and plasticisers (Kolliphor® P188, P237 and RH40) were purchased from Corbion purac and BASF, respectively.

Acetonitrile, acetic acid and acetone were of HPLC grade and from Sigma Aldrich.

Dichloromethane (DCM) was reagent grade and purchased from Sigma Aldrich.

5.3.2 Rheology

Rheological evaluation was performed using a TA instrument Discovery hybrid parallel plate rheometer with a 40 mm cross-hatch steel plate and a 500 µm gap height.

Linear Viscoelastic region

Initially an oscillation amplitude assessment was performed for each sample to determine the linear viscoelastic region. Each test was performed at a constant frequency (5 rad/s) with stress between 1×10^{-3} and 1×10^4 Pa and five temperature measurements (80, 100, 120, 140 and 180 °C).

Viscosity

Flow temperature ramp assessments were run over the temperature range of 80-180 °C, at constant stress within the viscoelastic region.

5.3.3 Thermal stability

Drug stability at manufacture temperature

The thermal stability of IRN, PTV, CAP and DSF were determined by individually weighing 10 mg of each drug into a glass vial, which were then placed in an oven at 80 °C for DSF and 120 °C for IRN, PTV and CAP, with vials (n=4) removed at 10, 30, 60, and 120 minutes. The content of each vial was subsequently analysed by dissolving the drug in 10 mL of HPLC mobile phase and analysing using the appropriate HPLC method (section 5.3.4 HPLC).

Crystallinity profile of formulation using DSC

The thermal behaviour of the polymer, drug, and formulated drug and excipient mixture were analysed using a TA instruments Q200 DSC. 5-10 mg of sample was weighed into an aluminium pan and analysed, with an empty aluminium pan was used as a reference. All calorimetric scans were subjected to four consecutive steps; 1) 5-minutes isothermal at 25 °C, 2) heating ramp at 5 °C/min, to 200 °C, 3) end temperature 1-minute isothermal, 4) cooling ramp at 5 °C/min, down to 25 °C.

5.3.4 HPLC

For both IRN-PTV-DSF-CoGlu and IRN-CAP-DSF drug combinations, the chromatographic column used was Thermo Scientific Synchronis, C18 (150 mm × 4.6 mm; 5 µm, 100 Å, 16 % carbon loading). The mobile phase consisted of water:acetonitrile:acetic acid mixture (30:70:0.1, v/v/v for IRN-PTV-DSF-DDC_Cu and 30:70:0.2, v/v/v for IRN-CAP-DSF), being pumped at a flow rate of 1 mL/min. Injection volume was 10 µL and detection wavelength was 245 nm. All experiments were performed at 27 °C and the total peak area was used to quantify each drug. Prior to sample injection the column was purged and equilibrated for 30 minutes using the mobile phase.

5.3.5 Swelling study

To investigate the swelling behaviour of different plasticisers, for each IRN-PTV-DSF-CoGlu and IRN-CAP-DSF multidrug treatments, three different formulations were made using three different plasticisers; RH40, P188 and P237, as per the manufacturing method (section 5.3.6).

For each formulation completely dry implants (n=4), with length and diameter dimensions pre-measured were fully immersed in 10mL of sink (2% SDS) and bio (H₂O) release medium. The samples were then transferred to an orbital shaking incubator set at 37 °C 60 rpm. Dimensions of each implant was then measured at 6, 24, 48 and 120 hours. Percentage swelling over time was then calculated and a graph plotted.

5.3.6 Micro extrusion

Preparation of raw material

In order to ensure the homogeneity of the final implant the particle size of the initial starting materials were reduced to similar sizes. Granules of PLGA (5002 and 5004) and P188 were cooled to -80 °C, in order to increase their brittleness and then subsequently crushed to a fine powder using an electric grinder. The drugs were supplied as fine powders.

Manufacturing of implantable drug delivery devices

Components ratio and processing temperature for each formulation are listed in Table 5.2. A 500 mg mixture consisting of drug, polymer and plasticiser were manually mixed in a 5mL beaker for 20 minutes. Once mixed, the content was transferred to a 1 mL plastic syringe with a piece of 2mm diameter silicon tubing attached. The syringe was then placed into an oven set at the processing temperature for 40 min. Once complete, the content of the syringe was then extruded out into the attached silicon tubing. Once cooled to room temperature, each formulation was then cut to dimension (2mmx2mm) to produce individual drug-loaded layers. To make the IRN-PTV-DSF-CoGlu and IRN-CAP-DSF multi drug implants, individual layers containing each drug were glued together using surgical glue to produce a 3 or 4 drug combination implant.

Table 5.2: Components ratio and processing temperature for each drug formulation. Each drug was either formulated using PLGA 5004 or 5002.

Formulation Drug:Polymer:Plasticiser	Loading ratio (%) Drug:Polymer:Plasticiser	Processing temperature (°C)
IRN:PLGA5004:P188	30:50:20	110
PTV:PLGA5004:P188	30:50:20	120
DSF:PLGA5004:P188	30:50:20	70
CAP:PLGA5004:P188	30:60:10	120
CoGlu:PLGA5004:P188	30:50:20	110
IRN:PLGA5002	30:70	120
PTV:PLGA5002	30:70	120
DSF:PLGA5002	30:70	80
CAP:PLGA5002	30:70	120
CoGlu:PLGA5002	30:70	120

5.3.7 Implant drug content

Each pre-weighed implant (n=8) was placed in a glass vial containing 5 mL of DCM and dissolved. The DCM was then evaporated off in a water bath set at 65°C. Once evaporated, 10 mL of HPLC mobile phase was added allowing the drug to re-dissolve into solution whilst the plasticiser and PLGA precipitated out. This solution was then filtered using a 0.25 µm syringe filter and analysed by HPLC to determine drug content. The results were then compared against the theoretical content calculated from the total mass of the implant to determine the reliability of the manufacturing process. A limit of $\pm 10\%$ of the theoretical content was deemed acceptable

5.3.8 Dissolution test, *in-vitro* drug release

Each individual implant (n=4) was placed into a glass vial and the release media added. For bio release, 3 mL of HPLC-grade water was used, while for sink release, 5 mL of 2 % SDS solution was used. The vials were then placed in an orbital shaking incubator set at 37 °C and 60 RPM. Samples were taken at 1, 2.5, 6 and 24 hours followed by 3, 5, 7, 9, 11, 14, 16, 21 and 28 days, with complete media replacement at each sampling point. The release media was subsequently analysed using the appropriate HPLC method.

5.4 Results and discussion

5.4.1 Rheological assessment of polymer and plasticisers

Due to the large variation in the physicochemical properties (molecular size, hydrophilicity, melting point and charge) of IRN, PTV, CAP, DSF and CoGlu, (Chapter one, 1.4 Drugs that may be suitable for repurposing to treat Glioblastoma, Table 1.2) the mechanism for drug release is expected to vary between the drugs with some releasing primarily via diffusion and others via the erosion of matrix system. 50/50 PLGA polymers were selected because of their relatively fast degradation rate (1-2 months) to enable any drugs with extremely slow diffusion rate to release, eliminating the potential for large variation in drug release between the drugs [162].

Initially the melt rheology of low, medium and high molecular weight 50/50 PLGA polymers were studied; 5002a (~ 10 kDa), 5004 (~ 20 kDa) and 5010 (~ 90 kDa) [417]. In order to

model each polymer extrusion profile and its manufacturing processing parameters a viscosity temperature sweep was performed on each polymer. For all three polymers viscosity decreased with an increase in temperature (Figure 5.3). The melt viscosity profile was influenced by the molecular weight, with a higher molecular weight resulting in a higher viscosity profile. For a small scale pharmaceutical extruder the optimum viscosity range is between 10^3 - 10^4 Pa.s, since higher viscosity would require unattainable amount of torque and lower viscosity would result in an extrudate that is too fluid and would therefore not take the form of the die [398, 418]. All three polymers were demonstrated to be extrudable but at different temperatures. Low and medium molecular weight polymers 5002a and 5004 had a viscosity between 10^3 - 10^4 Pa.s at 80-95 and 97-123 °C, respectively, while the high molecular weight polymer 5010 had a 10^4 Pa.s viscosity at 150 °C (Figure 5.3).

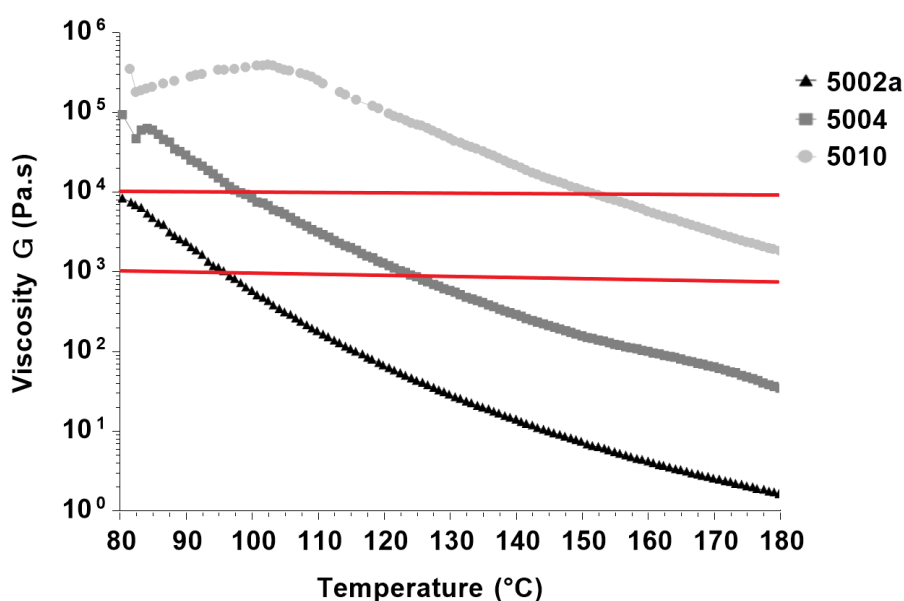


Figure 5.3: Temperature sweep data between 80 to 180 °C for PLGA 5002, 5004 and 5010. Optimum viscosity range for extrusion (10^3 - 10^4 Pa.s) is represent by red lines.

Unfortunately for heat sensitive drugs such as DSF an increase in processing temperature above 80 °C may lead to decomposition [419]. Hence for 5004 and 5010 polymers the addition of a plasticiser maybe required to reduce their melt viscosity. To confirm this, the melt rheology of drug mixed with low (5002), medium (5004) and high (5010) molecular weight PLGA polymers, at 30:70 drug-polymer ratio, were investigated. For the 5002, the melt viscosity of polymer mixed with CAP and DSF were noticeably lower than IRN, PTV and

CoGlu (Figure 5.4). This was also observed with 5004 but only at temperatures above 110 °C (Figure 5.4). Additionally, all 5002 and 5004 drug-polymer mixtures were demonstrated to be temperature dependant, with the exception for IRN-5004 drug-polymer mixture as the viscosity remained consistent at 10^4 Pa.s between 140 to 180 °C (Figure 5.4). For the 5010 polymer, extremely high viscosities $>10^6$ Pa.s were demonstrated during initial viscosity readings at the start of the rheology run across all of the samples. Due to this high viscosity, most runs were terminated prematurely by the equipment, higher starting temperatures (110, 140 and 160 °C) were trialled but with similar outcome.

For the 5002 polymer, IRN, PTV and CoGlu reached the 10^3 - 10^4 Pa.s viscosity range at 80-95 °C, while for CAP and DSF much lower melt viscosities were observed, and according to their extrapolated melt viscosity curves it is anticipated that they would require extrusion processing temperatures of 60-75 °C (Figure 5.4). Higher melt viscosities were observed for the 5004 drug-polymer mixtures with a 10^4 Pa.s melt viscosity achieved at temperatures of 130, 127, 110, 107 and 90 °C, for IRN, PTV, CoGlu, CAP and DSF respectively (Figure 5.4).

Therefore, with anticipated processing temperatures below 95 °C for PLGA 5002, the drug-polymer mixture possesses the appropriate melt viscosity properties for use in a low temperature extrusion process and thus does not require the addition of a plasticiser. However, much higher processing temperatures would be needed for PLGA 5004 and 5010 (90-130 °C for 5004 and < 180 °C for 5010) and thus the addition of a plasticiser is required to reduce their melt viscosity and provide acceptable processing temperatures.

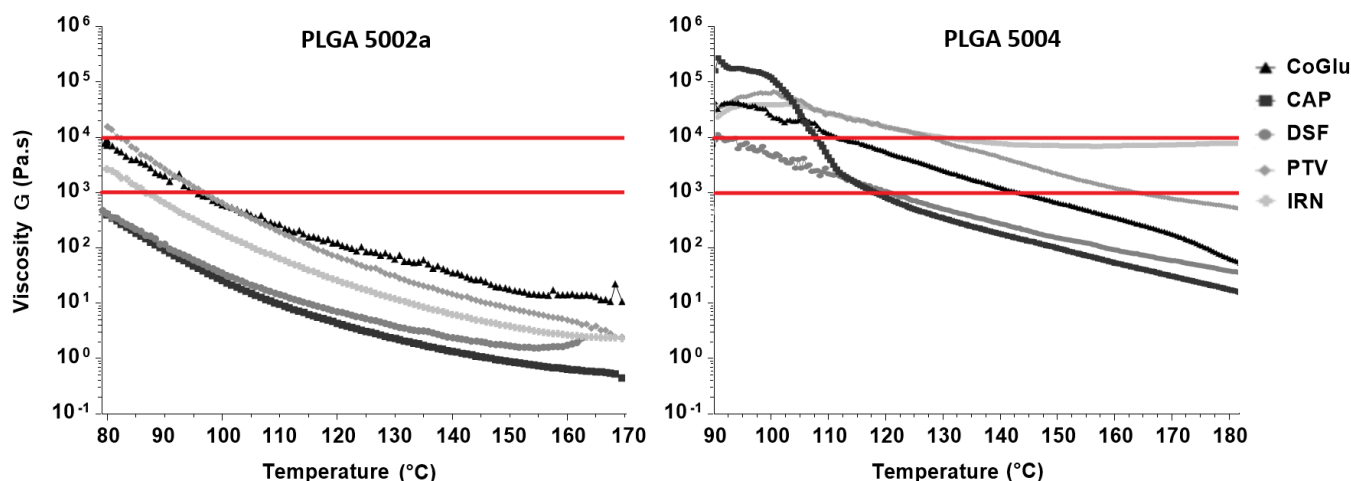


Figure 5.4: Temperature sweep data for the drug-polymer mixture at 30:70 % ratio. Drugs investigated were IRN, PTV, DSF, CAP and CoGlu, and polymers were PLGA 5002a and 5004. For the 5002 polymer the temperature sweep was performed at 80-170 °C, slightly higher temperature range, 90-180 °C, was selected for the 5004 polymer due its higher viscosity. Optimum viscosity range for extrusion (10^3 - 10^4 Pa.s) is represent by red lines.

Both 5004 and 5010 melt viscosities were investigated with the addition of plasticisers (Figure 5.5). Three plasticisers were trialled: RH40, P188 and p237 at either 10 or 30 % (w/w) and all three were proven to be sufficient at lowering the melt viscosity of 5004 and 5010 polymers with RH40 having the greatest influence. For 5004, the addition of 10% w/w plasticiser was sufficient at achieving 10^3 - 10^4 Pa.s viscosity within a relatively low temperature range of 90-120 °C (Figure 5.5). However, the addition of 10 % w/w plasticiser (w/w) to the 5010 polymer did not achieved this and at 10^4 Pa.s viscosity the corresponding temperatures were 120, 147 and 153 °C for RH40, P237 and P188, respectively (Figure 5.5). Increasing the plasticiser loading to 30% w/w improved the melt viscosity curves for the 5010 polymer, but still did not achieve the required melt viscosities for low temperature extrusion, with a 10^4 Pa.s viscosity achieved at temperatures of 105, 133 and 147 °C for RH40, P237 and P188, respectively (Figure 5.5).

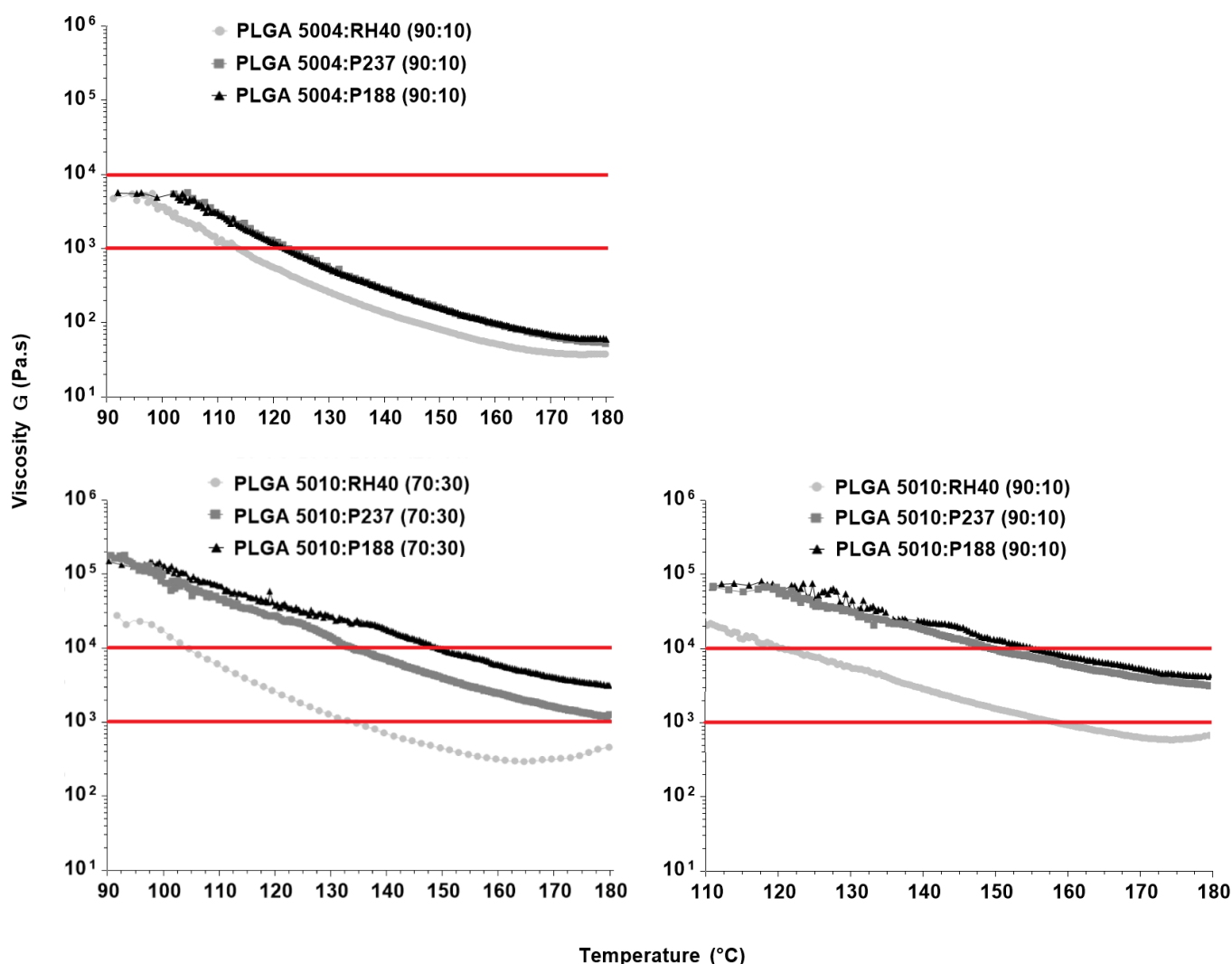


Figure 5.5: Temperature sweep data for the polymer-plasticiser mixture at different ratios. Plasticisers investigated were RH40, P188 and P237, and polymers were PLGA 5004 and 5010. For the 5004:plasticiser (90:10) and 5010:plasticiser (70:30) ratio the temperature sweep was performed at 90-180 °C, slightly higher initial temperature was selected for 5010:plasticiser (90:10) due to its higher viscosity. Optimum viscosity range for extrusion (10^3 - 10^4 Pa.s) is represent by red lines.

In order to achieve an acceptable melt viscosity within a reasonable temperature range for the 5010 polymer plasticiser loadings of >30% would be required. Such loadings may greatly affect the biocompatibility and drug release profile of an implantable device, and would thus require a more rigid safety testing to be accepted for use in a pharmaceutical product by the regulatory authority [420]. Because of this the 5010 polymer was phased out from any further development. Additionally, the melt viscosity data has shown that all three

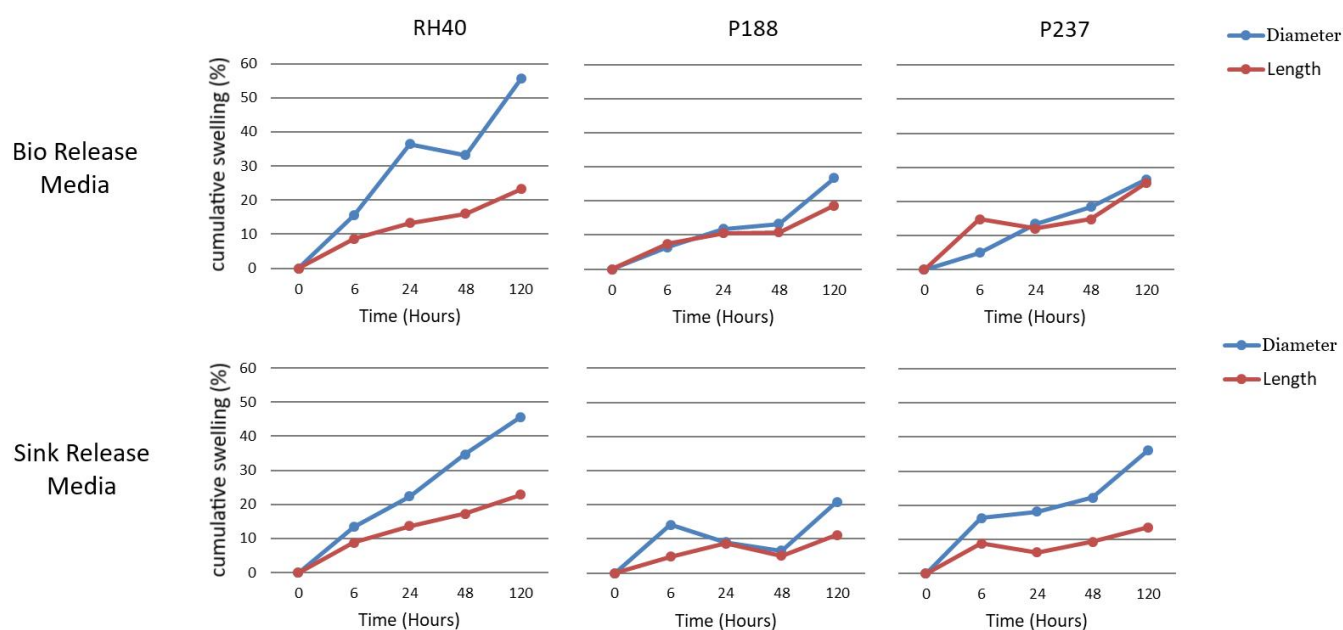
plasticisers, RH40, P237 and P188 were suitable for lowering the melt viscosity profile of 50/50 PLGA polymers.

5.4.2 Influence of plasticiser type and loading on the swelling of the implants

The use of plasticisers within a drug delivery device have previously been linked to increased swelling and for brain tumour this may contribute to cerebral oedema [421-423]. Therefore, to ensure that the developed drug delivery device is safe, a swelling study was performed where the IRN-CAP-DSF and IRN-PTV-DSF-CoGlu combination implants were placed in release media and their dimensions recorded over a 5 day incubation period (120 hours). Following 5 days of incubation both the IRN-CAP-DSF and IRN-PTV-DSF-CoGlu combination implants containing the RH40 plasticiser increased in length and diameter by 50% and 20 %, respectively (Figure 5.6). For P188 plasticiser, the implants size increased by 7 and 28 % in diameter and length, respectively, whilst for the P237 implants the size increased by 9 and 40 %, respectively (Figure 5.6).

Therefore, although the swelling of implants is inevitable and was observed across all formulations, the implants produced from p188 plasticiser demonstrated the least swelling as only a small change in size was recorded following a 5 day incubation period. Hence P188 plasticiser was selected for use in the implants.

Three Layer Drug Implant IRN-CAP-DSF



Four Layer Drug Implant IRN-PTV-DSF-CoGlu

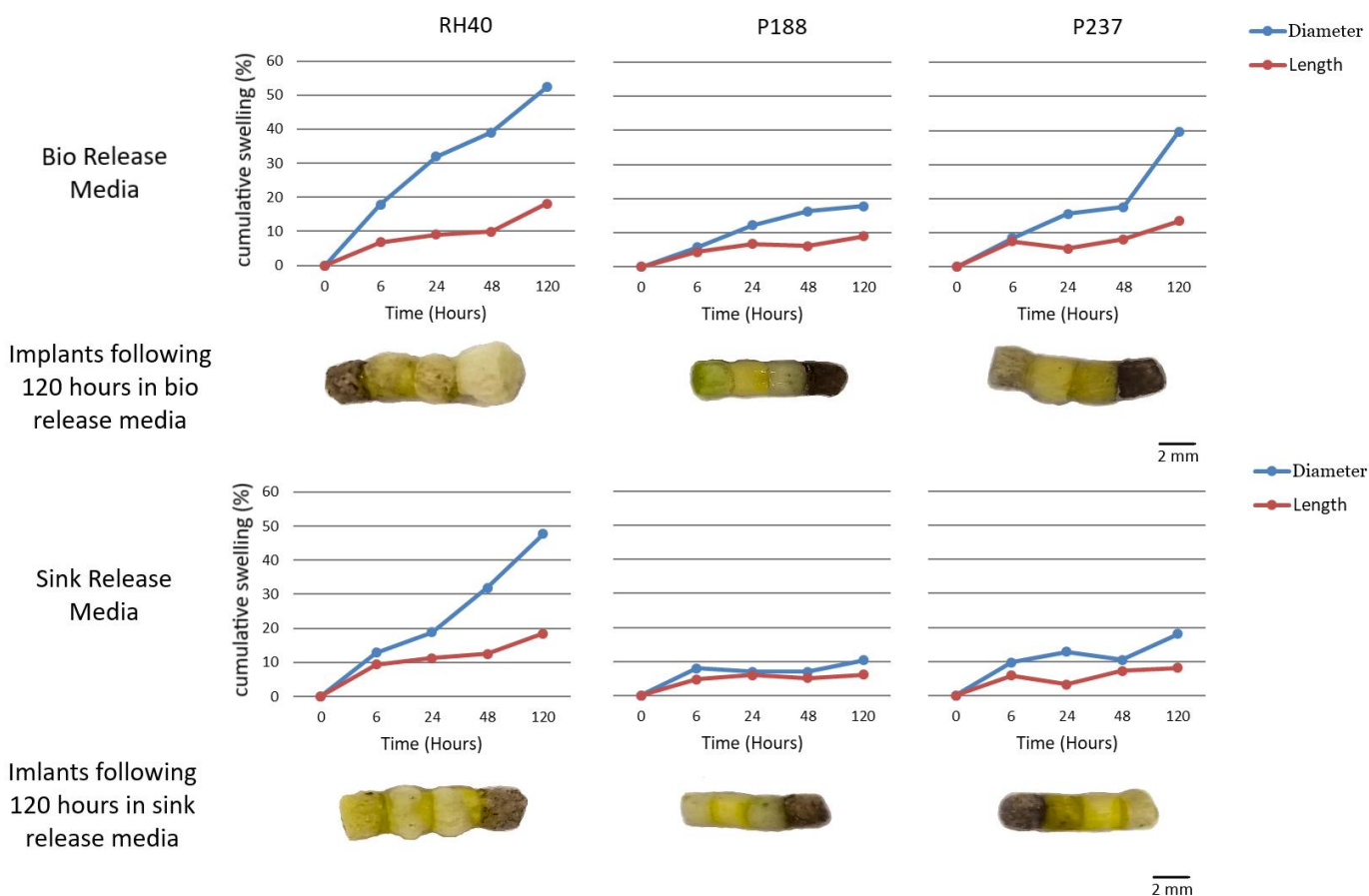


Figure 5.6: Swelling profile of IRN-PTV-DSF-CoGlu and IRN-CAP-DSF drug combination implants made from 5004 polymer and either RH40, P188 or P237 plasticiser.

5.4.3 Thermal stability during manufacture

Drug stability at manufacture temperature

A thermal stability HPLC analysis was performed to assess the effects of high processing temperatures on the stability of IRN, PTV, CAP and DSF at 120, 120, 120 and 80 °C respectively. HPLC analysis revealed no change in mass, with the recovery data for all drugs at 100% \pm 3 % RSD (Figure 5.7).

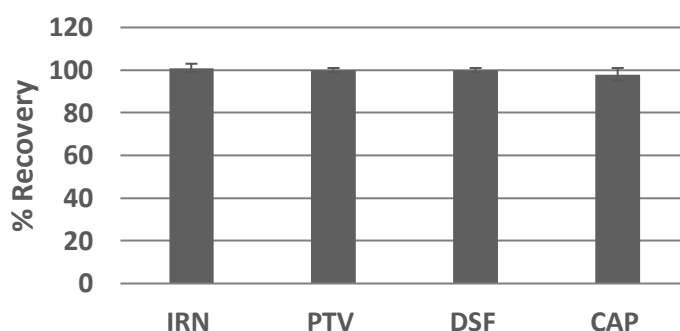


Figure 5.7: Thermal stability % recovery data for IRN, PTV, DSF and CAP. n=4, \pm %RSD is indicated as error bars.

Crystallinity profile of formulation using DSC

To determine the appropriate processing temperature range a DSC study was performed on each drug and excipients individually as well as in combination to ensure that there are no interactions between the drug and excipients. Peak shifts were used as a measure for drug-excipient interactions. Peak intensity was not assessed due to the likely variation in homogeneity, as although a larger 500 mg drug-excipient batch mixture was produced to minimise this variation, the polymer powder used was coarse and led to immediate loss of homogeneity during the re-weighing of the small amount required for assay (5-10 mg).

Both PLGA 5002A and 5004 thermograms exhibited an endothermic glass transition peak at 42 °C (Figure 5.8, A). No other peaks were observed during both the heating and cooling runs. Therefore, both samples were demonstrated to be completely amorphous as no crystallisation and melting peaks were observed. The P188 thermogram has an endothermic melting peak at 55 °C during heating, while during the cooling run, an exothermic crystallisation peak is observed at 30 °C, demonstrating that there was sufficient time for the material to crystallise (Figure 5.8, A). For IRN a broad endothermic peak was observed at

123 °C corresponding to its crystal form phase transition (Figure 5.8, B). However, with the physical mixture of IRN and excipients this peak has shifted to 86 and 73 °C for IRN-5004-P188 and IRN-5002a mixtures, respectively (Figure 5.8, B). This is attributed to the solid state interaction of IRN with PLGA during the heating process, transitioning IRN from the crystal state to amorphous state. To evaluate this further, the DSC of formulated IRN implants were also analysed and this peak was not detected in the thermogram indicating the complete disappearance of the IRN crystal form. A similar outcome has previously been reported with irinotecan's metabolic product, SN-38 demonstrating that when mixed with PLGA a phase transition from the crystal to amorphous form occurs [424]. Additionally, within the IRN-excipients mixtures both of the PLGA glass transition peaks and the P188 melting peak were detected at the exact same temperature positions (Figure 5.8, B). If there was an interaction between IRN and either PLGA or P188, these peaks would also have shifted. The thermogram of PTV pure drug revealed no phase transition peaks demonstrating that the drug is in its amorphous form (Figure 5.8, B). The thermograms of PTV and excipient mixtures shows only PLGA and P188 endothermic phase transition peaks, demonstrating that the drug has not lost its properties and does not show any type of interactions with the excipients. For the other drugs; DSF, CAP and CoGlu, the thermograms of pure drugs all show a phase transition melting peak at 74, 108 and 172 °C, respectively, which are all in line with their melting points from the literature (Figure 5.8, B) [171, 179, 181]. When mixed with the excipients, the aforementioned phase transition peaks were detected for each drug, with no peak shifts observed, confirming that there were no interactions with the excipients (Figure 5.8, B).

To conclude only IRN was shown to have a peak shift. This is due to it dissolving in the PLGA as a result of the PLGA melting and thus forming an amorphous solid solution. This type of scenario is quite prevalent for drug and polymer molecular mixtures [425]. The formation of a solid solution is likely to result in a faster dissolution rate of IRN, which can be controlled, if need be, via adjusting drug-loading in the formulation [426]. Furthermore,

amorphous drug forms are high energy solids and tend to recrystallize, which can be assessed via an accelerated stability study.

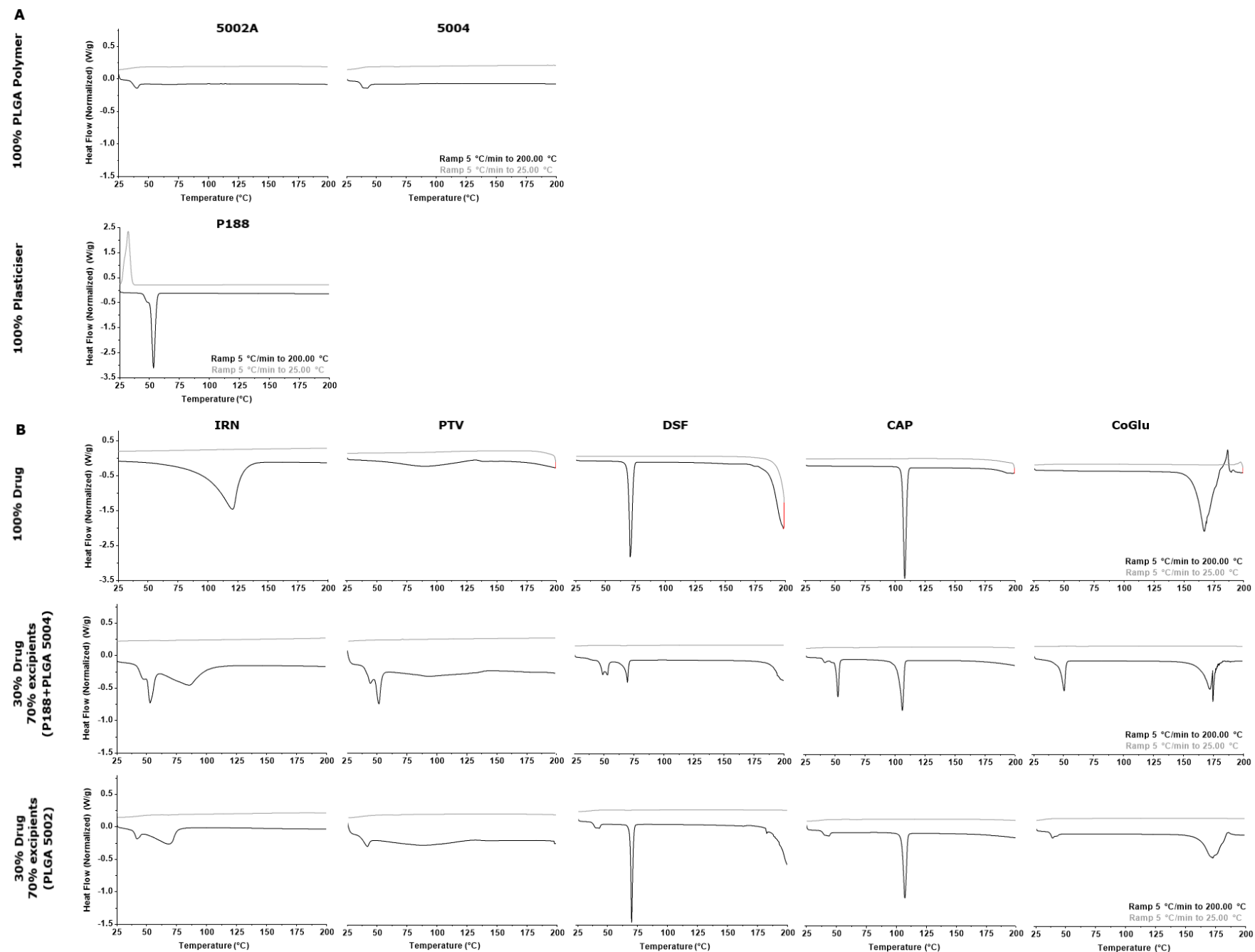


Figure 5.8: DSC diagram of (A) All excipients tested individually: PLGA 5002A, PLGA 5004 and P188 Plasticisers (B) Drug product tested three times; as pure compound (100% drug), drug in combination with p188 and PLGA 5004 (Drug:P188:PLGA 5004, 30:20:50%) and drug in combination with PLGA 5002 (Drug:5002A 30:70%).

5.4.4 Micro-extrusion and characterisation of implants

Uniformity of size and mass

IRN-PTV-DSF-CoGlu and IRN-CAP-DSF drug combination delivery devices were

manufactured from two different formulations, either with PLGA5002a or PLGA5004+P188.

To assess the reliability of the manufacturing process, size, weight and content analysis were performed. Uniformity of size measurements (diameter and length) for the individual drug-loaded layers reveals that they were consistent in size with a ± 10 % deviation. The weight of the individual layers is also shown to be consistent with PTV:PLGA5002a showing the highest degree of variation, with a %RSD value of 14 % (Table 5.3).

Table 5.3: Mass distribution data for the individual drug 2x2mm implants

30:70 Drug:PLGA5004+P188					
	IRN	PTV	DSF	CoGlu	CAP
Average (n=20) 2x2mm implant mass (mg)	8.36	7.95	7.47	9.23	7.66
RSD	0.83	0.49	0.65	0.81	0.87
% RSD	9.95	6.16	8.75	8.78	11.41
30:70 Drug:PLGA5002					
	IRN	PTV	DSF	CoGlu	CAP
Average (n=20) 2x2mm implant mass (mg)	9.56	8.45	8.27	9.09	9.23
RSD	1.18	1.20	0.81	0.83	0.58
% RSD	12.36	14.19	9.75	9.11	6.33

Uniformity of drug content

Four of the drugs, IRN, PTV, DSF and CAP, were measured for content uniformity within both the IRN-PTV-DSF-CoGlu and IRN-CAP-DSF implants. The content of CoGlu wasn't investigated as it cannot be detected via DAD/HPLC assay.

Both IRN-PTV-DSF-CoGlu implants demonstrated good content uniformity for IRN and PTV, with results between 94-112 % and % RSD values below 20 % across (Table 5.4).

However, for DSF the content was poor, measuring less than 35 % and for the PLGA5004+P188 formulation, the % RSD value was 60 %, demonstrating poor content uniformity between the different implants (Table 5.4). This low DSF content was predictable,

as it undergoes a known chelation reaction with CoGlu to form the DDC_Cu complex, this reaction is relatively quick and occur in solution during drug extraction [233]. This was confirmed during HPLC analysis of DSF, with 0.1-0.4 mg of DDC_Cu detected. Moreover, the content analysis for single DSF implants produced from the same batch were performed and results show significantly higher DSF drug content, > 90 % with % RSD values below 25 % for both formulations (Table 5.4).

For both IRN-CAP-DSF implants content uniformity was good, with contents between 80-120 % and % RSD values below 25 % across, except for CAP:PLGA5002a where the % RSD value was high, measuring at 50 %, demonstrating poor content uniformity (Table 5.4).

Table 5.4: Drug content, RSD and % RSD values for each drug within IRN-PTV-DSF-CoGlu, IRN-CAP-DSF and DSF only drug delivery devices.

IRN-PTV-DSF-CoGlu combination						
	30:70 Drug:PLGA5004+P188			30:70 Drug:PLGA5002a		
	IRN	PTV	DSF	IRN	PTV	DSF
Drug Content (%) (n=6)	112.38	93.56	19.60	110.23	94.13	34.93
RSD	17.80	13.48	11.73	4.94	15.16	3.90
% RSD	15.84	14.41	59.87	4.49	16.10	11.16
IRN-CAP-DSF combination						
	30:70 Drug:PLGA5004+P188			30:70 Drug:PLGA5002a		
	IRN	CAP	DSF	IRN	CAP	DSF
Drug Content (%) (n=6)	119.93	93.27	80.70	106.14	94.16	80.54
RSD	13.97	17.29	9.25	8.45	46.90	18.82
% RSD	11.65	18.53	11.60	7.96	49.81	23.66
DSF Single drug						
	30:70 Drug:PLGA5004+P188			30:70 Drug:PLGA5002a		
	DSF			DSF		
Drug Content (%) (n=6)	94.99			94.13		
RSD	12.48			22.68		
% RSD	13.14			24.10		

Overall the uniformity of size and mass was acceptable across all individual drug implants. The content uniformity for the implants varied depending of the formulation. IRN and PTV had good content uniformity across both combinations and formulations. For DSF the data was varied, within the IRN-PTV-DSF-CoGlu implant, the content uniformity for DSF was poor due its interactions with CoGlu, whereas when DSF was measured within IRN-CAP-

DSF combination or as a single drug layer the content uniformity was good. Finally, with CAP good content values were measured, but the content uniformity within the 5002a formulation was poor with a % RSD value above 50 %.

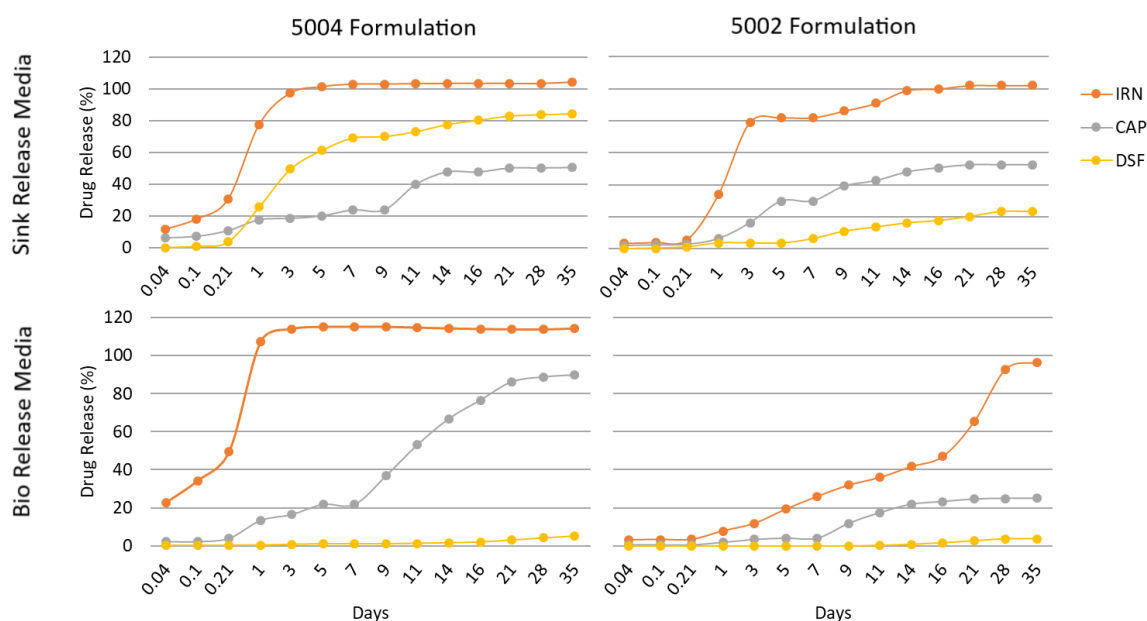
In-vitro drug release

The dissolution profile of IRN-CAP-DSF and IRN-PTV-DSF-CoGlu drug combination implants, formulated using two different PLGA polymers; 5004 and 5002a were assessed. Figure 5.9 shows the release profiles of IRN, PTV, CAP and DSF from both the 3 layer and 4 layer implants with two different PLGAs and into two different (biorelevant and sink conditioned) dissolution medias. For the IRN released from the 5004 formulation, an initial burst release was obtained and by day one 80 % of IRN was released under both sink and biorelevant release conditions. In comparison the IRN from the 5002a formulation demonstrated a more sustained release with a plateau reached by week 2 and 4 for both sink and biorelevant release, respectively. CAP demonstrated a controlled release across both formulations and dissolution media. However, under biorelevant conditions the rate of release varied between the two formulations, as following 35 days of dissolution, the 5004 formulation attained 90 % release whereas only 23 % was released from the 5002a. Under sink condition there was no variation in CAP release between the two formulations with both reaching a plateau at between 50-55 %. For DSF, little or no release was demonstrated under biorelevant condition, with the exception for the four layer 5002a implant which released 38 %. Additionally, for the four layer drug implant under biorelevant condition, less than 6×10^{-3} mg of DDC_Cu was formed, demonstrating almost no DSF+ CoGlu reaction taking place which is likely because DSF was not releasing and dissolving in the biorelevant media. However, under sink condition, DSF demonstrated a controlled and steady release across both formulations with the 5004 achieving 82 and 62 % of DSF release for the three and four layer combination implant, respectively. While for the 5002a, 21-22 % of DSF was released across both drug combinations. Additionally, for the four layer drug combination, 0.05 and 0.5 mg of DDC_Cu was released alongside DSF for the 5004 and 5002a formulations, respectively. PTV achieved fast drug release for the 5004 formulation reaching

a plateau following 1 and 7 days for both the sink and biorelevant conditions, respectively. A much slower PTV release was achieved with the 5002a formulation, with a plateau reached following 3 weeks.

Overall the implants produced using the 5004 PLGA polymer achieved much faster drug release rates than 5002a. As an initial dissolution study, this data clearly demonstrates that the release rate of each drug can be optimised to the desired profile via adjusting the polymer matrix. For instance, for the three layer drug implant, if a simultaneous release of IRN, CAP and DSF over the course of 3 weeks is desired then to achieve this IRN can be formulated with PLGA 5002a, whereas DSF and CAP would be formulated using the 5004 PLGA.

Three layer drug implant IRN-CAP-DSF



Four layer drug implant IRN-PTV-DSF-CoGlu

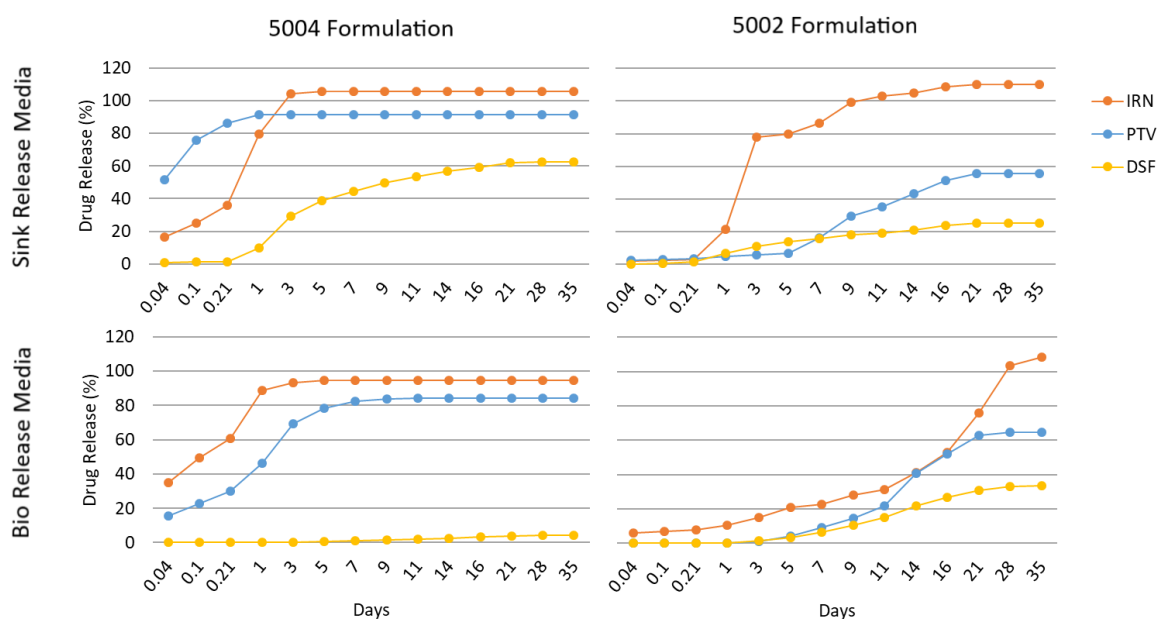


Figure 5.9: Simultaneous drug dissolution profiles of IRN, PTV, CAP and DSF within three (IRN-CAP-DSF) or four (IRN-PTV-DSF-CoGlu) layer combination drug implant. The dissolution profiles of two distinct formulations: 5004 and 5002 were tested under both sink and biorelevant conditions.

5.6 Conclusion

In this study, the selection of formulation composition and implant manufacturing processes were evaluated. Based on rheology, swelling and thermal stability data, two formulations for IRN-PTV-DSF-CoGlu and IRN-CAP-DSF combination implants were evaluated. Each implant was characterised for drug content and in vitro release with the data revealing good

content uniformity (+/- 20 %) and sustained drug release. More importantly this data provides a good starting point for the development of an implantable device capable of the delivery of multiple drugs at independent release rates. Furthermore, the release of each drug can be tailored based on the choice of PLGA.

6. CHAPTER SIX: CONCLUSION

Detailed conclusions were written at the end of each chapter. This conclusion chapter presents the overall outcome of the thesis and future progress ideas.

Starting from chapter two, the work initially explored whether currently FDA approved drugs used for the treatment of other diseases would be effective against glioma tumours. Eight mono-therapeutic drug treatments were tested against human derived tumour cells: IRN, PTV, DSF, CoGlu, CAP, CXB, TCL, ITZ. At $\leq 100 \mu\text{M}$ dose most of those drugs were proven to be more effective than the current chemotherapeutic treatment, TMZ. We then questioned if the same repurposed drugs in combination would be even more effective against glioma cancer, by targeting multiple cancer growth promoting pathways simultaneously. The data from chapter three testing this theory was very positive, with two of the tested combination drug treatments, IRN-PTV-DSF-CoGlu and IRN-CAP-DSF proven to be highly effective across most patients samples and at low dose (630 nM). The work presented in this thesis then followed to develop those two combination drug treatments into an implantable drug delivery device. In chapter four two analytical HPLC techniques capable of separating, detecting and quantifying IRN-PTV-DSF-DDC_Cu and IRN-CAP-DSF drug combinations were developed and validated. These methods were then used in part to develop IRN-PTV-DSF-CoGlu and IRN-CAP-DSF combination drug treatments into a suitable formulation. In chapter five an implantable drug delivery device was developed from material that is: FDA approved, biodegradable in physiological environment without inducing adverse reactions, can be easily manufactured by common techniques (such as extrusion) and capable of delivering the combination drug treatment at sustained-release rate. The drug delivery device composed of multilayer segments with each segment composed of therapeutic agent incorporated homogenously within either a 5002a PLGA polymer or 5004 PLGA polymer plus p188 plasticiser matrix.

For the future translation of this novel combination drug delivery device from the laboratory to the clinic we will describe some of the work done so far which can either be optimised or advanced further:

- 1- In this study equal molar ratios of the IRN-PTV-DSF-CoGlu and IRN-CAP-DSF combination drug treatments were investigated against human derived glioma cells. A future dose profiling of the combinations using box-behnken design of experiment approach could investigate if there is an optimum therapeutic molar ratio. This study could lead to further reduction in dosage requirement for some drugs.
- 2- To investigate the formulated multidrug delivery device effectiveness against glioma, 3D *in-vitro* cell culture as well as *in-vivo* patient derived xenograft (PDX) mouse models could be utilised to replicate the complex biology and heterogeneity of glioma. Allowing to evaluate the multidrug delivery device for safety and efficacy in a highly representative clinical model.
- 3- Two HPLC analytical techniques for IRN-PTV-DSF-DDC_Cu and IRN-CAP-DSF drug combinations were developed. While the single injection analytical method is very good as it is, it could benefit from testing whether lower acetic acid mobile phase content could achieve equivalent specificity, linearity, accuracy, precision data. This is because DSF molecule is known to be more stable at intermediate pH values so it could be worthwhile to refine the method slightly particularly for use in future forced degradation and long-term stability testing of drug delivery device [427]. Furthermore, the developed HPLC method could not detect CoGlu, hence a second highly selective analytical method such as atomic absorption spectrometry (AAS) or titration could be developed to quantify CoGlu within the drug delivery device.
- 4- During the *in-vitro* drug release study for IRN-PTV-DSF-CoGlu combination drug delivery device, small amount of DDC_Cu was detected due to DSF and CoGlu reacting together to form DDC_Cu. Future reaction kinetic study assessing DSF and CoGlu reaction rate under *in-vitro* test conditions could be useful to predict the maximum DDC_Cu dose reached *in-vivo*. Since both reactants and products may possess some

clinical activity, the potency and clinical effectiveness of each may vary depending on the speed at which the DSF and CoGlu reaction proceeds. To illustrate if the speed at which reactants are converted into products is slow, then the efficacy of treatment would mainly be from the DSF and CoGlu drug treatment, whereas if the reaction is quick, then the reaction process as well as DDC_Cu concentration could be the main reason for response to treatment.

- 5- In-vitro drug release testing was so far only performed at 30% drug loading, to further explore the pharmaceutical efficacy of treatment drug release testing at different drug loadings (e.g 10, 20, 30 and 40 %) could be evaluated.
- 6- A forced degradation study for each drug is needed to generate a degradation profile that mimics what would be observed in a stability study under ICH conditions.
- 7- For the formulated implantable drug delivery device accelerated stability testing (at relatively high temperatures and/or humidity) could be performed to determine the type of degradation products which may be found after long-term storage. This study could also determine the appropriate storage conditions for the drug delivery device.
- 8- A product sterilisation method such as applying gamma radiation to eliminate, remove, kills, or deactivates all forms of life (such as fungi, bacteria, viruses, spores, unicellular eukaryotic organisms such as Plasmodium, etc.) and other biological agents like prions must be developed. Additionally, radiation impact on drug stability and release characteristics must be evaluated.
- 9- So far, we have only formulated our multi-drug delivery device using a piloted small-scale manual micro-extrusion method, to properly evaluate our full product performance (e.g drug release, content uniformity and drug stability) future formulation of product using a pharmaceutical extruder is needed.

REFERENCES

1. Brodbelt A, Greenberg D, Winters T, Williams M, Vernon S, Collins VP: **Glioblastoma in England: 2007–2011**. *European Journal of Cancer* 2015, **51**(4):533-542.
2. **Glioblastoma Multiforme** [<http://www.aans.org/Patients/Neurosurgical-Conditions-and-Treatments/Glioblastoma-Multiforme>]
3. Kofman AV, Abounader R: **When tumor cells make blood vessels: implications for glioblastoma therapy**. *Future Oncology (London, England)* 2011, **7**(7):841-843.
4. Wesseling P, Capper D: **WHO 2016 Classification of gliomas**. *Neuropathology and applied neurobiology* 2018, **44**(2):139-150.
5. Pekmezci M, Rice T, Molinaro AM, Walsh KM, Decker PA, Hansen H, Sicotte H, Kollmeyer TM, McCoy LS, Sarkar G *et al*: **Adult infiltrating gliomas with WHO 2016 integrated diagnosis: additional prognostic roles of ATRX and TERT**. *Acta Neuropathologica* 2017, **133**(6):1001-1016.
6. Louis DN, Perry A, Reifenberger G, von Deimling A, Figarella-Branger D, Cavenee WK, Ohgaki H, Wiestler OD, Kleihues P, Ellison DW: **The 2016 World Health Organization Classification of Tumors of the Central Nervous System: a summary**. *Acta Neuropathologica* 2016, **131**(6):803-820.
7. Friedman GK, Spiller SE, Harrison DK, Fiveash JB, Reddy AT: **Treatment of Children With Glioblastoma With Conformal Radiation, Temozolomide, and Bevacizumab as Adjuncts to Surgical Resection**. *Journal of Pediatric Hematology/Oncology* 2013, **35**(3):e123-e126.
8. Ostrom QT, Gittleman H, Liao P, Rouse C, Chen Y, Dowling J, Wolinsky Y, Kruchko C, Barnholtz-Sloan J: **CBTRUS Statistical Report: Primary Brain and Central Nervous System Tumors Diagnosed in the United States in 2007–2011**. *Neuro-Oncology* 2014, **16**(Suppl 4):iv1-iv63.
9. Sun T, Warrington NM, Luo J, Brooks MD, Dahiya S, Snyder SC, Sengupta R, Rubin JB: **Sexually dimorphic RB inactivation underlies mesenchymal glioblastoma prevalence in males**. *The Journal of Clinical Investigation* 2014, **124**(9):4123-4133.
10. Ostrom QT, Bauchet L, Davis FG, Deltour I, Fisher JL, Langer CE, Pekmezci M, Schwartzbaum JA, Turner MC, Walsh KM *et al*: **The epidemiology of glioma in adults: a “state of the science” review**. *Neuro-Oncology* 2014, **16**(7):896-913.
11. de Andrade M, Barnholtz JS, Amos CI, Adatto P, Spencer C, Bondy ML: **Segregation analysis of cancer in families of glioma patients**. *Genetic epidemiology* 2001, **20**(2):258-270.
12. Melin BS, Barnholtz-Sloan JS, Wrensch MR, Johansen C, Il'yasova D, Kinnersley B, Ostrom QT, Labreche K, Chen Y, Armstrong G *et al*: **Genome-wide association study of glioma subtypes identifies specific differences in genetic susceptibility to glioblastoma and non-glioblastoma tumors**. *Nature genetics* 2017, **49**(5):789-794.
13. Ellor SV, Pagano-Young TA, Avgeropoulos NG: **Glioblastoma: background, standard treatment paradigms, and supportive care considerations**. *The Journal of law, medicine & ethics : a journal of the American Society of Law, Medicine & Ethics* 2014, **42**(2):171-182.
14. Weller M, van den Bent M, Hopkins K, Tonn JC, Stupp R, Falini A, Cohen-Jonathan-Moyal E, Frappaz D, Henriksson R, Balana C *et al*: **EANO guideline for the diagnosis and treatment of anaplastic gliomas and glioblastoma**. *The Lancet Oncology* 2014, **15**(9):e395-e403.
15. Altman DA, Atkinson DS, Brat DJ: **Glioblastoma Multiforme**. *RadioGraphics* 2007, **27**(3):883-888.
16. Ohgaki H, Kleihues P: **Genetic Pathways to Primary and Secondary Glioblastoma**. *The American Journal of Pathology* 2007, **170**(5):1445-1453.
17. Stupp R, Mason WP, van den Bent MJ, Weller M, Fisher B, Taphoorn MJB, Belanger K, Brandes AA, Marosi C, Bogdahn U *et al*: **Radiotherapy plus Concomitant and Adjuvant Temozolomide for Glioblastoma**. *New England Journal of Medicine* 2005, **352**(10):987-996.
18. Schapira AH: **Neurology and clinical neuroscience**; 2007.

19. J Dinnes CC, S Huang, K Major, R Milne: **The effectiveness and cost-effectiveness of temozolomide for the treatment of recurrent malignant glioma: a rapid and systematic review.** In.; 2001.
20. Wasserfallen J-B, Ostermann S, Leyvraz S, Stupp R: **Cost of temozolomide therapy and global care for recurrent malignant gliomas followed until death.** *Neuro-Oncology* 2005, **7**(2):189-195.
21. Bristol-Myers Squibb Pharmaceuticals Pty. Ltd: **Product information- Lomustine.** In.: www.medicines.org.au; 2015.
22. Merck & Co.: **Highlights of prescribing information** In. USA: www.FDA.gov; 2016.
23. Genentech: **Highlights of prescribing information** In.: www.FDA.gov; 2009.
24. Bristol-Myers Squibb Company: **Carmustine for injection.** In.: www.FDA.gov; 2007.
25. Eisai Inc: **Highlights of prescribing information** In.: www.FDA.gov; 2013.
26. NextSource Biotechnology: **Highlights of prescribing information.** In.; 2016.
27. Heritage Pharmaceuticals: **Highlights of prescribing information.** In.: FDA; 2016.
28. Parodi A, Rudzińska M, Deviatkin AA, Soond SM, Baldin AV, Zamyatnin AA, Jr.: **Established and Emerging Strategies for Drug Delivery Across the Blood-Brain Barrier in Brain Cancer.** *Pharmaceutics* 2019, **11**(5):245.
29. Smith SJ, Tyler B, Gould TWA, Veal GJ, Gorelick NL, Rowlinson J, Serra R, Ritchie AA, Berry P, Otto A *et al*: **Overall survival in malignant glioma is significantly prolonged by neurosurgical delivery of etoposide and temozolomide from a thermo-responsive biodegradable paste.** *Clinical Cancer Research* 2019:clincanres.3850.2018.
30. de Gooijer MC, de Vries NA, Buckle T, Buil LCM, Beijnen JH, Boogerd W, van Tellingen O: **Improved Brain Penetration and Antitumor Efficacy of Temozolomide by Inhibition of ABCB1 and ABCG2.** *Neoplasia* 2018, **20**(7):710-720.
31. Ostermann S, Csajka C, Buclin T, Leyvraz S, Lejeune F, Decosterd LA, Stupp R: **Plasma and cerebrospinal fluid population pharmacokinetics of temozolomide in malignant glioma patients.** *Clinical cancer research : an official journal of the American Association for Cancer Research* 2004, **10**(11):3728-3736.
32. Bower M, Newlands ES, Bleehen NM, Brada M, Begent RJ, Calvert H, Colquhoun I, Lewis P, Brampton MH: **Multicentre CRC phase II trial of temozolomide in recurrent or progressive high-grade glioma.** *Cancer Chemother Pharmacol* 1997, **40**(6):484-488.
33. Bae SH, Park M-J, Lee MM, Kim TM, Lee S-H, Cho SY, Kim Y-H, Kim YJ, Park C-K, Kim C-Y: **Toxicity Profile of Temozolomide in the Treatment of 300 Malignant Glioma Patients in Korea.** *Journal of Korean Medical Science* 2014, **29**(7):980-984.
34. Portnow J, Badie B, Chen M, Liu A, Blanchard S, Synold TW: **THE NEUROPHARMACOKINETICS OF TEMOZOLOMIDE IN PATIENTS WITH RESECTABLE BRAIN TUMORS: POTENTIAL IMPLICATIONS FOR THE CURRENT APPROACH TO CHEMORADIATION.** *Clinical cancer research : an official journal of the American Association for Cancer Research* 2009, **15**(22):7092-7098.
35. Jain RK: **Normalizing tumor vasculature with anti-angiogenic therapy: a new paradigm for combination therapy.** *Nat Med* 2001, **7**(9):987-989.
36. Carmeliet P, Ferreira V, Breier G, Pollefeyt S, Kieckens L, Gertsenstein M, Fahrig M, Vandenhoek A, Harpal K, Eberhardt C *et al*: **Abnormal blood vessel development and lethality in embryos lacking a single VEGF allele.** *Nature* 1996, **380**(6573):435-439.
37. Oku T, Tjuvajev JG, Miyagawa T, Sasajima T, Joshi A, Joshi R, Finn R, Claffey KP, Blasberg RG: **Tumor growth modulation by sense and antisense vascular endothelial growth factor gene expression: effects on angiogenesis, vascular permeability, blood volume, blood flow, fluorodeoxyglucose uptake, and proliferation of human melanoma intracerebral xenografts.** *Cancer research* 1998, **58**(18):4185-4192.
38. Xu C, Wu X, Zhu J: **VEGF Promotes Proliferation of Human Glioblastoma Multiforme Stem-Like Cells through VEGF Receptor 2.** *The Scientific World Journal* 2013, **2013**:8.

39. Presta LG, Chen H, O'Connor SJ, Chisholm V, Meng YG, Krummen L, Winkler M, Ferrara N: **Humanization of an anti-vascular endothelial growth factor monoclonal antibody for the therapy of solid tumors and other disorders.** *Cancer research* 1997, **57**(20):4593-4599.
40. Ferrara N, Hillan KJ, Gerber H-P, Novotny W: **Discovery and development of bevacizumab, an anti-VEGF antibody for treating cancer.** *Nature Reviews Drug Discovery* 2004, **3**:391.
41. Friedman HS, Prados MD, Wen PY, Mikkelsen T, Schiff D, Abrey LE, Yung WK, Paleologos N, Nicholas MK, Jensen R *et al*: **Bevacizumab alone and in combination with irinotecan in recurrent glioblastoma.** *Journal of clinical oncology : official journal of the American Society of Clinical Oncology* 2009, **27**(28):4733-4740.
42. Wenger KJ, Wagner M, You S-J, Franz K, Harter PN, Burger MC, Voss M, Ronellenfitsch MW, Fokas E, Steinbach JP *et al*: **Bevacizumab as a last-line treatment for glioblastoma following failure of radiotherapy, temozolomide and lomustine.** *Oncology Letters* 2017, **14**(1):1141-1146.
43. Narita Y: **Bevacizumab for glioblastoma.** *Therapeutics and Clinical Risk Management* 2015, **11**:1759-1765.
44. Cohen MH, Shen YL, Keegan P, Pazdur R: **FDA drug approval summary: bevacizumab (Avastin) as treatment of recurrent glioblastoma multiforme.** *Oncologist* 2009, **14**(11):1131-1138.
45. Gilbert MR, Dignam JJ, Armstrong TS, Wefel JS, Blumenthal DT, Vogelbaum MA, Colman H, Chakravarti A, Pugh S, Won M *et al*: **A Randomized Trial of Bevacizumab for Newly Diagnosed Glioblastoma.** *New England Journal of Medicine* 2014, **370**(8):699-708.
46. Macdonald DR, Cascino TL, Schold SC, Cairncross JG: **Response criteria for phase II studies of supratentorial malignant glioma.** *Journal of Clinical Oncology* 1990, **8**(7):1277-1280.
47. Chamberlain MC: **Bevacizumab for the treatment of recurrent glioblastoma.** *Clinical Medicine Insights Oncology* 2011, **5**:117-129.
48. Levin VA, Wilson CB: **Nitrosourea chemotherapy for primary malignant gliomas.** *Cancer treatment reports* 1976, **60**(6):719-724.
49. Shapiro WR, Young DF: **Chemotherapy of malignant glioma with CCNU alone and CCNU combined with vincristine sulfate and procarbazine hydrochloride.** *Transactions of the American Neurological Association* 1976, **101**:217-220.
50. Batchelor TT, Mulholland P, Neyns B, Nabors LB, Campone M, Wick A, Mason W, Mikkelsen T, Phuphanich S, Ashby LS *et al*: **Phase III randomized trial comparing the efficacy of cediranib as monotherapy, and in combination with lomustine, versus lomustine alone in patients with recurrent glioblastoma.** *Journal of clinical oncology : official journal of the American Society of Clinical Oncology* 2013, **31**(26):3212-3218.
51. Taal W, Oosterkamp HM, Walenkamp AME, Dubbink HJ, Beerepoot LV, Hanse MCJ, Buter J, Honkoop AH, Boerman D, de Vos FYF *et al*: **Single-agent bevacizumab or lomustine versus a combination of bevacizumab plus lomustine in patients with recurrent glioblastoma (BELOB trial): a randomised controlled phase 2 trial.** *The Lancet Oncology* 2014, **15**(9):943-953.
52. Nikolova T, Roos WP, Krämer OH, Strik HM, Kaina B: **Chloroethylating nitrosoureas in cancer therapy: DNA damage, repair and cell death signaling.** *Biochimica et Biophysica Acta (BBA) - Reviews on Cancer* 2017, **1868**(1):29-39.
53. Heiland DH, Masalha W, Franco P, Machein MR, Weyerbrock A: **Progression-free and overall survival in patients with recurrent Glioblastoma multiforme treated with last-line bevacizumab versus bevacizumab/lomustine.** *Journal of Neuro-Oncology* 2016, **126**(3):567-575.
54. Bartzatt R: **Lomustine analogous drug structures for intervention of brain and spinal cord tumors: the benefit of in silico substructure search and analysis.** *Chemotherapy research and practice* 2013, **2013**:360624-360624.

55. Gerson SL, Caimi PF, William BM, Creger RJ: **Chapter 57 - Pharmacology and Molecular Mechanisms of Antineoplastic Agents for Hematologic Malignancies**. In: *Hematology (Seventh Edition)*. Edited by Hoffman R, Benz EJ, Silberstein LE, Heslop HE, Weitz JI, Anastasi J, Salama ME, Abutalib SA: Elsevier; 2018: 849-912.
56. Woolley PV, Dion RL, Kohn KW, Bono VH: **Binding of 1-(2-chloroethyl)-3-cyclohexyl-1-nitrosourea to L1210 cell nuclear proteins**. *Cancer research* 1976, **36**(4):1470-1474.
57. Kohn KW: **Interstrand cross-linking of DNA by 1,3-bis(2-chloroethyl)-1-nitrosourea and other 1-(2-haloethyl)-1-nitrosoureas**. *Cancer research* 1977, **37**(5):1450-1454.
58. Kann HE, Jr.: **Comparison of biochemical and biological effects of four nitrosoureas with differing carbamoylating activities**. *Cancer research* 1978, **38**(8):2363-2366.
59. Bota DA, Desjardins A, Quinn JA, Affronti ML, Friedman HS: **Interstitial chemotherapy with biodegradable BCNU (Gliadel®) wafers in the treatment of malignant gliomas**. *Therapeutics and Clinical Risk Management* 2007, **3**(5):707-715.
60. Ramirez YP, Weatherbee JL, Wheelhouse RT, Ross AH: **Glioblastoma multiforme therapy and mechanisms of resistance**. *Pharmaceuticals (Basel, Switzerland)* 2013, **6**(12):1475-1506.
61. Gerson SL: **Clinical relevance of MGMT in the treatment of cancer**. *Journal of clinical oncology : official journal of the American Society of Clinical Oncology* 2002, **20**(9):2388-2399.
62. Dobson JM, Hohenhaus AE, Peaston AE: **Chapter 15 - Cancer chemotherapy**. In: *Small Animal Clinical Pharmacology (Second Edition)*. Edited by Maddison JE, Page SW, Church DB. Edinburgh: W.B. Saunders; 2008: 330-366.
63. Attenello F, Raza SM, Dimeco F, Olivi A: **Chapter 22 - Chemotherapy for brain tumors with polymer drug delivery**. In: *Handbook of Clinical Neurology*. Edited by Aminoff MJ, Boller F, Swaab DF, vol. 104: Elsevier; 2012: 339-353.
64. Wait SD, Prabhu RS, Burri SH, Atkins TG, Asher AL: **Polymeric drug delivery for the treatment of glioblastoma**. *Neuro Oncol* 2015, **17** Suppl 2:ii9-ii23.
65. Fleming AB, Saltzman WM: **Pharmacokinetics of the carmustine implant**. *Clin Pharmacokinet* 2002, **41**(6):403-419.
66. Ashby LS, Smith KA, Stea B: **Gliadel wafer implantation combined with standard radiotherapy and concurrent followed by adjuvant temozolomide for treatment of newly diagnosed high-grade glioma: a systematic literature review**. *World Journal of Surgical Oncology* 2016, **14**:15.
67. Westphal M, Hilt DC, Bortey E, Delavault P, Olivares R, Warnke PC, Whittle IR, Jääskeläinen J, Ram Z: **A phase 3 trial of local chemotherapy with biodegradable carmustine (BCNU) wafers (Gliadel wafers) in patients with primary malignant glioma**. *Neuro-Oncology* 2003, **5**(2):79-88.
68. Westphal M, Ram Z, Riddle V, Hilt D, Bortey E: **Gliadel wafer in initial surgery for malignant glioma: long-term follow-up of a multicenter controlled trial**. *Acta neurochirurgica* 2006, **148**(3):269-275; discussion 275.
69. Valtonen S, Timonen U, Toivanen P, Kalimo H, Kivipelto L, Heiskanen O, Unsgaard G, Kuurne T: **Interstitial chemotherapy with carmustine-loaded polymers for high-grade gliomas: a randomized double-blind study**. *Neurosurgery* 1997, **41**(1):44-48; discussion 48-49.
70. Lee M, Desai A: **Gibaldi's Drug Delivery Systems in Pharmaceutical Care**: American society of health system pharmacists; 2007.
71. Hart MG, Garside R, Rogers G, Somerville M, Stein K, Grant R: **Chemotherapy wafers for high grade glioma**. *Cochrane Database of Systematic Reviews* 2011(3).
72. Sathornsumetee S, Desjardins A, Vredenburgh JJ, McLendon RE, Marcello J, Herndon JE, Mathe A, Hamilton M, Rich JN, Norfleet JA et al: **Phase II trial of bevacizumab and erlotinib in patients with recurrent malignant glioma**. *Neuro-Oncology* 2010, **12**(12):1300-1310.

73. Peschillo S, Caporlingua A, Diana F, Caporlingua F, Delfini R: **New therapeutic strategies regarding endovascular treatment of glioblastoma, the role of the blood–brain barrier and new ways to bypass it.** *Journal of NeuroInterventional Surgery* 2016, **8**(10):1078.
74. Weidle UH, Niewohner J, Tiefenthaler G: **The Blood-Brain Barrier Challenge for the Treatment of Brain Cancer, Secondary Brain Metastases, and Neurological Diseases.** *Cancer genomics & proteomics* 2015, **12**(4):167-177.
75. Pardridge WM: **Drug and gene targeting to the brain with molecular Trojan horses.** *Nature reviews Drug discovery* 2002, **1**(2):131-139.
76. Hendricks BK, Cohen-Gadol AA, Miller JC: **Novel delivery methods bypassing the blood-brain and blood-tumor barriers.** *Neurosurgical focus* 2015, **38**(3):E10.
77. Reith MEA: **Handbook of Neurochemistry and Molecular Neurobiology: Neural Membranes and Transport**, vol. 3. New York, USA: Springer; 2007.
78. Arvanitis CD, Ferraro GB, Jain RK: **The blood–brain barrier and blood–tumour barrier in brain tumours and metastases.** *Nature Reviews Cancer* 2020, **20**(1):26-41.
79. Sarkaria JN, Hu LS, Parney IF, Pafundi DH, Brinkmann DH, Laack NN, Giannini C, Burns TC, Kizilbash SH, Laramy JK *et al*: **Is the blood-brain barrier really disrupted in all glioblastomas? A critical assessment of existing clinical data.** *Neuro-oncology* 2018, **20**(2):184-191.
80. Karim R, Palazzo C, Evrard B, Piel G: **Nanocarriers for the treatment of glioblastoma multiforme: Current state-of-the-art.** *J Control Release* 2016, **227**:23-37.
81. Bastiancich C, Danhier P, Preat V, Danhier F: **Anticancer drug-loaded hydrogels as drug delivery systems for the local treatment of glioblastoma.** *J Control Release* 2016, **243**:29-42.
82. Vogelbaum MA, Aghi MK: **Convection-enhanced delivery for the treatment of glioblastoma.** *Neuro-Oncology* 2015, **17**(suppl_2):ii3-ii8.
83. Zhou J, Atsina K-B, Himes BT, Strohhahn GW, Saltzman WM: **Novel Delivery Strategies for Glioblastoma.** *Cancer journal (Sudbury, Mass)* 2012, **18**(1):10.1097/PPO.1090b1013e318244d318248ae.
84. Burgess A, Shah K, Hough O, Hynynen K: **Focused ultrasound-mediated drug delivery through the blood–brain barrier.** *Expert Review of Neurotherapeutics* 2015, **15**(5):477-491.
85. Vera M, Barcia E, Negro S, Marcianes P, García-García L, Slowing K, Fernández-Carballido A: **New celecoxib multiparticulate systems to improve glioblastoma treatment.** *International Journal of Pharmaceutics* 2014, **473**(1):518-527.
86. Steiniger SCJ, Kreuter J, Khalansky AS, Skidan IN, Bobruskin AI, Smirnova ZS, Severin SE, Uhl R, Kock M, Geiger KD *et al*: **Chemotherapy of glioblastoma in rats using doxorubicin-loaded nanoparticles.** *International journal of cancer* 2004, **109**(5):759-767.
87. Xin H, Sha X, Jiang X, Zhang W, Chen L, Fang X: **Anti-glioblastoma efficacy and safety of paclitaxel-loading Angiopep-conjugated dual targeting PEG-PCL nanoparticles.** *Biomaterials* 2012, **33**(32):8167-8176.
88. Hadjipanayis CG, Machaidze R, Kaluzova M, Wang L, Schuette AJ, Chen H, Wu X, Mao H: **EGFRvIII Antibody–Conjugated Iron Oxide Nanoparticles for Magnetic Resonance Imaging–Guided Convection-Enhanced Delivery and Targeted Therapy of Glioblastoma.** *Cancer research* 2010, **70**(15):6303-6312.
89. Gelperina SE, Khalansky AS, Skidan IN, Smirnova ZS, Bobruskin AI, Severin SE, Turowski B, Zanella FE, Kreuter J: **Toxicological studies of doxorubicin bound to polysorbate 80-coated poly(butyl cyanoacrylate) nanoparticles in healthy rats and rats with intracranial glioblastoma.** *Toxicology Letters* 2002, **126**(2):131-141.
90. Lu J, Liong M, Zink JJ, Tamanoi F: **Mesoporous Silica Nanoparticles as a Delivery System for Hydrophobic Anticancer Drugs.** *Small* 2007, **3**(8):1341-1346.
91. Wohlfart S, Khalansky AS, Gelperina S, Maksimenko O, Bernreuther C, Glatzel M, Kreuter J: **Efficient Chemotherapy of Rat Glioblastoma Using Doxorubicin-Loaded PLGA Nanoparticles with Different Stabilizers.** *PLOS ONE* 2011, **6**(5):e19121.

92. Xin H, Chen L, Gu J, Ren X, wei Z, Luo J, Chen Y, Jiang X, Sha X, Fang X: **Enhanced anti-glioblastoma efficacy by PTX-loaded PEGylated poly(ϵ -caprolactone) nanoparticles: In vitro and in vivo evaluation.** *International Journal of Pharmaceutics* 2010, **402**(1):238-247.
93. Dong X: **Current Strategies for Brain Drug Delivery.** *Theranostics* 2018, **8**(6):1481-1493.
94. Saraiva C, Praça C, Ferreira R, Santos T, Ferreira L, Bernardino L: **Nanoparticle-mediated brain drug delivery: Overcoming blood–brain barrier to treat neurodegenerative diseases.** *Journal of Controlled Release* 2016, **235**:34-47.
95. Zhou Y, Peng Z, Seven ES, Leblanc RM: **Crossing the blood-brain barrier with nanoparticles.** *Journal of Controlled Release* 2018, **270**:290-303.
96. Saucier-Sawyer JK, Deng Y, Seo Y-E, Cheng CJ, Zhang J, Quijano E, Saltzman WM: **Systemic delivery of blood-brain barrier-targeted polymeric nanoparticles enhances delivery to brain tissue.** *Journal of drug targeting* 2015, **23**(7-8):736-749.
97. Wilson B, Samanta MK, Santhi K, Kumar KPS, Paramakrishnan N, Suresh B: **Targeted delivery of tacrine into the brain with polysorbate 80-coated poly(n-butylcyanoacrylate) nanoparticles.** *European Journal of Pharmaceutics and Biopharmaceutics* 2008, **70**(1):75-84.
98. Zhou Z, Singh R, Souweidane MM: **Convection-Enhanced Delivery for Diffuse Intrinsic Pontine Glioma Treatment.** *Current neuropharmacology* 2017, **15**(1):116-128.
99. Kunwar S, Chang S, Westphal M, Vogelbaum M, Sampson J, Barnett G, Shaffrey M, Ram Z, Piepmeier J, Prados M *et al*: **Phase III randomized trial of CED of IL13-PE38QQR vs Gliadel wafers for recurrent glioblastoma.** *Neuro-Oncology* 2010, **12**(8):871-881.
100. Nieder C, Grosu AL, Astner S, Molls M: **Treatment of unresectable glioblastoma multiforme.** *Anticancer Res* 2005, **25**(6c):4605-4610.
101. Maximilian I. Ruge SG, Harald Treuer and Volker Sturm: **Stereotactic Brachytherapy for Brain Tumors:** IntechOpen; 2012.
102. Potters L, Morgenstern C, Calugaru E, Fearn P, Jassal A, Presser J, Mullen E: **12-Year Outcomes Following Permanent Prostate Brachytherapy in Patients with Clinically Localized Prostate Cancer.** *The Journal of Urology* 2008, **179**(5, Supplement):S20-S24.
103. Nag S, Erickson B, Thomadsen B, Orton C, Demanes JD, Petereit D: **The American Brachytherapy Society recommendations for high-dose-rate brachytherapy for carcinoma of the cervix.** *International Journal of Radiation Oncology*Biophysics* 2000, **48**(1):201-211.
104. Schäfer R, Strnad V, Polgár C, Uter W, Hildebrandt G, Ott OJ, Kauer-Dorner D, Knauerhase H, Major T, Lyczek J *et al*: **Quality-of-life results for accelerated partial breast irradiation with interstitial brachytherapy versus whole-breast irradiation in early breast cancer after breast-conserving surgery (GEC-ESTRO): 5-year results of a randomised, phase 3 trial.** *The Lancet Oncology* 2018, **19**(6):834-844.
105. Ricke J, Wust P: **Computed Tomography–Guided Brachytherapy for Liver Cancer.** *Seminars in Radiation Oncology* 2011, **21**(4):287-293.
106. Barbarite E, Sick JT, Berchmans E, Bregy A, Shah AH, Elsayyad N, Komotar RJ: **The role of brachytherapy in the treatment of glioblastoma multiforme.** *Neurosurgical Review* 2017, **40**(2):195-211.
107. Betancourt T, Brown B, Brannon-Peppas L: **Doxorubicin-loaded PLGA nanoparticles by nanoprecipitation: preparation, characterization and in vitro evaluation.** *Nanomedicine (London, England)* 2007, **2**(2):219-232.
108. Zembko I, Ahmed I, Farooq A, Dail J, Tawari P, Wang W, McConville C: **Development of Disulfiram-Loaded Poly(Lactic-co-Glycolic Acid) Wafers for the Localised Treatment of Glioblastoma Multiforme: A Comparison of Manufacturing Techniques.** *Journal of pharmaceutical sciences* 2014, **104**(3):1076-1086.
109. McConville C, Tawari P, Wang W: **Hot melt extruded and injection moulded disulfiram-loaded PLGA millirods for the treatment of glioblastoma multiforme via stereotactic injection.** *International Journal of Pharmaceutics* 2015, **494**(1):73-82.

110. Najlah M, Ahmed Z, Iqbal M, Wang Z, Tawari P, Wang W, McConville C: **Development and characterisation of disulfiram-loaded PLGA nanoparticles for the treatment of non-small cell lung cancer.** *European Journal of Pharmaceutics and Biopharmaceutics* 2017, **112**:224-233.
111. Gavenis K, Schneider U, Groll J, Schmidt-Rohlfing B: **BMP-7-loaded PGLA microspheres as a new delivery system for the cultivation of human chondrocytes in a collagen type I gel: the common nude mouse model.** *The International journal of artificial organs* 2010, **33**(1):45-53.
112. Andreas K, Zehbe R, Kazubek M, Grzeschik K, Sternberg N, Baumler H, Schubert H, Sittinger M, Ringe J: **Biodegradable insulin-loaded PLGA microspheres fabricated by three different emulsification techniques: investigation for cartilage tissue engineering.** *Acta Biomater* 2011, **7**(4):1485-1495.
113. Jeong YI, Na HS, Seo DH, Kim DG, Lee HC, Jang MK, Na SK, Roh SH, Kim SI, Nah JW: **Ciprofloxacin-encapsulated poly(DL-lactide-co-glycolide) nanoparticles and its antibacterial activity.** *Int J Pharm* 2008, **352**(1-2):317-323.
114. Farazuddin M, Alam M, Khan AA, Khan N, Parvez S, Dutt GU, Mohammad O: **Efficacy of amoxicillin bearing microsphere formulation in treatment of *Listeria monocytogenes* infection in Swiss albino mice.** *Journal of drug targeting* 2010, **18**(1):45-52.
115. Zolnik BS, Burgess DJ: **Evaluation of in vivo-in vitro release of dexamethasone from PLGA microspheres.** *J Control Release* 2008, **127**(2):137-145.
116. Larjavaara S, Mäntylä R, Salminen T, Haapasalo H, Raitanen J, Jääskeläinen J, Auvinen A: **Incidence of gliomas by anatomic location.** *Neuro-oncology* 2007, **9**(3):319-325.
117. Markert JM: **The role of early resection vs biopsy in the management of low-grade gliomas.** *Jama* 2012, **308**(18):1918-1919.
118. Lara-Velazquez M, Al-Kharboosh R, Jeanneret S, Vazquez-Ramos C, Mahato D, Tavanaiepour D, Rahmathulla G, Quinones-Hinojosa A: **Advances in Brain Tumor Surgery for Glioblastoma in Adults.** *Brain sciences* 2017, **7**(12):166.
119. Eljamel S: **5-ALA Fluorescence Image Guided Resection of Glioblastoma Multiforme: A Meta-Analysis of the Literature.** *International Journal of Molecular Sciences* 2015, **16**(5):10443-10456.
120. Diez Valle R, Tejada Solis S, Idoate Gastearena MA, Garcia de Eulate R, Dominguez Echavarri P, Aristu Mendiroz J: **Surgery guided by 5-aminolevulinic fluorescence in glioblastoma: volumetric analysis of extent of resection in single-center experience.** *J Neurooncol* 2011, **102**(1):105-113.
121. Eljamel MS, Goodman C, Moseley H: **ALA and Photofrin fluorescence-guided resection and repetitive PDT in glioblastoma multiforme: a single centre Phase III randomised controlled trial.** *Lasers in medical science* 2008, **23**(4):361-367.
122. Eljamel S, Petersen M, Valentine R, Buist R, Goodman C, Moseley H, Eljamel S: **Comparison of intraoperative fluorescence and MRI image guided neuronavigation in malignant brain tumours, a prospective controlled study.** *Photodiagnosis and photodynamic therapy* 2013, **10**(4):356-361.
123. Kremer P, Fardanesh M, Ding R, Pritsch M, Zoubaa S, Frei E: **Intraoperative fluorescence staining of malignant brain tumors using 5-aminofluorescein-labeled albumin.** *Neurosurgery* 2009, **64**(3 Suppl):ons53-60; discussion ons60-51.
124. Panciani PP, Fontanella M, Schatlo B, Garbossa D, Agnoletti A, Ducati A, Lanotte M: **Fluorescence and image guided resection in high grade glioma.** *Clinical neurology and neurosurgery* 2012, **114**(1):37-41.
125. Stummer W, Pichlmeier U, Meinel T, Wiestler OD, Zanella F, Reulen HJ: **Fluorescence-guided surgery with 5-aminolevulinic acid for resection of malignant glioma: a randomised controlled multicentre phase III trial.** *The Lancet Oncology* 2006, **7**(5):392-401.

126. Della Puppa A, Ciccarino P, Lombardi G, Rolma G, Cecchin D, Rossetto M: **5-Aminolevulinic acid fluorescence in high grade glioma surgery: surgical outcome, intraoperative findings, and fluorescence patterns.** *BioMed research international* 2014, **2014**:232561.
127. Hadjipanayis CG, Widhalm G, Stummer W: **What is the Surgical Benefit of Utilizing 5-ALA for Fluorescence-Guided Surgery of Malignant Gliomas?** *Neurosurgery* 2015, **77**(5):663-673.
128. Lopez WOC, Trippel M, Doostkam S, Reithmeier T: **Interstitial brachytherapy with iodine-125 seeds for low grade brain stem gliomas in adults: Diagnostic and therapeutic intervention in a one-step procedure.** *Clinical neurology and neurosurgery* 2013, **115**(8):1451-1456.
129. Tanaka K, Kamo K-i, Tateoka K, Asanuma O, Sato K, Takeda H, Sakata K-i, Takada J: **A comparison of the dose distributions between the brachytherapy 125I source models, STM1251 and Oncoseed 6711, in a geometry lacking radiation equilibrium scatter conditions.** *Journal of Radiation Research* 2015, **56**(2):366-371.
130. Pantelis E, Papagiannis P, Anagnostopoulos G, Baltas D: **New (125)I brachytherapy source IsoSeed I25.S17plus: Monte Carlo dosimetry simulation and comparison to sources of similar design.** *Journal of contemporary brachytherapy* 2013, **5**(4):240-249.
131. Al-Qaisieh B, Smith DW, Brearley E, St. Clair S, Bownes P: **Comprehensive I-125 multi-seed comparison for prostate brachytherapy: Dosimetry and visibility analysis.** *Radiotherapy and Oncology* 2007, **84**(2):140-147.
132. Chaurasia A, Park SH, Seo JW, Park CK: **Immunohistochemical Analysis of ATRX, IDH1 and p53 in Glioblastoma and Their Correlations with Patient Survival.** *J Korean Med Sci* 2016, **31**(8):1208-1214.
133. Thon N, Kreth S, Kreth FW: **Personalized treatment strategies in glioblastoma: MGMT promoter methylation status.** *OncoTargets and therapy* 2013, **6**:1363-1372.
134. Lv S, Teugels E, Sadones J, Quartier E, Huylebrouck M, Du Four S, Le Mercier M, De Witte O, Salmon I, Michotte A *et al*: **Correlation between IDH1 gene mutation status and survival of patients treated for recurrent glioma.** *Anticancer Research* 2011, **31**(12):4457-4463.
135. Liu XY, Gerges N, Korshunov A, Sabha N, Khuong-Quang DA, Fontebasso AM, Fleming A, Hadjadj D, Schwartzentruber J, Majewski J *et al*: **Frequent ATRX mutations and loss of expression in adult diffuse astrocytic tumors carrying IDH1/IDH2 and TP53 mutations.** *Acta Neuropathol* 2012, **124**(5):615-625.
136. Verhaak RG, Hoadley KA, Purdom E, Wang V, Qi Y, Wilkerson MD, Miller CR, Ding L, Golub T, Mesirov JP *et al*: **Integrated genomic analysis identifies clinically relevant subtypes of glioblastoma characterized by abnormalities in PDGFRA, IDH1, EGFR, and NF1.** *Cancer cell* 2010, **17**(1):98-110.
137. Brennan CW, Verhaak RGW, McKenna A, Campos B, Noushmehr H, Salama SR, Zheng S, Chakravarty D, Sanborn JZ, Berman SH *et al*: **The Somatic Genomic Landscape of Glioblastoma.** *Cell* 2013, **155**(2):462-477.
138. Touat M, Idbaih A, Sanson M, Ligon KL: **Glioblastoma targeted therapy: updated approaches from recent biological insights.** *Annals of Oncology* 2017, **28**(7):1457-1472.
139. Markovsky E, Baabur-Cohen H, Satchi-Fainaro R: **Anticancer polymeric nanomedicine bearing synergistic drug combination is superior to a mixture of individually-conjugated drugs.** *Journal of Controlled Release* 2014, **187**(Supplement C):145-157.
140. Daniele S, Costa B, Zappelli E, Da Pozzo E, Sestito S, Nesi G, Campiglia P, Marinelli L, Novellino E, Rapposelli S *et al*: **Combined inhibition of AKT/mTOR and MDM2 enhances Glioblastoma Multiforme cell apoptosis and differentiation of cancer stem cells.** *Scientific reports* 2015, **5**:9956.
141. Shchors K, Massaras A, Hanahan D: **Dual Targeting of the Autophagic Regulatory Circuitry in Gliomas with Repurposed Drugs Elicits Cell-Lethal Autophagy and Therapeutic Benefit.** *Cancer cell* 2015, **28**(4):456-471.

142. Jiang P, Mukthavavam R, Chao Y, Bharati IS, Fogal V, Pastorino S, Cong X, Nomura N, Gallagher M, Abbasi T *et al*: **Novel anti-glioblastoma agents and therapeutic combinations identified from a collection of FDA approved drugs**. *Journal of Translational Medicine* 2014, **12**:13-13.
143. Yuan S, Wang F, Chen G, Zhang H, Feng L, Wang L, Colman H, Keating MJ, Li X, Xu R-H *et al*: **Effective Elimination of Cancer Stem Cells By a Novel Drug Combination Strategy**. *STEM CELLS* 2013, **31**(1):23-34.
144. Signore M, Pelacchi F, di Martino S, Runci D, Biffoni M, Giannetti S, Morgante L, De Majo M, Petricoin EF, Stancato L *et al*: **Combined PDK1 and CHK1 inhibition is required to kill glioblastoma stem-like cells in vitro and in vivo**. *Cell Death & Disease* 2014, **5**:e1223.
145. Nonnenmacher L, Westhoff MA, Fulda S, Karpel-Massler G, Halatsch ME, Engelke J, Simmet T, Corbacioglu S, Debatin KM: **RIST: a potent new combination therapy for glioblastoma**. *International journal of cancer* 2015, **136**(4):E173-187.
146. Sottoriva A, Spiteri I, Piccirillo SGM, Touloumis A, Collins VP, Marioni JC, Curtis C, Watts C, Tavaré S: **Intratumor heterogeneity in human glioblastoma reflects cancer evolutionary dynamics**. *Proceedings of the National Academy of Sciences* 2013, **110**(10):4009-4014.
147. Friedmann-Morvinski D: **Glioblastoma heterogeneity and cancer cell plasticity**. *Critical reviews in oncogenesis* 2014, **19**(5):327-336.
148. Bonavia R, Inda M-d-M, Cavenee W, Furnari F: **Heterogeneity Maintenance in Glioblastoma: a social network**. *Cancer research* 2011, **71**(12):4055-4060.
149. Meacham CE, Morrison SJ: **Tumor heterogeneity and cancer cell plasticity**. *Nature* 2013, **501**(7467):328-337.
150. Ene CI, Holland EC: **Personalized Medicine for Gliomas**. *Surgical Neurology International* 2015, **6**(Suppl 1):S89-S95.
151. Berenguer-Daizé C, Astorgues-Xerri L, Odore E, Cayol M, Cvitkovic E, Noel K, Bekradda M, MacKenzie S, Rezai K, Lokiec F *et al*: **OTX015 (MK-8628), a novel BET inhibitor, displays in vitro and in vivo antitumor effects alone and in combination with conventional therapies in glioblastoma models**. *International journal of cancer* 2016, **139**(9):2047-2055.
152. Soffietti R, Trevisan E, Bertero L, Cassoni P, Morra I, Fabrini MG, Pasqualetti F, Lolli I, Castiglione A, Ciccone G *et al*: **Bevacizumab and fotemustine for recurrent glioblastoma: a phase II study of AINO (Italian Association of Neuro-Oncology)**. *Journal of Neuro-Oncology* 2014, **116**(3):533-541.
153. Clarke JL, Molinaro AM, Phillips JJ, Butowski NA, Chang SM, Perry A, Costello JF, DeSilva AA, Rabbitt JE, Prados MD: **A single-institution phase II trial of radiation, temozolomide, erlotinib, and bevacizumab for initial treatment of glioblastoma**. *Neuro-Oncology* 2014, **16**(7):984-990.
154. Stupp R, Hegi ME, Gorlia T, Erridge SC, Perry J, Hong Y-K, Aldape KD, Lhermitte B, Pietsch T, Grujicic D *et al*: **Cilengitide combined with standard treatment for patients with newly diagnosed glioblastoma with methylated MGMT promoter (CENTRIC EORTC 26071-22072 study): a multicentre, randomised, open-label, phase 3 trial**. *The Lancet Oncology* 2014, **15**(10):1100-1108.
155. Bao S, Wu Q, McLendon RE, Hao Y, Shi Q, Hjelmeland AB, Dewhirst MW, Bigner DD, Rich JN: **Glioma stem cells promote radioresistance by preferential activation of the DNA damage response**. *Nature* 2006, **444**(7120):756-760.
156. Eramo A, Ricci-Vitiani L, Zeuner A, Pallini R, Lotti F, Sette G, Piloizzi E, Larocca LM, Peschle C, De Maria R: **Chemotherapy resistance of glioblastoma stem cells**. *Cell death and differentiation* 2006, **13**(7):1238-1241.
157. Kalkan R: **Glioblastoma Stem Cells as a New Therapeutic Target for Glioblastoma**. *Clinical Medicine Insights Oncology* 2015, **9**:95-103.

158. Singh SK, Hawkins C, Clarke ID, Squire JA, Bayani J, Hide T, Henkelman RM, Cusimano MD, Dirks PB: **Identification of human brain tumour initiating cells.** *Nature* 2004, **432**(7015):396-401.
159. Lathia JD, Mack SC, Mulkearns-Hubert EE, Valentim CLL, Rich JN: **Cancer stem cells in glioblastoma.** *Genes & development* 2015, **29**(12):1203-1217.
160. Bradshaw A, Wickremsekera A, Tan ST, Peng L, Davis PF, Itinteang T: **Cancer Stem Cell Hierarchy in Glioblastoma Multiforme.** *Frontiers in Surgery* 2016, **3**:21.
161. Dirkse A, Golebiewska A, Buder T, Nazarov PV, Muller A, Poovathingal S, Brons NHC, Leite S, Sauvageot N, Sarkisjan D *et al*: **Stem cell-associated heterogeneity in Glioblastoma results from intrinsic tumor plasticity shaped by the microenvironment.** *Nature Communications* 2019, **10**(1):1787.
162. Major I, Lastakchi S, Dalton M, McConville C: **Chapter 7. Implantable drug delivery systems.** In: *Engineering Drug Delivery Systems*. Edited by Ali Seyfoddin SD: Woodhead Publishing; 2020.
163. Kumar A, Pillai J: **Chapter 13 - Implantable drug delivery systems: An overview.** In: *Nanostructures for the Engineering of Cells, Tissues and Organs*. Edited by Grumezescu AM: William Andrew Publishing; 2018: 473-511.
164. Ahmad J, Kohli K, Mir SR, Amin S: **Lipid based Nanocarriers for Oral Delivery of Cancer Chemotherapeutics: An Insight in the Intestinal Lymphatic Transport.** *Drug Delivery Letters* 2013, **3**:38-46.
165. Kumar S: **Development and characterization of Irinotecan loaded colloidal drug delivery system.** *Journal of Pharmaceutical Sciences and Research* 2018, **10**:434-438.
166. Vredenburgh JJ, Desjardins A, Reardon DA, Friedman HS: **Experience with irinotecan for the treatment of malignant glioma.** *Neuro Oncol* 2009, **11**(1):80-91.
167. Vredenburgh JJ, Desjardins A, Reardon DA, Friedman HS: **Experience with irinotecan for the treatment of malignant glioma.** *Neuro-Oncology* 2009, **11**(1):80-91.
168. Kajinami K, Takekoshi N, Saito Y: **Pitavastatin: Efficacy and Safety Profiles of A Novel Synthetic HMG-CoA Reductase Inhibitor.** *Cardiovascular Drug Reviews* 2003, **21**(3):199-215.
169. Dhanalakshmi M, Nagajyothi N, Thenmozhi S, Manjuladevi K, Kameshwaran S: **Formulation and evaluation of pitavastatin nanosuspension.** *International Journal of Pharmacy & Life Sciences* 2014, **5**(2).
170. Johansson B: **Plasma protein binding of disulfiram and its metabolite diethylthiocarbamic acid methyl ester.** *Journal of Pharmacy and Pharmacology* 1990, **42**(11):806-807.
171. Borchert P, Wattenberg LW: **Inhibition of Macromolecular Binding of Benzo[a]pyrene and Inhibition of Neoplasia by Disulfiram in the Mouse Forestomach².** *JNCI: Journal of the National Cancer Institute* 1976, **57**(1):173-179.
172. Loo TW, Clarke DM: **Blockage of drug resistance in vitro by disulfiram, a drug used to treat alcoholism.** *Journal of the National Cancer Institute* 2000, **92**(11):898-902.
173. Kast RE, Karpel-Massler G, Halatsch M-E: **CUSP9* treatment protocol for recurrent glioblastoma: aprepitant, artesunate, auranofin, captopril, celecoxib, disulfiram, itraconazole, ritonavir, sertraline augmenting continuous low dose temozolomide.** *Oncotarget* 2014, **5**(18):8052-8082.
174. Hothi P, Martins TJ, Chen L, Deleyrolle L, Yoon J-G, Reynolds B, Foltz G: **High-Throughput Chemical Screens Identify Disulfiram as an Inhibitor of Human Glioblastoma Stem Cells.** *Oncotarget* 2012, **3**(10):1124-1136.
175. Liu P, Brown S, Goktug T, Channathodiyil P, Kannappan V, Hugnot JP, Guichet PO, Bian X, Armesilla AL, Darling JL *et al*: **Cytotoxic effect of disulfiram/copper on human glioblastoma cell lines and ALDH-positive cancer-stem-like cells.** *Br J Cancer* 2012, **107**(9):1488-1497.
176. Paranjpe A, Zhang R, Ali-Osman F, Bobustuc GC, Srivenugopal KS: **Disulfiram is a direct and potent inhibitor of human O6-methylguanine-DNA methyltransferase (MGMT) in brain**

- tumor cells and mouse brain and markedly increases the alkylating DNA damage. *Carcinogenesis* 2014, **35**(3):692-702.
177. Triscott J, Lee C, Hu K, Fotovati A, Berns R, Pambid M, Luk M, Kast RE, Kong E, Toyota E *et al*: **Disulfiram, a drug widely used to control alcoholism, suppresses self-renewal of glioblastoma and overrides resistance to temozolomide.** *Oncotarget* 2012, **3**(10):1112-1123.
 178. Lun X, Wells JC, Grinshtein N, King JC, Hao X, Dang N-H, Wang X, Aman A, Uehling D, Datti A *et al*: **Disulfiram when Combined with Copper Enhances the Therapeutic Effects of Temozolomide for the Treatment of Glioblastoma.** *Clinical Cancer Research* 2016, **22**(15):3860-3875.
 179. Company bAC: **Aldrich: Handbook of Fine Chemicals and Laboratory Equipment**; 2000.
 180. Kast RE, Boockvar JA, Brüning A, Cappello F, Chang W-W, Cvek B, Dou QP, Duenas-Gonzalez A, Efferth T, Focosi D *et al*: **A conceptually new treatment approach for relapsed glioblastoma: Coordinated undermining of survival paths with nine repurposed drugs (CUSP9) by the International Initiative for Accelerated Improvement of Glioblastoma Care.** *Oncotarget* 2013, **4**(4):502-530.
 181. Odović J, Karljicković-Rajić K, Trbojević-Stanković J, Stojimirović B, Vladimirov S: **Lipophilicity Examination of Some ACE inhibitors and Hydrochlorothiazide on Cellulose in RP Thin-Layer Chromatography.** *Iran J Pharm Res* 2012, **11**(3):763-770.
 182. Nakagawa T, Kubota T, Kabuto M, Koder T: **Captopril inhibits glioma cell invasion in vitro: involvement of matrix metalloproteinases.** *Anticancer Res* 1995, **15**(5b):1985-1989.
 183. Rooprai HK, Kandaneeratchi A, Rucklidge G, Pilkington GJ: **Influence of putative antiinvasive agents on matrix metalloproteinase secretion by human neoplastic glia in vitro.** *Annals of the New York Academy of Sciences* 1999, **878**:654-657.
 184. Rooprai HK, Kandaneeratchi A, Maidment SL, Christidou M, Trillo-Pazos G, Dexter DT, Rucklidge GJ, Widmer W, Pilkington GJ: **Evaluation of the effects of swainsonine, captopril, tangeretin and nobiletin on the biological behaviour of brain tumour cells in vitro.** *Neuropathology and applied neurobiology* 2001, **27**(1):29-39.
 185. Kast RE, Halatsch ME: **Matrix metalloproteinase-2 and -9 in glioblastoma: a trio of old drugs-captopril, disulfiram and nelfinavir-are inhibitors with potential as adjunctive treatments in glioblastoma.** *Archives of medical research* 2012, **43**(3):243-247.
 186. Takada Y, Hiwada K, Kokubu T: **Characterization and immunohistologic demonstration of angiotensin-converting enzyme in human renal cell carcinoma.** *Oncodevelopmental biology and medicine : the journal of the International Society for Oncodevelopmental Biology and Medicine* 1983, **4**(5):327-334.
 187. Ayalasomayajula SP, Kompella UB: **Retinal delivery of celecoxib is several-fold higher following subconjunctival administration compared to systemic administration.** *Pharmaceutical research* 2004, **21**(10):1797-1804.
 188. Primo F, Fröhlich P: **Celecoxib Identification Methods.** 2005, **24**.
 189. Sareddy GR, Geeviman K, Ramulu C, Babu PP: **The nonsteroidal anti-inflammatory drug celecoxib suppresses the growth and induces apoptosis of human glioblastoma cells via the NF-kappaB pathway.** *J Neurooncol* 2012, **106**(1):99-109.
 190. Kang KB, Zhu C, Yong SK, Gao Q, Wong MC: **Enhanced sensitivity of celecoxib in human glioblastoma cells: Induction of DNA damage leading to p53-dependent G1 cell cycle arrest and autophagy.** *Molecular cancer* 2009, **8**:66.
 191. Suzuki K, Gerelchuluun A, Hong Z, Sun L, Zenkoh J, Moritake T, Tsuboi K: **Celecoxib enhances radiosensitivity of hypoxic glioblastoma cells through endoplasmic reticulum stress.** *Neuro Oncol* 2013, **15**(9):1186-1199.
 192. Grossman SA, Olson J, Batchelor T, Peereboom D, Lesser G, Desideri S, Ye X, Hammour T, Supko JG: **Effect of phenytoin on celecoxib pharmacokinetics in patients with glioblastoma.** *Neuro Oncol* 2008, **10**(2):190-198.

193. Kesari S, Schiff D, Henson JW, Muzikansky A, Gigas DC, Doherty L, Batchelor TT, Longtine JA, Ligon KL, Weaver S *et al*: **Phase II study of temozolomide, thalidomide, and celecoxib for newly diagnosed glioblastoma in adults.** *Neuro Oncol* 2008, **10**(3):300-308.
194. Lewis DFV, Ito Y, Lake BG: **Quantitative structure-activity relationships (QSARs) for inhibitors and substrates of CYP2B enzymes: importance of compound lipophilicity in explanation of potency differences.** *Journal of Enzyme Inhibition and Medicinal Chemistry* 2010, **25**(5):679-684.
195. Martins FT, deLima PV, Azarias LC, de Abreu PJ, Neves PP, Legendre AO, de Andrade FM, de Oliveira GR, Ellena J, Doriguetto AC: **Increasing the symmetry of drug crystals: a monoclinic conformational polymorph of the platelet antiaggregating agent ticlopidine hydrochloride.** *CrystEngComm* 2011, **13**(19):5737-5743.
196. de Chasteigner S, Cavé G, Fessi H, Devissaguet J-P, Puisieux F: **Freeze-drying of itraconazole-loaded nanosphere suspensions: a feasibility study.** *Drug Development Research* 1996, **38**(2):116-124.
197. Six K, Verreck G, Peeters J, Binnemans K, Berghmans H, Augustijns P, Kinget R, Van den Mooter G: **Investigation of thermal properties of glassy itraconazole: identification of a monotropic mesophase.** *Thermochimica Acta* 2001, **376**(2):175-181.
198. Liu R, Li J, Zhang T, Zou L, Chen Y, Wang K, Lei Y, Yuan K, Li Y, Lan J *et al*: **Itraconazole suppresses the growth of glioblastoma through induction of autophagy: Involvement of abnormal cholesterol trafficking.** *Autophagy* 2014, **10**(7):1241-1255.
199. Fujita K-i, Kubota Y, Ishida H, Sasaki Y: **Irinotecan, a key chemotherapeutic drug for metastatic colorectal cancer.** *World journal of gastroenterology* 2015, **21**(43):12234-12248.
200. Xu Y, Villalona-Calero MA: **Irinotecan: mechanisms of tumor resistance and novel strategies for modulating its activity.** *Annals of Oncology* 2002, **13**(12):1841-1851.
201. Creemers GJ, Lund B, Verweij J: **Topoisomerase I inhibitors: topotecan and irinotecan.** *Cancer treatment reviews* 1994, **20**(1):73-96.
202. Singh S, Dwarakanath BS, Lazar Mathew T: **Role of topoisomerases in cytotoxicity induced by DNA ligand Hoechst-33342 and UV-C in a glioma cell line.** *Indian journal of experimental biology* 2005, **43**(4):313-323.
203. Friedman HS, Petros WP, Friedman AH, Schaaf LJ, Kerby T, Lawyer J, Parry M, Houghton PJ, Lovell S, Rasheed K *et al*: **Irinotecan therapy in adults with recurrent or progressive malignant glioma.** *Journal of clinical oncology : official journal of the American Society of Clinical Oncology* 1999, **17**(5):1516-1525.
204. Kawato Y, Aonuma M, Hirota Y, Kuga H, Sato K: **Intracellular Roles of SN-38, a Metabolite of the Camptothecin Derivative CPT-11, in the Antitumor Effect of CPT-11.** *Cancer research* 1991, **51**(16):4187.
205. Raymond E, Fabbro M, Boige V, Rixe O, Frenay M, Vassal G, Faivre S, Sicard E, Germa C, Rodier JM *et al*: **Multicentre phase II study and pharmacokinetic analysis of irinotecan in chemotherapy-naïve patients with glioblastoma.** *Annals of Oncology* 2003, **14**(4):603-614.
206. Crews KR, Stewart CF, Jones-Wallace D, Thompson SJ, Houghton PJ, Heideman RL, Fouladi M, Bowers DC, Chintagumpala MM, Gajjar A: **Altered irinotecan pharmacokinetics in pediatric high-grade glioma patients receiving enzyme-inducing anticonvulsant therapy.** *Clinical cancer research : an official journal of the American Association for Cancer Research* 2002, **8**(7):2202-2209.
207. Buckner JC, Reid JM, Wright K, Kaufmann SH, Erlichman C, Ames M, Cha S, O'Fallon JR, Schaaf LJ, Miller LL: **Irinotecan in the treatment of glioma patients.** *Cancer* 2003, **97**(S9):2352-2358.
208. Puduvalli VK, Giglio P, Groves MD, Hess KR, Gilbert MR, Mahankali S, Jackson EF, Levin VA, Conrad CA, Hsu SH *et al*: **Phase II trial of irinotecan and thalidomide in adults with recurrent glioblastoma multiforme.** *Neuro-Oncology* 2008, **10**(2):216-222.

209. Reardon DA, Desjardins A, Peters KB, Vredenburgh JJ, Gururangan S, Sampson JH, McLendon RE, Herndon JE, Coan A, Threatt S *et al*: **Phase 2 study of carboplatin, irinotecan, and bevacizumab for recurrent glioblastoma after progression on bevacizumab therapy.** *Cancer* 2011, **117**(23):5351-5358.
210. Hasselbalch B, Lassen U, Hansen S, Holmberg M, Sørensen M, Kosteljanetz M, Broholm H, Stockhausen M-T, Poulsen HS: **Cetuximab, bevacizumab, and irinotecan for patients with primary glioblastoma and progression after radiation therapy and temozolomide: a phase II trial.** *Neuro-Oncology* 2010, **12**(5):508-516.
211. Brandes AA, Tosoni A, Basso U, Reni M, Valduga F, Monfardini S, Amistà P, Nicolardi L, Sotti G, Ermani M: **Second-Line Chemotherapy With Irinotecan Plus Carmustine in Glioblastoma Recurrent or Progressive After First-Line Temozolomide Chemotherapy: A Phase II Study of the Gruppo Italiano Cooperativo di Neuro-Oncologia (GICNO).** *Journal of Clinical Oncology* 2004, **22**(23):4779-4786.
212. Ozel O, Kurt M, Ozdemir O, Bayram J, Akdeniz H, Koca D: **Complete response to bevacizumab plus irinotecan in patients with rapidly progressive GBM: Cases report and literature review.** *Journal of Oncological Sciences* 2016, **2**(2):87-94.
213. Herrlinger U, Schäfer N, Steinbach JP, Weyerbrock A, Hau P, Goldbrunner R, Friedrich F, Rohde V, Ringel F, Schlegel U *et al*: **Bevacizumab Plus Irinotecan Versus Temozolomide in Newly Diagnosed O6-Methylguanine–DNA Methyltransferase Nonmethylated Glioblastoma: The Randomized GLARIUS Trial.** *Journal of Clinical Oncology* 2016, **34**(14):1611-1619.
214. Reynés G, Martínez-Sales V, Vila V, Balañá C, Pérez-Segura P, Vaz MA, Benavides M, Gallego O, Palomero I, Gil-Gil M *et al*: **Phase II trial of irinotecan and metronomic temozolomide in patients with recurrent glioblastoma.** *Anti-Cancer Drugs* 2016, **27**(2):133-137.
215. Gruber ML, Buster WP: **Temozolomide in combination with irinotecan for treatment of recurrent malignant glioma.** *American journal of clinical oncology* 2004, **27**(1):33-38.
216. O'Reilly S, Rowinsky EK: **The clinical status of irinotecan (CPT-11), a novel water soluble camptothecin analogue: 1996.** *Critical Reviews in Oncology/Hematology* 1996, **24**(1):47-70.
217. Kreisl TN, Kim L, Moore K, Duic P, Royce C, Stroud I, Garren N, Mackey M, Butman JA, Camphausen K *et al*: **Phase II Trial of Single-Agent Bevacizumab Followed by Bevacizumab Plus Irinotecan at Tumor Progression in Recurrent Glioblastoma.** *Journal of Clinical Oncology* 2009, **27**(5):740-745.
218. Vredenburgh JJ, Desjardins A, Herndon JE, Marcello J, Reardon DA, Quinn JA, Rich JN, Sathornsumetee S, Gururangan S, Sampson J *et al*: **Bevacizumab Plus Irinotecan in Recurrent Glioblastoma Multiforme.** *Journal of Clinical Oncology* 2007, **25**(30):4722-4729.
219. Ramsay EC, Anantha M, Zastre J, Meijs M, Zonderhuis J, Strutt D, Webb MS, Waterhouse D, Bally MB: **Irinophore C: A Liposome Formulation of Irinotecan with Substantially Improved Therapeutic Efficacy against a Panel of Human Xenograft Tumors.** *Clinical Cancer Research* 2008, **14**(4):1208.
220. Verreault M, Strutt D, Masin D, Anantha M, Waterhouse D, Yapp DT, Bally MB: **Irinophore C, a lipid-based nanoparticulate formulation of irinotecan, is more effective than free irinotecan when used to treat an orthotopic glioblastoma model.** *J Control Release* 2012, **158**(1):34-43.
221. Jiang P, Mukthavaram R, Chao Y, Nomura N, Bharati IS, Fogal V, Pastorino S, Teng D, Cong X, Pingle SC *et al*: **In vitro and in vivo anticancer effects of mevalonate pathway modulation on human cancer cells.** *Br J Cancer* 2014, **111**(8):1562-1571.
222. Anjum K, Shagufta BI, Abbas SQ, Patel S, Khan I, Shah SAA, Akhter N, Hassan SSu: **Current status and future therapeutic perspectives of glioblastoma multiforme (GBM) therapy: A review.** *Biomedicine & Pharmacotherapy* 2017, **92**(Supplement C):681-689.

223. Koukourakis MI, Mitrakas AG, Giatromanolaki A: **Therapeutic interactions of autophagy with radiation and temozolomide in glioblastoma: evidence and issues to resolve.** *Br J Cancer* 2016, **114**(5):485-496.
224. Jiang P, Mukthavavam R, Chao Y, Sri Bharati I, Fogal V, Pastorino S, Cong X, Nomura N, Gallagher M, Abbasi T *et al*: **Correction to novel anti-glioblastoma agents and therapeutic combinations identified from a collection of FDA approved drugs [J TranslMed (2014) 12 13],** vol. 12; 2014.
225. Tsuboi Y, Kurimoto M, Nagai S, Hayakawa Y, Kamiyama H, Hayashi N, Kitajima I, Endo S: **Induction of autophagic cell death and radiosensitization by the pharmacological inhibition of nuclear factor-kappa B activation in human glioma cell lines.** *Journal of neurosurgery* 2009, **110**(3):594-604.
226. Zhang ZY, Zheng SH, Yang WG, Yang C, Yuan WT: **Targeting colon cancer stem cells with novel blood cholesterol drug pitavastatin.** *European review for medical and pharmacological sciences* 2017, **21**(6):1226-1233.
227. de Wolf E, Abdullah MI, Jones SM, Menezes K, Moss DM, Drijfhout FP, Hart SR, Hoskins C, Stronach EA, Richardson A: **Dietary geranylgeraniol can limit the activity of pitavastatin as a potential treatment for drug-resistant ovarian cancer.** *Scientific reports* 2017, **7**(1):5410-5410.
228. Nakai E, Park K, Yawata T, Chihara T, Kumazawa A, Nakabayashi H, Shimizu K: **Enhanced MDR1 expression and chemoresistance of cancer stem cells derived from glioblastoma.** *Cancer investigation* 2009, **27**(9):901-908.
229. Michael WN, Constance AG, Barbara AZ, Ralph HH, Peter CP, Stuart AG, Henry B, Colvin OM: **Multidrug resistance gene (MDR1) expression in human brain tumors.** *Journal of neurosurgery* 1991, **75**(6):941-946.
230. Garrigues A, Escargueil AE, Orlowski S: **The multidrug transporter, P-glycoprotein, actively mediates cholesterol redistribution in the cell membrane.** *Proceedings of the National Academy of Sciences* 2002, **99**(16):10347.
231. Fan Y, Nguyen DT, Akay Y, Xu F, Akay M: **Engineering a Brain Cancer Chip for High-throughput Drug Screening.** *Scientific reports* 2016, **6**:25062.
232. (TIP) Series, No. 49.) Chapter 3—Disulfiram. Available from: <https://www.ncbi.nlm.nih.gov/books/NBK64036/CfSATIAPIMPRMSAaMHSAUTIP>.
233. Lewis DJ, Deshmukh P, Tedstone AA, Tuna F, O'Brien P: **On the interaction of copper(II) with disulfiram.** *Chemical communications (Cambridge, England)* 2014, **50**(87):13334-13337.
234. Huang J, Campian JL, Gujar AD, Tran DD, Lockhart AC, DeWees TA, Tsien CI, Kim AH: **A phase I study to repurpose disulfiram in combination with temozolomide to treat newly diagnosed glioblastoma after chemoradiotherapy.** *J Neurooncol* 2016, **128**(2):259-266.
235. Huang J, L. Campian J, Gujar A, Tsien C, Ansstas G, Tran D, DeWees T, Craig Lockhart A, Kim A: **Final results of a phase I dose-escalation, dose-expansion study of adding disulfiram with or without copper to adjuvant temozolomide for newly diagnosed glioblastoma,** vol. 138; 2018.
236. Johansson B: **A review of the pharmacokinetics and pharmacodynamics of disulfiram and its metabolites.** *Acta psychiatrica Scandinavica Supplementum* 1992, **369**:15-26.
237. Agarwal RP, Phillips M, McPherson RA, Hensley P: **Serum albumin and the metabolism of disulfiram.** *Biochemical pharmacology* 1986, **35**(19):3341-3347.
238. Migdalof BH, Antonaccio MJ, McKinstry DN, Singhvi SM, Lan SJ, Egli P, Kripalani KJ: **Captopril: pharmacology, metabolism and disposition.** *Drug metabolism reviews* 1984, **15**(4):841-869.
239. Juillerat-Jeanneret L, Celerier J, Chapuis Bernasconi C, Nguyen G, Wostl W, Maerki HP, Janzer RC, Corvol P, Gasc JM: **Renin and angiotensinogen expression and functions in growth and apoptosis of human glioblastoma.** *Br J Cancer* 2004, **90**(5):1059-1068.
240. Tamba M, Torreggiani A: **Free radical scavenging and copper chelation: a potentially beneficial action of captopril.** *Free radical research* 2000, **32**(3):199-211.

241. Jones PH, Christodoulos K, Dobbs N, Thavasu P, Balkwill F, Blann AD, Caine GJ, Kumar S, Kakkar AJ, Gompertz N *et al*: **Combination antiangiogenesis therapy with marimastat, captopril and fragmin in patients with advanced cancer**. *British journal of cancer* 2004, **91**(1):30-36.
242. Krusche B, Arend J, Efferth T: **Synergistic Inhibition of Angiogenesis by Artesunate and Captopril In Vitro and In Vivo**. *Evidence-Based Complementary and Alternative Medicine* 2013, **2013**:10.
243. de Groot-Besseling RRJ, Ruers TJM, van Kraats AA, Poelen GJM, Ruiter DJ, de Waal RMW, Westphal JR: **Anti-tumor activity of a combination of plasminogen activator and captopril in a human melanoma xenograft model**. *International journal of cancer* 2004, **112**(2):329-334.
244. Chatterjee K, Parmley WW, Cohn JN, Levine TB, Awan NA, Mason DT, Faxon DP, Creager M, Gavras HP, Fouad FM *et al*: **A cooperative multicenter study of captopril in congestive heart failure: Hemodynamic effects and long-term response**. *American Heart Journal* 1985, **110**(2):439-447.
245. Shukla AC, Steven JM, McGowan FX: **CHAPTER 16 - Cardiac Physiology and Pharmacology**. In: *A Practice of Anesthesia for Infants and Children (Fourth Edition)*. Edited by Coté CJ, Lerman J, Todres ID. Philadelphia: W.B. Saunders; 2009: 361-395.
246. Kulp SK, Yang Y-T, Hung C-C, Chen K-F, Lai J-P, Tseng P-H, Fowble JW, Ward PJ, Chen C-S: **3-Phosphoinositide-Dependent Protein Kinase-1/Akt Signaling Represents a Major Cyclooxygenase-2-Independent Target for Celecoxib in Prostate Cancer Cells**. *Cancer research* 2004, **64**(4):1444-1451.
247. Backhus LM, Petasis NA, Uddin J, Schonthal AH, Bart RD, Lin Y, Starnes VA, Bremner RM: **Dimethyl celecoxib as a novel non-cyclooxygenase 2 therapy in the treatment of non-small cell lung cancer**. *The Journal of thoracic and cardiovascular surgery* 2005, **130**(5):1406-1412.
248. Zhu J, Huang JW, Tseng PH, Yang YT, Fowble J, Shiau CW, Shaw YJ, Kulp SK, Chen CS: **From the cyclooxygenase-2 inhibitor celecoxib to a novel class of 3-phosphoinositide-dependent protein kinase-1 inhibitors**. *Cancer research* 2004, **64**(12):4309-4318.
249. Kardosh A, Blumenthal M, Wang WJ, Chen TC, Schonthal AH: **Differential Effects of Selective COX-2 Inhibitors on Cell Cycle Regulation and Proliferation of Glioblastoma Cell Lines**. *Cancer Biology & Therapy* 2004, **3**(1):55-62.
250. Kardosh A, Golden EB, Pyrko P, Uddin J, Hofman FM, Chen TC, Louie SG, Petasis NA, Schonthal AH: **Aggravated endoplasmic reticulum stress as a basis for enhanced glioblastoma cell killing by bortezomib in combination with celecoxib or its non-coxib analogue, 2,5-dimethyl-celecoxib**. *Cancer research* 2008, **68**(3):843-851.
251. Nam DH, Park K, Park C, Im YH, Kim MH, Lee S, Hong SC, Shin HJ, Kim JH, Eoh W *et al*: **Intracranial inhibition of glioma cell growth by cyclooxygenase-2 inhibitor celecoxib**. *Oncology reports* 2004, **11**(2):263-268.
252. Kang KB, Wang TT, Woon CT, Cheah ES, Moore XL, Zhu C, Wong MC: **Enhancement of glioblastoma radioresponse by a selective COX-2 inhibitor celecoxib: inhibition of tumor angiogenesis with extensive tumor necrosis**. *International journal of radiation oncology, biology, physics* 2007, **67**(3):888-896.
253. Hsin-I Ma, Shih-Hwa Chiou, Dueng-Yuan Hueng, Lung-Kuo Tai, Pin-I Huang, Chung-Lan Kao, Yi-Wei Chen, Huey-Kang Sytwu: **Celecoxib and radioresistant glioblastoma-derived CD133+ cells: improvement in radiotherapeutic effects**. *Journal of neurosurgery* 2011, **114**(3):651-662.
254. Kang SG, Kim JS, Park K, Kim JS, Groves MD, Nam DH: **Combination celecoxib and temozolomide in C6 rat glioma orthotopic model**. *Oncology reports* 2006, **15**(1):7-13.
255. Walbert T, Gilbert MR, Groves MD, Puduvalli VK, Yung WK, Conrad CA, Bobustuc GC, Colman H, Hsu SH, Bekele BN *et al*: **Combination of 6-thioguanine, capecitabine, and celecoxib with**

- temozolomide or lomustine for recurrent high-grade glioma.** *J Neurooncol* 2011, **102**(2):273-280.
256. Penas-Prado M, Hess KR, Fisch MJ, Lagrone LW, Groves MD, Levin VA, De Groot JF, Puduvalli VK, Colman H, Volas-Redd G *et al*: **Randomized phase II adjuvant factorial study of dose-dense temozolomide alone and in combination with isotretinoin, celecoxib, and/or thalidomide for glioblastoma.** *Neuro-Oncology* 2015, **17**(2):266-273.
 257. Reardon DA, Quinn JA, Vredenburgh J, Rich JN, Gururangan S, Badruddoja M, Herndon JE, Dowell JM, Friedman AH, Friedman HS: **Phase II trial of irinotecan plus celecoxib in adults with recurrent malignant glioma.** *Cancer* 2005, **103**(2):329-338.
 258. Batchelor TT, Gilbert MR, Supko JG, Carson KA, Nabors LB, Grossman SA, Lesser GJ, Mikkelsen T, Phuphanich S: **Phase 2 study of weekly irinotecan in adults with recurrent malignant glioma: final report of NABTT 97-11.** *Neuro Oncol* 2004, **6**(1):21-27.
 259. Cloughesy TF, Filka E, Kuhn J, Nelson G, Kabbinnavar F, Friedman H, Miller LL, Elfring GL: **Two studies evaluating irinotecan treatment for recurrent malignant glioma using an every-3-week regimen.** *Cancer* 2003, **97**(9 Suppl):2381-2386.
 260. Dembo G, Park SB, Kharasch ED: **Central nervous system concentrations of cyclooxygenase-2 inhibitors in humans.** *Anesthesiology* 2005, **102**(2):409-415.
 261. Wojtukiewicz MZ, Hempel D, Sierko E, Tucker SC, Honn KV: **Antiplatelet agents for cancer treatment: a real perspective or just an echo from the past?** *Cancer Metastasis Reviews* 2017, **36**(2):305-329.
 262. Pantziarka P, Sukhatme V, Bouche G, Meheus L, Sukhatme VP: **Repurposing Drugs in Oncology (ReDO)—itraconazole as an anti-cancer agent.** *ecancermedicalscience* 2015, **9**:521.
 263. Aftab BT, Dobromilskaya I, Liu JO, Rudin CM: **Itraconazole inhibits angiogenesis and tumor growth in non-small cell lung cancer.** *Cancer research* 2011, **71**(21):6764-6772.
 264. Antonarakis ES, Heath EI, Smith DC, Rathkopf D, Blackford AL, Danila DC, King S, Frost A, Ajiboye AS, Zhao M *et al*: **Repurposing itraconazole as a treatment for advanced prostate cancer: a noncomparative randomized phase II trial in men with metastatic castration-resistant prostate cancer.** *Oncologist* 2013, **18**(2):163-173.
 265. Yang Y, Shi J, Tolomelli G, Xu H, Xia J, Wang H, Zhou W, Zhou Y, Das S, Gu Z *et al*: **RARalpha2 expression confers myeloma stem cell features.** *Blood* 2013, **122**(8):1437-1447.
 266. Kim J, Tang JY, Gong R, Kim J, Lee JJ, Clemons KV, Chong CR, Chang KS, Fereshteh M, Gardner D *et al*: **Itraconazole, a commonly used antifungal that inhibits Hedgehog pathway activity and cancer growth.** *Cancer cell* 2010, **17**(4):388-399.
 267. Kim DJ, Kim J, Spaunhurst K, Montoya J, Khodosh R, Chandra K, Fu T, Gilliam A, Molgo M, Beachy PA *et al*: **Open-label, exploratory phase II trial of oral itraconazole for the treatment of basal cell carcinoma.** *Journal of clinical oncology : official journal of the American Society of Clinical Oncology* 2014, **32**(8):745-751.
 268. Wang X, Wei S, Zhao Y, Shi C, Liu P, Zhang C, Lei Y, Zhang B, Bai B, Huang Y *et al*: **Anti-proliferation of breast cancer cells with itraconazole: Hedgehog pathway inhibition induces apoptosis and autophagic cell death.** *Cancer letters* 2017, **385**:128-136.
 269. You M, Varona-Santos J, Singh S, Robbins DJ, Savaraj N, Nguyen DM: **Targeting of the Hedgehog signal transduction pathway suppresses survival of malignant pleural mesothelioma cells in vitro.** *The Journal of thoracic and cardiovascular surgery* 2014, **147**(1):508-516.
 270. Tsubamoto H, Inoue K, Sakata K, Ueda T, Takeyama R, Shibahara H, Sonoda T: **Itraconazole Inhibits AKT/mTOR Signaling and Proliferation in Endometrial Cancer Cells.** *Anticancer Res* 2017, **37**(2):515-519.
 271. Gupta A, Unadkat JD, Mao Q: **Interactions of azole antifungal agents with the human breast cancer resistance protein (BCRP).** *Journal of pharmaceutical sciences* 2007, **96**(12):3226-3235.

272. Gupta S, Kim J, Gollapudi S: **Reversal of daunorubicin resistance in P388/ADR cells by itraconazole.** *J Clin Invest* 1991, **87**(4):1467-1469.
273. Kurosawa M, Okabe M, Hara N, Kawamura K, Suzuki S, Sakurada K, Asaka M: **Reversal effect of itraconazole on adriamycin and etoposide resistance in human leukemia cells.** *Annals of hematology* 1996, **72**(1):17-21.
274. Elewski B, Tavakkol A: **Safety and tolerability of oral antifungal agents in the treatment of fungal nail disease: a proven reality.** *Therapeutics and Clinical Risk Management* 2005, **1**(4):299-306.
275. Seidel S, Garvalov B, Acker T: **Isolation and Culture of Primary Glioblastoma Cells from Human Tumor Specimens**, vol. 1235; 2015.
276. Millau JF, Mai S, Bastien N, Drouin R: **p53 functions and cell lines: have we learned the lessons from the past?** *BioEssays : news and reviews in molecular, cellular and developmental biology* 2010, **32**(5):392-400.
277. Gazdar AF, Girard L, Lockwood WW, Lam WL, Minna JD: **Lung Cancer Cell Lines as Tools for Biomedical Discovery and Research.** *JNCI: Journal of the National Cancer Institute* 2010, **102**(17):1310-1321.
278. International BR: **Retracted: Tanshinone IIA Induces Apoptosis in Human Oral Cancer KB Cells through a Mitochondria-Dependent Pathway.** *BioMed research international* 2017, **2017**:1.
279. Zhang P, Yang Y, Zweidler-McKay P, Hughes DPM: **Retraction: Critical role of notch signaling in osteosarcoma invasion and metastasis.** *Clinical cancer research : an official journal of the American Association for Cancer Research* 2013, **19**(18):5256-5257.
280. Aum DJ, Kim DH, Beaumont TL, Leuthardt EC, Dunn GP, Kim AH: **Molecular and cellular heterogeneity: the hallmark of glioblastoma.** *Neurosurgical focus* 2014, **37**(6):E11.
281. Patel AP, Tirosch I, Trombetta JJ, Shalek AK, Gillespie SM, Wakimoto H, Cahill DP, Nahed BV, Curry WT, Martuza RL *et al*: **Single-cell RNA-seq highlights intratumoral heterogeneity in primary glioblastoma.** *Science (New York, NY)* 2014, **344**(6190):1396-1401.
282. Liu Y, Xu X, Yin L, Zhang X, Li L, Lu H: **Relationship between Glioblastoma Heterogeneity and Survival Time: An MR Imaging Texture Analysis.** *American Journal of Neuroradiology* 2017, **38**(9):1695.
283. Parker JJ, Canoll P, Niswander L, Kleinschmidt-DeMasters BK, Foshay K, Waziri A: **Intratumoral heterogeneity of endogenous tumor cell invasive behavior in human glioblastoma.** *Scientific reports* 2018, **8**(1):18002.
284. Jordan JP, Hand CM, Markowitz RS, Black P: **Test for chemotherapeutic sensitivity of cerebral gliomas: use of colorimetric MTT assay.** *Journal of Neuro-Oncology* 1992, **14**(1):19-35.
285. Nikkhah G, Tonn JC, Hoffmann O, Kraemer H-P, Darling JL, Schachenmayr W, Schönmayr R: **The MTT assay for chemosensitivity testing of human tumors of the central nervous system.** *Journal of Neuro-Oncology* 1992, **13**(1):13-24.
286. Stepanenko AA, Dmitrenko VV: **Pitfalls of the MTT assay: Direct and off-target effects of inhibitors can result in over/underestimation of cell viability.** *Gene* 2015, **574**(2):193-203.
287. Single A, Beetham H, Telford BJ, Guilford P, Chen A: **A Comparison of Real-Time and Endpoint Cell Viability Assays for Improved Synthetic Lethal Drug Validation.** *Journal of Biomolecular Screening* 2015, **20**(10):1286-1293.
288. !!! INVALID CITATION !!! {}.
289. Gürten B, Yenigül E, Sezer AD, Malta S: **Complexation and enhancement of temozolomide solubility with cyclodextrins.** *Brazilian Journal of Pharmaceutical Sciences* 2018, **54**.
290. Chemicals C: **Product information.** In.; 2020.

291. Ikeda Y, Kimura K, Hirayama F, Arima H, Uekama K: **Controlled release of a water-soluble drug, captopril, by a combination of hydrophilic and hydrophobic cyclodextrin derivatives.** *Journal of Controlled Release* 2000, **66**(2):271-280.
292. Kim H, Likhari P, Parker D, Statkevich P, Marco A, Lin CC, Nomeir AA: **High-performance liquid chromatographic analysis and stability of anti-tumor agent temozolomide in human plasma.** *Journal of pharmaceutical and biomedical analysis* 2001, **24**(3):461-468.
293. Chen X, Peer CJ, Alfaro R, Tian T, Spencer SD, Figg WD: **Quantification of Irinotecan, SN38, and SN38G in human and porcine plasma by ultra high-performance liquid chromatography-tandem mass spectrometry and its application to hepatic chemoembolization.** *Journal of pharmaceutical and biomedical analysis* 2012, **62**:140-148.
294. Yin T, Liu Q, Zhao H, Zhao L, Liu H, Li M, Cui M, Ren W: **LC-MS/MS assay for pitavastatin in human plasma and subsequent application to a clinical study in healthy Chinese volunteers.** *Asian Journal of Pharmaceutical Sciences* 2014, **9**(6):348-355.
295. Borges NC, Mendes GD, Borges A, Oliveira SE, Barrientos-Astigarraga RE, Nucci GD: **Ticlopidine quantification in human plasma by high-performance liquid chromatography coupled to electrospray tandem mass spectrometry. Application to bioequivalence study.** *J Mass Spectrom* 2004, **39**(12):1562-1569.
296. Dwivedi A, Singh B, Sharma S, Lokhandae RS, Dubey N: **Ultra-performance liquid chromatography electrospray ionization-tandem mass spectrometry method for the simultaneous determination of itraconazole and hydroxy itraconazole in human plasma.** *Journal of Pharmaceutical Analysis* 2014, **4**(5):316-324.
297. Thappali SRS, Varanasi K, Veeraraghavan S, Arla R, Chennupati S, Rajamanickam M, Vakkalanka S, Khagga M: **Simultaneous Determination of Celecoxib, Erlotinib, and its Metabolite Desmethyl-Erlotinib (OSI-420) in Rat Plasma by Liquid chromatography/Tandem Mass Spectrometry with Positive/Negative Ion-Switching Electrospray Ionisation.** *Scientia Pharmaceutica* 2012, **80**(3):633-646.
298. Vancea S, Imre S, Donath-Nagy G, Bela T, Nyulas M, Muntean T, Borka-Balas R: **Determination of free captopril in human plasma by liquid chromatography with mass spectrometry detection.** *Talanta* 2009, **79**(2):436-441.
299. Lee J, Kotliarova S, Kotliarov Y, Li A, Su Q, Donin NM, Pastorino S, Purow BW, Christopher N, Zhang W *et al*: **Tumor stem cells derived from glioblastomas cultured in bFGF and EGF more closely mirror the phenotype and genotype of primary tumors than do serum-cultured cell lines.** *Cancer cell* 2006, **9**(5):391-403.
300. Inagaki A, Soeda A, Oka N, Kitajima H, Nakagawa J, Motohashi T, Kunisada T, Iwama T: **Long-term maintenance of brain tumor stem cell properties under at non-adherent and adherent culture conditions.** *Biochemical and biophysical research communications* 2007, **361**(3):586-592.
301. Jiao Y, Killela PJ, Reitman ZJ, Rasheed AB, Heaphy CM, de Wilde RF, Rodriguez FJ, Rosenberg S, Oba-Shinjo SM, Nagahashi Marie SK *et al*: **Frequent ATRX, CIC, FUBP1 and IDH1 mutations refine the classification of malignant gliomas.** *Oncotarget* 2012, **3**(7):709-722.
302. Foote Michael B, Papadopoulos N, Diaz Luis A: **Genetic Classification of Gliomas: Refining Histopathology.** *Cancer cell* 2015, **28**(1):9-11.
303. Takano S, Ishikawa E, Sakamoto N, Matsuda M, Akutsu H, Noguchi M, Kato Y, Yamamoto T, Matsumura A: **Immunohistochemistry on IDH 1/2, ATRX, p53 and Ki-67 substitute molecular genetic testing and predict patient prognosis in grade III adult diffuse gliomas.** *Brain Tumor Pathology* 2016, **33**(2):107-116.
304. Chen Y-J, Hakin-Smith V, Teo M, Xinarianos GE, Jellinek DA, Carroll T, McDowell D, MacFarlane MR, Boet R, Baguley BC *et al*: **Association of Mutant TP53 with Alternative Lengthening of Telomeres and Favorable Prognosis in Glioma.** *Cancer research* 2006, **66**(13):6473.

305. Nguyen DN, Heaphy CM, de Wilde RF, Orr BA, Odia Y, Eberhart CG, Meeker AK, Rodriguez FJ: **Molecular and morphologic correlates of the alternative lengthening of telomeres phenotype in high-grade astrocytomas.** *Brain pathology (Zurich, Switzerland)* 2013, **23**(3):237-243.
306. Newcomb EW, Cohen H, Lee SR, Bhalla SK, Bloom J, Hayes RL, Miller DC: **Survival of patients with glioblastoma multiforme is not influenced by altered expression of p16, p53, EGFR, MDM2 or Bcl-2 genes.** *Brain pathology (Zurich, Switzerland)* 1998, **8**(4):655-667.
307. Hassan SB, Haglund C, A°leskog A, Larsson R, Lindhagen E: **Primary lymphocytes as predictors for species differences in cytotoxic drug sensitivity.** *Toxicology in Vitro* 2007, **21**(6):1174-1181.
308. Arora M: **Cell Culture Media: A Review.** In. United States: University of Pittsburgh Medical Center; 2013.
309. Lundholt BK, Scudder KM, Pagliaro L: **A Simple Technique for Reducing Edge Effect in Cell-Based Assays.** *Journal of Biomolecular Screening* 2003, **8**(5):566-570.
310. Azzalin A, Nato G, Parmigiani E, Garelo F, Buffo A, Magrassi L: **Inhibitors of GLUT/SLC2A Enhance the Action of BCNU and Temozolomide against High-Grade Gliomas.** *Neoplasia* 2017, **19**(4):364-373.
311. Lan F, Yang Y, Han J, Wu Q, Yu H, Yue X: **Sulforaphane reverses chemo-resistance to temozolomide in glioblastoma cells by NF-kappaB-dependent pathway downregulating MGMT expression.** *International journal of oncology* 2016, **48**(2):559-568.
312. Sanghez V, Chen M, Li S, Chou TF, Iacovino M, Lin HJ, Lasky JL, Panosyan EH: **Efficacy of Asparaginase Erwinia chrysanthemi With and Without Temozolomide Against Glioma Cells and Intracranial Mouse Medulloblastoma.** *Anticancer Res* 2018, **38**(5):2627-2634.
313. Kim SS, Rait A, Kim E, DeMarco J, Pirollo KF, Chang EH: **Encapsulation of temozolomide in a tumor-targeting nanocomplex enhances anti-cancer efficacy and reduces toxicity in a mouse model of glioblastoma.** *Cancer letters* 2015, **369**(1):250-258.
314. Ellis HP, Greenslade M, Powell B, Spiteri I, Sottoriva A, Kurian KM: **Current Challenges in Glioblastoma: Intratumour Heterogeneity, Residual Disease, and Models to Predict Disease Recurrence.** *Frontiers in Oncology* 2015, **5**(251).
315. Qazi MA, Vora P, Venugopal C, Sidhu SS, Moffat J, Swanton C, Singh SK: **Intratumoral heterogeneity: pathways to treatment resistance and relapse in human glioblastoma.** *Annals of oncology : official journal of the European Society for Medical Oncology* 2017, **28**(7):1448-1456.
316. Albert FK, Forsting M, Sartor K, Adams HP, Kunze S: **Early postoperative magnetic resonance imaging after resection of malignant glioma: objective evaluation of residual tumor and its influence on regrowth and prognosis.** *Neurosurgery* 1994, **34**(1):45-60; discussion 60-41.
317. Hegi ME, Diserens A-C, Gorlia T, Hamou M-F, de Tribolet N, Weller M, Kros JM, Hainfellner JA, Mason W, Mariani L et al: **MGMT Gene Silencing and Benefit from Temozolomide in Glioblastoma.** *New England Journal of Medicine* 2005, **352**(10):997-1003.
318. Gilbert MR, Wang M, Aldape KD, Stupp R, Hegi M, Jaeckle KA, Armstrong TS, Wefel JS, Won M, Blumenthal DT et al: **RTOG 0525: A randomized phase III trial comparing standard adjuvant temozolomide (TMZ) with a dose-dense (dd) schedule in newly diagnosed glioblastoma (GBM).** *Journal of Clinical Oncology* 2011, **29**(15_suppl):2006-2006.
319. Everhard S, Kaloshi G, Crinière E, Benouaich-Amiel A, Lejeune J, Marie Y, Sanson M, Kujas M, Mokhtari K, Hoang-Xuan K et al: **MGMT methylation: A marker of response to temozolomide in low-grade gliomas.** *Annals of Neurology* 2006, **60**(6):740-743.
320. Francesco P, Massimiliano Del B, Riccardo F, Ignazio GV, Alberto M, Luca A, Luca Maria S, Giovanni M, Luigi S, Bianca P et al: **Identification of residual tumor with intraoperative contrast-enhanced ultrasound during glioblastoma resection.** *Neurosurgical Focus FOC* 2016, **40**(3):E7.

321. Bunse T, Bunse L, Sahm F, Omokoko T, Stevanovic S, Von Deimling A, Sahin U, Schmitt M, Wick W, Platten M: **IMMUNE RESPONSES TO A MUTATION-SPECIFIC PEPTIDE VACCINE TARGETING IDH1R132H IN PATIENTS WITH IDH1R132H-MUTATED GLIOMAS.** *Neuro-Oncology*, **18**(s4):4-4.
322. Debus C, Waltenberger M, Floca R, Afshar-Oromieh A, Bougatf N, Adeberg S, Heiland S, Bendszus M, Wick W, Rieken S *et al*: **Impact of 18F-FET PET on Target Volume Definition and Tumor Progression of Recurrent High Grade Glioma Treated with Carbon-Ion Radiotherapy.** *Scientific Reports* 2018, **8**(1):7201.
323. Wu JS, Gong X, Song YY, Zhuang DX, Yao CJ, Qiu TM, Lu JF, Zhang J, Zhu W, Mao Y *et al*: **3.0-T intraoperative magnetic resonance imaging-guided resection in cerebral glioma surgery: interim analysis of a prospective, randomized, triple-blind, parallel-controlled trial.** *Neurosurgery* 2014, **61 Suppl 1**:145-154.
324. Mellinghoff IK, Penas-Prado M, Peters KB, Cloughesy TF, Burris HA, Maher EA, Janku F, Cote GM, De La Fuente MI, Clarke J *et al*: **Phase 1 study of AG-881, an inhibitor of mutant IDH1/IDH2, in patients with advanced IDH-mutant solid tumors, including glioma.** *Journal of Clinical Oncology* 2018, **36**(15_suppl):2002-2002.
325. Sampson JH, Archer GE, Mitchell DA, Heimberger AB, Bigner DD: **Tumor-specific immunotherapy targeting the EGFRvIII mutation in patients with malignant glioma.** *Seminars in Immunology* 2008, **20**(5):267-275.
326. Fenstermaker RA, Ciesielski MJ: **Immunotherapeutic Strategies for Malignant Glioma.** *Cancer Control* 2004, **11**(3):181-191.
327. Uram L, Misiorek M, Pichla M, Filipowicz-Rachwal A, Markowicz J, Wolowiec S, Walajtys-Rode E: **The Effect of Biotinylated PAMAM G3 Dendrimers Conjugated with COX-2 Inhibitor (celecoxib) and PPARgamma Agonist (Fmoc-L-Leucine) on Human Normal Fibroblasts, Immortalized Keratinocytes and Glioma Cells in Vitro.** *Molecules (Basel, Switzerland)* 2019, **24**(20).
328. Stanojkovic TP, Zizak Z, Mihailovic-Stanojevic N, Petrovic T, Juranic Z: **Inhibition of proliferation on some neoplastic cell lines-act of carvedilol and captopril.** *Journal of experimental & clinical cancer research : CR* 2005, **24**(3):387-395.
329. Jo HY, Kim Y, Park HW, Moon HE, Bae S, Kim J, Kim DG, Paek SH: **The Unreliability of MTT Assay in the Cytotoxic Test of Primary Cultured Glioblastoma Cells.** *Exp Neurobiol* 2015, **24**(3):235-245.
330. Chen W-H, Liao W-C, Sohn YS, Fadeev M, Cecconello A, Nechushtai R, Willner I: **Stimuli-Responsive Nucleic Acid-Based Polyacrylamide Hydrogel-Coated Metal–Organic Framework Nanoparticles for Controlled Drug Release.** *Advanced Functional Materials* 2018, **28**(8):1705137.
331. Böttcher MA, Held-Feindt J, Synowitz M, Lucius R, Traulsen A, Hattermann K: **Modeling treatment-dependent glioma growth including a dormant tumor cell subpopulation.** *BMC Cancer* 2018, **18**(1):376.
332. Soeda A, Hara A, Kunisada T, Yoshimura S-i, Iwama T, Park DM: **The Evidence of Glioblastoma Heterogeneity.** *Scientific reports* 2015, **5**:7979.
333. Johnson BE, Mazor T, Hong C, Barnes M, Aihara K, McLean CY, Fouse SD, Yamamoto S, Ueda H, Tatsuno K *et al*: **Mutational analysis reveals the origin and therapy-driven evolution of recurrent glioma.** *Science (New York, NY)* 2014, **343**(6167):189-193.
334. Reardon DA, Wen PY: **Unravelling tumour heterogeneity—implications for therapy.** *Nature Reviews Clinical Oncology* 2015, **12**:69.
335. Odia Y, Sul J, Shih JH, Kreisl TN, Butman JA, Iwamoto FM, Fine HA: **A Phase II trial of tandutinib (MLN 518) in combination with bevacizumab for patients with recurrent glioblastoma.** *CNS oncology* 2016, **5**(2):59-67.
336. Weathers S-P, Han X, Liu DD, Conrad CA, Gilbert MR, Loghin ME, O'Brien BJ, Penas-Prado M, Puduvalli VK, Tremont-Lukats I *et al*: **A randomized phase II trial of standard dose**

- bevacizumab versus low dose bevacizumab plus lomustine (CCNU) in adults with recurrent glioblastoma.** *Journal of Neuro-Oncology* 2016, **129**(3):487-494.
337. Brandes AA, Carpentier AF, Kesari S, Sepulveda-Sanchez JM, Wheeler HR, Chinot O, Cher L, Steinbach JP, Capper D, Specenier P *et al*: **A Phase II randomized study of galunisertib monotherapy or galunisertib plus lomustine compared with lomustine monotherapy in patients with recurrent glioblastoma.** *Neuro-Oncology* 2016, **18**(8):1146-1156.
 338. Chen M-J, Tsan Y-T, Liou J-M, Lee Y-C, Wu M-S, Chiu H-M, Wang H-P, Chen P-C: **Statins and the risk of pancreatic cancer in Type 2 diabetic patients—A population-based cohort study.** *International journal of cancer* 2016, **138**(3):594-603.
 339. Nielsen SF, Nordestgaard BG, Bojesen SE: **Statin use and reduced cancer-related mortality.** *The New England journal of medicine* 2012, **367**(19):1792-1802.
 340. Wang A, Aragaki AK, Tang JY, Kurian AW, Manson JE, Chlebowski RT, Simon M, Desai P, Wassertheil-Smoller S, Liu S *et al*: **Statin use and all-cancer survival: prospective results from the Women's Health Initiative.** *Br J Cancer* 2016, **115**(1):129-135.
 341. Zhou Y-Y, Zhu G-Q, Wang Y, Zheng J-N, Ruan L-Y, Cheng Z, Hu B, Fu S-W, Zheng M-H: **Systematic review with network meta-analysis: statins and risk of hepatocellular carcinoma.** *Oncotarget* 2016, **7**(16):21753-21762.
 342. Ananthakrishnan AN, Cagan A, Cai T, Gainer VS, Shaw SY, Churchill S, Karlson EW, Murphy SN, Liao KP, Kohane I: **Statin Use Is Associated With Reduced Risk of Colorectal Cancer in Patients With Inflammatory Bowel Diseases.** *Clinical Gastroenterology and Hepatology* 2016, **14**(7):973-979.
 343. Gaist D, Andersen L, Hallas J, Sorensen HT, Schroder HD, Friis S: **Use of statins and risk of glioma: a nationwide case-control study in Denmark.** *Br J Cancer* 2013, **108**(3):715-720.
 344. Bhavsar S, Hagan K, Arunkumar R, Potylchansky Y, Grasu R, Dang A, Carlson R, Cowels C, Arnold B, Rahlfs TF *et al*: **Preoperative statin use is not associated with improvement in survival after glioblastoma surgery.** *Journal of clinical neuroscience : official journal of the Neurosurgical Society of Australasia* 2016, **31**:176-180.
 345. Gaist D, Hallas J, Friis S, Hansen S, Sorensen HT: **Statin use and survival following glioblastoma multiforme.** *Cancer epidemiology* 2014, **38**(6):722-727.
 346. Seliger C, Schaertl J, Gerken M, Lubert C, Proescholdt M, Riemenschneider MJ, Leitzmann MF, Hau P, Klinkhammer-Schalke M: **Use of statins or NSAIDs and survival of patients with high-grade glioma.** *PLOS ONE* 2018, **13**(12):e0207858.
 347. Yanae M, Tsubaki M, Satou T, Itoh T, Imano M, Yamazoe Y, Nishida S: **Statin-induced apoptosis via the suppression of ERK1/2 and Akt activation by inhibition of the geranylgeranyl-pyrophosphate biosynthesis in glioblastoma.** *Journal of experimental & clinical cancer research : CR* 2011, **30**:74.
 348. Kerschbaumer J, Schmidt FA, Grams AE, Nowosielski M, Pinggera D, Brawanski KR, Petr O, Thome C, Tuettenberg J, Seiz M *et al*: **Dual Anti-angiogenic Chemotherapy with Temozolomide and Celecoxib in Selected Patients with Malignant Glioma Not Eligible for Standard Treatment.** *Anticancer Res* 2015, **35**(9):4955-4960.
 349. Shono K, Sumi A, Fujihara T, Nakajima K, Mizobuchi Y, Kitazato K, Nagahiro S, Mure H: **EXTH-72. CELECOXIB INHIBITS PROLIFERATION AND INDUCES APOPTOSIS IN GLIOMA STEM CELLS AND AN ANIMAL MODEL OF GLIOBLASTOMA.** *Neuro-Oncology* 2017, **19**(Suppl 6):vi88-vi89.
 350. Toloczko-Iwaniuk N, Dziemianczyk-Pakiela D, Nowaszewska BK, Celinska-Janowicz K, Milytk W: **Celecoxib in Cancer Therapy and Prevention - Review.** *Current drug targets* 2019, **20**(3):302-315.
 351. Yerokun T, Winfield LL: **Celecoxib and LLW-3-6 Reduce Survival of Human Glioma Cells Independently and Synergistically with Sulfasalazine.** *Anticancer Res* 2015, **35**(12):6419-6424.
 352. Welzel G, Gehweiler J, Brehmer S, Appelt J-U, von Deimling A, Seiz-Rosenhagen M, Schmiedek P, Wenz F, Giordano FA: **Metronomic chemotherapy with daily low-dose**

- temozolomide and celecoxib in elderly patients with newly diagnosed glioblastoma multiforme: a retrospective analysis.** *Journal of Neuro-Oncology* 2015, **124**(2):265-273.
353. Zhang T, Yang X, Liu P, Zhou J, Luo J, Wang H, Li A, Zhou Y: **Association between nonsteroidal anti-inflammatory drugs use and risk of central nervous system tumors: a dose-response meta analysis.** *Oncotarget* 2017, **8**(60):102486-102498.
 354. Purow B: **Repurposing existing agents as adjunct therapies for glioblastoma.** *Neuro-Oncology Practice* 2015, **3**(3):154-163.
 355. Raj L, Ide T, Gurkar AU, Foley M, Schenone M, Li X, Tolliday NJ, Golub TR, Carr SA, Shamji AF *et al*: **Selective killing of cancer cells by a small molecule targeting the stress response to ROS.** *Nature* 2011, **475**(7355):231-234.
 356. Tawari PE, Wang Z, Najlah M, Tsang CW, Kannappan V, Liu P, McConville C, He B, Armesilla AL, Wang W: **The cytotoxic mechanisms of disulfiram and copper(ii) in cancer cells.** *Toxicology Research* 2015, **4**(6):1439-1442.
 357. Wen X, Cheng X, Hu D, Li W, Ha J, Kang Z, Zhang M, Huang Y, Wu S: **Combination of Curcumin with an Anti-Transferrin Receptor Antibody Suppressed the Growth of Malignant Gliomas In vitro.** *Turkish neurosurgery* 2016, **26**(2):209-214.
 358. Odia Y, Kreisl TN, Aregawi D, Innis EK, Fine HA: **A phase II trial of tamoxifen and bortezomib in patients with recurrent malignant gliomas.** *Journal of Neuro-Oncology* 2015, **125**(1):191-195.
 359. Wu M, Fan Y, Lv S, Xiao B, Ye M, Zhu X: **Vincristine and temozolomide combined chemotherapy for the treatment of glioma: a comparison of solid lipid nanoparticles and nanostructured lipid carriers for dual drugs delivery.** *Drug delivery* 2016, **23**(8):2720-2725.
 360. Krauze AV, Myrehaug SD, Chang MG, Holdford DJ, Smith S, Shih J, Tofilon PJ, Fine HA, Camphausen K: **A Phase 2 Study of Concurrent Radiation Therapy, Temozolomide, and the Histone Deacetylase Inhibitor Valproic Acid for Patients With Glioblastoma.** *International Journal of Radiation Oncology*Biophysics* 2015, **92**(5):986-992.
 361. Lin L, Cai J, Jiang C: **Recent Advances in Targeted Therapy for Glioma.** *Current medicinal chemistry* 2017, **24**(13):1365-1381.
 362. Gorelick N, Jackson E, Tyler B, Brem H: **Chapter 11 - Interstitial Chemotherapy and Polymer Drug Delivery.** In: *Handbook of Brain Tumor Chemotherapy, Molecular Therapeutics, and Immunotherapy (Second Edition)*. Edited by Newton HB: Academic Press; 2018: 155-165.
 363. Arnone GD, Bhimani AD, Aguilar T, Mehta AI: **Localized targeted antiangiogenic drug delivery for glioblastoma.** *Journal of Neuro-Oncology* 2018, **137**(2):223-231.
 364. Viola-Rhenals M, Patel KR, Jaimes-Santamaria L, Wu G, Liu J, Dou QP: **Recent Advances in Antabuse (Disulfiram): The Importance of its Metal-binding Ability to its Anticancer Activity.** *Current medicinal chemistry* 2018, **25**(4):506-524.
 365. Eccleston DS, Horrigan MC, Ellis SG: **Rationale for local drug delivery.** *Seminars in interventional cardiology : SIIC* 1996, **1**(1):8-16.
 366. Li Y, Yin W, Wang X, Zhu W, Huang Y, Yan G: **Cholera toxin induces malignant glioma cell differentiation via the PKA/CREB pathway.** *Proceedings of the National Academy of Sciences* 2007, **104**(33):13438.
 367. Jellinger K: **Glioblastoma multiforme: Morphology and biology.** *Acta neurochirurgica* 1978, **42**(1):5-32.
 368. Fernandes C, Costa A, Osorio L, Lago RC, Linhares P, Carvalho B, Caeiro C: **Current Standards of Care in Glioblastoma Therapy.** In: *Glioblastoma*. Edited by De Vleeschouwer S. Brisbane (AU): Codon Publications
- Copyright: The Authors.; 2017.
369. Scicchitano BM, Sorrentino S, Proietti G, Lama G, Dobrowolny G, Catizone A, Binda E, Larocca LM, Sica G: **Levetiracetam enhances the temozolomide effect on glioblastoma stem cell proliferation and apoptosis.** *Cancer Cell International* 2018, **18**(1):136.

370. Peddi P, Ajit NE, Burton GV, El-Osta H: **Regression of a glioblastoma multiforme: spontaneous versus a potential antineoplastic effect of dexamethasone and levetiracetam.** *BMJ Case Reports* 2016, **2016**:bcr2016217393.
371. Cenciarini M, Valentino M, Belia S, Sforza L, Rosa P, Ronchetti S, D'Adamo MC, Pessia M: **Dexamethasone in Glioblastoma Multiforme Therapy: Mechanisms and Controversies.** *Frontiers in Molecular Neuroscience* 2019, **12**(65).
372. Brandao M, Ponde NF, Poggio F, Kotecki N, Salis M, Lambertini M, de Azambuja E: **Combination therapies for the treatment of HER2-positive breast cancer: current and future prospects.** *Expert review of anticancer therapy* 2018, **18**(7):629-649.
373. Najem A, Krayem M, Perdrix A, Kerger J, Awada A, Journe F, Ghanem G: **New Drug Combination Strategies in Melanoma: Current Status and Future Directions.** *Anticancer Res* 2017, **37**(11):5941-5953.
374. Nikolaou V, Anastasaki A, Alsubaie F, Simula A, Fox D, Haddleton D: **Copper(II) gluconate (a non-toxic food supplement/dietary aid) as a precursor catalyst for effective photo-induced living radical polymerisation of acrylates.** *Polym Chem* 2015, **6**.
375. Karamanakos PN, Trafalis DT, Papachristou DJ, Panteli ES, Papavasiliopoulou M, Karatzas A, Kardamakis D, Nasioulas G, Marselos M: **Evidence for the efficacy of disulfiram and copper combination in glioblastoma multiforme - A propos of a case.** *Journal of BUON : official journal of the Balkan Union of Oncology* 2017, **22**(5):1227-1232.
376. Dalecki AG, Haeili M, Shah S, Speer A, Niederweis M, Kutsch O, Wolschendorf F: **Disulfiram and Copper Ions Kill *Mycobacterium tuberculosis* in a Synergistic Manner.** *Antimicrobial Agents and Chemotherapy* 2015, **59**(8):4835.
377. Singh V: **Synthesis, electrochemical, fluorescence and antimicrobial studies of 2-chloro-3-amino-1,4-naphthoquinone bearing mononuclear transition metal dithiocarbamate complexes [M{2S,S-S2C-piperazine-C2H4N(H)CINQ}n].** *RSC Advances* 2015, **5**.
378. 5.0 EP: **2.2.46. Chromatograph Separation Techniques**
379. Samba I, Hernandez R, Rescignano N, Mijangos C, Kenny JM: **Nanocomposite hydrogels based on embedded PLGA nanoparticles in gelatin.** *Nanocomposites* 2015, **1**(1):46-50.
380. Wang Q, Wang J, Lu Q, Detamore MS, Berkland C: **Injectable PLGA based colloidal gels for zero-order dexamethasone release in cranial defects.** *Biomaterials* 2010, **31**(18):4980-4986.
381. Malik S, Bahal R: **Investigation of PLGA nanoparticles in conjunction with nuclear localization sequence for enhanced delivery of anti-miR phosphorothioates in cancer cells in vitro.** *Journal of Nanobiotechnology* 2019, **17**(1):57.
382. Wei H, Song J, Li H, Li Y, Zhu S, Zhou X, Zhang X, Yang L: **Active loading liposomal irinotecan hydrochloride: Preparation, in vitro and in vivo evaluation.** *Asian Journal of Pharmaceutical Sciences* 2013, **8**(5):303-311.
383. Alagona P, Jr.: **Pitavastatin: evidence for its place in treatment of hypercholesterolemia.** *Core Evid* 2010, **5**:91-105.
384. Ramadhani N, Shabir M, McConville C: **Preparation and characterisation of Kolliphor® P 188 and P 237 solid dispersion oral tablets containing the poorly water soluble drug disulfiram.** *International Journal of Pharmaceutics* 2014, **475**(1):514-522.
385. Wehbe M, Anantha M, Shi M, Leung AW-Y, Dragowska WH, Sanche L, Bally MB: **Development and optimization of an injectable formulation of copper diethyldithiocarbamate, an active anticancer agent.** *Int J Nanomedicine* 2017, **12**:4129-4146.
386. Tariq M, Negi LM, Talegaonkar S, Ahmad FJ, Iqbal Z, Khan AM: **Liquid Chromatographic Method for Irinotecan Estimation: Screening of P-gp Modulators.** *Indian J Pharm Sci* 2015, **77**(1):14-23.

387. Satheesh Kumar N, Nisha N, Jayabalan N, N S, Bagyalakshmi J: **HPLC Determination of Pitavastatin Calcium in Pharmaceutical Dosage Forms.** *Pharmaceutica Analytica Acta* 2011, **02**.
388. Baffoe CS, Nguyen N, Boyd P, Wang W, Morris M, McConville C: **Disulfiram-loaded immediate and extended release vaginal tablets for the localised treatment of cervical cancer.** *Journal of Pharmacy and Pharmacology* 2015, **67**(2):189-198.
389. Hutchins SR, Haddad PR, Dilli S: **Reversed-phase high-performance liquid chromatography of diethyldithiocarbamate complexes using radial compression columns.** *Journal of Chromatography A* 1982, **252**:185-192.
390. Li K, Tan L, Zhou JA: **HPLC determination of captopril in human plasma and its pharmacokinetic study.** *Biomedical chromatography : BMC* 1996, **10**(5):237-239.
391. Timmins P, Jackson I, Wang Y: **Factors affecting captopril stability in aqueous solution.** *International Journal of Pharmaceutics* 1982, **11**:329–336.
392. Owens PK, Svensson LA, Vessman J: **Direct separation of captopril diastereoisomers including their rotational isomers by RP-LC using a teicoplanin column.** *Journal of pharmaceutical and biomedical analysis* 2001, **25**(3):453-464.
393. Mansour FR, Danielson ND: **Separation methods for captopril in pharmaceuticals and biological fluids.** *Journal of separation science* 2012, **35**(10-11):1213-1226.
394. Shabir GAJJovt: **Step-by-step analytical methods validation and protocol in the quality system compliance industry.** 2005, **10**:314-325.
395. Bunn GP: **Good Manufacturing Practices for Pharmaceuticals, Seventh Edition:** crc press taylor and francis group 2019.
396. Phan-Thien N: **Understanding viscoelasticity : an introduction to rheology** In., 2nd ed. edn. Heidelberg: Heidelberg : Springer; 2013.
397. Tanzi MC, Farè S, Candiani G: **Chapter 2 - Mechanical Properties of Materials.** In: *Foundations of Biomaterials Engineering.* Edited by Tanzi MC, Farè S, Candiani G: Academic Press; 2019: 105-136.
398. Vlachopoulos J, Strutt D: **The Role of Rheology in Polymer Extrusion.** *Extrusion Minitex and Conference: From Basics to Recent Developments* 2003.
399. Dealy JM, Wissbrun KF: **Role of Rheology in Extrusion.** In: *Melt Rheology and Its Role in Plastics Processing: Theory and Applications.* Edited by Dealy JM, Wissbrun KF. Dordrecht: Springer Netherlands; 1999: 441-490.
400. Cogswell FN: **Chapter Six - Rheology in Polymer Processing.** In: *Polymer Melt Rheology.* Edited by Cogswell FN: Woodhead Publishing; 2003: 111-131.
401. Sakka L, Coll G, Chazal J: **Anatomy and physiology of cerebrospinal fluid.** *Eur Ann Otorhinolaryngol Head Neck Dis* 2011, **128**(6):309-316.
402. Brown PD, Davies SL, Speake T, Millar ID: **Molecular mechanisms of cerebrospinal fluid production.** *Neuroscience* 2004, **129**(4):955-968.
403. Weber EL, Goebel EA: **Cerebral edema associated with Gliadel wafers: two case studies.** *Neuro-oncology* 2005, **7**(1):84-89.
404. Lin Z-X: **Glioma-related edema: new insight into molecular mechanisms and their clinical implications.** *Chin J Cancer* 2013, **32**(1):49-52.
405. Xing WK, Shao C, Qi ZY, Yang C, Wang Z: **The role of Gliadel wafers in the treatment of newly diagnosed GBM: a meta-analysis.** *Drug Des Devel Ther* 2015, **9**:3341-3348.
406. Loftsson T: **Drug Stability for Pharmaceutical Scientists:** Elsevier Science.
407. Qiu F, Scrivens G: **Accelerated predictive stability (APS) : fundamentals and pharmaceutical industry practices:** London, United Kingdom : Academic Press, an imprint of Elsevier, 2018.; 2018.
408. Blessy M, Patel RD, Prajapati PN, Agrawal YK: **Development of forced degradation and stability indicating studies of drugs—A review.** *Journal of Pharmaceutical Analysis* 2014, **4**(3):159-165.

409. Knopp MM, Löbmann K, Elder DP, Rades T, Holm R: **Recent advances and potential applications of modulated differential scanning calorimetry (mDSC) in drug development.** *European Journal of Pharmaceutical Sciences* 2016, **87**:164-173.
410. El-Houssiny A, Ward A, Mostafa D, Abd-El-Messieh s, Nour K, Darwish M, Khalil W: **Drug–polymer interaction between glucosamine sulfate and alginate nanoparticles: FTIR, DSC and dielectric spectroscopy studies.** *Advances in Natural Sciences: Nanoscience and Nanotechnology* 2016, **7**:025014.
411. Ceschel GC, Badiello R, Ronchi C, Maffei P: **Degradation of components in drug formulations: a comparison between HPLC and DSC methods.** *Journal of pharmaceutical and biomedical analysis* 2003, **32**(4):1067-1072.
412. Chen Y, Gao Z, Duan JZ: **Chapter 13 - Dissolution Testing of Solid Products.** In: *Developing Solid Oral Dosage Forms (Second Edition)*. Edited by Qiu Y, Chen Y, Zhang GGZ, Yu L, Mantri RV. Boston: Academic Press; 2017: 355-380.
413. Anand O, Yu LX, Conner DP, Davit BM: **Dissolution testing for generic drugs: an FDA perspective.** *AAPS J* 2011, **13**(3):328-335.
414. Kimura H, Ogura Y, Hashizoe M, Nishiwaki H, Honda Y, Ikada Y: **A new vitreal drug delivery system using an implantable biodegradable polymeric device.** *Investigative Ophthalmology & Visual Science* 1994, **35**(6):2815-2819.
415. Siepmann J, Göpferich A: **Mathematical modeling of bioerodible, polymeric drug delivery systems.** *Advanced Drug Delivery Reviews* 2001, **48**(2):229-247.
416. Solorio L, Carlson A, Zhou H, Exner AA: **Implantable Drug Delivery Systems.** In: *Engineering Polymer Systems for Improved Drug Delivery*. 2014: 189-225.
417. Allen RP, Bolandparvaz A, Ma JA, Manickam VA, Lewis JS: **Microparticles Latent, Immunosuppressive Nature of Poly(lactic-co-glycolic acid).** *ACS Biomater Sci Eng* 2018, **4**(3):900-918.
418. Kolter K, Karl M, Gryczke A: **Hot-melt extrusion with BASF pharma polymers.** In: *Hot melt extrusion & solubilizer compendia by BASF*.
419. Boyd P, Major I, Wang W, McConville C: **Development of disulfiram-loaded vaginal rings for the localised treatment of cervical cancer.** *Eur J Pharm Biopharm* 2014, **88**(3):945-953.
420. Snejdova E, Dittrich M: **Pharmaceutically Used Plasticizers** In: *Recent Advances in Plasticizers*. Edited by Luqma M. Czech Republic; 2011.
421. Panda B, Parihar AS, Mallick S: **Effect of plasticizer on drug crystallinity of hydroxypropyl methylcellulose matrix film.** *International Journal of Biological Macromolecules* 2014, **67**:295-302.
422. Jaiswar D, Pawar J, Amin P: **Hot Melt Extrusion: Continuous Process of Preparation of Sustained Released Matrix Tablet by Using Hydroxypropylcellulose.** *American Journal of Pharmtech Research* 2016.
423. Quinten T, De Beer T, Onofre F, Mendez-Montealvo G, Wang Y-J, Remon j, Vervaet C: **Sustained-Release and Swelling Characteristics of Xanthan Gum/Ethylcellulose-Based Injection Moulded Matrix Tablets: in Vitro and in Vivo Evaluation.** *Journal of pharmaceutical sciences* 2011, **100**:2858-2870.
424. Sepehri N, Rouhani H, Tavassolian F, Montazeri H, Khoshayand MR, Ghahremani MH, Ostad SN, Atyabi F, Dinarvand R: **SN38 polymeric nanoparticles: In vitro cytotoxicity and in vivo antitumor efficacy in xenograft balb/c model with breast cancer versus irinotecan.** *International Journal of Pharmaceutics* 2014, **471**(1):485-497.
425. Grohgan H, Löbmann K, Priemel P, Tarp Jensen K, Graeser K, Strachan C, Rades T: **Amorphous drugs and dosage forms.** *Journal of Drug Delivery Science and Technology* 2013, **23**(4):403-408.
426. Datta S, Grant DJW: **Crystal structures of drugs: advances in determination, prediction and engineering.** *Nature Reviews Drug Discovery* 2004, **3**(1):42-57.
427. Pharmacopeia US: **USP Method for HPLC Analysis of Disulfiram.** In.; 2002.

Appendix A

Pathology results, previous treatment and MTT LogIC₅₀ data summary for single drug treatments.

Patient	Tumour Grade	Mutation						Previous treatments	Tumour Fragment	LogIC ₅₀ (nM)									
		IDH ₁		ATRX		MGMT				TMZ	DSF	CoGlu	CAP	TCL	ITZ	CXB	IRN	PTV	
		Wild-type	Mutant	Wild-type	Mutant	Methylated	Un-methylated												
1	N/A	N/A		N/A		N/A		N/A	TC	>5	-	-	-	-	-	-	4.2	-	
2	IV	✓		✓		✓		Dexamethasone	TC	>5	-	-	-	-	-	-	3.4	-	
									BAT	>5	>5	>5	>5	>5	>5	5.0	>5	>5	
3	IV	✓		✓		✓		Steroids	TC	>5	>5	>5	>5	>5	4.8	3.8	4.6	3.3	
4	IV	✓		✓		Low level methylation		None	TC	>5	>5	4.7	>5	>5	>5	4.2	4.5	2.3	
									BAT	>5	>5	>5	>5	5.0	>5	4.8	4.0	>5	
5	III		✓	✓			✓	2x resection Radiotherapy TMZ Levetiracetam	TC	-	-	-	-	-	-	-	-	-	
									BAT	>5	>5	>5	>5	>5	>5	4.8	3.4	>5	
6	III		✓		✓		✓	Radiotherapy TMZ Lomustine	TC	>5	>5	4.5	5.0	>5	4.8	4.4	4.3	2.5	
7	IV	N/A		✓			✓	Dexamethasone Lansoprazole Levetiracetam	TC	>5	>5	4.9	>5	>5	4.1	3.6	4.0	2.3	
8	IV	✓		✓		N/A		Dexamethasone	TC	>5	4.8	>5	>5	>5	>5	4.0	4.0	3.5	3.0
									BAT	2.8	>5	>5	>5	>5	>5	4.5	>5	3.0	
9	IV	✓		✓		Low level methylation		N/A	TC	>5	3.4	>5	>5	>5	>5	5.0	>5	>5	
									BAT	>5	2.8	>5	>5	>5	>5	3.0	2.4	2.8	
10	IV	✓		N/A			✓	3x resection	TC	>5	>5	5.0	>5	>5	>5	4.3	4.4	2.4	
11	IV	✓		✓			✓	Steroids	TC	>5	>5	>5	>5	>5	>5	>5	3.3	2.0	
12	III	N/A			✓		✓	Resection Levetiracetam	TC	>5	5.0	4.8	5.0	>5	4.3	4.3	4.5	>5	

List of abbreviations: IDH₁, isocitrate dehydrogenase 1; ATRX, alpha-thalassemia/mental retardation X-linked; MGMT, O-6-methylguanine-DNA methyltransferase; TC, tumour core; BAT, brain around tumour; TMZ, temozolomide; IRN, irinotecan; PTV, pitavastatin; DSF, disulfiram; CoGlu, copper Gluconate; CAP, captopril; CXB, celecoxib; ITZ, itraconazole; TCL, ticlopidine. n/a indicates that the data could not be determined.

Appendix B

Pathology results, previous treatment and MTT LogIC₅₀ data summary for combination drug treatments.

Patient	Tumour Grade	Mutation						Previous treatments	Tumour Fragment	LogIC ₅₀ (nM)				
		IDH ₁		ATRX		MGMT				Drug Combination				
		Wild-type	Mutant	Wild-type	Mutant	Methylated	Un-methylated			TMZ	IRN-PTV-DSF-CoGlu	IRN-CAP-CXB-ITZ	IRN-CAP-DSF	IRN-PTV-CAP-TCL
2	IV	✓		✓		✓		Dexamethasone	TC	>5	-	-	-	-
									TIC	>5	2.8	>5	>5	>5
3	IV	✓		✓		✓		Steroids	TC	>5	4.0	4.3	3.2	4.9
4	IV	✓		✓		Low level methylation		None	TC	>5	2.8	4.6	3.5	4.0
									TIC	>5	2.3	4.3	3.9	4.8
5	III		✓	✓			✓	2x resection Radiotherapy TMZ Levetiracetam	TC	-	-	-	-	-
									TIC	>5	2.5	4.3	3.1	2.4
6	III		✓		✓		✓	Radiotherapy TMZ Lomustine	TC	>5	2.4	4.0	3.3	4.7
7	IV	N/A		✓			✓	Dexamethasone Lansoprazole Levetiracetam	TC	>5	2.1	4.6	4.0	2.4
8	IV	✓		✓		N/A		Dexamethasone	TC	>5	2.4	4.3	4.0	4.2
									TIC	2.8	2.3	4.3	3.9	2.6
9	IV	✓		✓		Low level methylation		N/A	TC	>5	2.8	4.6	3.6	4.0
									TIC	>5	3.0	3.9	3.3	2.9
10	IV	✓		N/A			✓	3x resection	TC	>5	2.3	3.8	3.7	2.5
11	IV	✓		✓			✓	Steroids	TC	>5	2.5	3.8	3.5	3.0
12	III	N/A			✓		✓	Resection Levetiracetam	TC	>5	2.4	4.5	3.4	4.8

List of abbreviations: IDH₁, isocitrate dehydrogenase 1; ATRX, alpha-thalassemia/mental retardation X-linked; MGMT, O-6-methylguanine-DNA methyltransferase; TC, tumour core; BAT, brain around tumour; TMZ, temozolomide; IRN, irinotecan; PTV, pitavastatin; DSF, disulfiram; CoGlu, copper Gluconate; CAP, captopril; CXB, celecoxib; ITZ, itraconazole; TCL, ticlopidine. n/a indicates that the data could not be determined.